NASA CR 72086
TRW ER 6661-9

TRW INC.

NASA

CARBON DIOXIDE CONCENTRATION SYSTEM

By

A. D. Babinsky, D. L. DeRespiris, and S. J. Derezinski

Prepared for

NATIONAL AERONAUTICS AND SPACE ADMINISTRATION

CONTRACT NAS 3-7638

TRW EQUIPMENT LABORATORIES
A DIVISION OF TRW INC. • CLEVELAND, OHIO 44117

NOTICE

This report was prepared as an account of Government sponsored work. Neither the United States, nor the National Aeronautics and Space Administration (NASA), nor any person acting on behalf of NASA:

A.) Makes any warranty or representation, expressed or implied, with respect to the accuracy, completeness, or usefulness of the information contained in this report, or that the use of any information, apparatus, method, or process disclosed in this report may not infringe privately owned rights; or

B.) Assumes any liabilities with respect to the use of, or for damages resulting from the use of any information, apparatus, method or process disclosed in this report.

As used above, "person acting on behalf of NASA" includes any employee or contractor of NASA, or employee of such contractor, to the extent that such employee or contractor of NASA, or employee or such contractor prepares, disseminates, or provides access to, any information pursuant to his employment or contract with NASA, or his employment with such contractor.

Request for copies of this report should be referred to

National Aeronautics and Space Administration
Office of Scientific and Technical Information
Attention: AFSS-A
Washington, D. C. 20546

NASA CR-72086

TRW ER-6661-9

FINAL REPORT

CARBON DIOXIDE CONCENTRATION SYSTEM

by

A. D. Babinsky, D. L. DeRespiris, and S. J. Derezinski

prepared for

NATIONAL AERONAUTICS AND SPACE ADMINISTRATION

July 30, 1966

CONTRACT NAS 3-7638

Technical Management
NASA Lewis Research Center
Cleveland, Ohio
Solar and Chemical Power Branch
Meyer R. Unger

TRW EQUIPMENT LABORATORIES
New Products Department
23555 Euclid Avenue
Cleveland, Ohio 44117

CARBON DIOXIDE CONCENTRATION SYSTEM

by

A. D. Babinsky, D. L. DeRespiris, and S. J. Derezinski

ABSTRACT

Under contract NAS 3-7638 an experimental program was conducted to determine the feasibility of an electrochemical means of concentrating CO_2 from cabin air while obtaining engineering design data for future system prototype design.

Studies were made using both small laboratory type cells and large (12" x 12" electrode area) test cells. The first two stages of the three stage system used an electrolyte of potassium carbonate while the third stage utilized sulfuric acid. The large carbonate cells had end plates fabricated of gold and nickel plated magnesium, while PVDC plastic was used for the acid cell end plates.

Short term parametric tests were conducted for current densities ranging from 15 to 45 ASF, and cell temperatures ranging from 90° to 140°F for Stage I, 122° to 176°F for Stage II and 172° to 195°F for Stage III.

Two cells of each stage were put on a extended duration life test. Due to materials difficulties all cell testing was terminated short of the 250 hour goal. The process functioned satisfactorily prior to the onset of the materials difficulties.

TABLE OF CONTENTS

LIST OF FIGURES

LIST OF FIGURES (CONTINUED)

LIST OF FIGURES (CONTINUED)

LIST OF FIGURES (CONTINUED)

LIST OF TABLES

CARBON DIOXIDE CONCENTRATION SYSTEM

by

A. D. Babinsky, D. L. DeRespiris, and S. J. Derezinski

SUMMARY

The objective of contract NAS 3-7638 was to obtain engineering data for the design of an electrochemical carbon dioxide concentration system suitable to perform as a life support system in space. During the program only individual cells were tested.

The system consists of three connected electrochemical cell stages which extract CO_2 from air processed through the system. From an air stream containing 0.5% CO_2 the first stage transfers a gas mixture of 57% CO_2 and 43% O_2 to the second stage. The second stage transfers from this gas a mixture consisting of approximately 74% CO_2 and 26% O_2. The third stage cell removes O_2 from thismixture leaving essentially pure CO_2 as the end product. Potassium carbonate solution is used as the electrolyte for Stage I and II, while aqueous sulfuric acid is used for the Stage III cell electrolyte.

A preliminary system analysis was completed to permit the subsequent design of the large experimental cells. To avoid scale up problems at a later date the electrode area used was 12" x 12". First and second stage cell end plates were fabricated of magnesium and plated with nickel and gold. The results of studies conducted to determine suitable materials for the acid electrolyte third stage cells indicated that 2-mil non-porous gold plated magnesium was a suitable material for that purpose. However, its high cost was not compatible with the program, hence a plastic (PVDC) cell with 2-mil gold plated copper current collector inserts were used for this experimental program.

Two test rigs were designed and assembled. A test rig for small (3" x 3") cell testing was used for testing of a small plastic acid stage cell and a small non-porous gold plated magnesium cell. The test stand for the large cells was designed to permit individual installation and test of each stage while allowing the use of common gas analysis and recording instrumentation.

Provisions were made for automatic cell temperature control and cell inlet humidity control for each stage.

Small cell testing included plastic cell tests and four test series (M-1 thru M-4) using a small gold plated acid test cell. The object of these tests was to examine the acid stage polarization time dependence and materials compatibility. The common result of all tests was an initial voltage increase ranging from 75 to 90 mv over the first seven hours of cell operation. It was concluded that progressive oxidation of the tantalum screen appeared to be the cause of this voltage increase with time. The gold plated end plates performed satisfactorily as evidenced by the 185 hour run during test M-3. Nominal operating voltage was 1.060 volts at a current density of 40 ASF.

Parametric testing of the large cells was conducted for a four hour period at each operating point. These tests are summarized in the Table below.

Large Cell Parametric Testing

Stage I Cell Operating Potential, Volts

	$T_c \sim 90^\circ F$	$T_c \sim 116^\circ F$	$T_c \sim 140^\circ F$
2 x S Flow			
I ~ 15 ASF	1.22	1.10	0.93
I ~ 30 ASF	1.53	1.30	1.13
I ~ 45 ASF	--	1.52	1.25
5 x S Flow			
I ~ 30 ASF	--	1.40	--
1 x S Flow			
I ~ 30 ASF	--	1.22	1.08

Stage II Cell Operating Potential, Volts

	$T_c \sim 122^\circ F$	$T_c \sim 176^\circ F$
1 x S Flow		
I ~ 15 ASF	0.982	0.715
I ~ 22.5 ASF	1.171	--
I ~ 30 ASF	1.332	0.938
I ~ 45 ASF	--	1.088

Stage III Cell Operating Potential, Volts

	$T_c \sim 172^\circ F$	$T_c \sim 195^\circ F$
1.3 x S Flow		
I ~ 17 ASF	1.021	0.970
I ~ 35 ASF	1.090	1.038
I ~ 52 ASF	1.194	1.074

System optimization and thermal balance studies were completed based on the parametric test results. Results of these studies indicate that a system can be made which has self-regulating temperature control by evaporative cooling of water from liquid reservoirs in the cells. Optimum operating conditions are:

	Stage I	Stage II	Stage III
Cell Temperature	$140^\circ F$	$176^\circ F$	$195^\circ F$
Cell Current Density	30 ASF	30 ASF	50 ASF

Two cells of each stage were put on life test with the objective of a minimum run of 250 hours for at least one cell of each stage. All cells stopped short of this goal as indicated below. Satisfactory operation ceases when the cell polarization becomes excessive (greater than 1.5 volts cell potential) and or the CO_2 or O_2 transfer rate decreases substantially (less than 80% of initial rate).

	Maximum Satisfactory Operating Time	Cause of Failure	
		Cell #1	Cell #2
Stage I	70 hours - Cell #2	Corrosion	Corrosion
Stage II	60 hours	Corrosion	Electrical short; corrosion
Stage III	140 hours	Electrical short	Electrical short

Corrosion of the nickel electrode screen and plating on end plates is the prime difficulty in Stage I and II. In Stage III, lack of strength in the matrix led to contact of anode and cathode screens.

The CO_2 concentrating process functions properly and an attractive system could be developed with solution of the materials problems.

1.0 INTRODUCTION

This is the Final Report covering the work carried out at TRW Equipment Laboratories under contract NAS 3-7638. Under this contract, individual cells of a three-stage electrochemical carbon dioxide concentration system for space applications are to be designed, fabricated and tested. The electrochemical concept being used for carbon dioxide concentration was developed by TRW and the cells used in the system are called "Carbonation Cells". This system, using these cells, offers the following desirable features:

1. CO_2 would be removed from the cabin air on a continuous, non-cyclic basis.
2. The output CO_2 is free of diluent gas contamination (N_2).
3. If required, the system is capable of concentrating carbon dioxide from air at any partial pressure down to normal atmospheric concentration of 0.03%.

The Carbonation Cell system is composed of a series of three cell stages, each stage transferring a different gas composition. In the first stage air is supplied to the cathode of the cell and carbon dioxide and oxygen are transferred to the anode. The first stage anode gas is transferred to the second stage cathode. Here, due to the high CO_2 partial pressure, the ion species transferred across the cell changes, and a higher CO_2 percentage is obtained from the second stage anode gas. This mixture is fed to a third stage which preferentially transfers oxygen, leaving essentially pure carbon dioxide.

The objective of this contract was to obtain parametric test data and life test data on electrochemical carbon dioxide concentration cells used in the carbon dioxide concentration system developed by TRW. To avoid problems of "scale-up" in the design of a prototype system using the cell test data, large cells (12" x 12") were used in the test program.

This process for electrochemically concentrating carbon dioxide was shown to be feasible for multi-man capacity systems. With the large cell hardware, short term test results obtained were better than had been predicted, based on the results achieved with small plastic cells in past TRW programs.

An area of major difficulty which did occur was materials compatibility. Long term materials degradation appeared in all three stages during the life tests.

A thermal balance study was performed to demonstrate a feasible method of system thermal control and to provide coolant flow requirements for use in system integration studies.

2.0 CARBONATION CELL CONCEPT

2.1 General Principles

When various electrodes and electrolytes are combined to form electro-chemical cells, two general classes of cells may result: (1) chemical cells in which the voltage is due to a chemical reaction occurring within the cell (e.g., batteries); and (2) concentration cells, in which the voltage is due to the free energy decrease associated with the transfer of matter from one part of the cell to another. The TRW "Carbonation Cell" is a specific cell which is typical of class (2) electro-chemical cells. The voltage impressed upon the Carbonation Cell results in concentration gradients of carbon dioxide and oxygen gases at the electrodes.

Consider an oxygen-carbon dioxide concentration cell shown schematically below:

$$O_2\ (aP_{O_2}),\ CO_2\ (aP_{CO_2}),\ M \,\|\, \underset{\text{electrolyte}}{CO_3^{=}} \,\|\, M,\ CO_2\ (cP_{CO_2}),\ O_2\ (cP_{O_2})$$

where:

aP_{O_2} = anode partial pressure of oxygen

cP_{O_2} = cathode partial pressure of oxygen

M = metallic porous electrode.

For the above cell the reactions are:

Cathode: $1/2\ O_2 + H_2O + 2e^- \rightleftharpoons 2OH^-$ (1)

Catholyte: $CO_2 + 2OH^- \rightleftharpoons H_2O + CO_3^{=}$ (2)

Anode: $2OH^- \rightleftharpoons 1/2\ O_2 + H_2O + 2e^-$ (3)

Anolyte: $H_2O + CO_3^{=} \rightleftharpoons CO_2 + 2OH^-$ (4)

Net cell reaction:

$$1/2\ O_2\ (cP_{O_2}) + CO_2\ (cP_{CO_2}) \longrightarrow 1/2\ O_2\ (aP_{O_2}) + CO_2\ (aP_{CO_2}) \qquad (5)$$

The theoretical electrical energy, 2FE, for the spontaneous, isothermal transfer of 1/2 mole of oxygen and one mole of carbon dioxide from the cathode at pressure cP_{O_2} and cP_{CO_2} to the anode is given by

$$2FE = -RT \ln \frac{(aP_{O_2})^{1/2}(aP_{CO_2})}{(cP_{O_2})^{1/2}(cP_{CO_2})} \qquad (6)$$

where:

E is the cell reversible potential

F is the Faraday constant.

In the above derivation the bicarbonate transfer mechanism was not considered since it is important only when cP_{CO_2} is high, as in the second stage cell.

2.2 Three Stage CO_2 Concentration System

To separate carbon dioxide from air at one atmosphere and maintain a carbon dioxide concentration of 0.005 atm. according to reaction (5), it is seen from equation (6) that an external source of energy is required, since $(.2)(.005)^2 < (.333)(.666)^2$; i.e., the reaction is not spontaneous. The three stage concentration system uses a series of three electrically powered cell stages, each stage transferring a different gas composition. The electrolyte in the first two stages is potassium carbonate, while sulfuric acid is used in the third stage.

In the first stage, air is supplied to the cathode of the cell and carbon dioxide and oxygen are transferred to the anode. These gases are transferred through the electrolyte solution as carbonate, bicarbonate, and hydroxyl ions. At the anode hydroxyl ions are discharged and oxygen is evolved. This in turn drives the discharge of CO_2 from carbonate ions to replace the diminished hydroxyl ion pool. Figure 2-1 schematically represents this transfer mechanism. The ratio of the various ionic species depends on the carbon dioxide partial pressure at the cathode. The gas composition at the anode, which depends on the ratio of ionic species, also depends on the cathode carbon dioxide partial pressure. This relationship is shown in Figure 2-2, which is based on experimental data. A cathode gas with 0.5 mole percent CO_2 at one atmosphere has a partial pressure of CO_2 equal to 3.8 mm Hg and yields an anode mixture of 57 mole percent CO_2 and 43 mole percent O_2.

This mixture is transferred to the cathode of the second stage cells. Here, due to a higher CO_2 partial pressure, a greater proportion of bicarbonate ions are formed. With the example above, the anode gas cavity of the second stage cells evolves a mixture of 79% CO_2 and 21% O_2. This mixture is fed to a third stage which preferentially transfers oxygen, leaving essentially pure carbon dioxide. The third stage cell is shown schematically in Figure 2-3. A blower is required to provide air to the first stage only, since the cells produce sufficient gas pressure to transfer gas for subsequent processing.

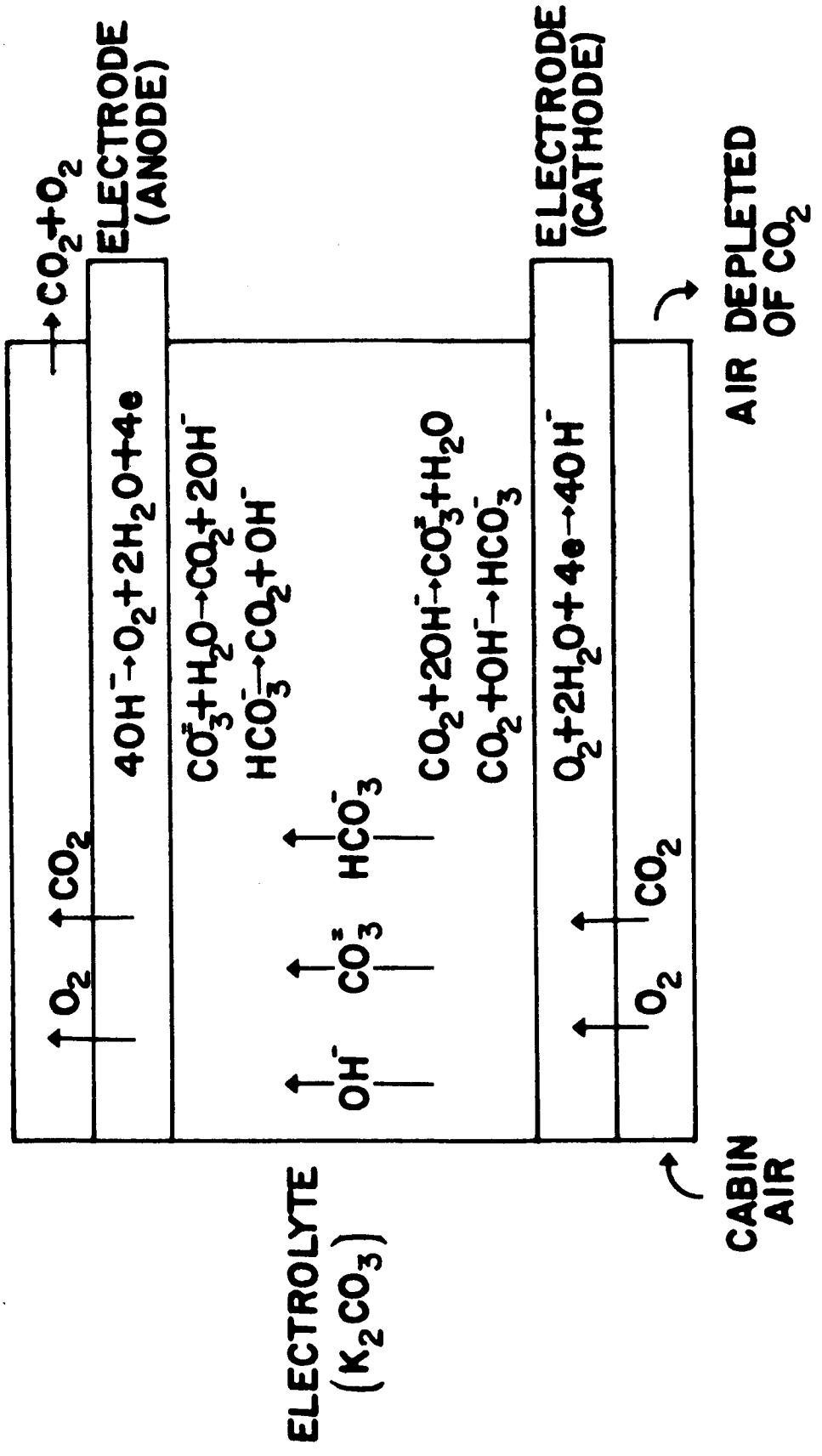

FIGURE 2-1 STAGE I CELL - SCHEMATIC REPRESENTATION

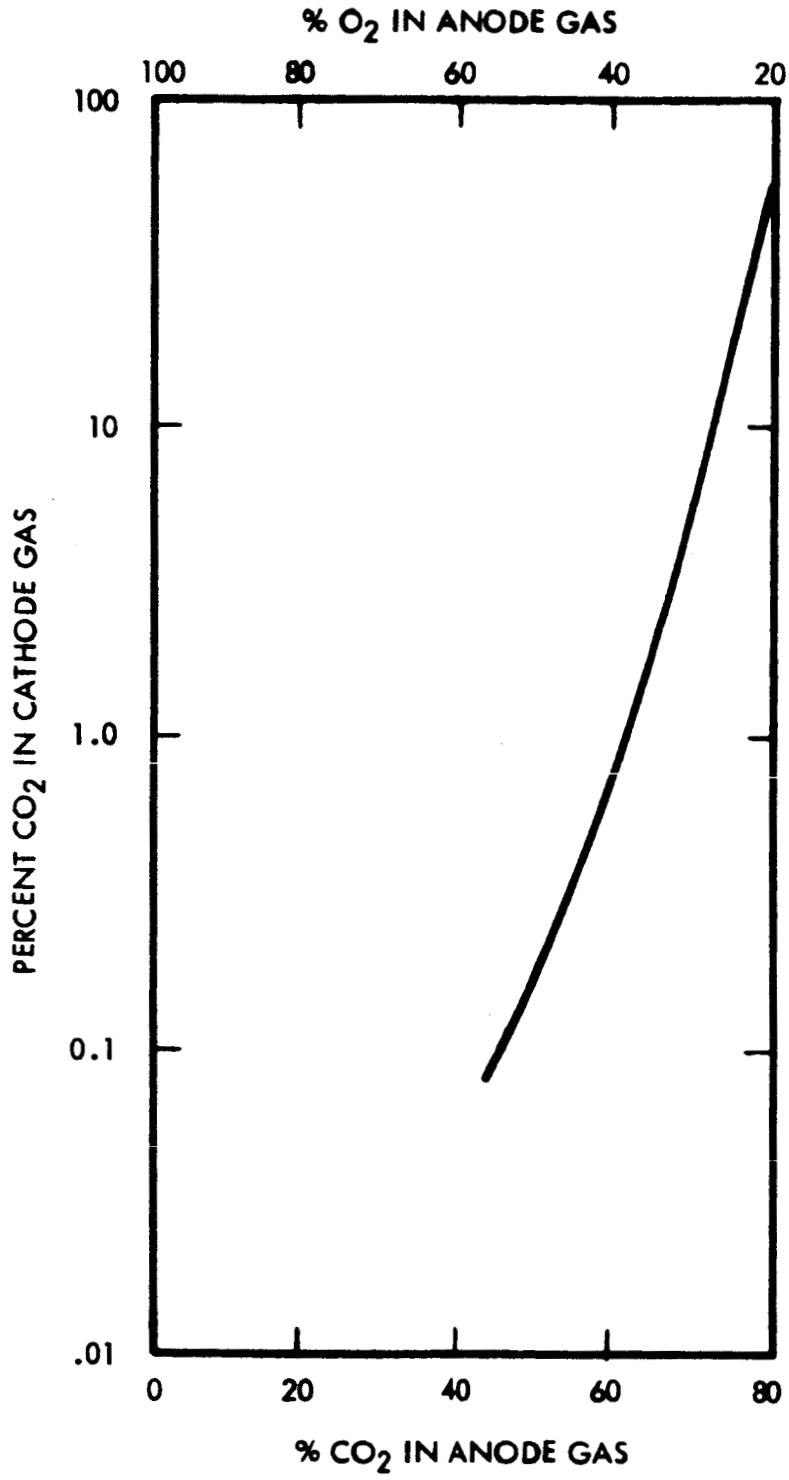

FIGURE 2-2 ANODE GAS MIXTURE AS FUNCTION OF CATHODE GAS MIXTURE FOR CARBONATION CELL

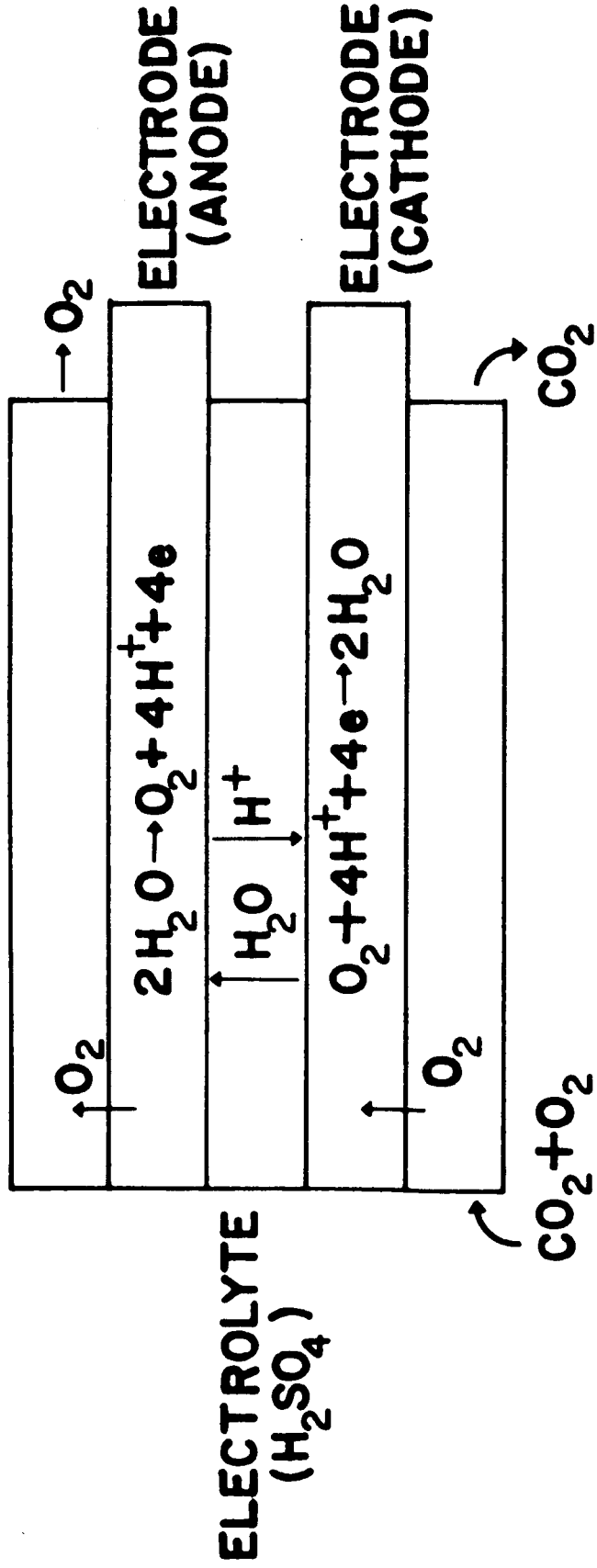

FIGURE 2-3 STAGE III CELL - SCHEMATIC REPRESENTATION

The system summarized above is capable of concentrating carbon dioxide from air at any partial pressure down to the normal atmospheric concentration of 0.03%.

Figure 2-4 presents a schematic of the three-stage Carbonation Cell carbon dioxide concentration system.

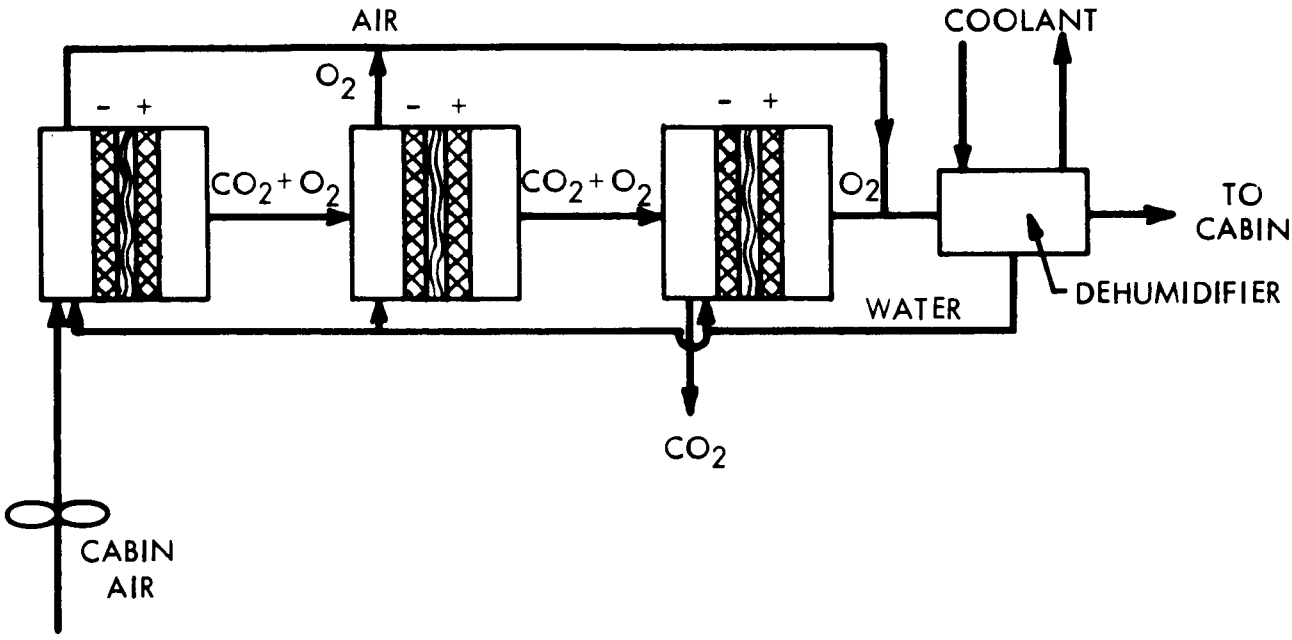

FIGURE 2-4 SCHEMATIC OF CARBONATION CELL CARBON DIOXIDE CONCENTRATION SYSTEM

3.0 DESIGN DISCUSSION

3.1 Preliminary Analysis of Four-Man Prototype

To determine the design characteristics of the large experimental cells, an analysis of a four-man prototype system was performed. The major objective of this preliminary analysis was to evolve a control method which would allow for both the thermal and humidity balance to be accomplished within the cell. A further consideration was to exercise this control without the aid of external cooling or humidification, thereby minimizing system complexity and weight.

A schematic of the design model used in this analysis is shown in Figure 3-1. Since the process gas entering the cathode chamber is at a lower dew point temperature than the cell electrolyte, water is evaporated from the membrane surface to the gas stream. Thus the heat of vaporization of water is used to remove the heat generated within the cell. The equilibrium partial pressure of water vapor that results in the gas cavity will determine the mean cell electrolyte concentration and temperature.

The equilibrium partial pressure of water vapor will be a function of the process gas flow rate, dew point, and the cell terminal voltage. Preliminary analysis indicates that the above method of control is applicable to the second and third stage units but is a marginal control scheme when applied to the first stage unit. For example, a 1st stage unit operating at relatively high process gas flow rates (5 x stoichiometric CO_2) and low dew point temperatures (30% R. H.) would approach an equilibrium temperature near or below ambient and electrolyte concentrations not far removed from saturation.

An alternate approach for the thermal control of the 1st stage unit would be in the use of the process gas to remove cell heat. The humidity control would have to be accomplished by external means. In this mode of operation the process gas will experience a temperature increase at a constant dew point temperature which in turn will cause a gradient in the electrolyte concentration. The magnitude of this gradient is a strong function of the process gas flow rate. Calculations indicate that allowable concentration gradients are realized only at flow rates approaching 10 x stoichiometric CO_2. Sample calculations are shown in Appendix A.

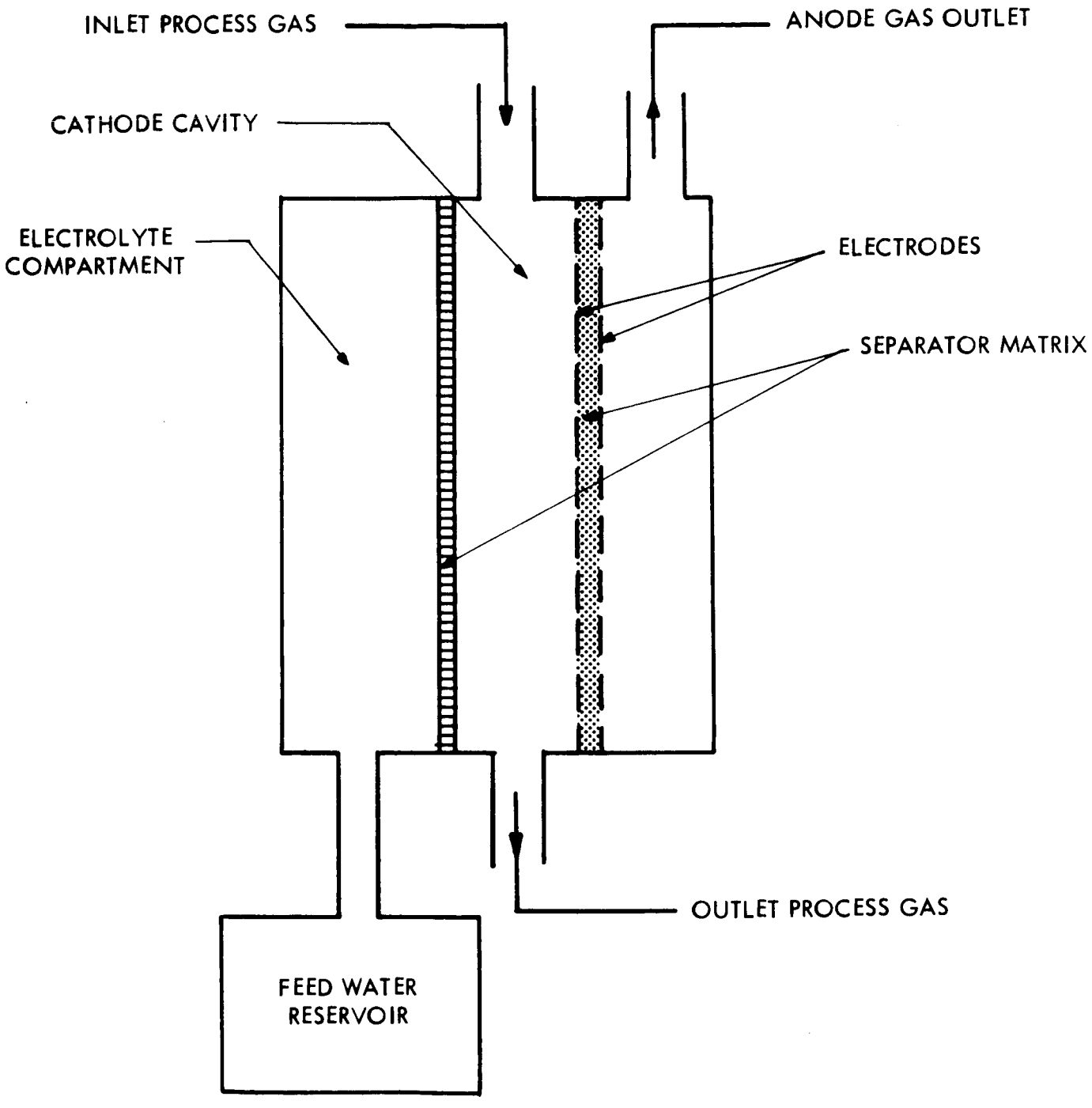

FIGURE 3-1 CELL DESIGN MODEL FOR PRELIMINARY ANALYSIS

The preliminary analysis summary presented in Table 3-1 was based upon several simplifying assumptions:

a) No external heat transfer to or from the cell.
b) Linear thermal and concentration gradients within the cell, if any.
c) 1st stage ion transfer 100% $CO_3^=$; 2nd stage ion transfer 100% HCO_3^-.
d) Negligible heat transfer from cell to process gas in 2nd and 3rd stage.
e) Instantaneous mixing of process gas and of evaporation water in 2nd and 3rd stage.

Vapor pressure data for the Stage I and II K_2CO_3 electrolyte and Stage III H_2SO_4 electrolyte used in the analysis are presented in Table 3-2.

A thermal balance study is presented in Section 8.0 which was performed in Task IV based on the results of the experimental data for all three stages operating with variable parameters.

3.2 Experimental Test Cells

For use in the experimental program, 12" x 12" active area cells were designed. These cells used American Cyanamid fuel cell electrodes measuring 12" x 12". (Types AA1 and AB6X were evaluated.) The logic behind using large cells was to prevent any scale-up problems in going from experimental cells to a flight configuration. Consistent with the desire to build experimental cells which correspond with flight cells, materials were also selected with this in mind. The cells for Stage I and Stage II therefore used gold-plated magnesium to yield a low weight system. The gold plated magnesium eventually proved to be unsatisfactory during life testing. The Stage III acid cell materials problems are discussed in Section 4.0.

Although experimental cells were all single cell units, all porting and flow patterns were designed so that bipolar plate designs could be substantially copied from the experimental cell designs. Experimental cell components were also designed to reduce the number of drawings required and to permit interchangeability of components as much as possible. To accomplish this, three basic end plate designs were necessary - an anode plate for use on all three stages; a first stage cathode plate to accommodate the high flow of the first stage; and a cathode plate for the Stage II and III cells which incorporates a wicking system for water addition and was designed for lower gas flow than the first stage cathode.

The cell end plate, fabricated of a single piece of magnesium, combined a number of functions into the single piece:

TABLE 3-2

VAPOR PRESSURE DATA FOR AQUEOUS K_2CO_3 AND H_2SO_4 SOLUTIONS

	VAPOR PRESSURE (mm Hg)							
Wt. % K_2CO_3	30°C	40°C	50°C	60°C	70°C	80°C	90°C	100°C
17.2	29.62	51.58	86.35	139.6	219	333	494	712
32.6	25.8	44.97	75.3	122.2	192	294	437	633
45.3	19.62	34.42	58.1	94.6	150	232	348	505
52.5	14.5	25.6	43.3	71.2	115	181	272	410

Wt. % H_2SO_4	35°C	45°C	55°C	65°C	75°C	85°C	95°C	100°C
20	37.2	63.3	106	167	256	385	580	678
30	31.9	54.7	91.0	145	222	333	493	590
40	24.3	41.0	69.0	110	171	261	390	474
50	15.4	26.7	45.5	73.7	115	178	268	326

	(H_2O)														
Temp. °C	30	35	40	45	50	55	60	65	70	75	80	85	90	95	100
	31.82	42.17	55.32	71.88	92.51	118.04	149.30	187.54	233.7	289.1	355.1	433.6	525.8	633.9	760

TABLE 3-1

PRELIMINARY ANALYSIS SUMMARY

	Cabin Air to Pre-conditioner	Stage I			Stage II			Stage III		
		Cathode In	Cathode Out	Anode Out	Cathode In	Cathode Out	Anode Out	Cathode In	Cathode Out	Anode Out
Design Conditions for 4-Man System										
Carbon Dioxide ~ gm moles/hr	40	40	36	4	4	0	4	4	4	0
Oxygen ~ gm moles/hr	1680	1680	1678	2	2	1	1	1	0	1
Nitrogen ~ gm moles/hr	3700	3700	3700	-	-	-	-	-	-	-
Water Vapor ~ gm moles/hr	85	935	934	1	1	2.4	11.9	11.9	20.05	5.1
Gas Temperature ~ °C	20	46	51.7	58.8	58.8	82.5	82.5	82.5	87.4	87.4
Gas Dew Point ~ °C	8	46	46	46	46	80.5	80.5	80.5	85.0	85.0
Cell Temp. ~ °C		56	61.7		82.5	82.5		87.4	87.4	
Electrolyte Concentration ~ wgt%		45.3	52.5		17.2	17.2		20.0	20.0	
Power Density ~ watts/ft^2		50			50			50		
Total Area ~ ft^2		6			3			3		
Cell Power ~ watts		300			150			150		
Design Conditions for Prototype Cells										
Cell Area ~ ft^2		1			1			1		
Maximum Current Density ~ ASF		50			50			50		
Maximum Gas Flow ~ cfm/cell		8.5			0.5			0.5		
Cooling Method		Process Gas and Conduction			Water Evap. and Conduction			Water Evap. and Conduction		

a) Cell end sealing plate
b) Pressure clamping plate
c) Gas distribution (manifolding and pin structure)
d) Current collector
e) Integral structure for attachment of flow line fittings.

Uniform compression of the cell matrix and good electrical contact with the electrode was provided by the pin strucutre (0.06" square pins). The cells were sealed with a large diameter O-ring and assembled with 28 bolts to assure uniform compression.

No baffling for flow pattern control was incorporated in the cells. For Stages II and III baffling was added during assembly by inserting pieces of epoxy fiber board between adjacent rows of pins, thereby providing a means for establishing desired flow patterns.

Variation in cathode gas flow pattern for Stage I consisted of air flowing from bottom to top of cell or from top to bottom. Gas flow from top to bottom of cell will carry out any condensed liquid which tends to pool in cell bottom if too much moisture is added to cell. Cathode gas flowing from bottom to top of cell will not carry out pooled liquid.

Upon referring to Figures 3-2 and 3-3, Cell Assembly Drawings, the configuration of the cells may be seen. The active portion of the cell, composed of two electrodes (one on each side of an asbestos electrolyte matrix), is compressed between two cell end plates. The current leads are attached directly to the end plates, with electrical contact to the electrodes being through the pin structure. Electrically insulating washers are used on the compression bolts to insulate one end plate from the other. The Teflon tape shown on the assembly drawings, intended to establish the desired end plate spacing and electrolyte matrix compression, was not required.

A variable height electrolyte pool was provided for by an asbestos wick used to separate a water cavity from the cathode gas compartment. The wick was held firmly in place by tantalum screening on either side of the asbestos. The asbestos-tantalum screen wick assembly was clamped between the pins of the end plate water cavity and the pins of the gas diffusion plate. The gas diffusion plate, shown in Figure 3-4, provided an even flow distribution of cathode gases between the wick

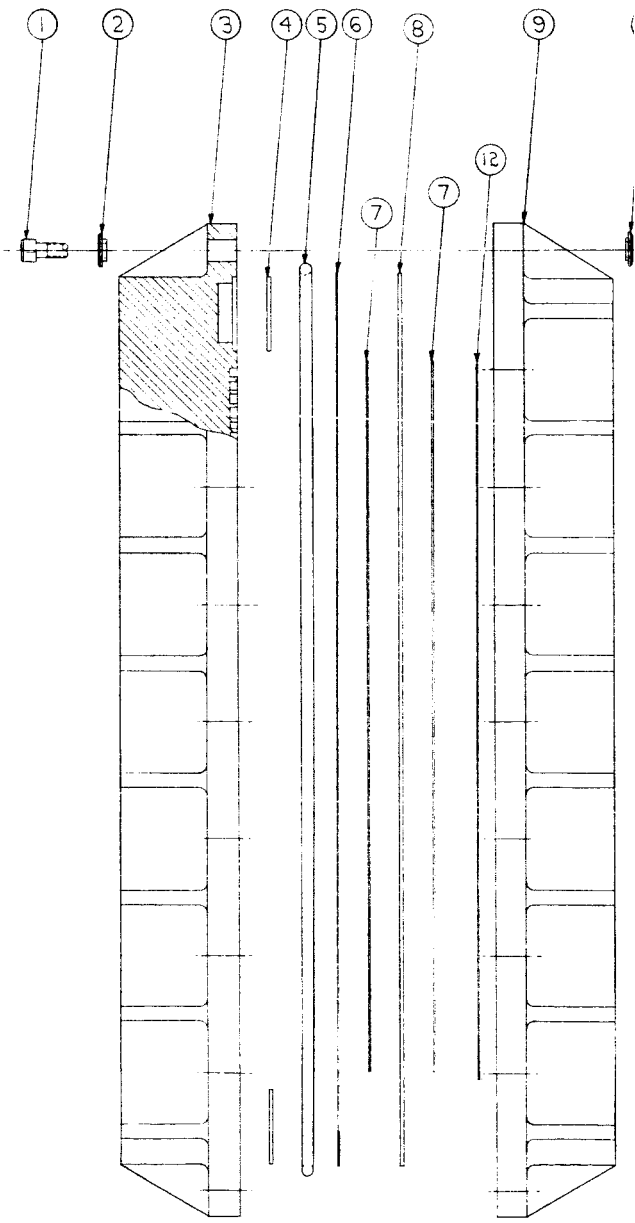

19-1

REVISIONS			
SYM.	DESCRIPTION	DATE	APPROVED

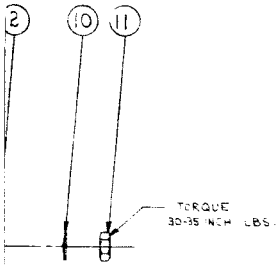

DASH NO.	(8) SPACER	(7) ELECTRODE
-1	310101-1	310102-1
-2	310101-1	310102-2
-3	310101-2	310102-1
-4	310101-2	310102-2
-5	310101-3	310102-1
-6	310101-3	310102-2

QTY REQ'D	ITEM NO.	PART OR IDENTIFYING NO.	NOMENCLATURE OR DESCRIPTION	REFERENCE OR NOTE
1	12	310100	SEAL PLATE	TRW
2	11	1/4-20	NUT	QPL
2	10	1/4	WASHER, BELVILLE	QPL
1	9	310096	ANODE END PLATE	TRW
1	8	SEE CHART	SPACER, ASBESTOS	TRW
2	7	SEE CHART	ELECTRODE	TRW
AR	6	# 55	TAPE, FLUROCARBON	3M
1	5	2-387	"O" RING (VITON)	PARKER
2	4	310097	PLATE, SEAL	TRW
1	3	310094	CATHODE END PLATE	TRW
2	2	SW-25	WASHER, SHOULDER	WECKESSER
2	1	1/4-20 x 1 1/2 LG	SCREW, SOC. HD. CAP	QPL

LIST OF MATERIALS OR PARTS LIST

310090

DRAWING RELEASED FROM NEW PRODUCT RESEARCH DIVISION OF THOMPSON RAMO WOOLDRIDGE INC. DATE 9-10-65 BY [illegible]

UNLESS OTHERWISE SPECIFIED DIMENSIONS ARE IN INCHES
TOL. ON ANGLES ±
TOL. ON TWO-PLACE DEC. ±
TOL. ON THREE-PLACE DEC. ±
FOUR PLACE DECIMAL DIMENSIONS WITHOUT TOLERANCE ARE BASIC.
MATERIAL
HEAT TREAT
WELD OR BRAZE
SURFACE TREATMENT
INSPECTION STAMP

DFTM.	[illegible]	8-11-65
CHKD.	GJD	9-10-65
APPD.		
ENGR.	[illegible]	9/10/65
ENGR.	[illegible]	9/10/65
MAT'L APPR.		
MFR.		
APPROVAL		
APPROVAL		

TAPCO
A DIVISION OF THOMPSON RAMO WOOLDRIDGE INC.
CLEVELAND, OHIO, U.S.A.

TITLE
ASSEMBLY
STAGE I
CARBONATION CELL PROTOTYPE

NEXT ASSY. (REF.)

CODE IDENT. NO.	SIZE	DRAWING NO.
59875	E	310090

SCALE NONE SHEET 1 OF 1

512-004918-08

FIGURE 3-2

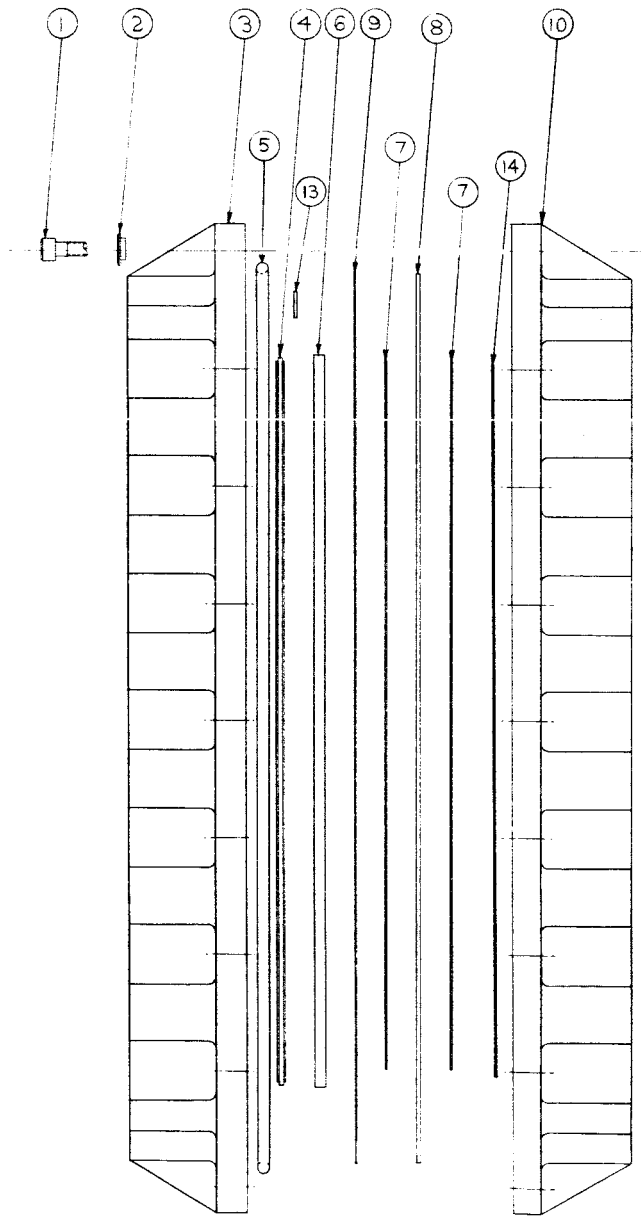
1
2
3
4
6
9
8
10
5
13
7
7
14

REVISIONS			
SYM.	DESCRIPTION	DATE	APPROVED
A	PICTURE CHANGE SEE RDC 13176		

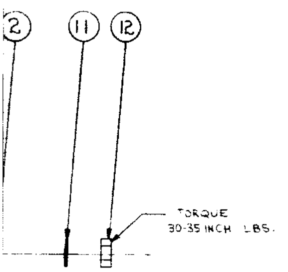

STAGE II

DASH NO.	SPACER (8)	ELECTRODE (7)
-1	310101-1	310102-1
-2	310101-1	310102-2
-3	310101-2	310102-1
-4	310101-2	310102-2
-5	310101-3	310102-1
-6	310101-3	310102-2

STAGE III

DASH NO.	SPACER (8)	ELECTRODE (7)
-7	310101-1	310102-1
-8	310101-1	310102-2
-9	310101-2	310102-1
-10	310101-2	310102-2
-11	310101-3	310102-1
-12	310101-3	310102-2

DRAWING RELEASED FROM NEW PRODUCT RESEARCH THOMPSON RAMO WOOLDRIDGE INC DATE 9-10-65 BY TRW

QTY REQ'D	ITEM NO.	PART OR IDENTIFYING NO.	NOMENCLATURE OR DESCRIPTION	REFERENCE OR NOTE
1	14	310100	SEAL PLATE	TRW
2	13	310098	SEAL PLATE	TRW
28	12	1/4-20	NUT	QPL
28	11	# 1/4	WASHER, BELVILLE	QPL
1	10	310096	ANODE END PLATE	TRW
AR	9	#55	TAPE, FLUROCARBON	3M
1	8	SEE CHART	SPACER, ASBESTOS	TRW
2	7	SEE CHART	ELECTRODE	TRW
1	6	310092	PLATE, GAS DIFFUSING	TRW
1	5	2-387	"O" RING (VITON)	PARKER
1	4	310093	WICK ASSEMBLY	TRW
1	3	310095	CATHODE END PLATE	TRW
56	2	SW-25	WASHER, SHOULDER	WECKESSER
28	1	1/4-20 x 1 3/4 LG.	SCREW, SOC. HD. CAP	QPL

LIST OF MATERIALS OR PARTS LIST

UNLESS OTHERWISE SPECIFIED DIMENSIONS ARE IN INCHES
TOL. ON ANGLES ±
TOL. ON TWO-PLACE DEC. ±
TOL. ON THREE-PLACE DEC. ±
FOUR-PLACE DECIMAL DIMENSIONS WITHOUT TOLERANCE ARE BASIC.

DFTM. 8-12-65 · CHKD. SJD 9-10-65 · 9/10/65 · 9/10/65

TAPCO
A DIVISION OF THOMPSON RAMO WOOLDRIDGE INC.
CLEVELAND, OHIO, U.S.A.

TITLE: ASSEMBLY STAGE II & III CARBONATION CELL PROTOTYPE

CODE IDENT. NO. 59875 · SIZE E · DRAWING NO. 310091 · SHEET 1 OF 1

310091 A

512-004918-08

FIGURE 3-3

20

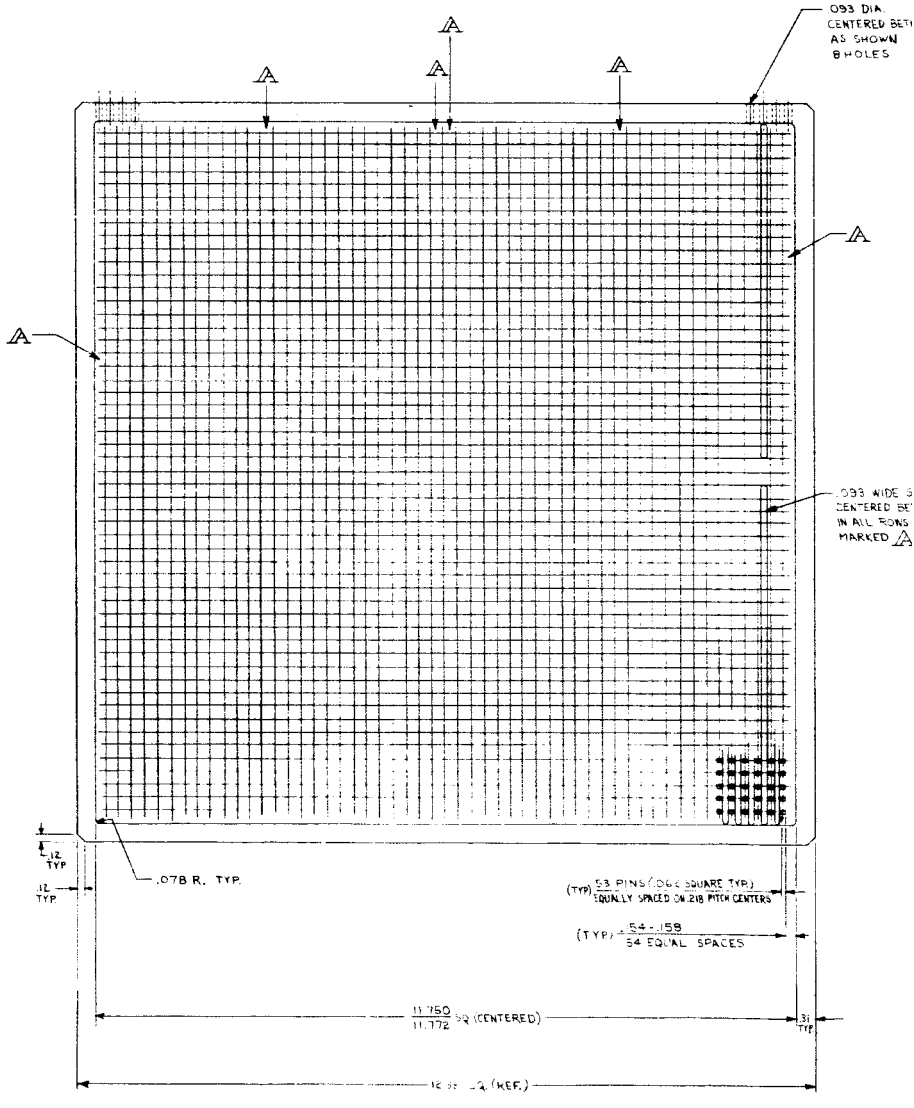
.093 DIA.
CENTERED BET
AS SHOWN
8 HOLES
.093 WIDE S
CENTERED BE
IN ALL RONS
MARKED A
.078 R. TYP.
.12
TYP
.12
TYP
(TYP) 53 PINS (.06 SQUARE TYP.)
EQUALLY SPACED ON .218 PITCH CENTERS
(TYP.) 54 - .158
54 EQUAL SPACES
11.750
11.772 SQ (CENTERED)
.31
TYP

21-1

REVISIONS			
SYM.	DESCRIPTION	DATE	APPROVED
A	WAS .031 DIMENSION SEE RDC 13183		

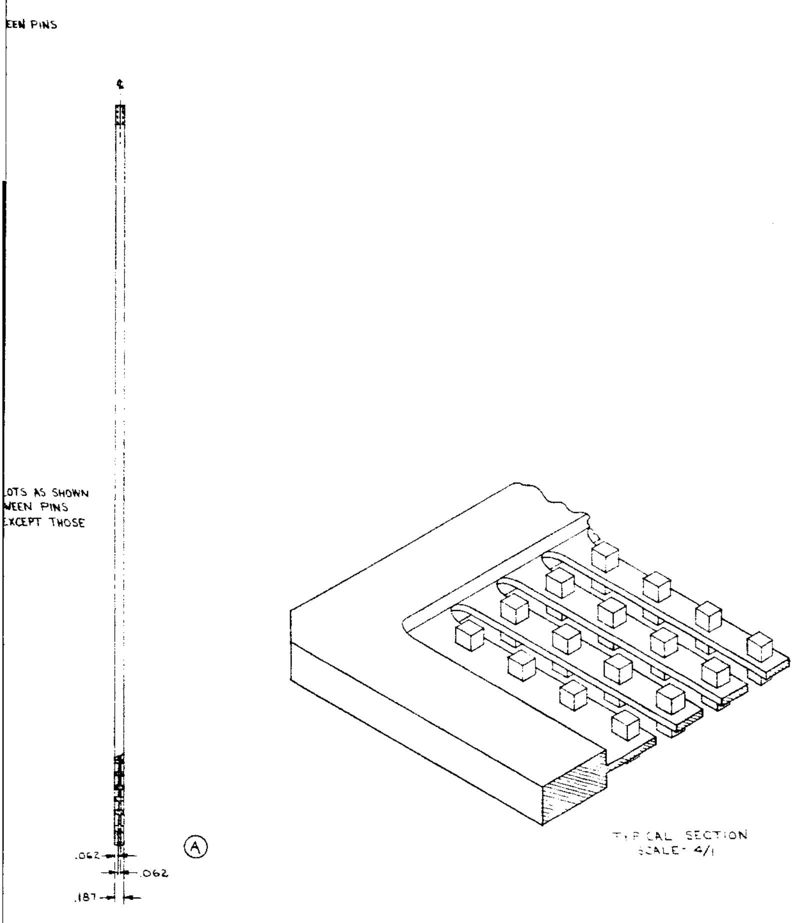

TYPICAL SECTION
SCALE 4/1

310092

DRAWING RELEASED FROM ... RESEARCH ... DATE 9-10-65

QTY REQ'D	ITEM NO.	PART OR IDENTIFYING NO.	NOMENCLATURE OR DESCRIPTION	REFERENCE OR NOTE

LIST OF MATERIALS OR PARTS LIST

UNLESS OTHERWISE SPECIFIED DIMENSIONS ARE IN INCHES
TOL. ON ANGLES ± 2°
TOL. ON TWO-PLACE DEC. ± .015
TOL. ON THREE-PLACE DEC. ± .010
FOUR-PLACE DECIMAL DIMENSIONS WITHOUT TOLERANCE ARE BASIC

MATERIAL AZ31B TYPE 2 MAGNESIUM PLATE

HEAT TREAT

WELD OR BRAZE

SURFACE TREATMENT | INSPECTION SPECS.

DFTM.		8-10-65
CHKD	SJD	9-10-65
APPD.		
ENG. APPD.		9/10/65
ENG. APPD.		9/10/65
MATL. APPD.		
MFG.		

APPROVAL

APPROVAL

TAPCO
A DIVISION OF
THOMPSON RAMO WOOLDRIDGE INC.
CLEVELAND, OHIO, U. S. A.

TITLE
PLATE, GAS DIFFUSING
STAGE II, III
CARBONATION CELL PROTOTYPE

NEXT ASSY. (REF.)

CODE IDENT. No.	SIZE	DRAWING No.
59875	E	310092

SCALE 1/1 SHEET 1 OF 1

512-00491B-08

FIGURE 3-4

and electrode surfaces. Electrical continuity to the electrode was from the end plate to the rim of the gas diffusion plate and then to the pins on the diffusion plate touching the electrode.

Control of the Stage II and III cell electrolyte concentrations was aided by the use of the variable height electrolyte pool. The anode gas pressure was maintained higher than the cathode pressure and the cathode pressure greater than the electrolyte pool cavity pressure. Thus any free electrolyte pooling in the cell bottom was forced in the electrolyte pool cavity. At the start of a test, with proper electrolyte charge concentration, the electrolyte pool height was noted. If operating conditions were such that an excess of moisture was being introduced into the cell by condensation causing the electrolyte to be diluted, the pool height in the sight glass tube would rise. Conversely if the cathode gas is deficient in moisture, water evaporates from the pool wick causing the level to drop. Cell operating conditions were controlled by adjustment of cell temperature or humidifier temperature to maintain the electrolyte pool height at the proper level thus maintained the desired electrolyte concentration.

The gas distribution system was designed so that each cell can handle five times stoichiometric flow at 50 amperes per square foot with a maximum pressure drop of 0.2 psi. To control the flow pattern the major drop is across the distribution holes connecting the flow channels with the cell field. The field drop is very low and therefore non controlling. Drops of water or irregularities in the cell will therefore not materially affect the flow patterns. Inlet ports and manifolding on the cell end plates are seen on the photographs of the representative experimental cell components, Figures 3-5, 3-6, and 3-7.

The small recession provided in each manifold slot is for insertion of a plastic seal plate to complete each manifold chamber. Clearly shown on the back of the end plates are provisions for:

a) Attachment of power lugs
b) Mounting of thermocouples
c) Connection of pressure gauges
d) Attachment of inlet/outlet flow line fittings
e) Installation of liquid level sight glass for the Stage II and III water cavities.

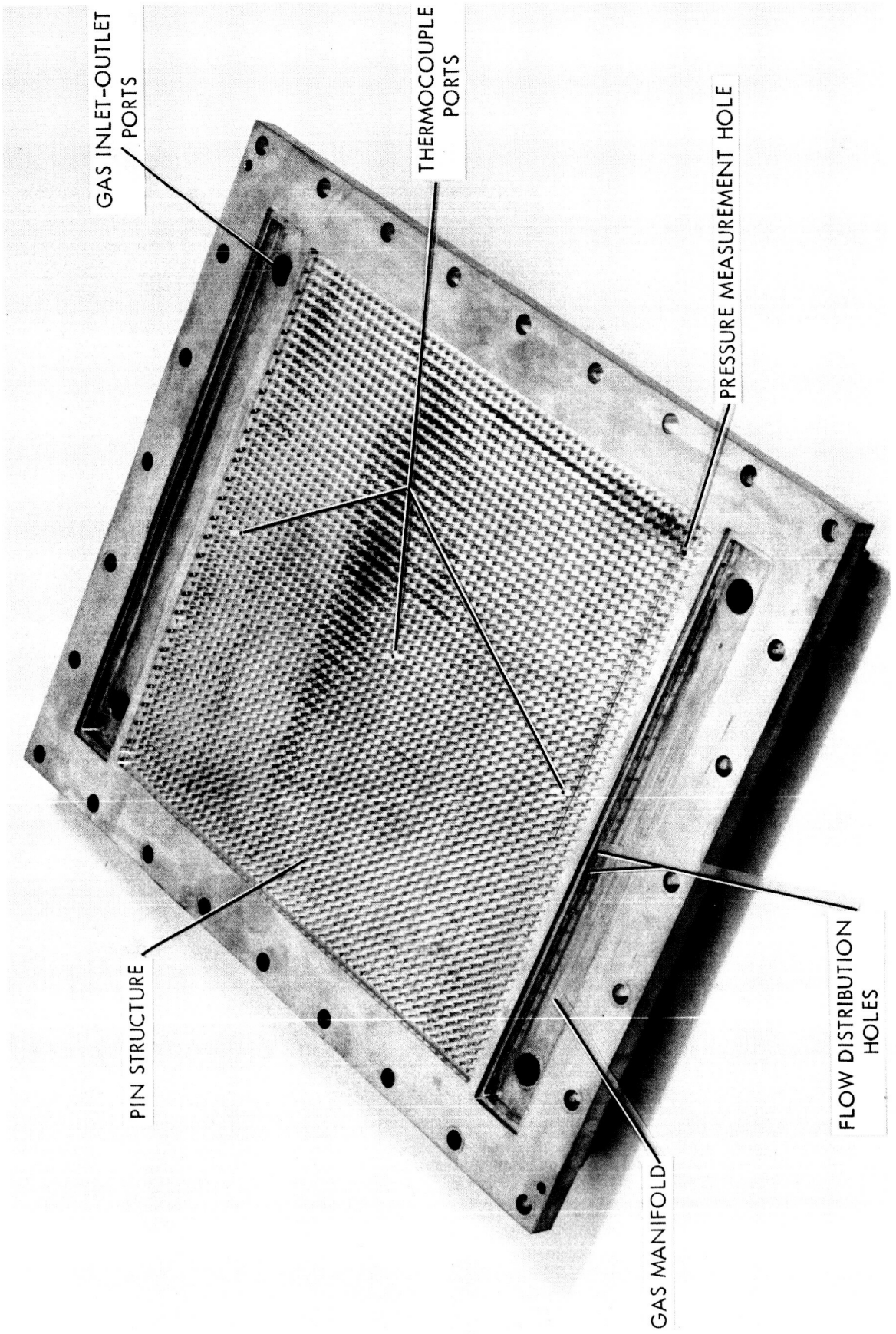

FIGURE 3-5 STAGE I CELL CATHODE END PLATE

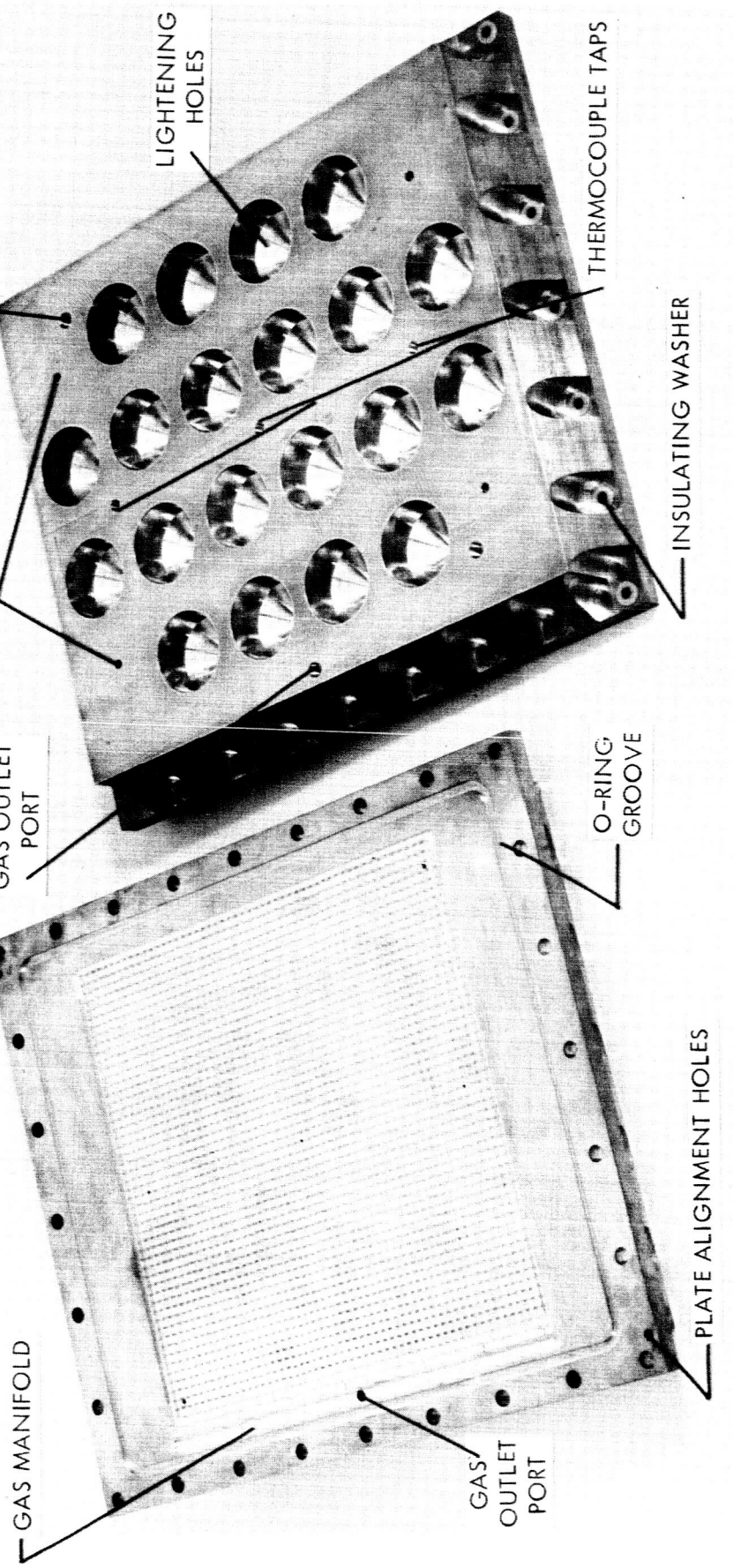

FIGURE 3-6 STAGE I, II, AND III CELL ANODE PLATE

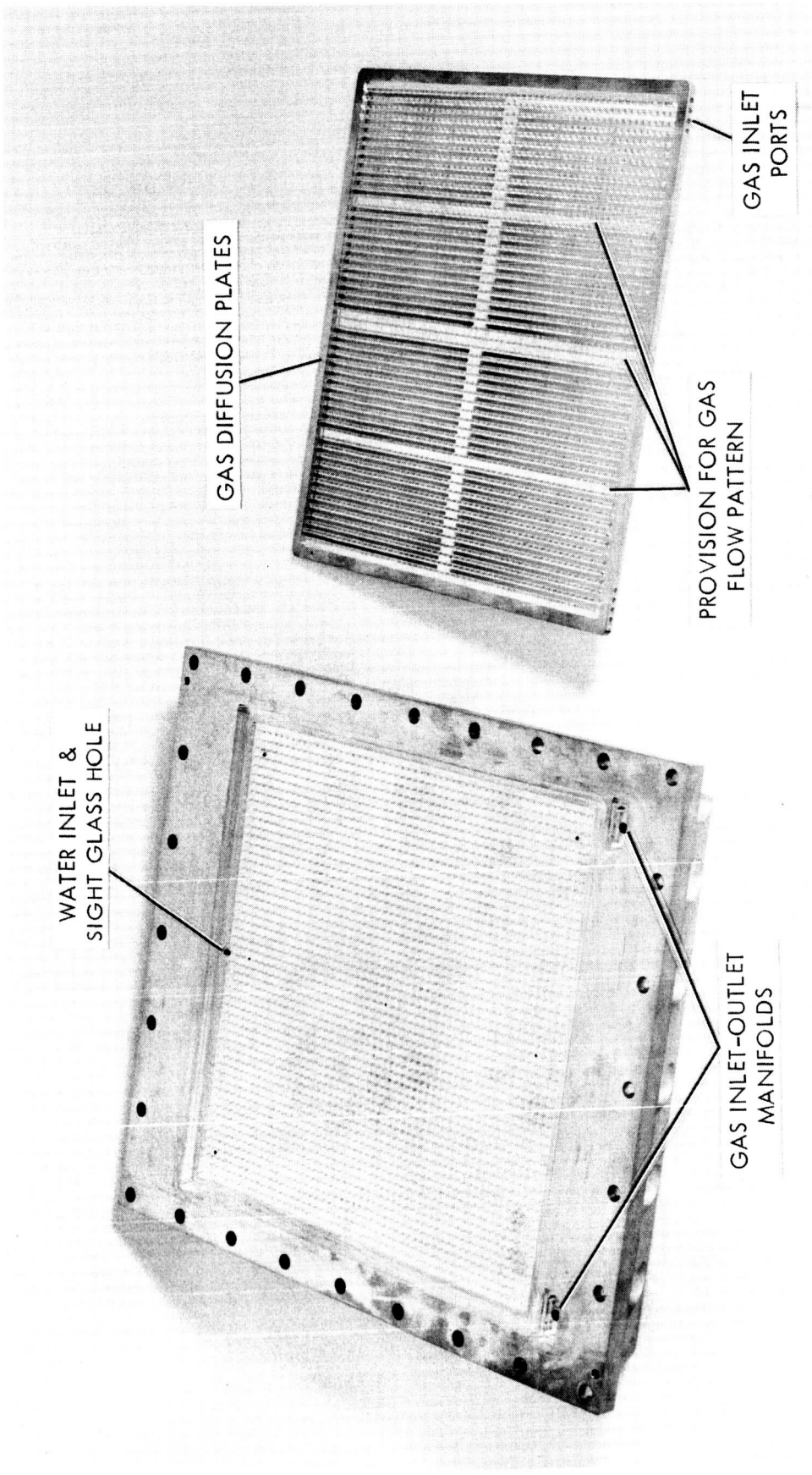

FIGURE 3-7 STAGE II AND III CELL CATHODE AND GAS DIFFUSION PLATE

The large two-inch diameter holes on the back side of the plates are merely holes to decrease the weight of the structures. Design of the holes was such as to minimize machining requirements and to insure that cell deflection at center of cell would not exceed 0.001 inch when all 28 bolts are properly tightened. This lightening structure is by no means optimum. For a flight unit a much more intricate cast type pressure clamping plate would be used. The first Stage I cathode end plate was machined with rectangular shaped, undercut, lightening holes. This configuration provides a 20% lighter weight piece, but the machining time associated with the process was too high. Thus, the design was changed to the round holes. Figure 3-8 is a photograph of the gold plated cathode end plate and a gold plated gas diffusion plate.

Figures 3-9 and 3-10 are photographs of a partially assembled Stage II cell. These can be compared to Figure 3-11 which shows the components of the Stage III acid cell. A more detailed discussion of the acid cell configuration is given in Section 4.0 on materials selection.

3.3 Test Stands

3.3.1 Small Cell Test Rig - Small test cells were used to check out problem areas expected on the large experimental cells and to examine in detail unexpected or strange performance in the large cells. Figure 3-12 presents a schematic of the set-up used for this testing. Provisions were made for precise control of cell temperature and feed gas humidity. Inlet gas composition was known (analyzed cylinder gas) and the outlet gas composition was monitored by an oxygen analyzer. Provision was made for inlet and outlet flow rate measurement. Figure 3-13 presents a schematic of the electrical measuring circuits used to analyze cell electrical performance. Figure 3-14 presents a photographic view showing the major components of the test rig.

3.3.2 Large Cell Test Stand - The large cell test stand was designed such that cells could be tested individually during the parametric short term testing and also used for life testing of six cells concurrently. Figure 3-15 presents a schematic of the full test stand. As indicated, gas feed to the first stage is by a mixture of laboratory air and bottled CO_2. Stage II and III gas feed is from premixed bottles. A large vacuum pump is connected to a common manifold connecting the gas outlets of all three stages to maintain cell operating pressures in the necessary sub-ambient range. Common manifolding enables the use of

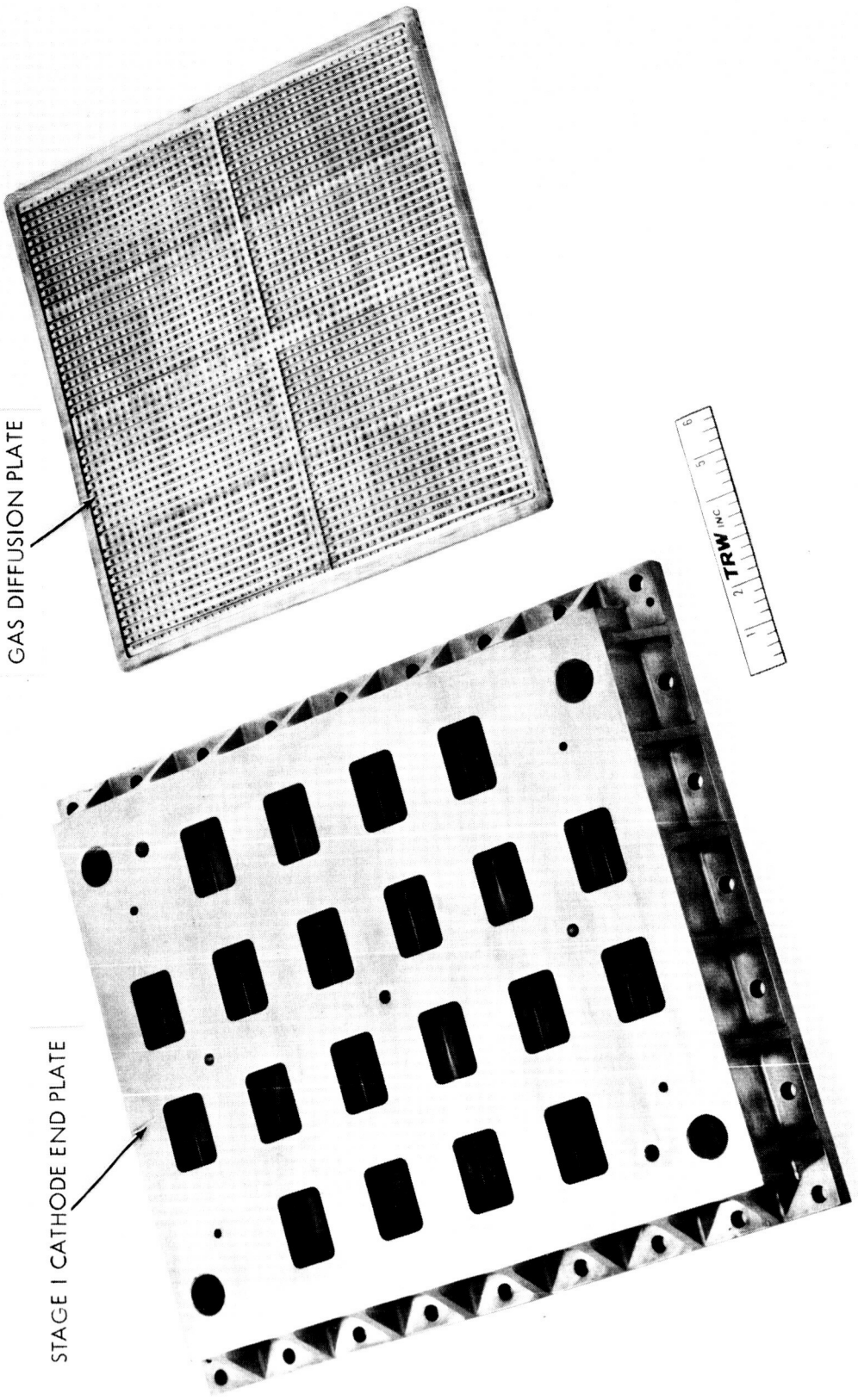

STAGE I & II CELL COMPONENTS - GOLD PLATED

STAGE II CELL - PARTIALLY ASSEMBLED - LIQUID SIDE OF GAS DIFFUSION PLATE

FIGURE 3-9

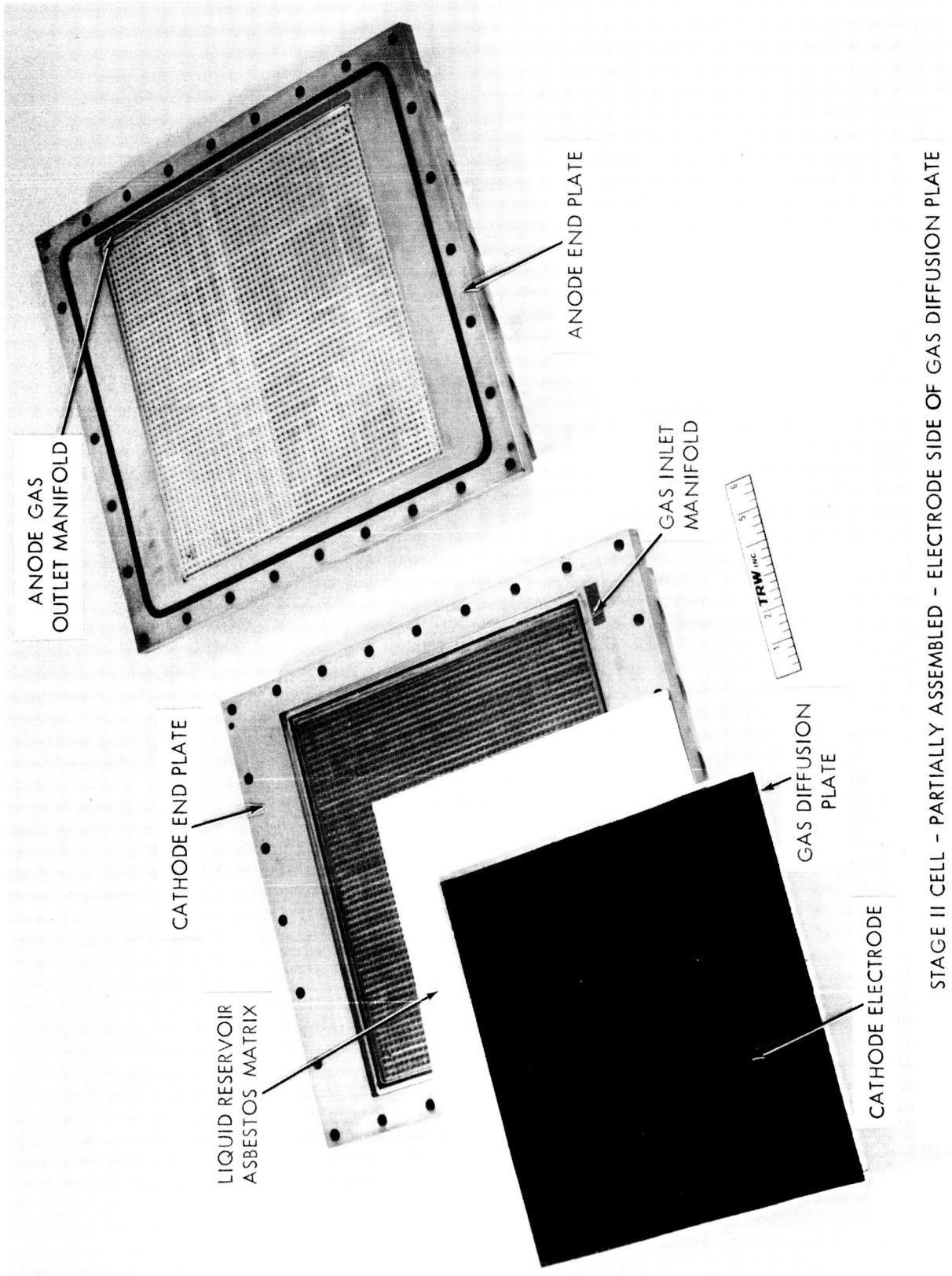

STAGE II CELL - PARTIALLY ASSEMBLED - ELECTRODE SIDE OF GAS DIFFUSION PLATE

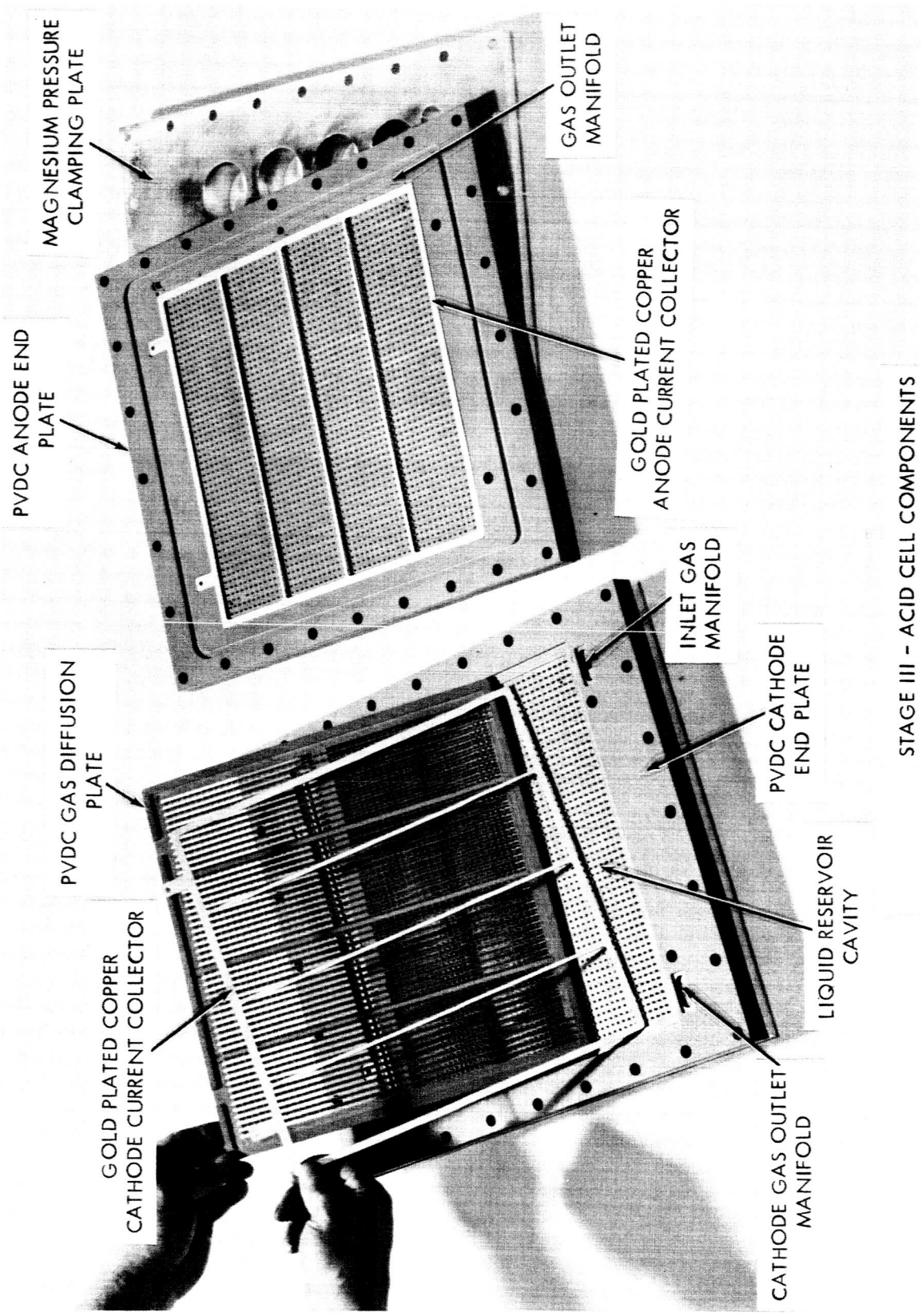

STAGE III - ACID CELL COMPONENTS

FIGURE 3-11

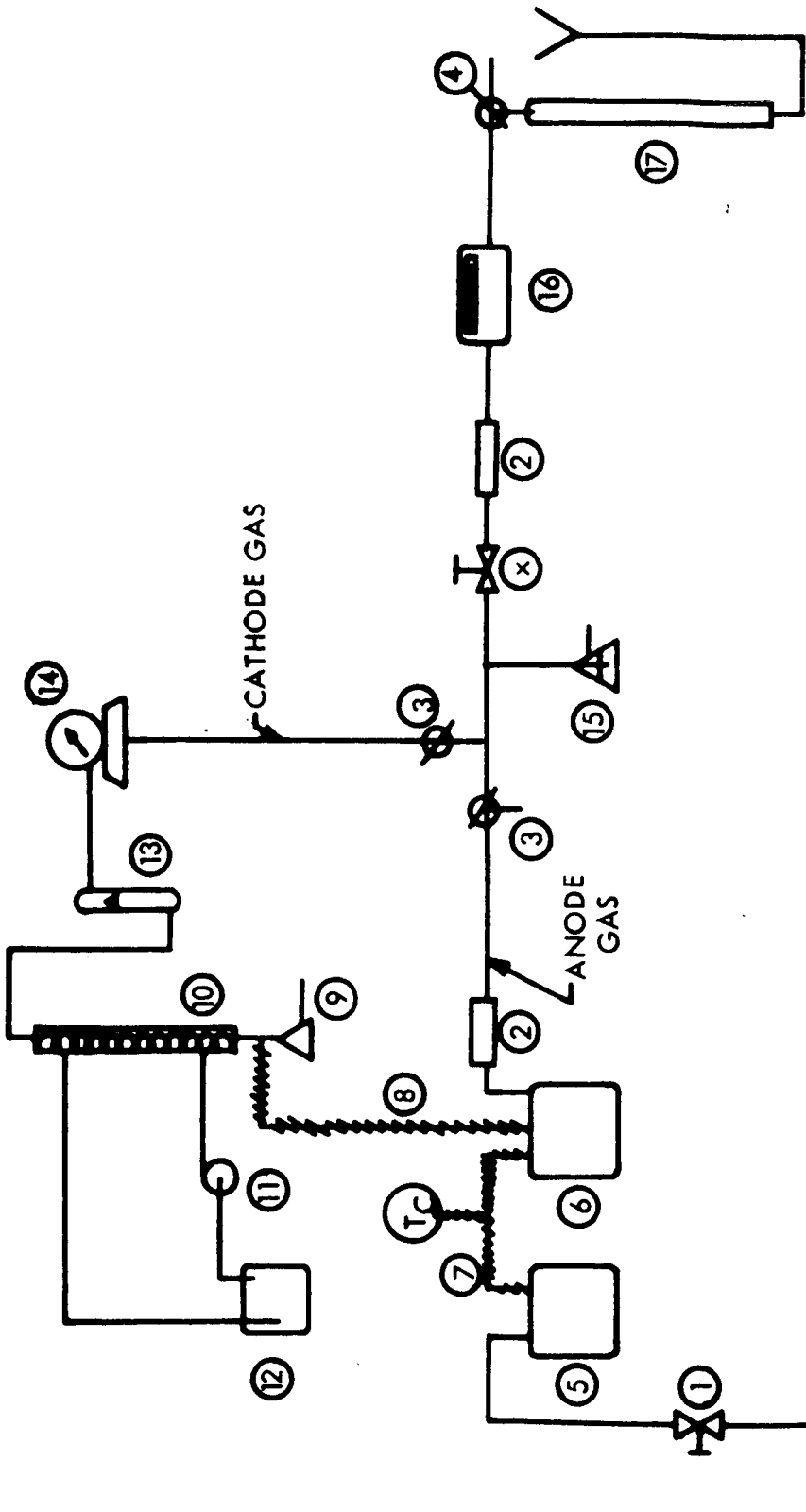

1. Needle Valve
2. $CaSO_4$ Drying Tube
3. Two-Way Stopcock
4. Three-Way Stopcock
5. Humidifier & Constant Temp. Water Bath
6. Cell & Constant Temp. Water Bath
7. Thermostated Heating Tape
8. Insulated Line
9. Condensate Reservoir
10. Condenser
11. Water Pump (Coolant)
12. Coolant Reservoir
13. Rotameter
14. Wet Test Meter
15. Static Pressure Regulator
16. Beckman D-2 Oxygen Analyzer
17. Gas Burrett & Leveling Bulb

FIGURE 3-12 TEST STAND SCHEMATIC - SMALL EXPERIMENTAL CELLS

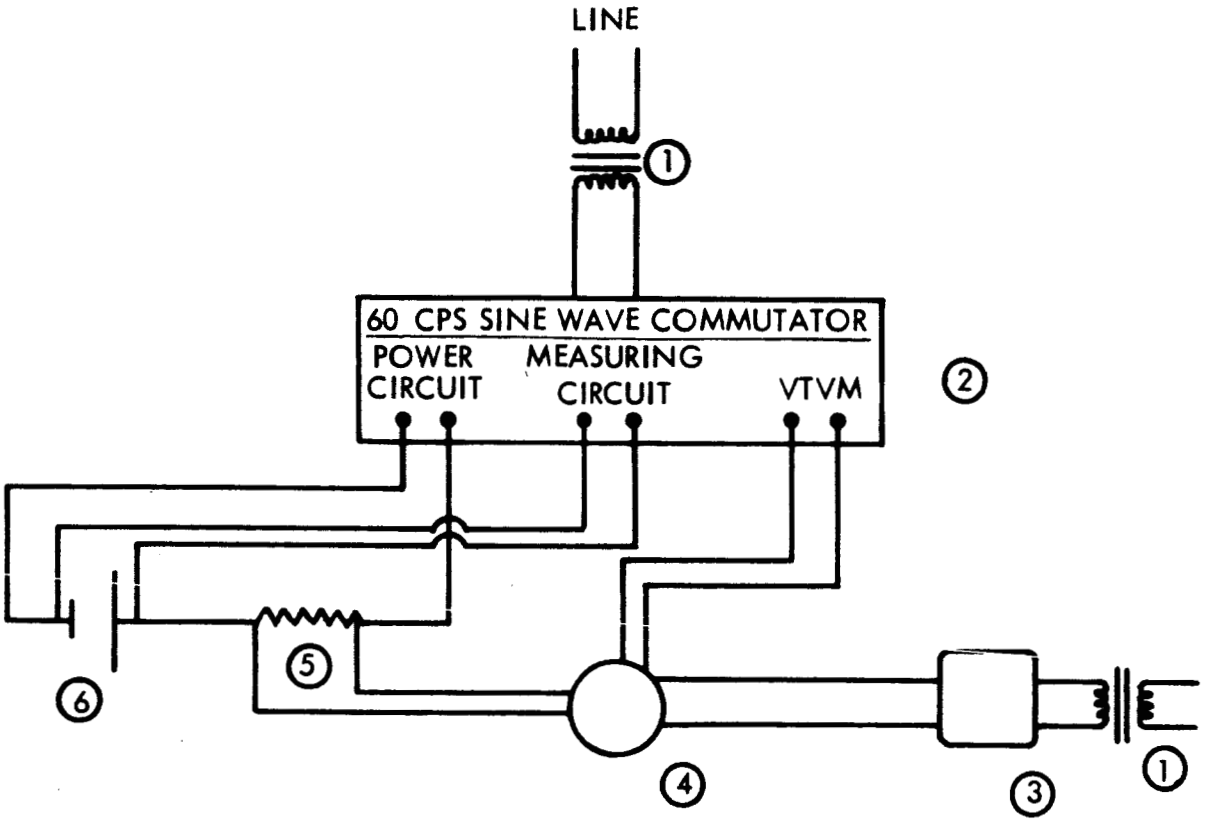

1 - CONSTANT VOLTAGE TRANSFORMER
2 - TRANSISTORIZED 60 CPS SINE WAVE COMMUTATOR. (POLLNOW, KAY, JOUR. ELEC. SOC., 109, 648)
3 - JOHN FLUKE DIFFERENTIAL VOLTMETER
4 - ROTARY SWITCH
5 - WESTON 50 MV - 5 AMP PRECISION SHUNT
6 - TEST CELL

FIGURE 3-13 ELECTRICAL TEST MEASURING CIRCUIT

SMALL CELL TEST RIG

FIGURE 3-14

NOTES: UNLESS OTHERWISE SPECIFIED

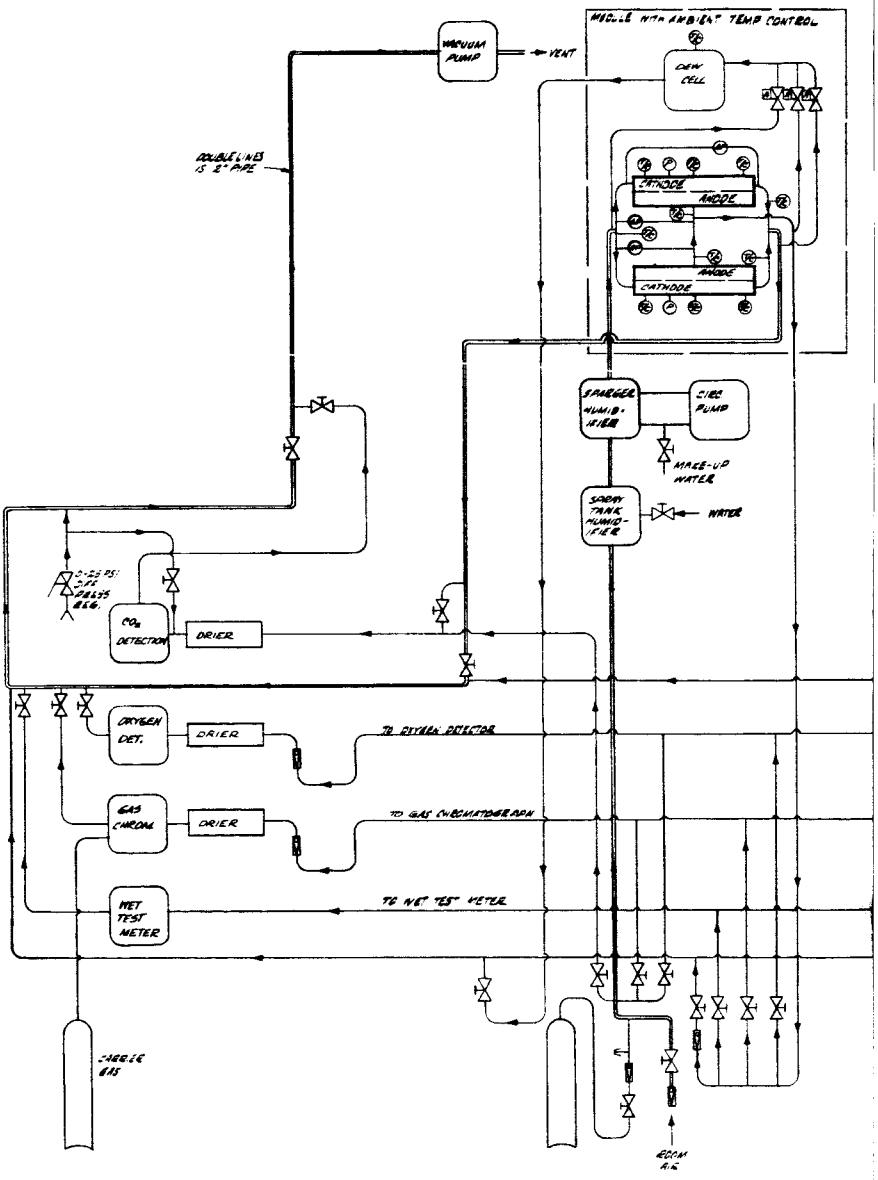

SHEET NO.	REVISIONS ZONE	LTR	DESCRIPTION	D.C.N.	DATE	APPROVED

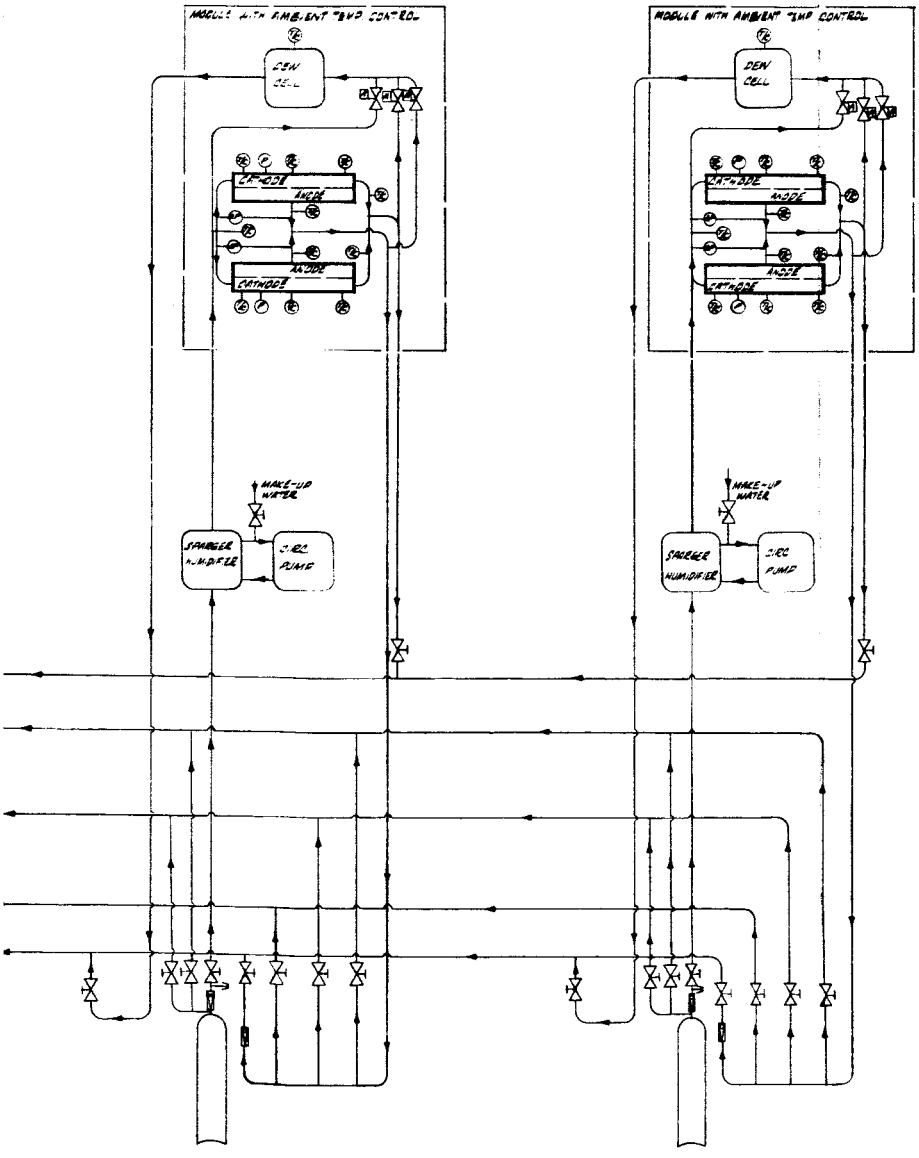

QTY REQ'D	ITEM NO	PART OR IDENTIFYING NO.	NOMENCLATURE OR DESCRIPTION	MATERIAL AND SPECIFICATION	REFERENCE OR NOTE
← ASSY DASH NO.		LIST OF MATERIALS OR PARTS LIST			

APPLICABLE SPECIFICATIONS UNLESS OTHERWISE SPECIFIED	UNLESS OTHERWISE SPECIFIED	DRTH	TRW ELECTROMECHANICAL DIVISION THOMPSON RAMO WOOLDRIDGE INC. CLEVELAND OHIO U.S.A.
DWG. INTERPRETATION PER MIL-STD-8	DIMENSIONS ARE IN INCHES TOL ON ANGLES TOL ON FRACTIONS TOL ON TWO-PLACE DEC. TOL ON THREE-PLACE DEC.	CHKD APPD ENG APPD PROJ ENGR	TITLE
THREAD DIMENSIONS AND DESIGNATIONS PER HANDBOOK H-28 AND MIL-STD-8 RESPECTIVELY.	FOUR-PLACE DECIMAL DIMENSIONS WITHOUT TOLERANCE ARE "BASIC" REMOVE ALL BURRS BREAK EDGES .005 .015 CORNER FILLETS .005 .020R	MAT'L APPD	NEXT ASSY MFR. CODE
SURFACE ROUGHNESS SYMBOLS PER	MATERIAL	MFG.	CODE IDENT NO. 59875 SIZE E DRAWING NO.
PART MARKING PER TRW SPEC. 02-3000.		APPROVAL	SCALE DWG. STATUS SHEET
WELDING SYMBOLS PER JAN STD 19	HEAT TREAT	APPROVAL	

FIGURE 3-15

a single O_2 analyzer and CO_2 detector, to measure the composition of gases in each stage. Individual humidity detectors are provided for each stage.

Figures 3-16 and 3-17 are photographs of the test stand. One end of the stand, Figure 3-16, is the control panel, which is used to set gas flow rates, control temperatures, and route gases to gas analysis instrumentation. In Figure 3-12 is seen the main portion of the stand. The bottom houses the plumbing, vacuum pump, gas humidifiers, and cell power supply. The upper portion consists of three lucite-enclosed sections which house the test cells. Each section encloses two cells of one stage.

Individual cells are installed on modules for ease in installation in the test stand. Each module consists of two cells, a small frame, instrumentation, and all necessary fluid and electrical connections. The modules are installed in the test enclosure by merely connecting four tube fittings, electrical interconnections, and thermocouple jacks. Figure 3-18 is a photograph of a partially assembled module.

3.3.2.1 Thermal Control - An independent ambient air temperature control, which has a range up to 175°F, is provided for each stage. Heat is supplied in the top of each enclosure by nine light bulbs (300 watts per bulb). Two of the bulbs have their power level controlled by a variac while the remaining seven are cycled on-off by a temperature controller to maintain desired enclosure temperature level. The air heated by the bulbs is circulated by two externally mounted blowers per stage. The hollow framework members of the test stand form the duct work which carries the hot air from the top of the enclosure to the bottom of the enclosure and onto the test cells.

3.3.2.2 Humidity Control - Precise control of inlet gas humidity is necessary in order to study cell moisture balance. It is accomplished by passing inlet gases through thermally-controlled water baths, measuring 30" tall and 10" in diameter. The gas passes through spargers in the bottom of each tank. The gas passes upward through the bath which are maintained at a controlled uniform temperature by a temperature controller, variac, heater, and mixing pump. At the exit a baffle arrangement stops droplet carryover.

Figure 3-19 is a photograph of the test stand with the bottom panels removed to expose some of the components used to control temperature and humidity.

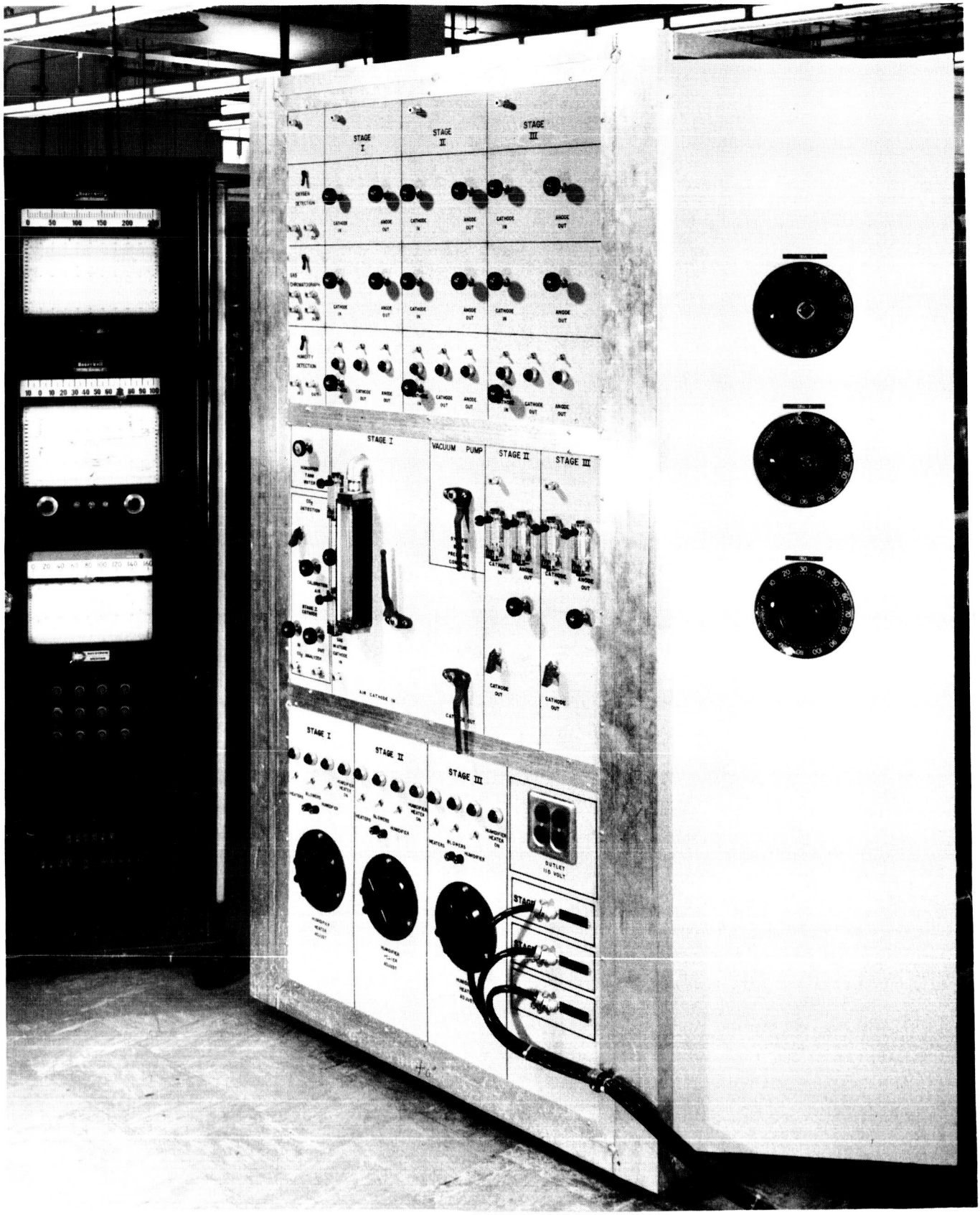

TEST STAND CONTROL PANEL

FIGURE 3-16

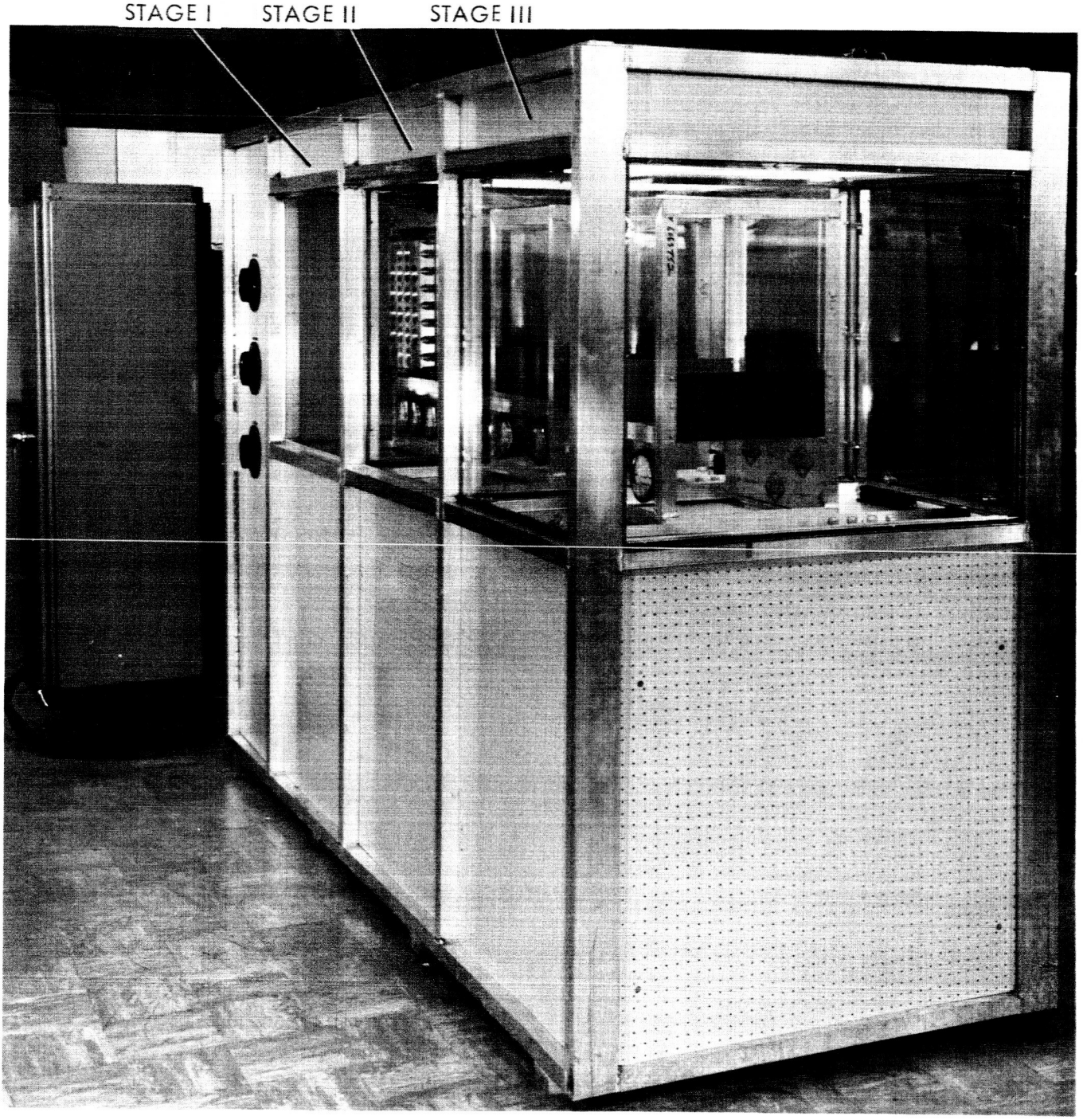

TEST STAND

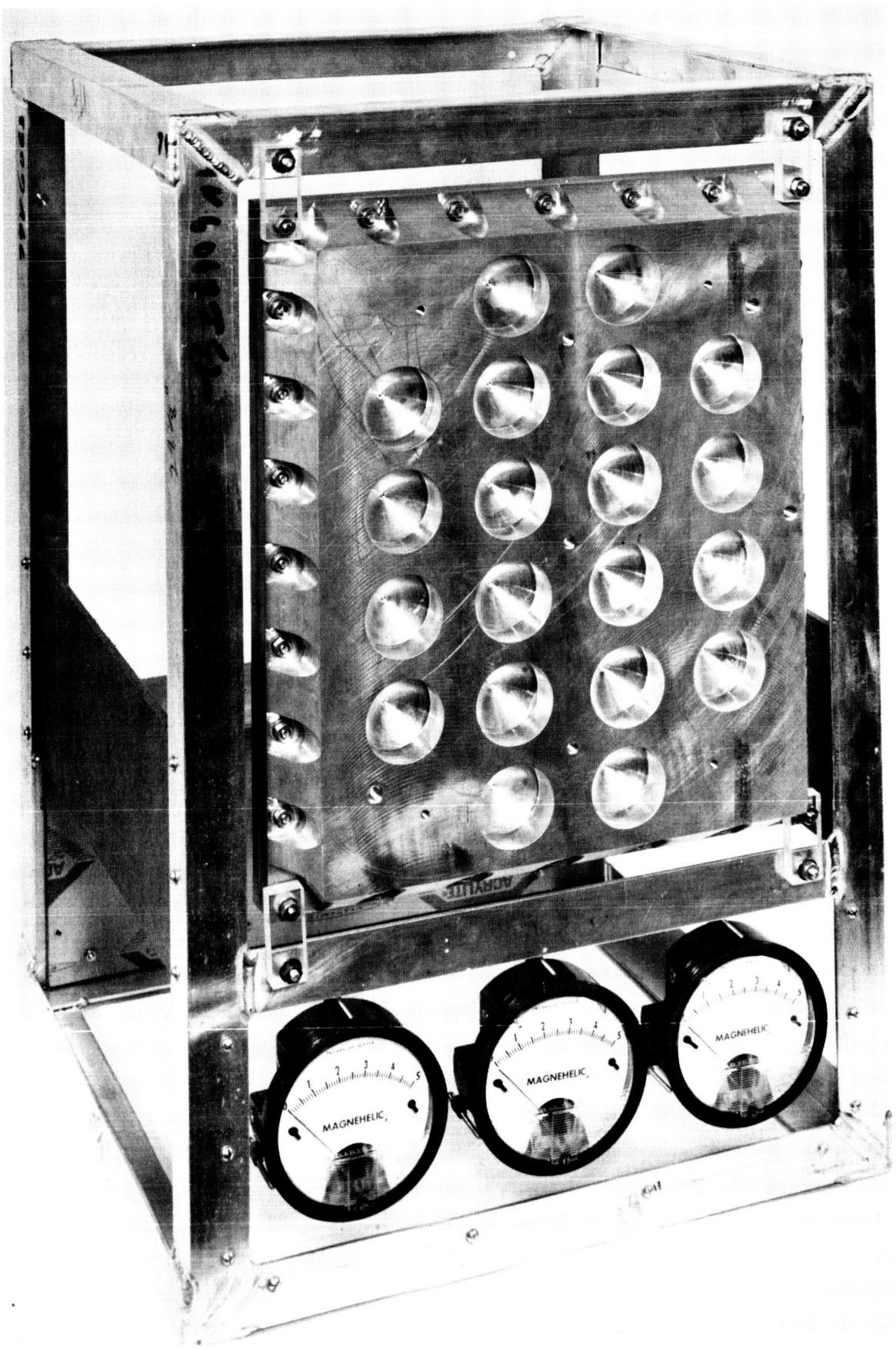

STAGE I MODULE - ONE CELL MOUNTED

FIGURE 3-18

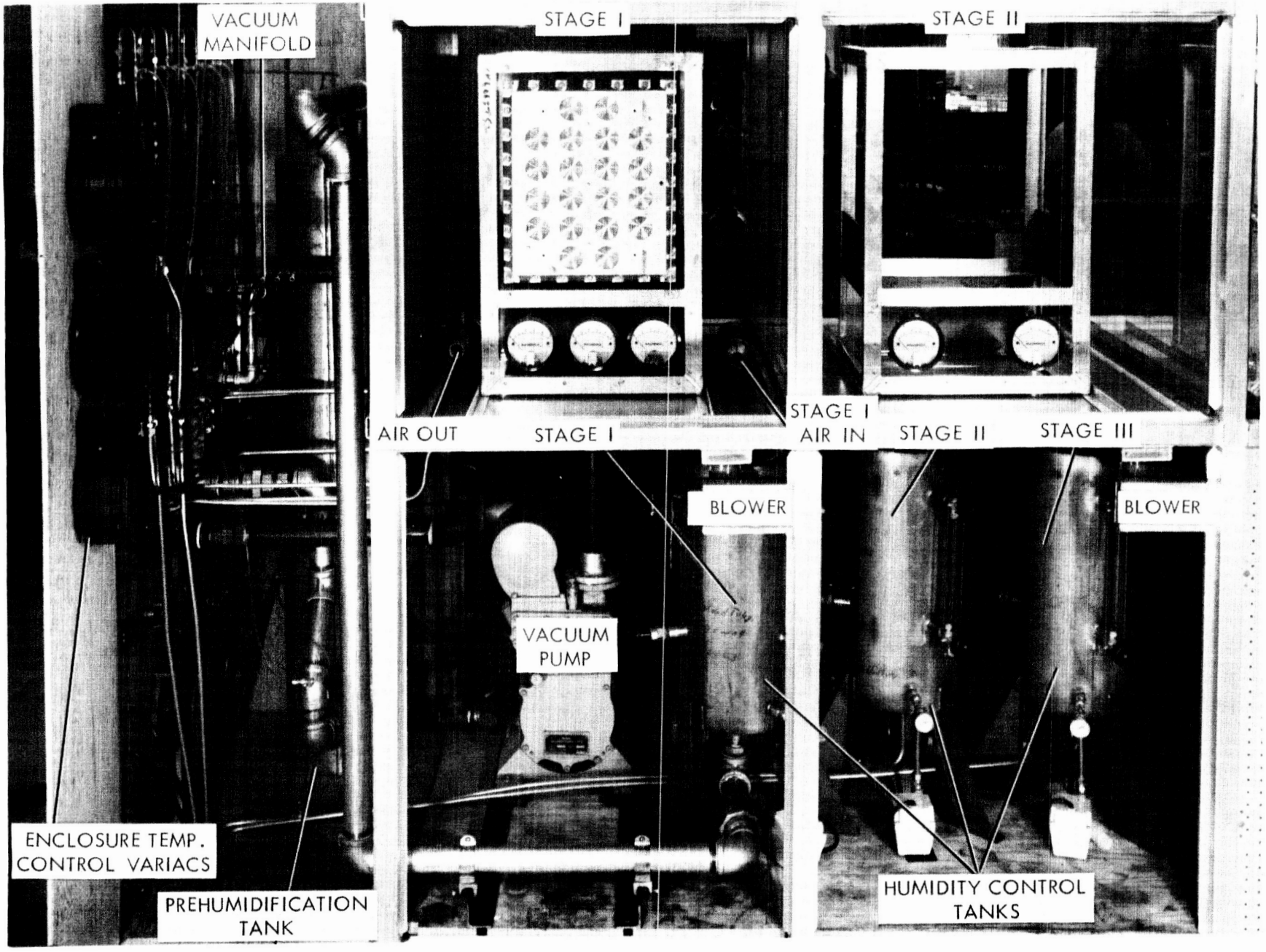

THERMAL AND HUMIDITY CONTROL COMPONENTS

FIGURE 3-19

3.3.2.3 Instrumentation -

a) Gas Analysis. A "Critical Orifice Carbon Dioxide Analyzer" (Harvard Apparatus Co., Dover, Mass.) was used to monitor the carbon dioxide content of the inlet and outlet 1st stage process gas. The instrument has a range of 0 - 10% CO_2 with a stated accuracy of $\pm$0.05% CO_2.

The "Beckman E-2 Oxygen Analyzer" was also used. It is a continuous sampling multirange instrument which determines oxygen partial pressure by measuring the sample's magnetic susceptibility. This unit, together with suitable manifolding, monitors the anode and cathode gas streams of all stages. The carbon dioxide content of the gas stream can then be determined by difference (in the absence of internal gas leakage).

b) Dew Point Temperatures. The dew point temperature of any one of the three gas streams associated with a given stage can be monitored by a "Honeywell dew probe sensor" (SSP129-C). The sensor is rated at a maximum dew point temperature of 160°F.

c) Cell Temperature, Voltage, and Current were continuously recorded with a multipoint potentiometric recorder. The use of suitable voltage divider circuits and precision shunts determined the operation range of the various channels.

d) Gas Flow Measurement. All cathode flows were monitored by rotameters of the variable area type. Anode gas flows and low cathode flows were monitored with a Precision Scientific wet test meter.

e) Pressures. Cell operating pressures were measured by compound type pressure gauges while differential pressure measurements were made by "Dwyer Magnehelic Gauges". These gauges were mounted on the individual modules.

4.0 MATERIALS

4.1 Stage I and II Cells

Material selection for the Stage I and II cells was based on experience at TRW on similar cells. A compilation of these materials is given in Table 4-1.

TABLE 4-1

STAGE I AND II CELL MATERIALS

Component	Material	Remarks
End Plates	AZ31B Type 2 Magnesium Plate	Gold Plates as follows: a) Zinc immersion (molecular) b) 0.1 to 0.3 mil copper c) 1.5 mil electroless nickel d) 0.03-0.05 mil gold.
Electrodes	American Cyanamid Type - AB6	Gold plated nickel screen with 9 mgm/cm^2 of platinum
Electrolyte Matrix	Asbestos	Fuel cell board (20 mils thick)
O-Ring	Neoprene	
Gas Diffusion Plate	Same as End Plates	
Wick Assembly (Stage II)	Tantalum Wire screen and asbestos	
Seal Plates	Epoxy Fiber Board	

4.2 Stage III Acid Cell

The Stage III material selection is a difficult problem in view of the sulfuric acid electrolyte and high cell operating potential (anode).

4.2.1 Materials Screening - A material screening and evaluation program was conducted in an effort to select a cell material for the Stage III cell construction. The material selected should meet the following requirements:

a) Resistant to sulfuric acid corrosion under electrochemical action.

b) Low cost raw material.

c) Easily machinable into intricate forms.

d) Sufficient mechanical strength.

e) Electrical conductor.

f) Impervious to gas.

g) Available in proper form and within schedule framework.

Table 4-2 lists the materials which were considered for possible use on the program. They were all eliminated from consideration for not meeting one or more of the above listed requirements. This then forced the use of end plate assemblies which were composed of a number of different pieces fabricated of different materials. Table 4-3 gives the materials used for Stage III cell. Some minor design modifications were made to accommodate the use of these materials. The end plate was divided into two pieces, a plastic pin structure and a metal clamping plate. A metal grid current collector is imbedded in the pin structure of each end plate to provide electrical contact with the electrodes. The components are seen in Figure 3-11.

TABLE 4-3

STAGE III CELL END PLATE MATERIALS

Part	Material	Remarks
Pin Structure and End Plate	Polyvinyldichloride (PVDC)	Thick enough to accept all fittings
Pressure Clamping Plate	Magnesium Plate	Unplated
Current Collector	Gold Plated Copper Grid	Embedded in pin structure-electroplated gold 2 mils thick
Gas Diffusion Plate	PVDC	

4.2.2 Non Porous Gold Plated Magnesium Evaluation - Except for the high cost of gold plating, magnesium with a 2-mil thick non-porous gold plating would be our choice for the third stage end plates. As such, test samples have been put through a number of corrosion tests.

Three 3" x 5" magnesium test plates containing a machined pin structure were plated as follows:

a) Zinc immersion (molecular)

b) 0.1 to 0.3 mil copper

TABLE 4-2

STAGE III CELL-MATERIALS EVALUATION

Structure Type	Cost		Availability		Mech. Prop.	Elec. Prop.	Remarks
	Material	Fabrication	Size	Schedule			
Carbon - ATJ Type	Low	Low	Yes	Yes	No*	Poor	Gas permeability too high, weak and brittle
Carbon - High Density Type (ER-1924)	High*	Low	No*	No	Ques-tionable	Good	Cost too high - not available in large enough pieces
Gold Plated Carbon	Moderate	Low	Yes	Yes	Ques-tionable*	Good	Questionable Strength
Magnesium - Non Porous Gold Plate	High*	Low	Yes	Yes	Good	Good	Gold plating cost too high - would be used for flight hardware.
Electroclad Tantalum on Carbon Pin Structure	Moderate	Moderate	Yes	Yes	Good	Ques. *	Use of Tantalum Questionable - See Section 4.2.3.
Other Inert Metals	High*	Moderate	Yes	Yes	Good	Good	Material cost too high
Plastic Pin Structure - Gold Plated Current Collector	Low	Low	Yes	Yes	Satis-factory	Good	Must use multiple type structure - will be used for experimental cells

*Major reasons for elimination

c) 1.5 mil electroless nickel

d) 0.5 mil gold

All of the above plating was done by Furniture City Plating Co. except for the gold plating (SEL-REX-CO.). The gold plate was applied by electrolytic deposition. The results of several corrosion tests are summarized in Table 4-4. All tests involved immersion of one half of the test plate in a 6 normal aqueous solution of sulfuric acid. The test plate served as the anode of an electrolysis cell couple. Figure 4-1 is a photograph of the test samples as described below.

A post test (no. 1) microscopic examination of the unused portion of plate No. 1 revealed several pin holes which may have been the centers of attack. The brownish deposit observed in tests no. 1 and no. 4 is an oxide of gold which readily formed at the operating potential of 1.8 to 1.9 volts with respect to a standard calomel electrode. This brown oxide is easily rubbed off leaving a smooth unpitted surface (Figure 4-1, plate no. 2). The pinkish coloration imparted to the test solution is probably due to the formation of a gold sol, formed by the reduction of gold oxide particles which migrate to the cathode by forced convection.

The results of tests 2 to 5 indicate that the base metal is well protected from either chemical or electrochemical attack. In test no. 5 a platinum electrode was placed in intimate contact with the test plate simulating a typical cell assembly. No formation of gold oxide was evident, indicating that the test plate is functioning only as an electron exchange medium and is not involved in any electrochemical reaction. The small black spots on the test sample used in test no. 5 are the points at which the electrode was spot-welded to the gold plated magnesium.

Further evaluation of the gold plated magnesium was conducted by the use of a small test cell fabricated of this material.

4.2.3 Small Cell Tests - Small cell testing was conducted to examine those areas posing problems in the large cell testing program. The small cell testing profram was also intended to examine in detail large cell test results which were at variance with expected results. During this phase of the present program only the materials problem of the third stage cell was studied by testing of three cell types:

TABLE 4-4

CORROSION TESTS GOLD-PLATED MAGNESIUM

Test No.	Temp. (°C)	Test Duration (Hours)	Plate Potential (Volts)[1]	End of Test Observations		Solution[2] Analysis
				Solution	Test Plate	
1 Plate #1	25	15	+1.9 at 0.5 amps (constant)	Pinkish coloration brownish - purple particles dispersed in solution	Brown adherent deposit, random distribution of pin holes. Severe attack at one point on edge of plate.	High Ni, Mg, Ca, Cu, Fe, Au.
2 Plate #2	25	72	None	No change	No change	--
3 Plate #2	90	29	None	No change	No change	--
4 Plate #2	25	17	+1.8 at 0.5 amps (constant)	Pinkish coloration	Brown adherent deposit. No pin holes observed.	--
5 Upper half Plate #2 AA-1 Elec. Spotwelded to Plate	25	23	+1.8 at 0.5 amps (constant)	No change	No deposit on plates. No pinholes observed. Black spots due to spotwelding electrode in place.	None

(1) With respect to a saturated calomel electrode, counter electrode - 50 mesh tantalum screen. Potential given is minimum at start of test — a slight increase with time occurred but was not measured.

(2) Spectrophotometric

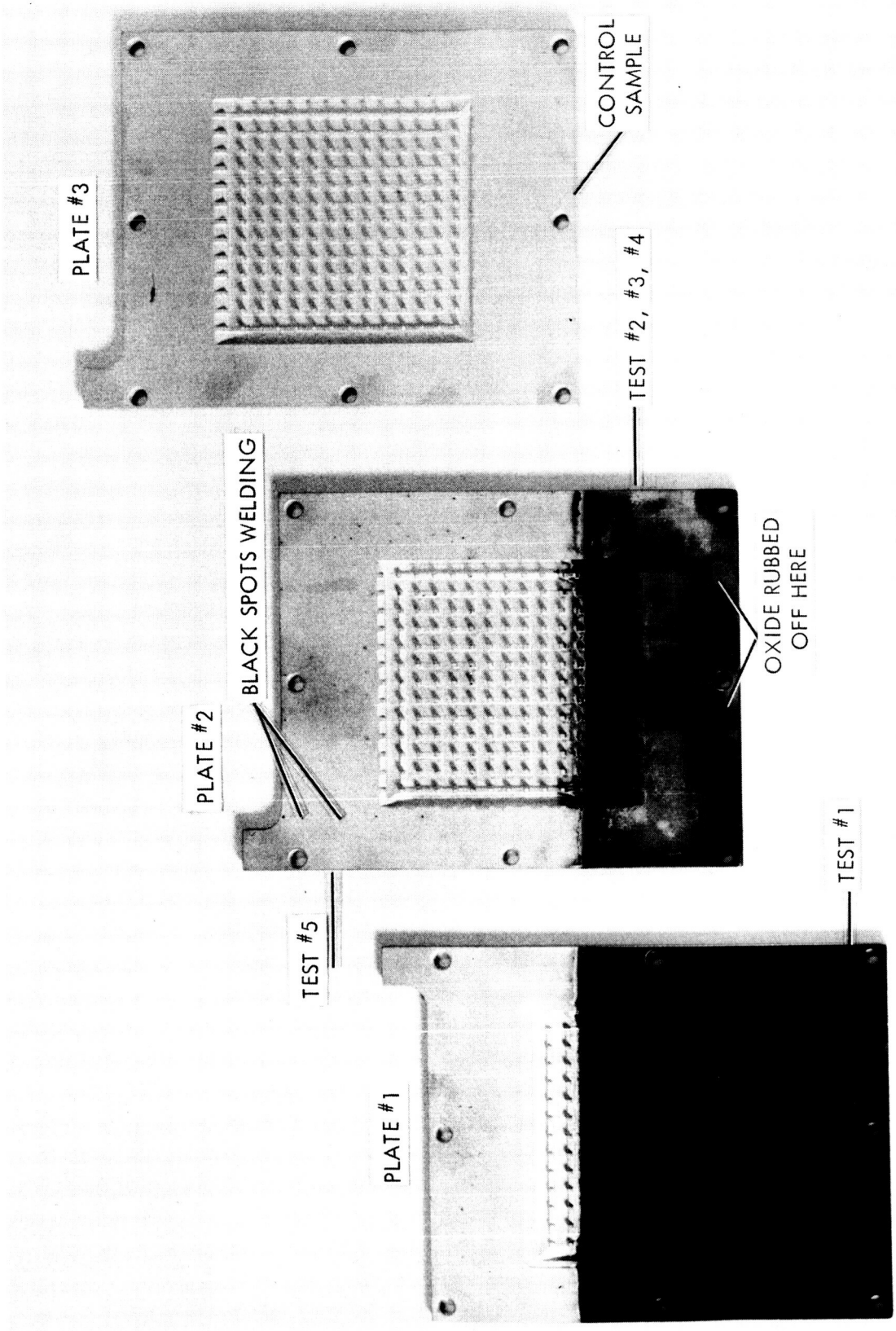

FIGURE 4-1 GOLD PLATE EVALUATION TEST SAMPLES

a) Carbon end plates

b) Plastic end plates with tantalum current collector inserts

c) Non-porous gold plated Magnesium end plates.

4.2.3.1 Carbon Cell - A set of carbon end plates was fabricated to study the applicability of using readily available grades (ATJ) of carbon for the Stage III end plates. No electrical performance tests were conducted as the permeability of the carbon end plates allowed leakage of gases at operating pressures. The low mechanical strength of the carbon is evident in Figure 4-2, as the upper end plate is cracked where the current lug had been attached to the back of the cell.

4.2.3.2 Plastic Cell with Metal Inserts - A total of 35 hours of testing was accumulated on the plastic test cell (Figure 4-2). (Lucite end plates containing an integral pin and baffle structure.) The current collector recessed in the end plate consists of a vertically ribbed tantalum frame. All testing was conducted in the test system described in Section 3.3.1. Test conditions were as follows:

Electrodes: AC No. AA-1 (Active area 127 CM^2)
Electrolyte: 6N H_2SO_4/Whatman No. GF-B Glass Filter Paper
Cell Pressure: Ambient
Cell Temperature: $35^{\circ}C \pm 0.1^{\circ}C$
Current Density: 31.5 MA/CM^2
Cathode Gas: 80% CO_2 - 20% O_2 - 276 cc STP/min - 4 x stoichiometric (O_2)

In all tests a polarization-time dependence was noted of the order of 0.5 MV/min. Figure 4-3 is a plot of the cell "IR" free voltage as a function of time at load for a typical run.

Difficulties were encountered in sealing the test cell (internal). As a result, an accurate determination of the anode gas purity was not possible. Additional difficulty was encountered in maintaining proper cell dew point owing to the fact that the plastic cell acts as an insulator and prevents the internal temperature of the cell from matching the water bath temperature.

Several possibilities exist as to the cause of the polarization-time dependence:

a) Progressive oxidation of the tantalum screen and current collector, resulting in an increased overall cell resistance.

FIGURE 4-2 SMALL TEST CELLS

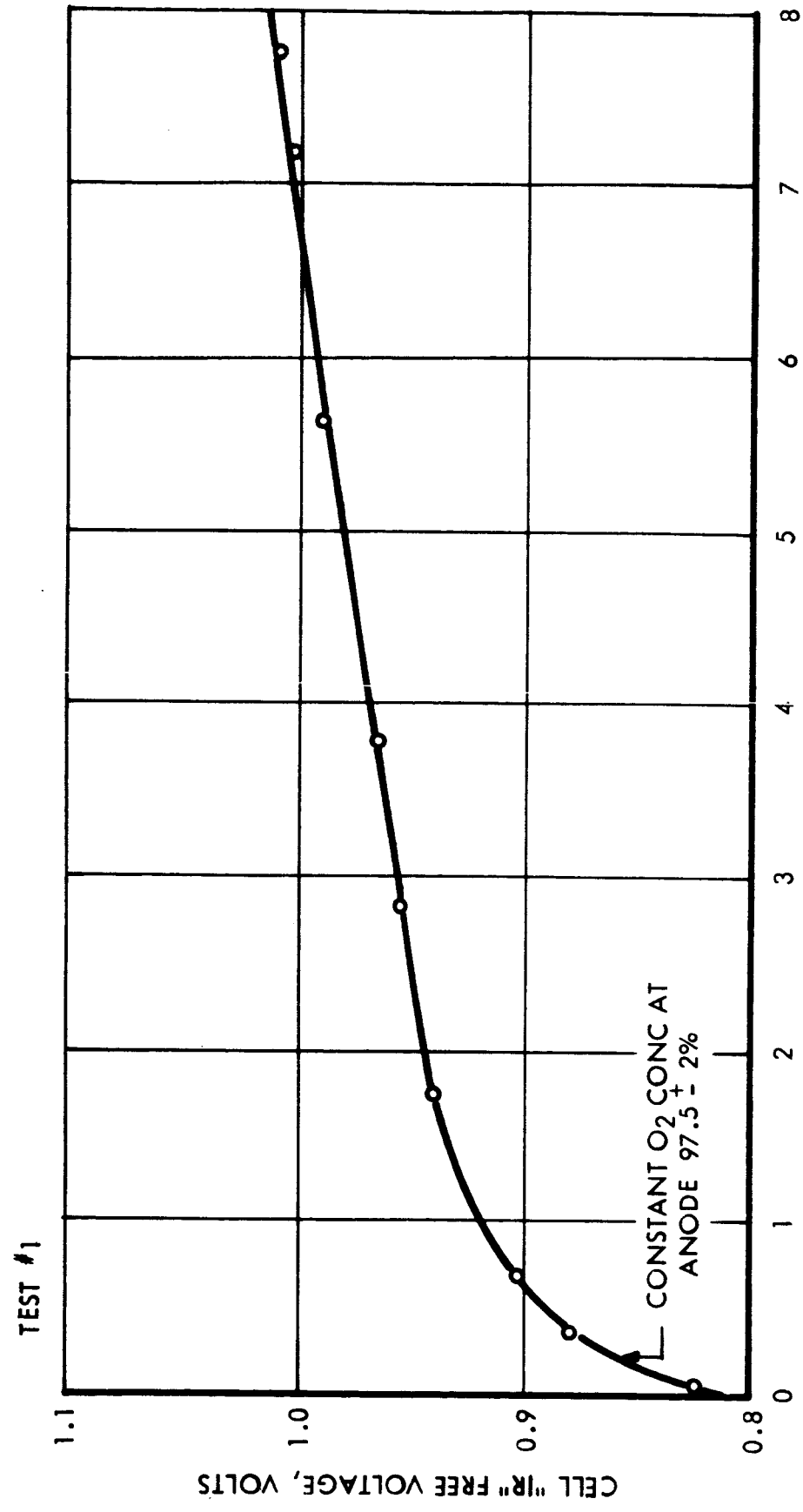

FIGURE 4-3 PLASTIC CELL - POLARIZATION TIME DEPENDENCE

b) Reduction of the carbon dioxide at the cathode, with the resulting formation of carbon monoxide - the carbon monoxide being irreversibly adsorbed on the electrode.

c) Internal cell temperatures higher than the ambient would result in a recession of the electrode-electrolyte interface since the entering gas dew point is based upon ambient cell temperature.

4.2.3.3 Gold Plated Magnesium Cell - Based on the materials screening program results, a gold plated magnesium cell was selected for further evaluation in the small cell test program.

Cell Description

The gold plated magnesium cell end plates are shown in Figure 4-4. Slight discolorations on the land areas are due to operation in the water bath during tests M-1 and M-2. This cell contains in the end plates an integral pin and baffle structure. Design characteristics of the pins are similar to the large cell units. The active electrode area contained by these cells is 0.0775 ft^2.

A compilation of the materials used in the cell is given in Table 4-5.

TABLE 4-5

GOLD PLATED MAGNESIUM ACID CELL MATERIALS

Component	Material	Remarks
End Plates	AZ31B Type 2 Magnesium Plate	Gold Plate as follows: a) Zinc immersion (molecular) b) 0.1 to 0.3 mil copper c) 1.5 mil nickel d) 1.5 mil electrolytic gold e) 0.5 mil electroless gold
Electrodes	American Cyanamid Type - AA1	Tantalum screen with 9 mgm/cm^2 of platinum
Electrolyte Matrix	Matted Structure	Whatman GFB glass fiber filter paper - (20 mils thick)
Gasket	Viton	

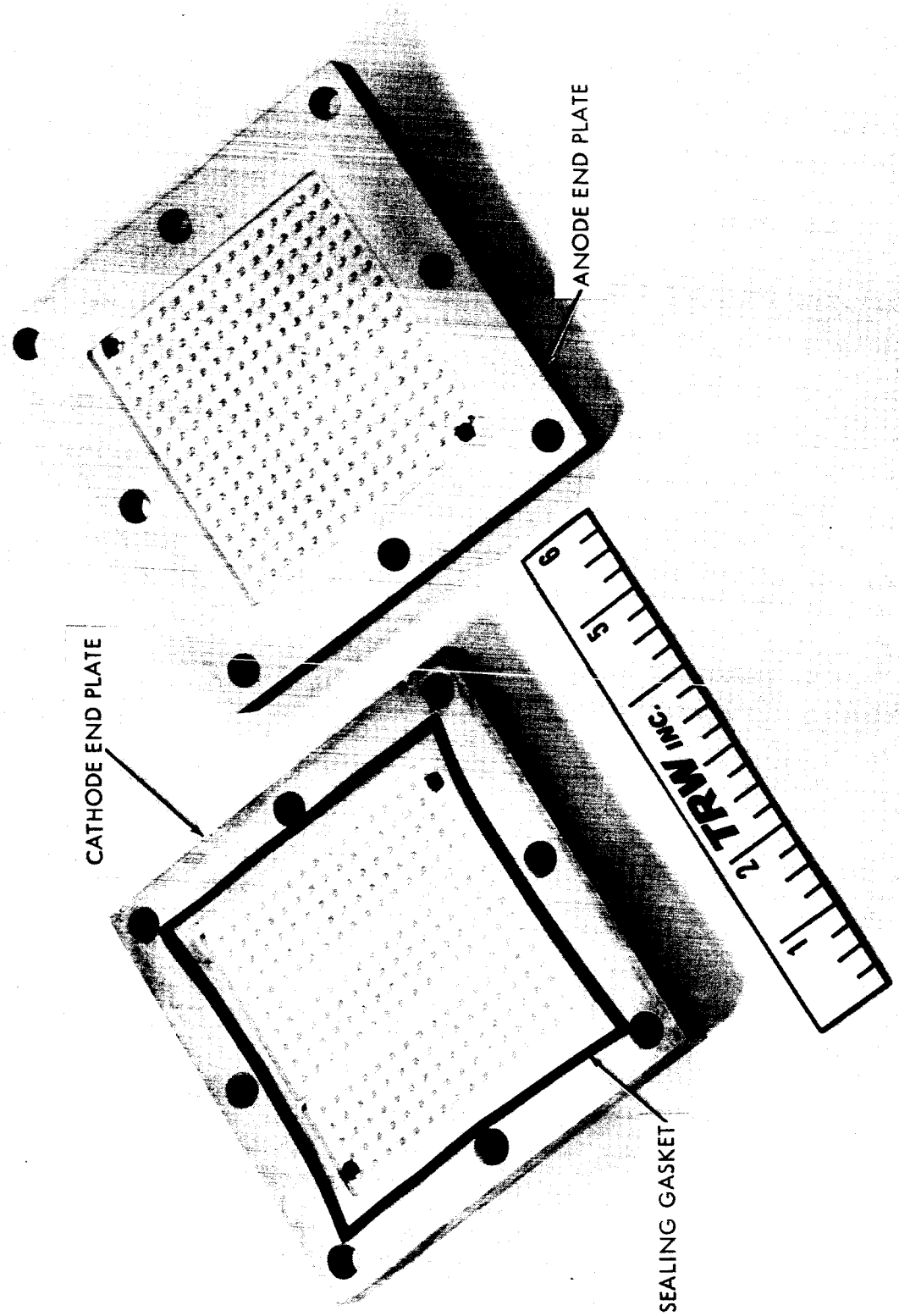
ANODE END PLATE
CATHODE END PLATE
SEALING GASKET
TRW INC.
GOLD PLATED MAGNESIUM ACID STAGE TEST CELL

FIGURE 4-4

a. Test No. M-1

Figure 4-5 shows the polarization time dependence obtained during the first experimental run with the gold plated magnesium cell. The total time at load for the test cell was approximately 58 hours. A break in performance, as indicated by the discontinuity, occurred at the end of six hours when the constant current power supply failed. The cell was returned to load with a new power supply and continued operation for another 52 hours. The test was terminated due to an internal gas leak caused by improper seating of an electrode resulting in matrix damage. Over the last 27 hours of the test the average rate of voltage increase was approximately 0.75 mv/hr, with the rate decreasing to 0.62 mv/hr over the last eight hours. It can thus be seen that the rate of increase in voltage was still decreasing with time. A post-test cell inspection revealed no corrosion of the end plates. Cathode gas flow rate was 307.5 cc STP/min, while the anode gas O_2 content varied from 97.5 to 99 per cent by volume as measured by Beckman O_2 Oxygen Analyzer.

b. Test No. M-2

Using new electrodes, the cell was reassembled in preparation for a repeat of the previous test for a longer time period. Initial operating conditions were identical to those of test run No. M-1. The polarization time dependence for the run is plotted in Figure 4-6.

Initial cell voltage was 0.932 volts, rising to 1.100 volts after three hours of operation. At the end of twenty-six (26) hours of operation, the cell terminal voltage was 1.186 volts. Over the last four and one-half hours, the average rate of voltage increase was 1.78 mv/hr. At this time, the CO_2 was removed from the cathode feed to see if the CO_2 actually was contributing to the cell degradation. Oxygen was used as the cathode feed for the balance of the test. Nominal cathode gas flow rate was 365 cc STP/min.

After switching to O_2 feed, the initial cell terminal voltage was 1.058 volts increasing rapidly (30 minutes) to 1.085 volts, then following a rate of increase close to the rate observed before the CO_2 was removed from the cathode feed. In addition to the periods of increasing cell voltage, periods of stable cell voltage and decreasing cell voltage were noted. During the sixty-five hour period from 77 hours at load to 142 hours at load, the average rate of voltage increase was 0.15 mv/hr, while from that point to the end of the test the terminal voltage decreased. The test was terminated when some type of intermittent short between the cell plates occurred. This short was believed to be due to contamination

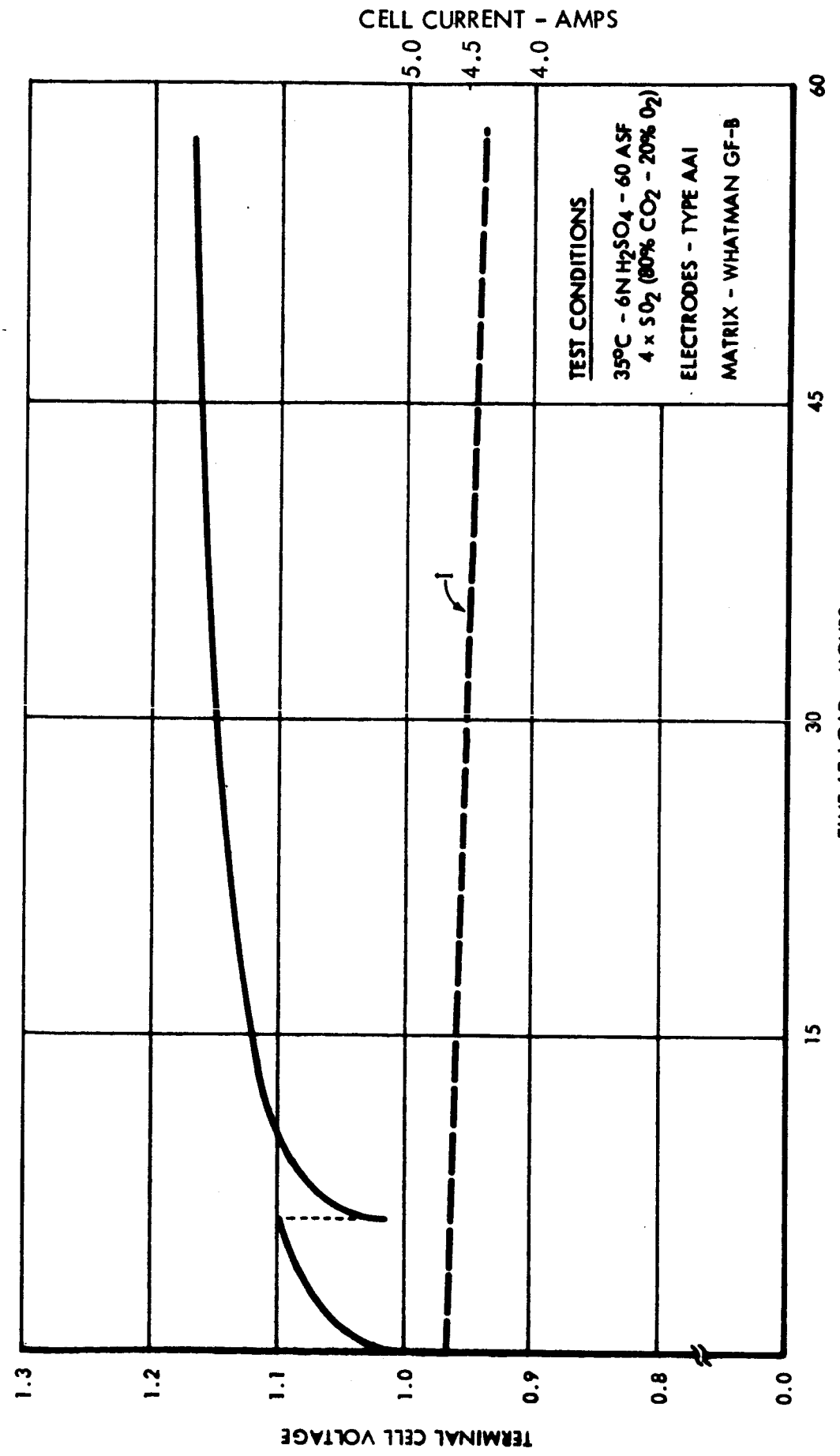

FIGURE 4-5 POLARIZATION TIME DEPENDENCE - STAGE III - TEST #M-1
(CELL TYPE MG/NI/AU)

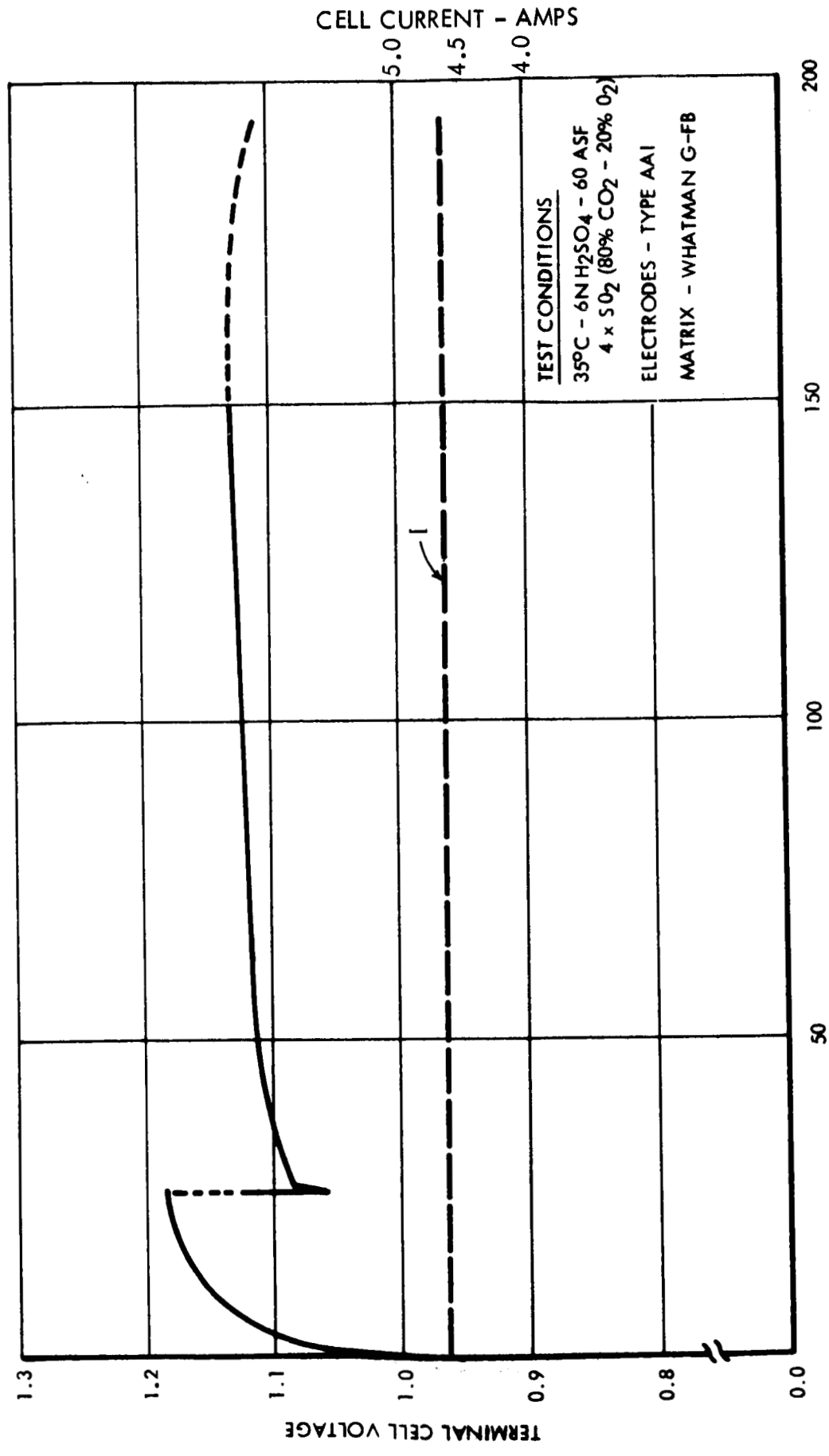

FIGURE 4-6 POLARIZATION TIME DEPENDENCE - STAGE III - TEST #M-2
(CELL TYPE MG/NI/AU)

in the cell constant temperature water bath. The anode gas O_2 content varied from 97.5 to 100 per cent by volume while on CO_2 - O_2 feed and 100 per cent while on pure O_2 feed.

Cell disassembly revealed a pinkish-red coloration on the cathode side of the matrix corresponding to the pin area. The cathode had a pinkish-red coloration on the pin contact side. With the exception of two small black pits no visible corrosion of the end plates was noted. By spectrographic analyses, the impurities on the electrodes and matrix were determined. The results of these analyses are presented in Table 4-6.

TABLE 4-6

SPECTOGRAPHIC ANALYSES OF ELECTRODES AND MATRIX

Samples Examined

Elements Detected in %	Matrix Cathode Side	Matrix Anode Side	Cathode	Anode	Unused Matrix
Au	A0.10	ND	0.8 to 1.0	ND	ND
Ni	0.01	0.01	0.01 to 0.10	0.01 to 0.10	ND
Cu	<0.01	<0.01	0.01 to 0.10	0.01 to 0.10	0.01
Zn	1.0 to 3.0	1.0 to 4.0	ND	ND	2.0 to 5.0
Mg	0.2 to 0.6	0.10 to 1.0	0.10 to 1.0	0.10 to 1.0	0.005 to 0.05

ND = Not Detected

A = Approximate

Results of the analyses indicate that the gold source is the cathode end plate. Gross corrosion products are not apparent. The magnesium detected may indicate a small crack in the plating, possibly in one of the gas ports which was somewhat scratched in the removal of a damaged plastic fitting.

It has been established by the supplier that the Whatman GFB glass fiber paper used as the matrix will disintegrate with time when immersed in 30% sulphuric acid. The rate of disintegration however is not known by the supplier. Using a glass fiber matrix material with 5N H_2SO_4 at 70°C, a single cell life test on a fuel cell was conducted by American Cyanamid Company. Stable operation over a period of 1100 hours was observed, indicating that the glass fiber matrix does not cause cell performance degradation.

It is felt that the voltage increase with time noted in the small acid cell testing program is due to the use of the tantalum screen electrodes. Referring to the plastic cell results presented in Figure 4-3 and tests M-1 and M-2, the voltage increase obtained between one and eight hours at load is as follows:

Test	ΔE (for 7 hours)
Plastic Cell	90 mv
M-1	75 mv
M-2	82 mv (with O_2 flow only)

It is seen that the same general increase is noted in each test, the common feature of each test was the type of electrode used, and the matrix material. Progressive oxidation of the tantalum screen appears to be a logical cause of the cell voltage increase with time.

c. Test M-3

The two small black pin-holes, noted at the completion of test M-2, were covered by a protective coating of epoxy. The cell was assembled in a manner identical to the M-1 and M-2 configuration and a series of three tests were completed; life test, polarization runs, and cathode gas flow rate effect determination.

Life Test - Operating conditions and results of the life test are shown in Figure 4-7. Initial cell voltage was 0.775 volts, rising to 0.995 volts after three hours of operation. At the end of forty-seven hours the voltage was 1.048 volts, while the current density had decreased to 40 ASF. From this point on the current density was maintained at 40 ASF. Total test duration was 185 hours. Voltage at termination of test was 1.060 volts. Over the last 115 hours of the test the rate of voltage increase was 0.043 mv/hr. The cell was completely operative upon termination of the life test. Nominal cathode gas flow rate was 186 cc STP/min. Anode gas oxygen content varied from 97.7 to 98.4 per cent at volume.

Polarization - Upon termination of the life test polarization runs were made using the same set-up as used for the life. A polarization curve is presented in Figure 4-8.

Cathode Gas Flow Rate - The effect of cathode gas flow rate was studied by varying the gas flow to the cathode while maintaining the current density of 103 ASF.

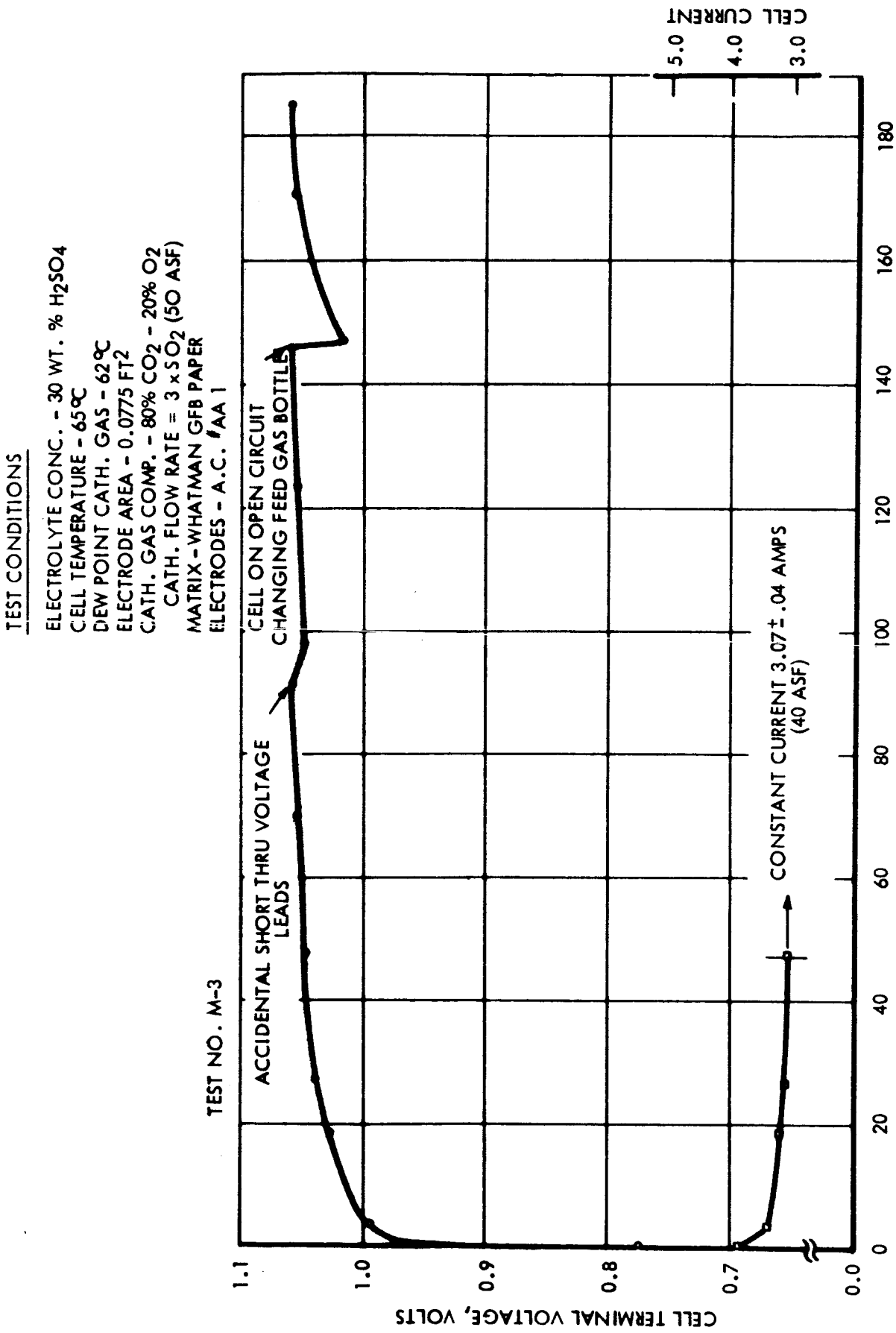

FIGURE 4-7 SMALL METAL CELL, POLARIZATION TIME DEPENDENCE

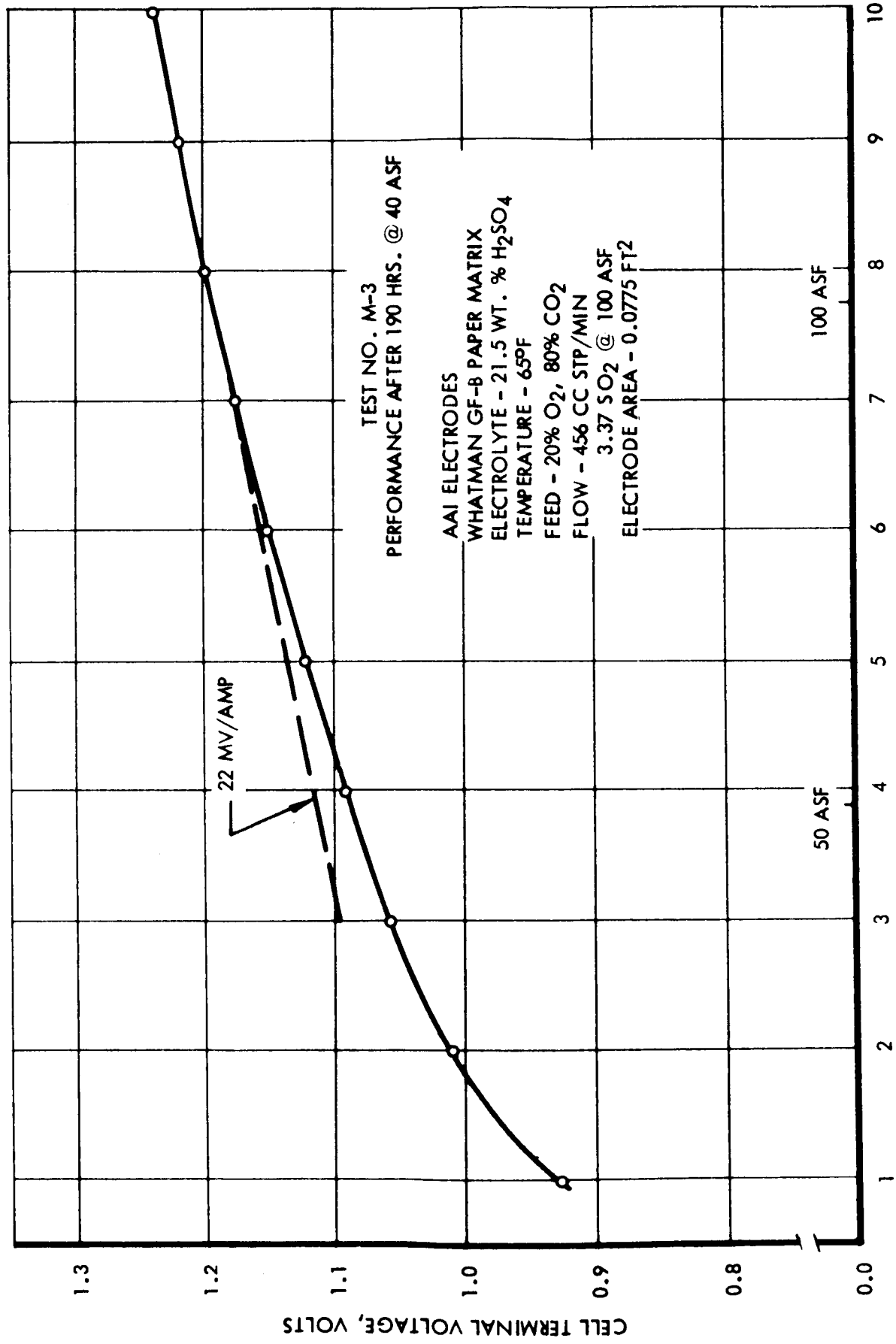

FIGURE 4-8 SMALL METAL CELL PERFORMANCE AS A FUNCTION OF CURRENT DENSITY

It was found that the lower limit on the cathode gas flow at this current density was 1.025 times stoichiometric flow. At this point a sharp rise in voltage was noted, Figure 4-9, as the flow ratio was dropped below 1.025 times stoichiometric flow.

Upon completion of these tests, the cell was disassembled and examined for corrosion. No corrosion was noted, as indicated by the photographs in Figures 4-10 and 4-11.

d. Test M-4

As a means of checking the small cell test set-up and test equipment a short run was made on a different test rig and cell. Cathode feed gas was 100% oxygen. Test M-4 was run for 27 hours with the polarization time dependence curve (Figure 4-12) almost exactly parallel to thatobtained in Test M-3 but at a slightly higher terminal voltage. The cell current was maintained at 3.87 amps (50ASF) with cathode gas flow rate much greater than stoichiometric oxygen requirements. Anode gas composition was not measured.

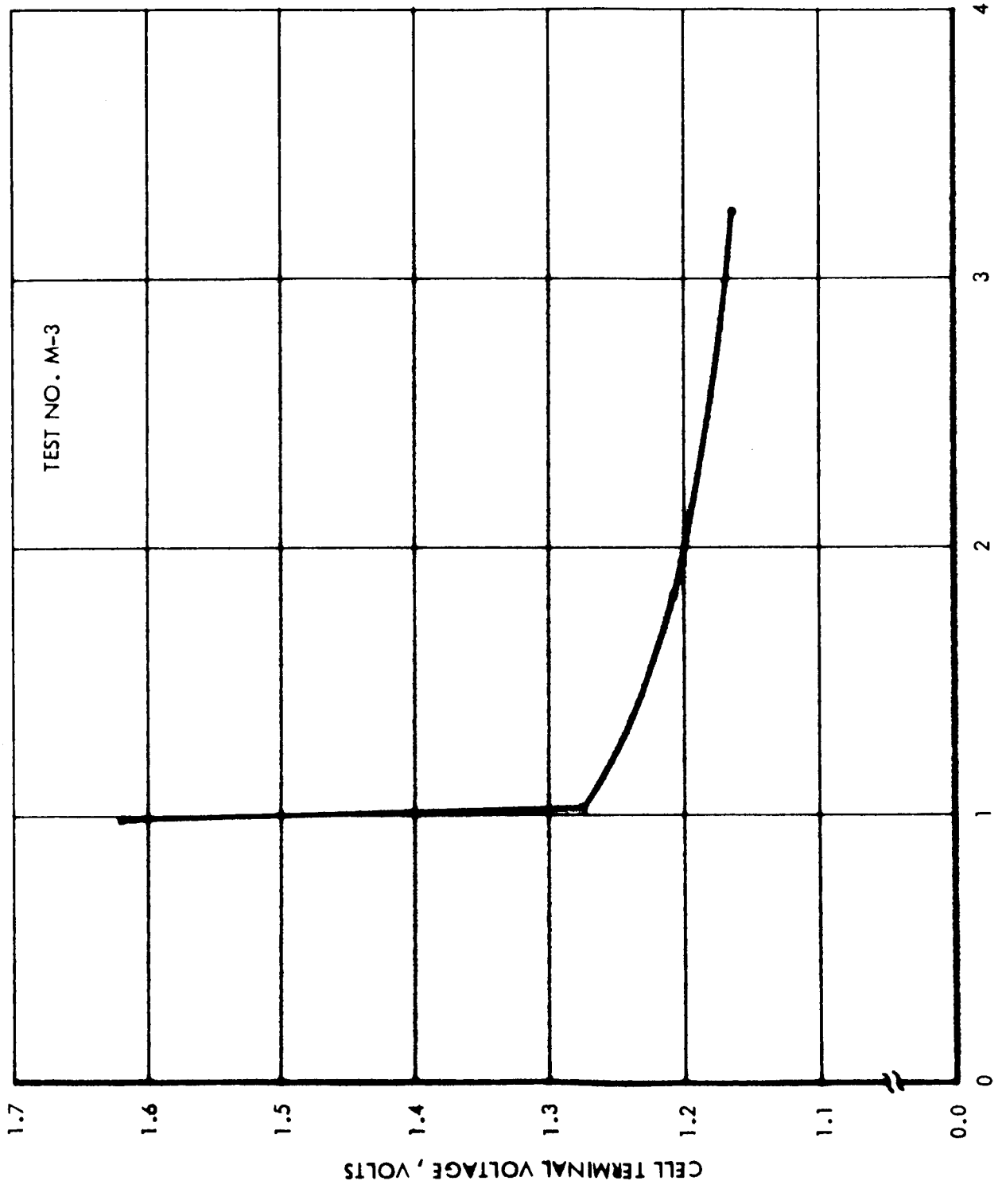

FIGURE 4-9 SMALL METAL CELL PERFORMANCE AS A FUNCTION OF CATHODE GAS FLOW RATE

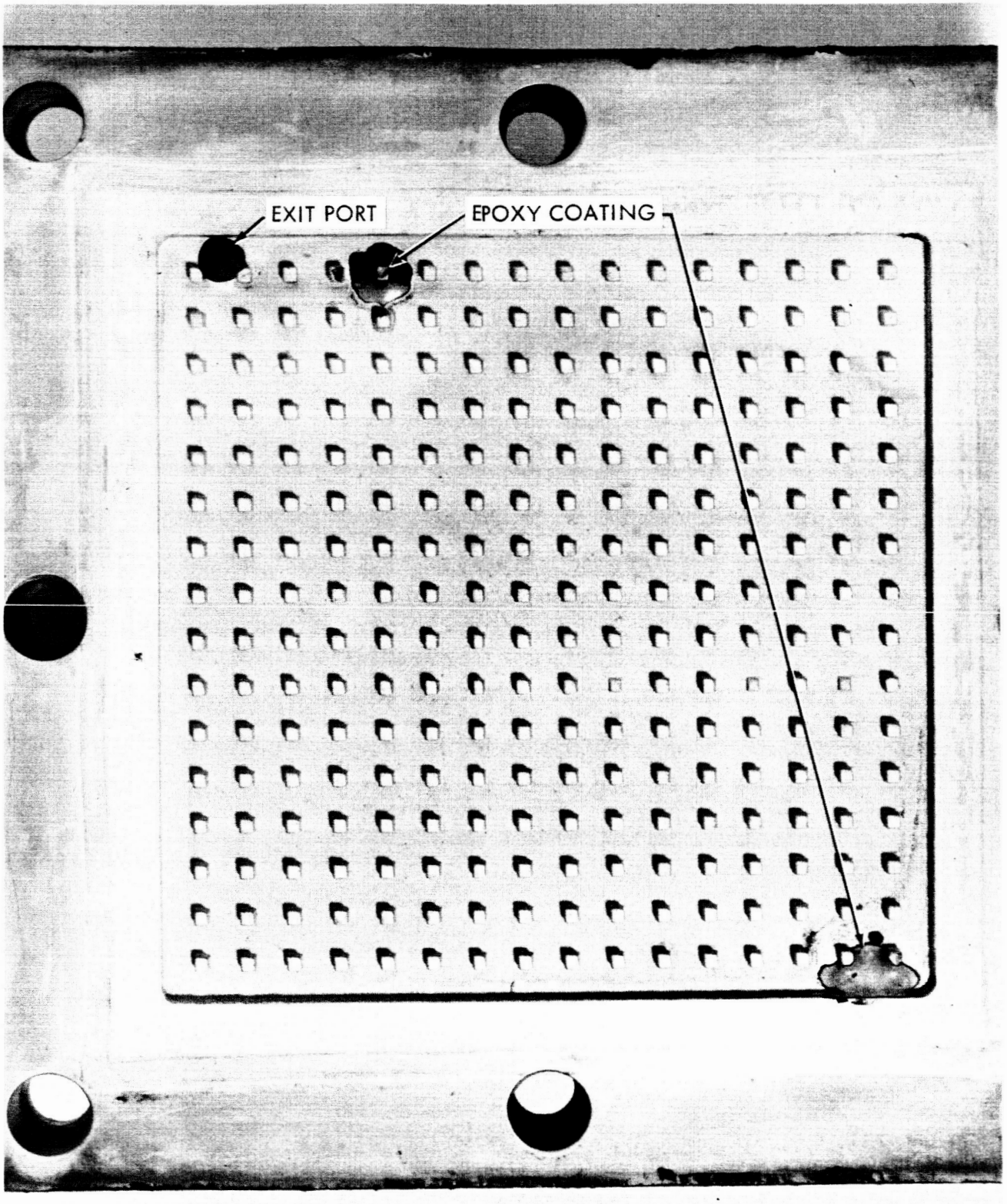

FIGURE 4-10 METAL CELL PLATE AFTER TEST, M-3 (ANODE)

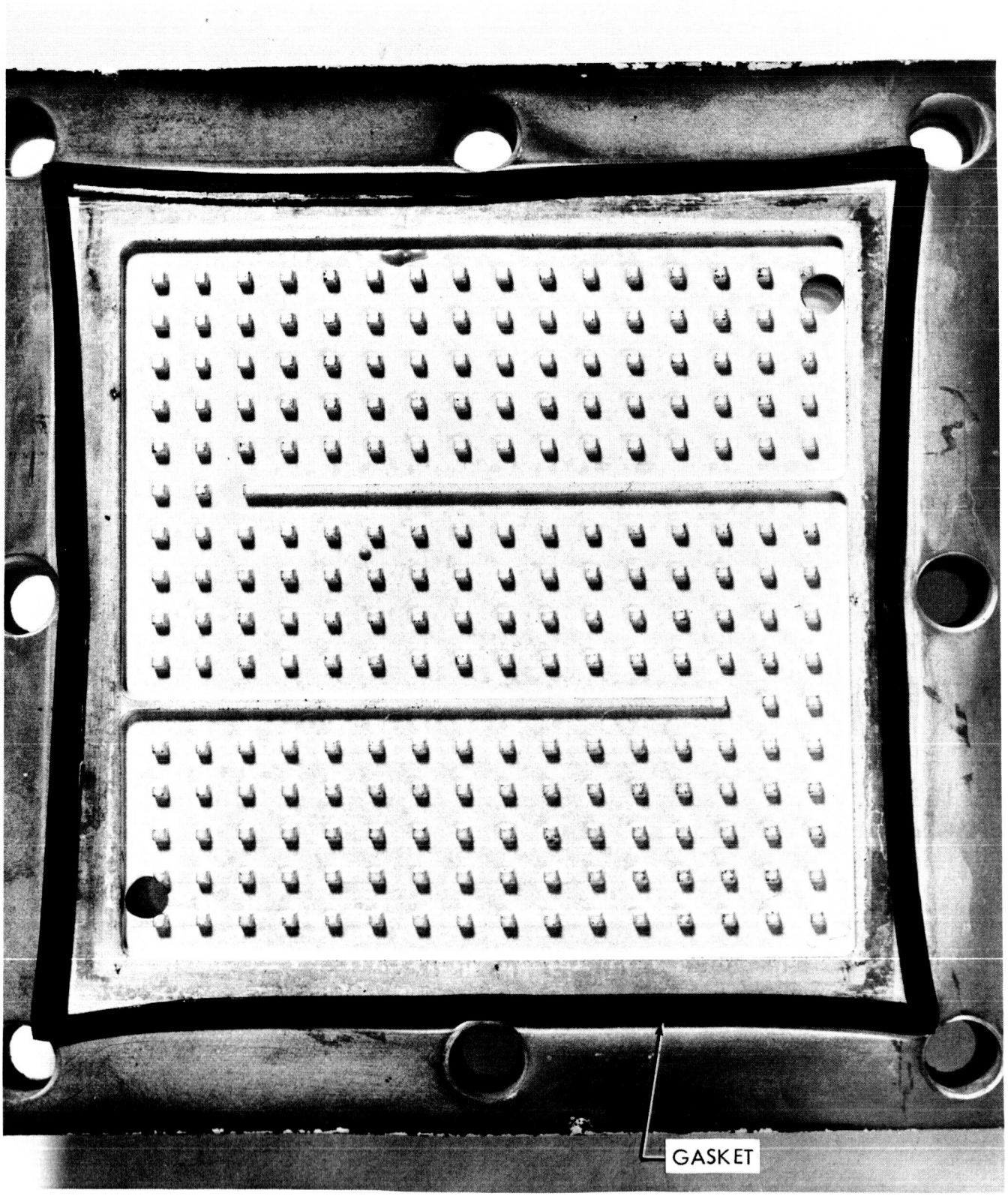

FIGURE 4-11 METAL CELL PLATE AFTER TEST, M-3 (CATHODE)

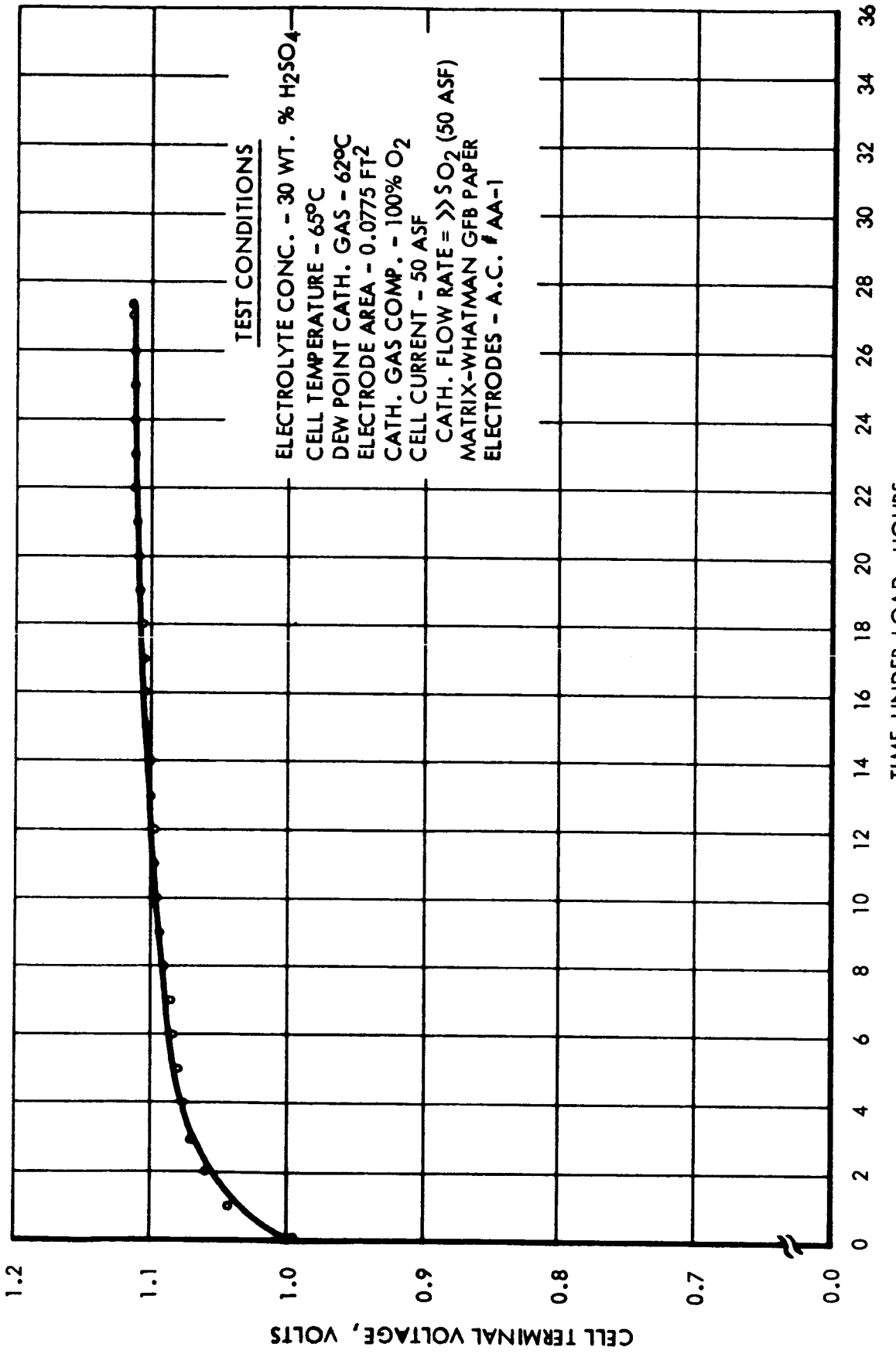

FIGURE 4-12 TEST NO. M-4, POLARIZATION TIME DEPENDENCE

5.0 TEST RIG CHECKOUT AND MODIFICATION

Upon completion of the test stand, a functional checkout was initiated. Control of the three thermal enclosures was maintained to within less than 1°F of the selected temperature (up to 160°F). The Stage II and III humidity control of inlet gases was satisfactory, maintaining a preset humidifier tank temperature to within 1°F of the set point temperature at rated gas flows. Testing of the Stage I humidifier indicated a need for:

1. Additional vacuum pump capacity to give the desired air flow rate at 10.0 psia. (A second vacuum pump was installed in parallel with the original pump.)
2. A higher capacity heater in the humidifier tank. (The original heater was converted to a 440 volt heater, approximately doubling the power output.)
3. A condenser to remove water from the air stream before it entered the vacuum pumps. (A gas-liquid heat exchanger with provision for condensate drain in the air side was installed between the cell and the vacuum pumps.)

The dew point temperature of gas out of the humidifier was checked with a Foxboro Dew Point Analyzer, correlating to within 2°F of the tank temperature. A check also was made on the amount of water removed from the condenser to check the accuracy of the Foxboro data.

During the first test runs with the Stage I large cell, a number of difficulties in operation of the test rig were encountered. The difficulties and corrective measured taken were as follows:

1. The pressure drop across the sparger plate in the humidifier gradually increased with operating time until it was impossible to achieve significant flow of air through the humidifier and cell. Due to the passage of carbon dioxide in the inlet air through the hot tap water, a carbonate type of deposit was forming in the sparger plate. The humidifier was removed from the rig and cleaned with acid and water to remove the

deposit. After reinstallation of the humidifier tank a distilled water feed system was installed to avoid further formation of water insoluble deposits.

2. Setting air flow rate and cell operating pressure was difficult and time consuming. Trim by-pass valves were installed in parallel with the flow control valve and back pressure regulator valve.

3. Additional capacity in condensate storage was required. Two parallel storage bottles with shut-off valves were installed.

4. Water was condensing in the anode gas sample outlet line and the dew point sample outlet line. Condensers and collector bottles were installed in these lines to remove unwanted condensation in test sample lines.

5. Varying water level in the humidifier tank was causing the dew point temperature out of the humidifier tank to vary. An automatic water level control was added to the distilled water feed circuit.

6. Gas inlet lines to the cathode and gas sample lines to the dew cell chamber were running at temperatures below the cell operating temperature. Temperature controlled heater tapes and insulation were added to lines where required.

7. Difficulties in sampling cathode and anode gases below atmospheric pressure were encountered with the oxygen analyzer, wet test meter, and CO_2 analyzer. The anode was replumbed to operate at ambient pressure and a vacuum pump was installed to draw gas samples from the cathode chamber.

8. Erratic readings of dew point temperatures were obtained from the "Dew Cell" sampling element. The element was removed from the rig, and tested and calibrated over the expected operating range.

Numerous other minor changes and modifications were made to improve the performance of the test rig and recording instrumentation as testing proceeded.

For the life testing phase separate anode outlet lines were provided for all cells to more adequately analyze performance of each cell.

6.0 LARGE CELL PARAMETRIC TESTING

6.1 Stage I

The Stage I cell had to be assembled twice before a satisfactory seal was achieved both externally and internally. After all bolts are torqued in a set pattern, the cell is checked for external leaks with the cell dry internally. If seal is satisfactory, the electrolyte charging procedure is initiated. The entire cell cavity is put under a vacuum and then electrolyte is allowed to completely fill the void. Excess electrolyte is then drained from the cell, leaving only that electrolyte which wets the matrix. Gas pressure is then applied to one gas cavity with the other cavity being open to the atmosphere. The fully charged matrix, after the second assembly, successfully withstood a 16 psi pressure differential from anode to cathode cavity.

The fully charged cell was installed in the module rack and installed in the test stand. A check of air flow through the system and the Stage I cathode chamber was made. Pressure drops across the cathode cell field and across the entire cathode chamber (including inlet and outlet ports) checked with the calculated design values.

Figures 6-1 and 6-2 show a typical cell instrumented and installed in the test rig.

Several early test runs were terminated due to difficulties with the test rig. The difficulties and the corrective action were discussed in Section 5.0.

Normal test procedure followed during parametric testing was as follows:

1. With cell isolated from rest of system, heat the cell and humidifier to desired operating temperature.

2. Establish gas flow through humidifier while bypassing cell cathode chamber.

3. Establish proper gas composition.

4. Switch gas flow through the cathode chamber.

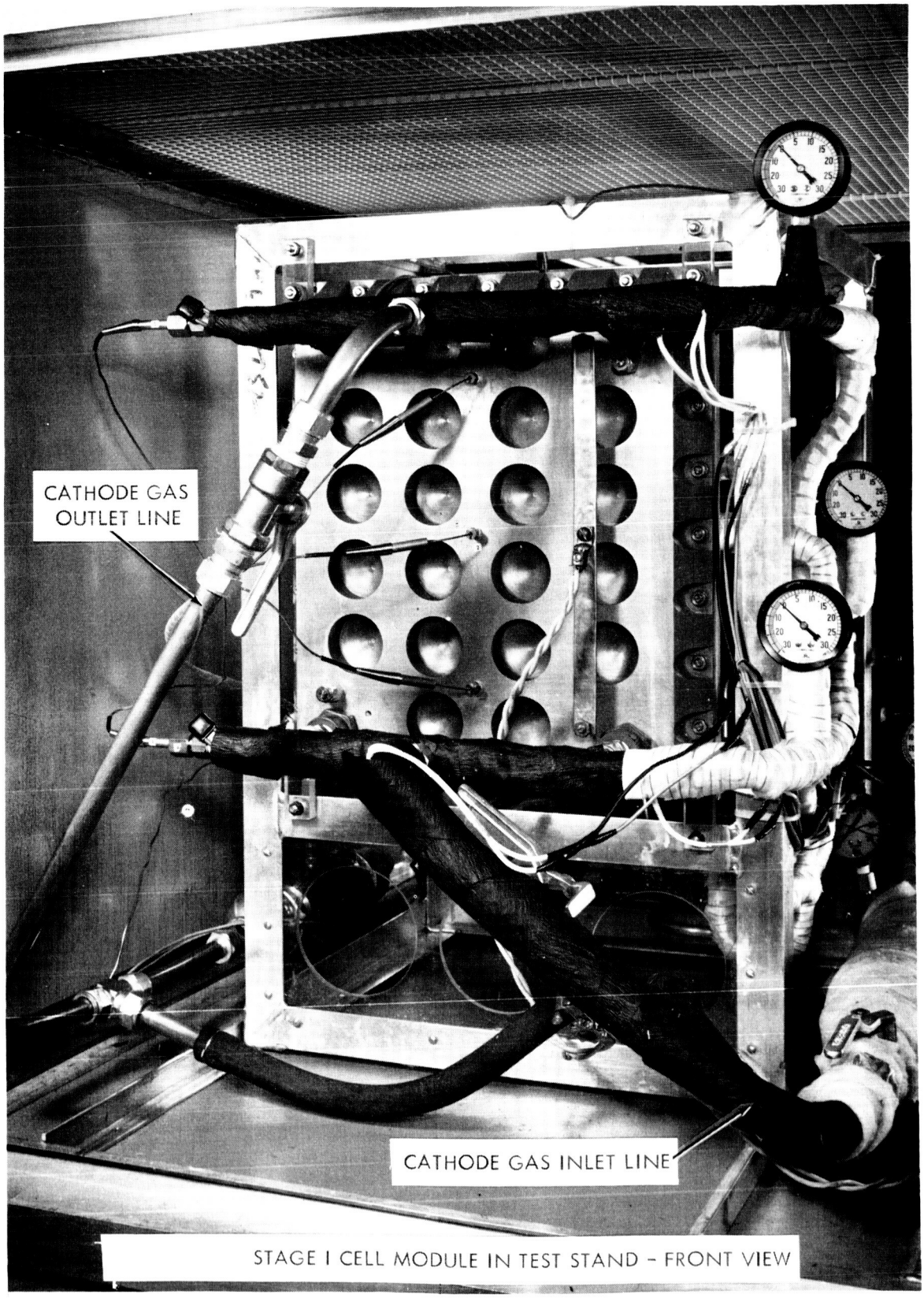

STAGE I CELL MODULE IN TEST STAND - FRONT VIEW

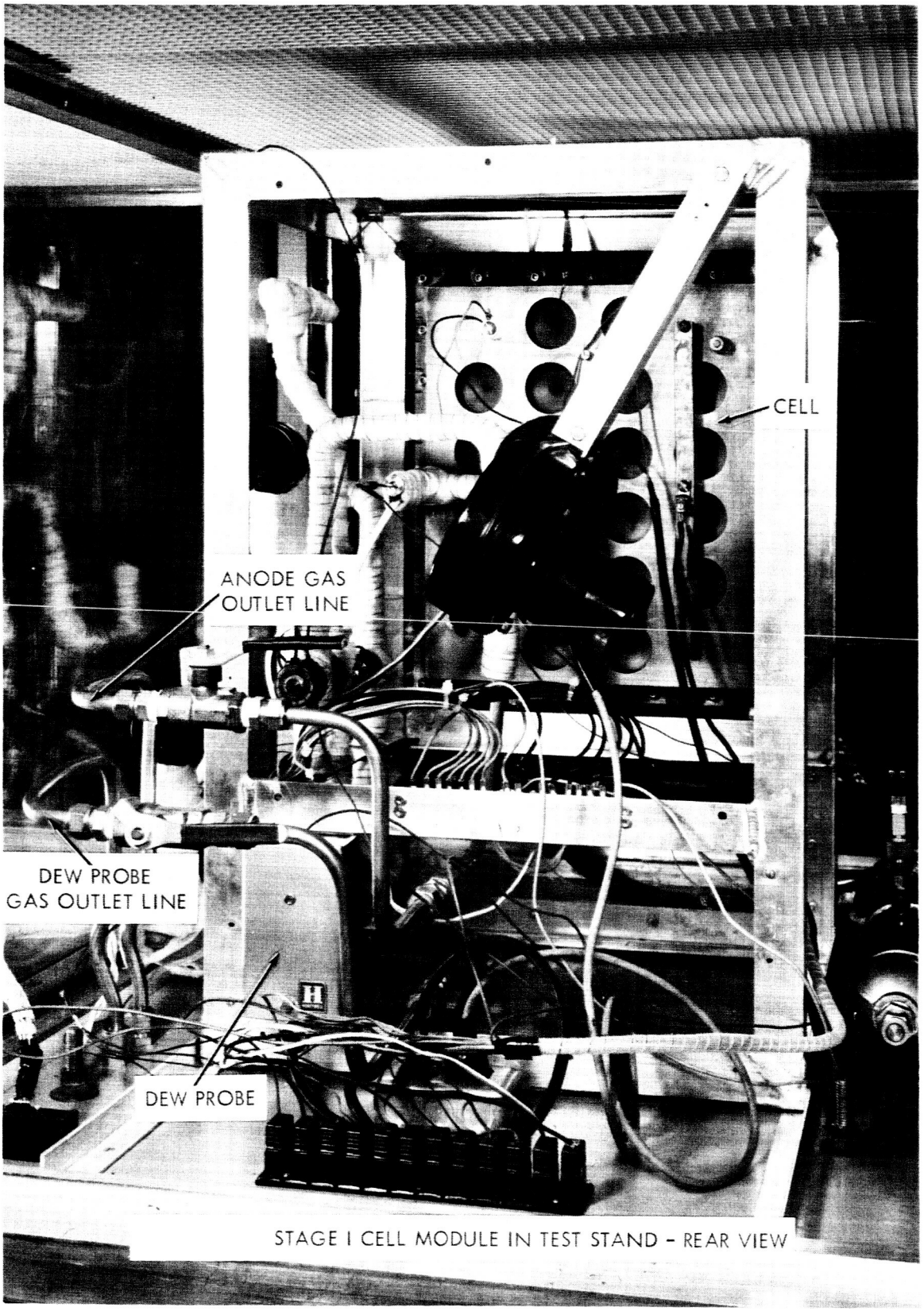

STAGE I CELL MODULE IN TEST STAND - REAR VIEW

5. Turn on cell power.

6. Periodically determine gas composition of cathode inlet gas, cathode outlet gas, and anode outlet gas. Measure anode gas flow rate.

7. Maintain operation for a four-hour period.

8. Cut off cell power.

9. Stop cathode gas flow.

10. Isolate cell cavity from rest of system to maintain proper cell water balance.

11. Repeat procedure for each desired cell operating point.

The direct current power supply used was not a constant current device, therefore some of the variations in cell performance were due to variations in the cell power applied.

6.1.1 Current Density Effect

Figure 6-3 presents the effect of cell current density on cell performance for three cell operating temperatures. The current, given in amperes, is the same value as the current density in amps/ft^2, since the cell active electrode area is one square foot. At a cell temperature of 90°F the 30 ampere point was maintained for only a short period (10 minutes) because of the high cell voltage. All the data points used are for a cathode gas flow rate based on twice the stoichiometric CO_2 requirement at a given cell operating current. It also should be noted that the electrolyte concentration was not identical for all runs due to the variations in make-up from batch to batch.

6.1.2 Cell Temperature Effect

Figure 6-4 is a cross-plot obtained from Figure 6-3, showing the strong effect cell temperature has on cell current density for a given voltage. Similar curves for the voltage as a function of cell temperature at a constant current can be drawn using the data from Figure 6-3.

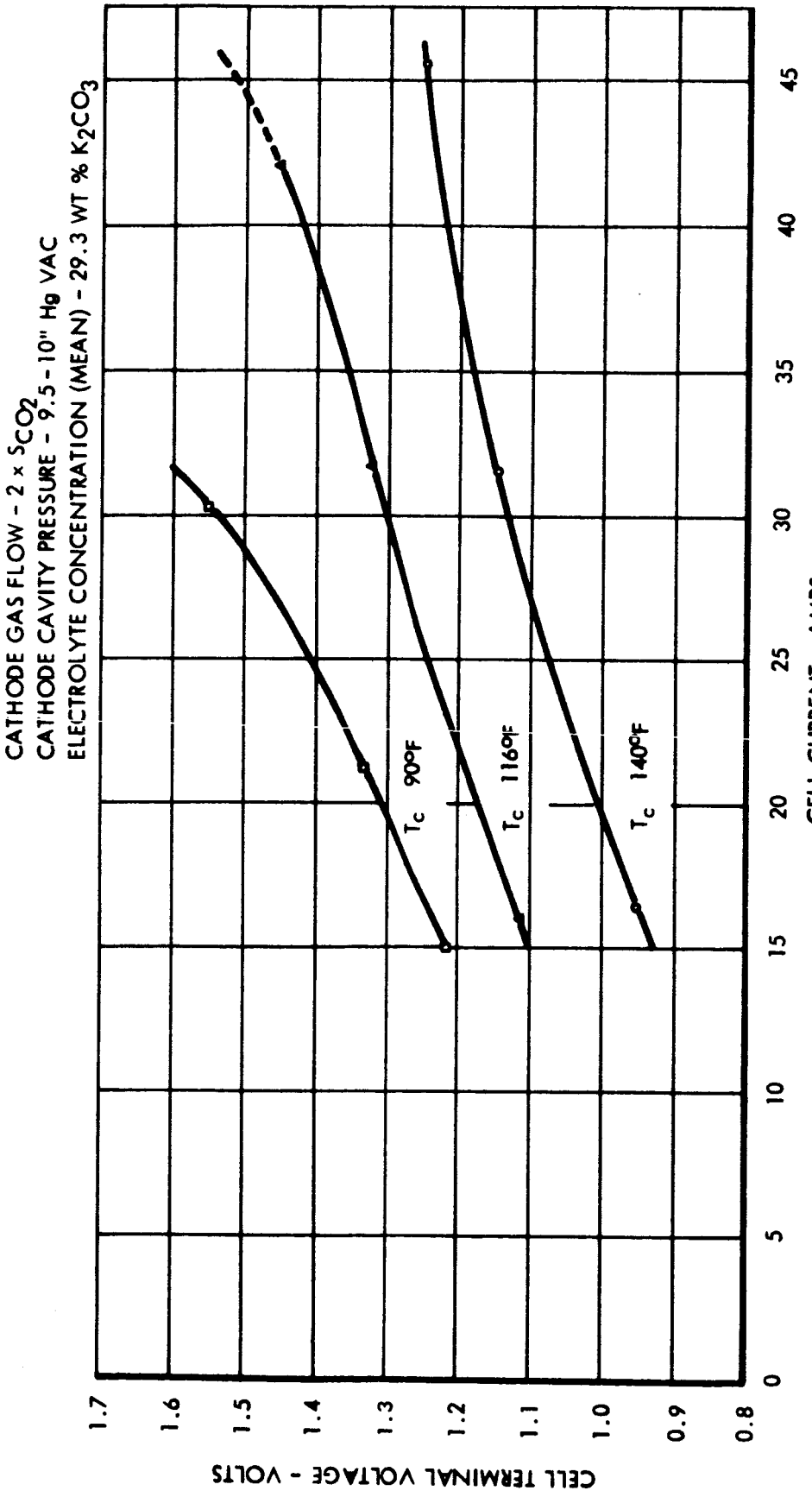

FIGURE 6-3 CELL VOLTAGE AS A FUNCTION OF CELL CURRENT STAGE I

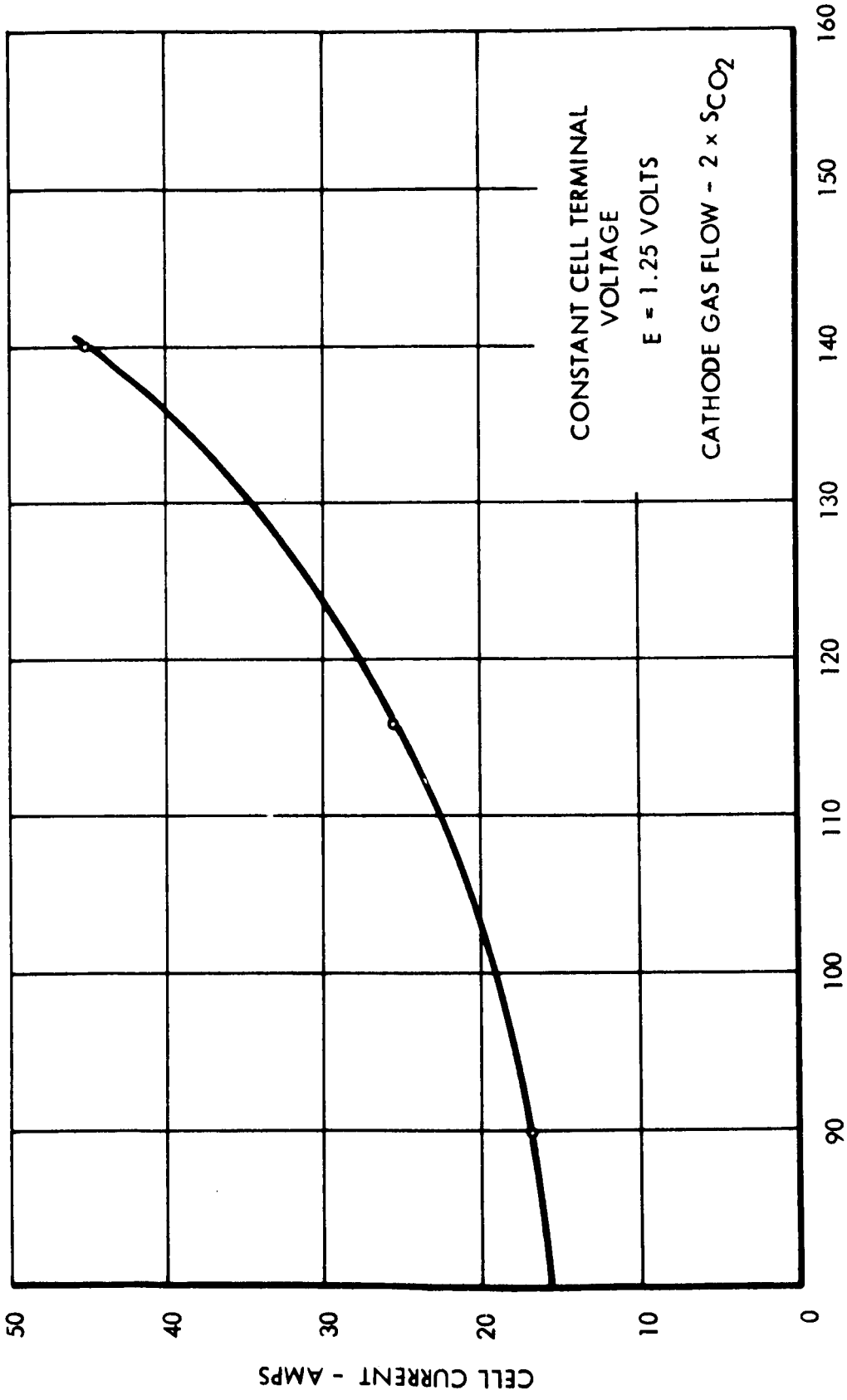

FIGURE 6-4 STAGE I CELL CURRENT AS A FUNCTION OF CELL TEMPERATURE

6.1.3 Cathode Gas Flow Rate Effects

The cathode gas flow was normally maintained at twice stoichiometric CO_2 with one run at a 5 x S_{CO_2} flow. There were however two runs made at a cathode flow of 1 x S_{CO_2}, made when the cell current was increased from 15 amps to 30 amps prior to increasing the cathode gas flow to match the higher current. Using the data obtained at these additional flow ratios, Figure 6-5 was plotted to show the effect of the stoichiometric flow ratio on cell voltage and per cent of CO_2 in the anode gas output. At the very low ratios, cell electrical performance improves at the expense of the per cent CO_2 transferred across the cell. The change in cell voltage at the low flow ratio may be due to a change in electrolyte composition as the average CO_2 partial pressure in the cathode cavity falls below a certain critical value as CO_2 is scrubbed from the air by the electrolyte.

6.1.4 Carbon Dioxide Transfer

The per cent of CO_2 in the anode gas and the CO_2 transfer rate as a function of cell current density are given in Figure 6-6 for the three cell temperatures. The apparent increase of the CO_2 transfer rate with current density between 15 and 30 ASF at 140°F is not statistically significant. The observed CO_2 transfer rate at 30 ASF has a deviation from the arithmetic mean which was twice as great as all other observations in this test series. However, it should be noted that the effect of increasing the current density at all temperatures was to significantly depress the CO_2 transfer rate.

6.1.5 Polarization Time Dependence

Figures 6-7 through 6-15 give the polarization time dependence for the required test conditions. Comments concerning some of the runs are given below. Where no comments for a run are given, no further data, other than that on the graph, is readily available to explain odd shapes in the polarization curves. As stated, the cell current in amperes is equivalent to the cell current density in amps/ft^2.

1. Figure 6-7. This was the first operating condition after the test rig modifications were completed. An overnight run was completed to check the rig for proper operation, resulting in a test run just short of 24 hours in duration.

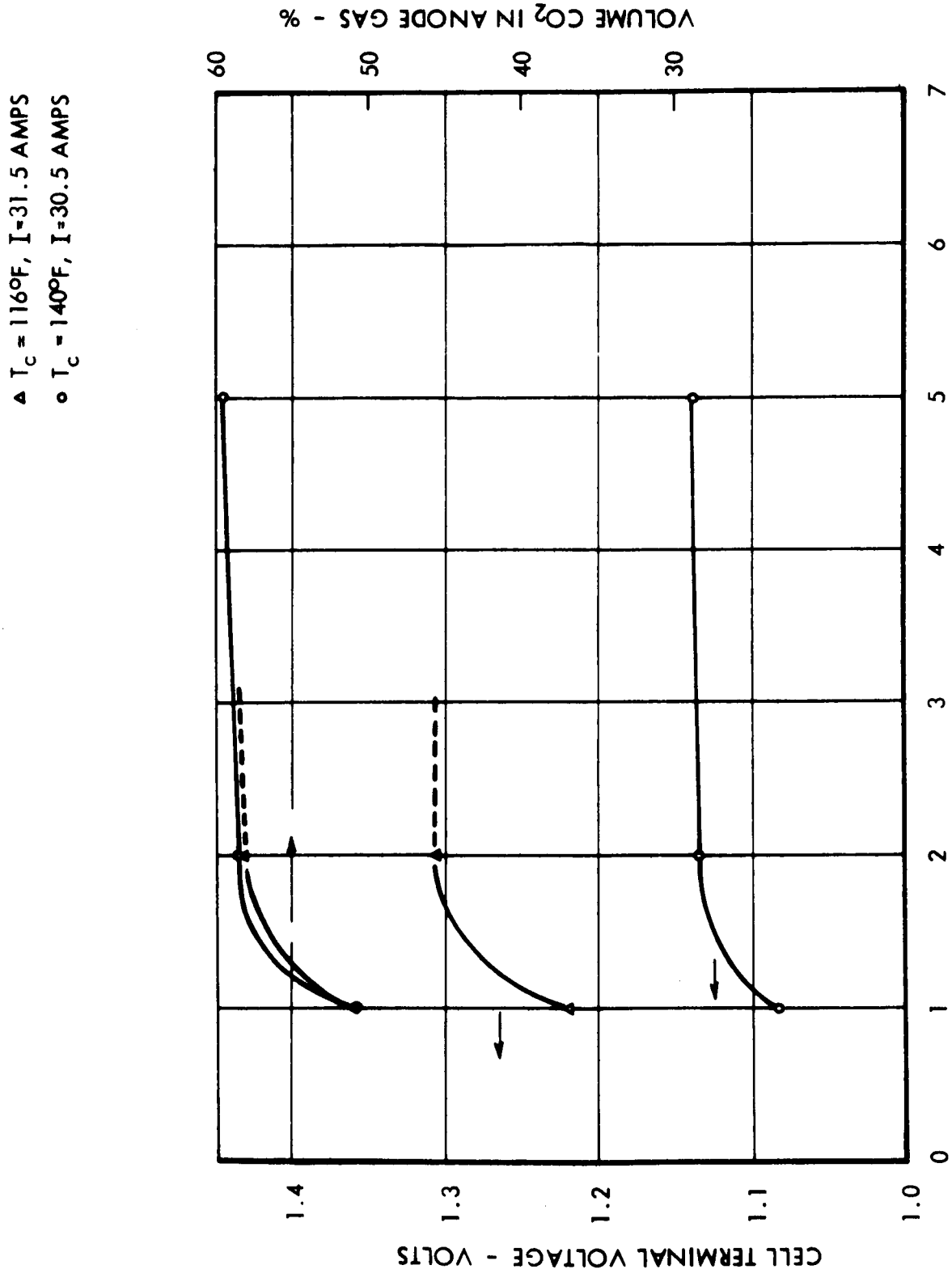

FIGURE 6-5 CELL PERFORMANCE AS A FUNCTION OF CATHODE GAS FLOW RATE
STAGE I

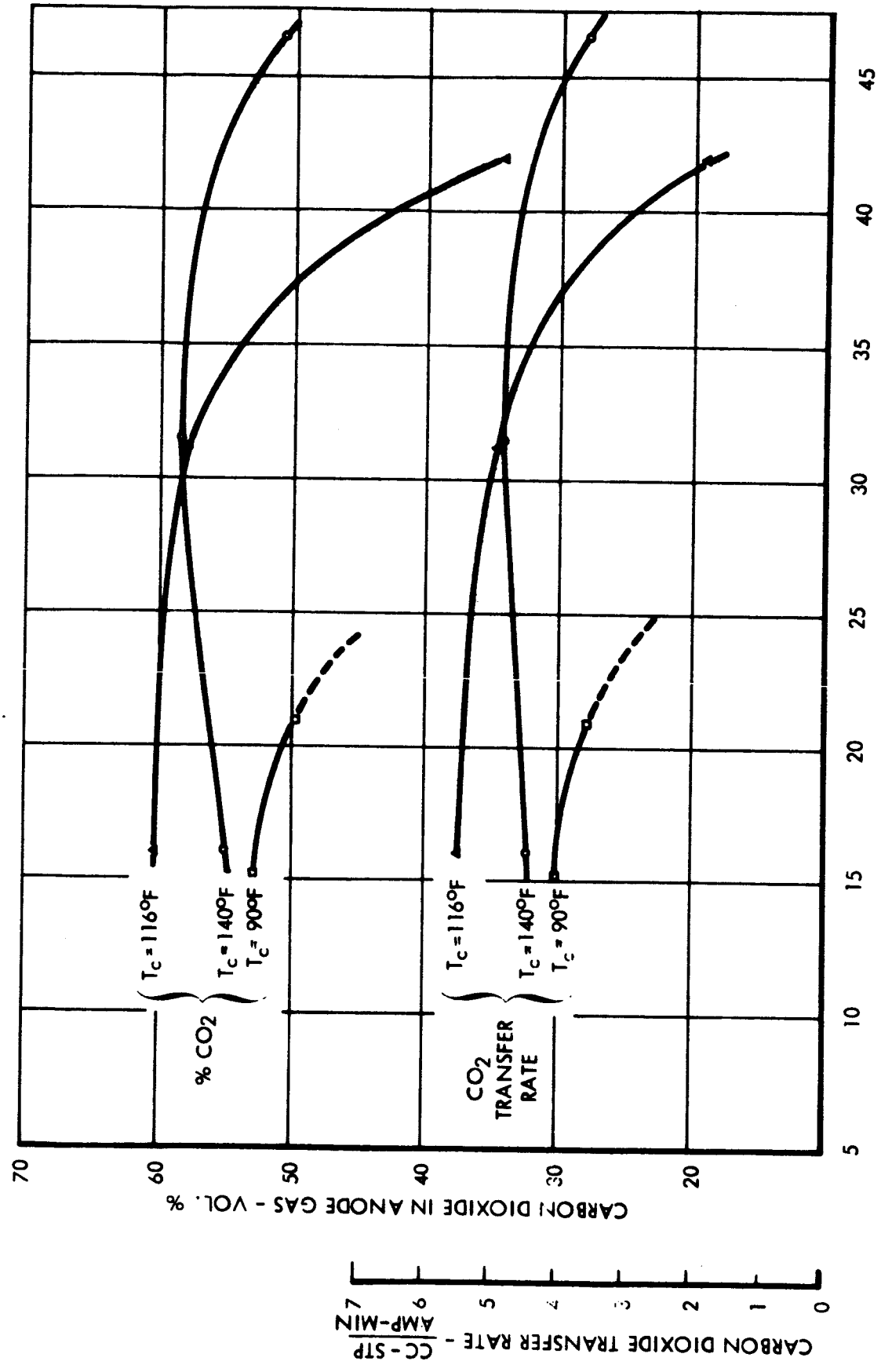

FIGURE 6-6 CARBON DIOXIDE TRANSFER AS A FUNCTION OF CELL CURRENT STAGE I

CELL CURRENT ~ 15 AMPS
CELL TEMPERATURE - 140°F
CATHODE GAS INLET DEW POINT - 133°F
CATHODE CAVITY PRESSURE - 9.5 - 10" Hg VAC
CATHODE GAS FLOW - $2 \times S_{CO_2}$ (15 AMPS)
ELECTROLYTE CONCENTRATION - 28.4 WT % K_2CO_3
T_c RANGE - 138.5 - 140.5°F
T_{DP} RANGE - 132 - 133.5°F

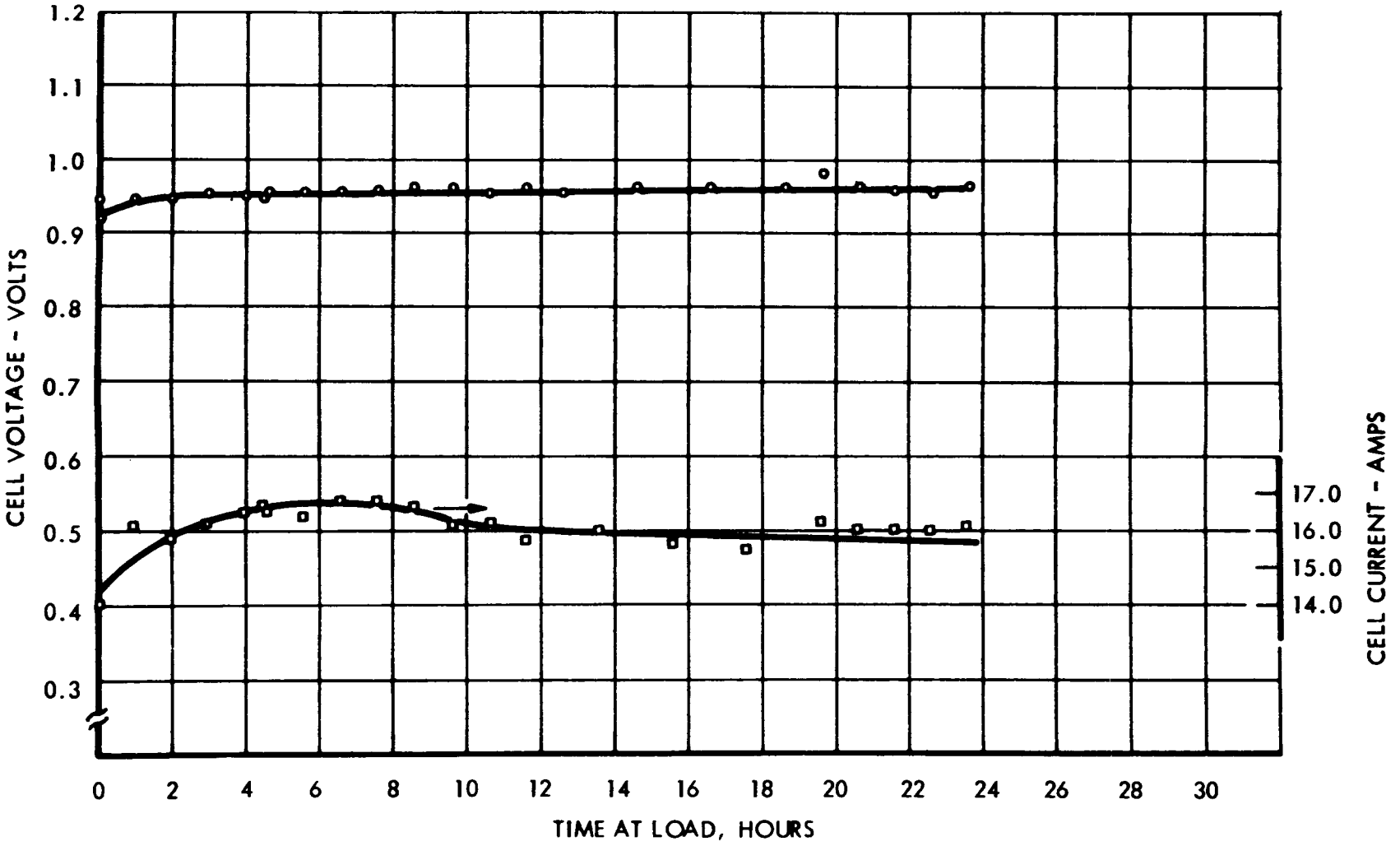

FIGURE 6-7 STAGE I CELL - POLARIZATION TIME DEPENDENCE, T = 140°F, I = 15

2. Figure 6-8. The cell current was decreased at t = 206 minutes to bring the current closer to the 30 ampere nominal operating point.

3. Figure 6-11. As indicated on the graph, adjustments in the cathode gas flow were made early in the run after the power to the cell had been turned on. The steady rise in cell voltage is due to the steady increase in the cell current density. At t = 200 minutes the power relay controlling the humidifier heater stuck in the on position. A rapid increase in the cell temperature and inlet gas dew point temperature caused a rapid decrease in cell voltage and increase in cell current. The high dew point of the incoming gas ($200^{\circ}F$) then rapidly flooded the cell causing complete deterioration in cell performance.

4. Figure 6-12. The large voltage fluctuations are due primarily to the wide cell temperature changes. Control of the cell temperature became difficult at the high power input level at this low operating temperature ($115^{\circ}F$). Nearing the end of the run, the cell stabilized as better temperature control of the cell was achieved.

5. Figure 6-14. After twelve minutes of operation, cell current was decreased from 30 amps to 21 amps without change in gas flow. Fluctuating cell temperature and inlet gas dew point temperature caused erratic operation. At t = 185 minutes, the cathode gas flow was adjusted to 2 x S_{CO_2} for the 20 amp operating level. Stable performance was achieved as proper humidifier and cell temperatures were established.

6. Figure 6-15. This run was at the 5 x S flow ratio. Again it is seen that the cell temperature ($136 - 143^{\circ}F$) and inlet gas dew point temperature ($131.5 - 134.5^{\circ}F$) varied over a considerable range contributing to variable cell performance. The cell current was adjusted at t = 212 minutes and t = 237 minutes.

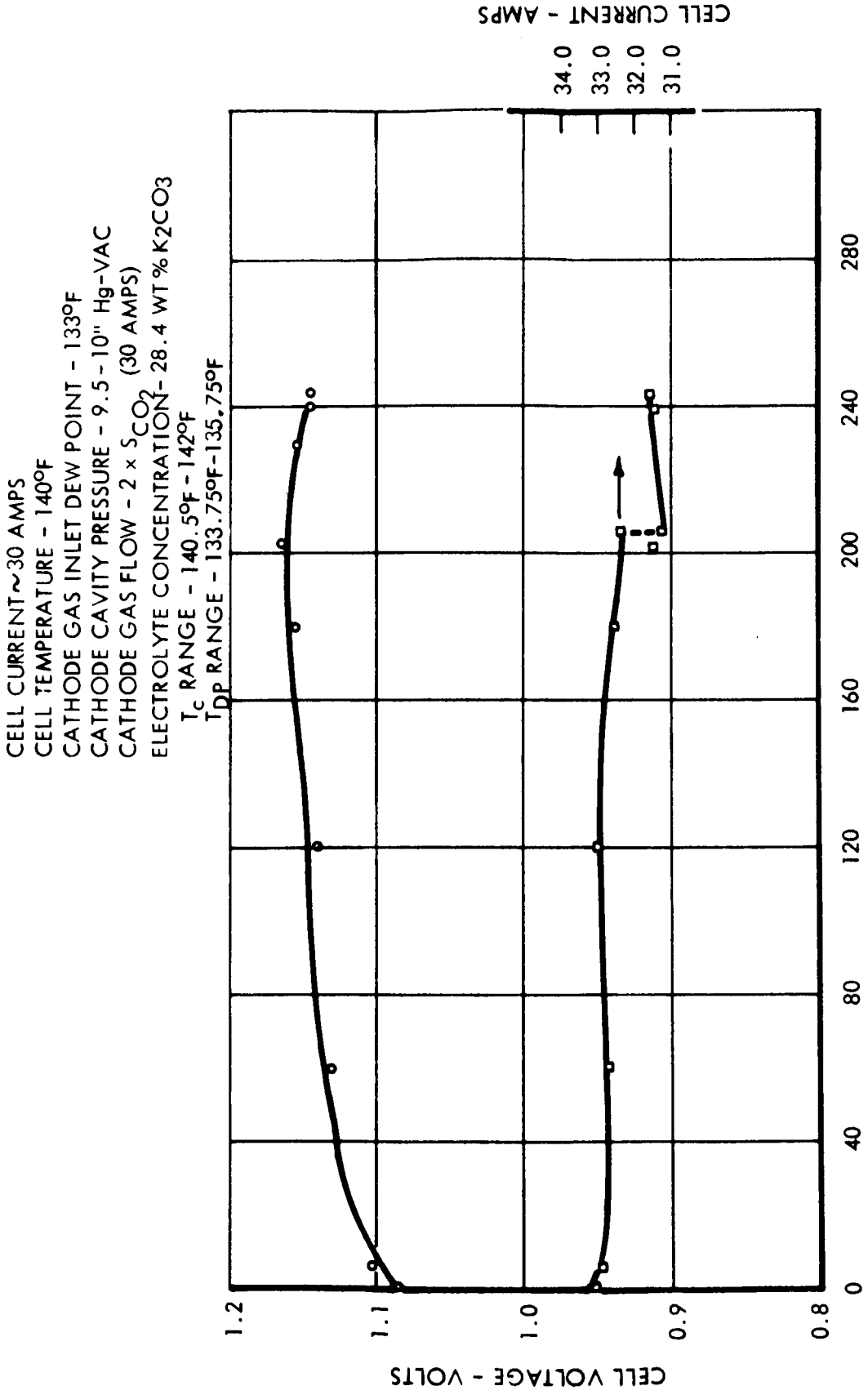

FIGURE 6-8 STAGE I CELL - POLARIZATION TIME DEPENDENCE, T = 140°F, I = 30

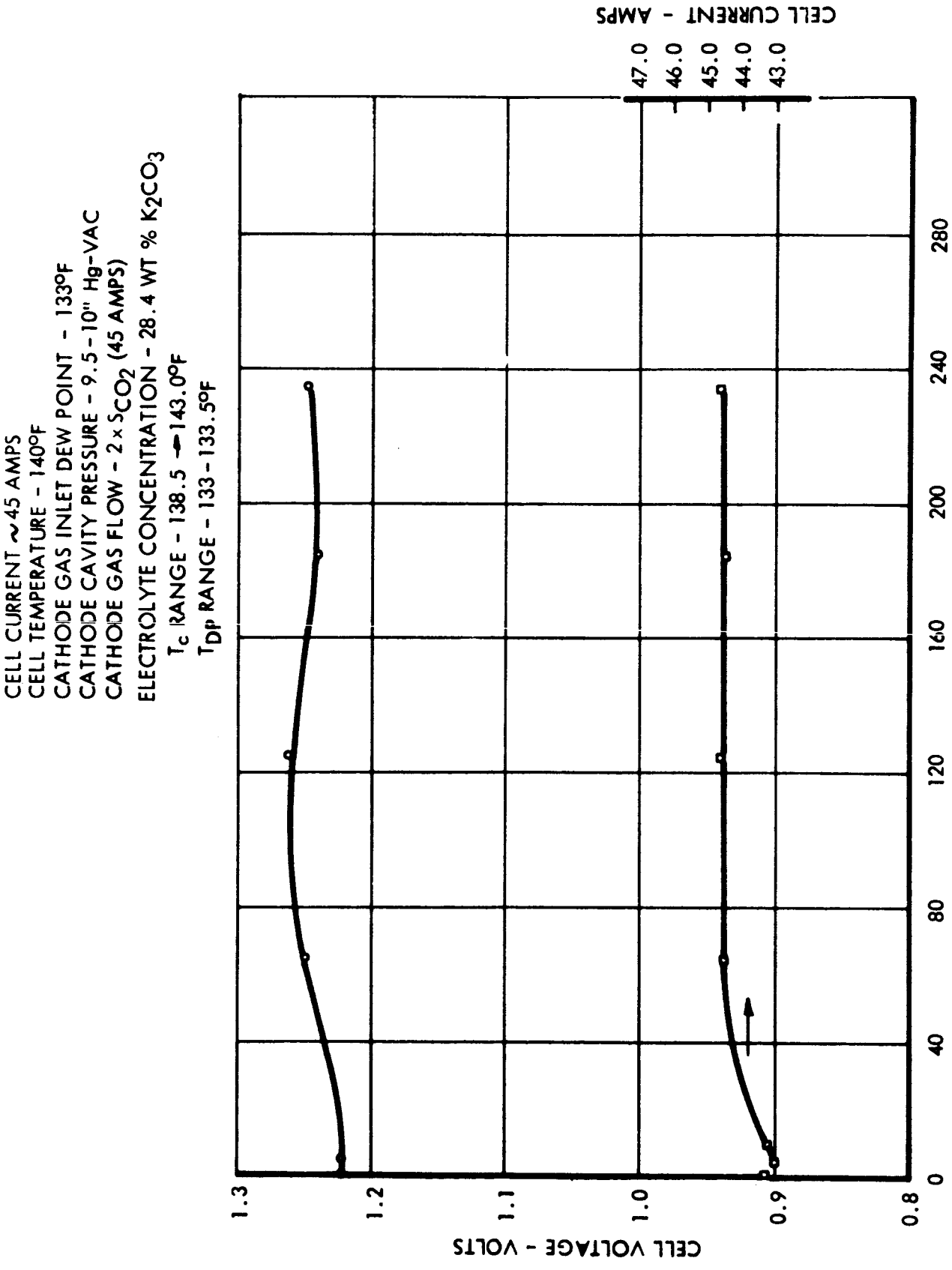

FIGURE 6-9 STAGE I CELL - POLARIZATION TIME DEPENDENCE, T = 140°F, I = 45

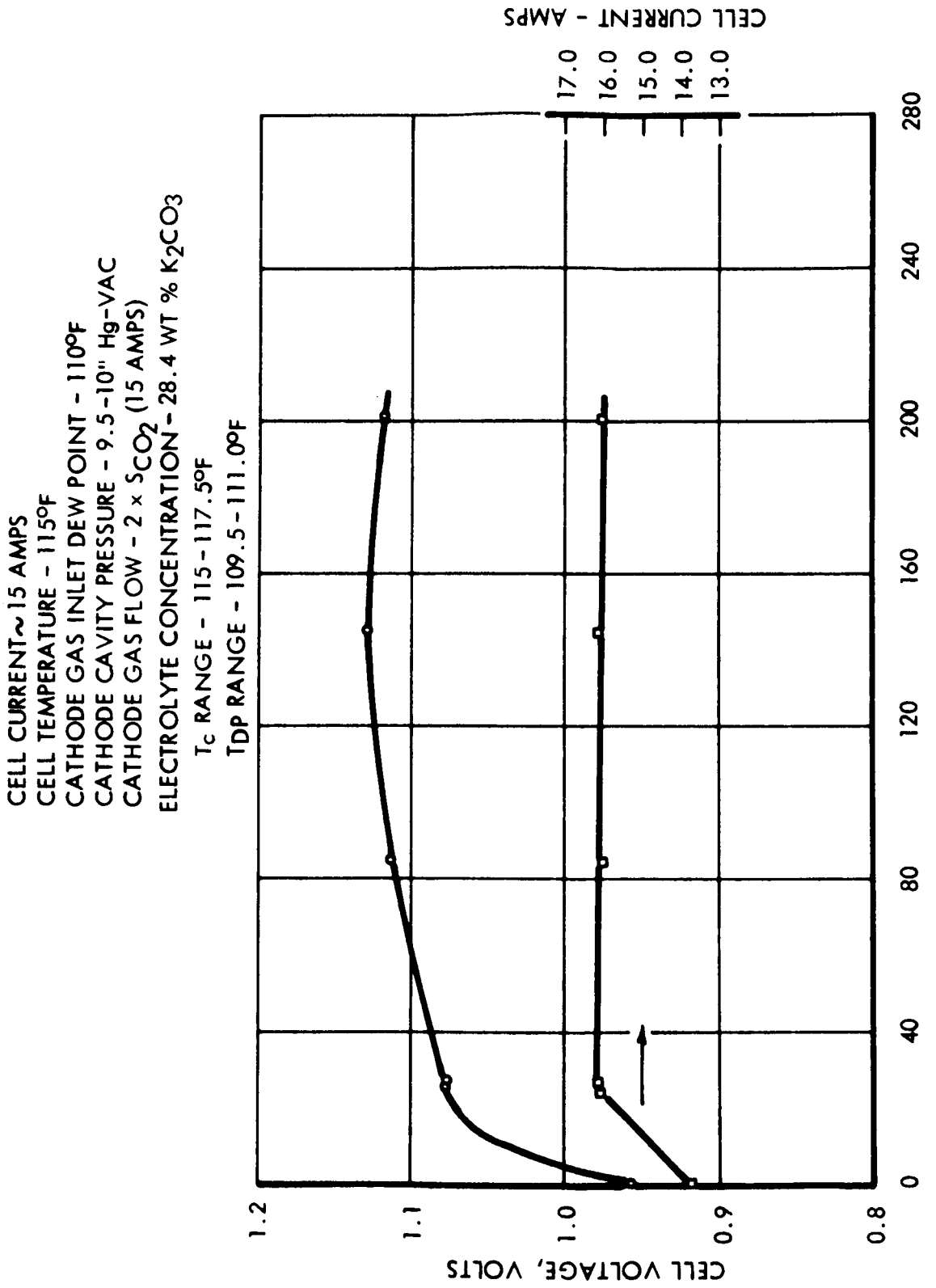

FIGURE 6-10 STAGE I CELL - POLARIZATION TIME DEPENDENCE, T = 115°F, I = 15

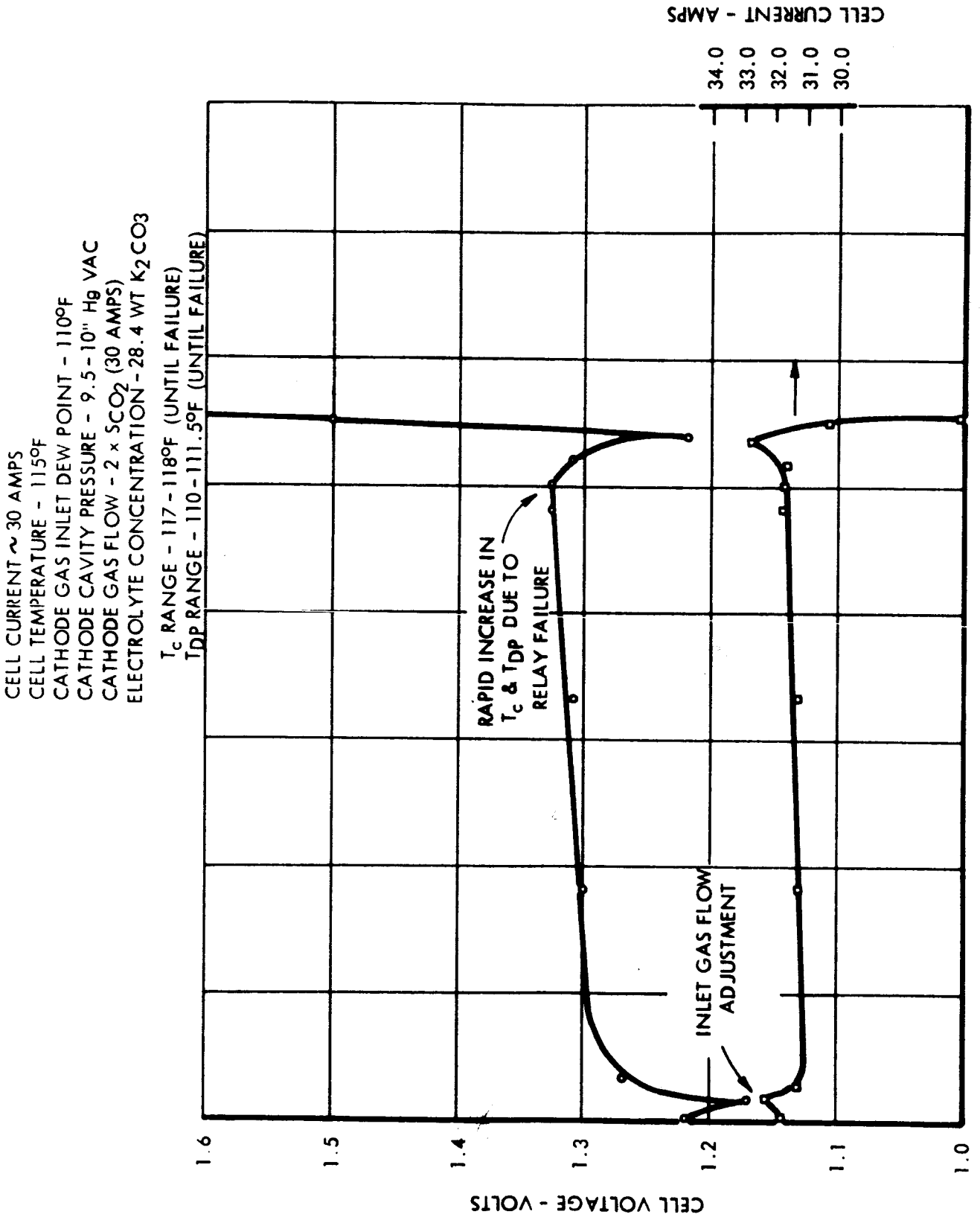

FIGURE 6-11 STAGE I CELL - POLARIZATION TIME DEPENDENCE, T = 115°F, I = 30

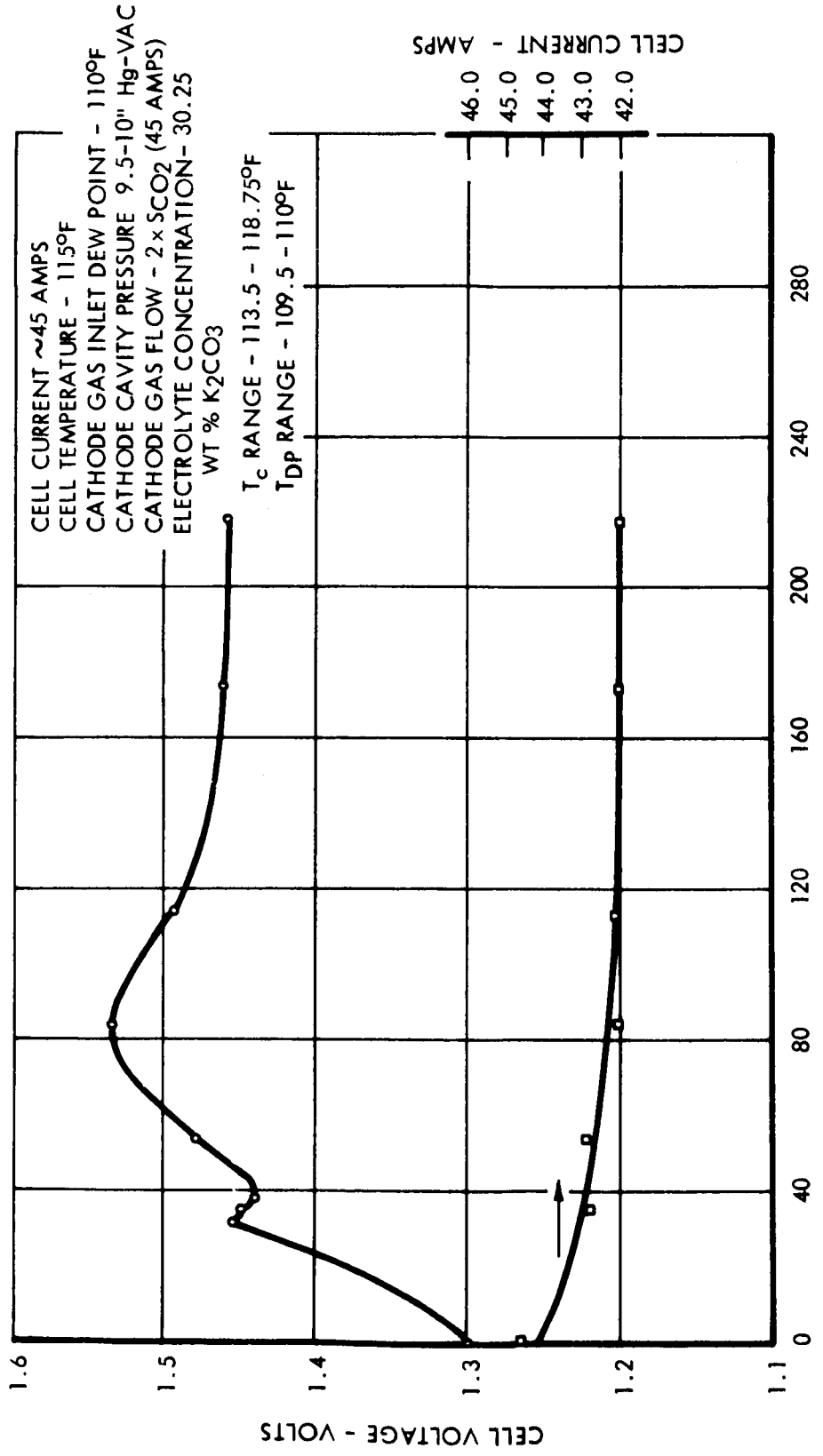

FIGURE 6-12 STAGE I CELL - POLARIZATION TIME DEPENDENCE, T=115°F, I=45

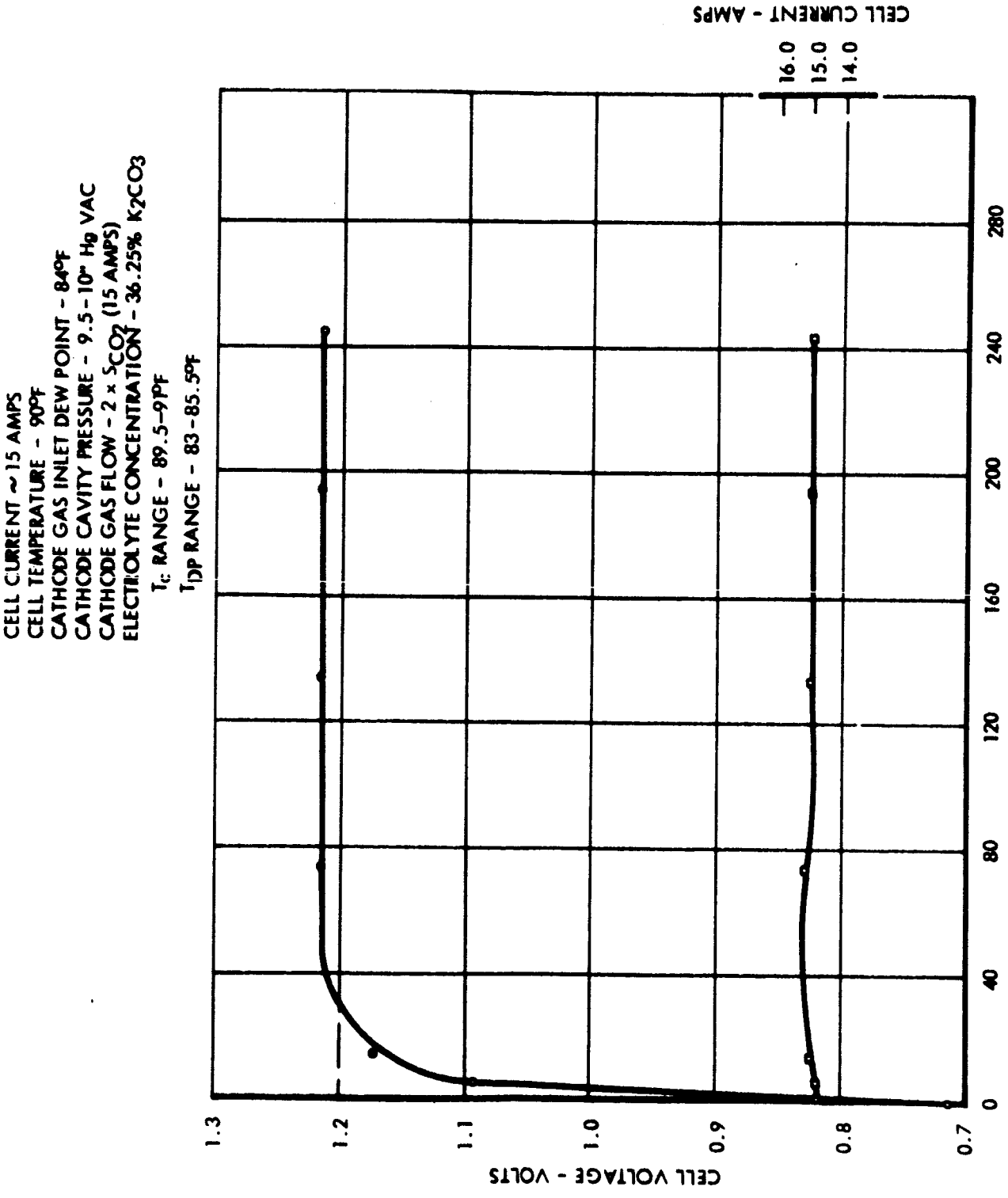

FIGURE 6-13 STAGE I CELL - POLARIZATION TIME DEPENDENCE, T = 90°F, I = 15

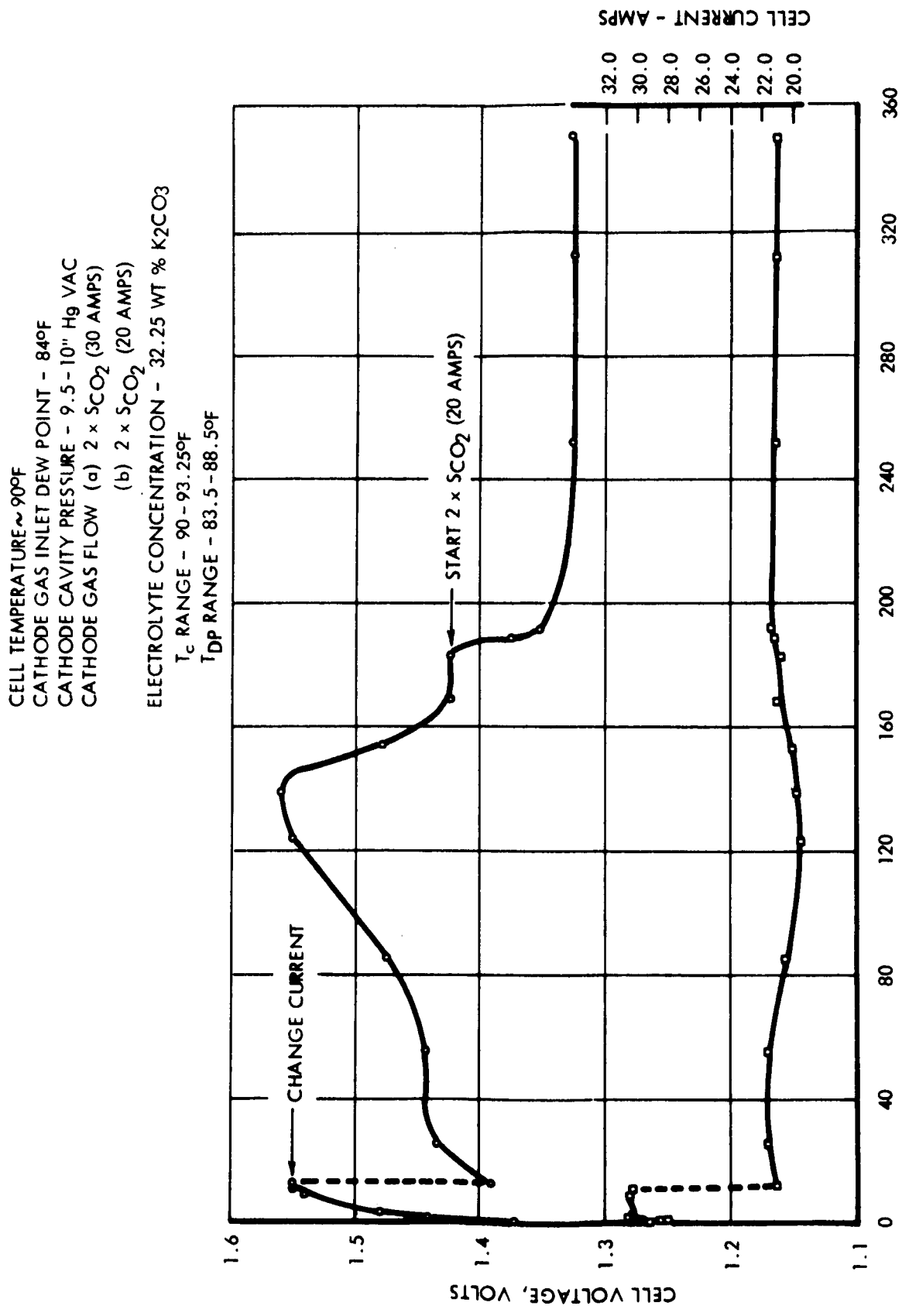

FIGURE 6-14 STAGE I CELL - POLARIZATION TIME DEPENDENCE, T = 90°F, I (20-30)

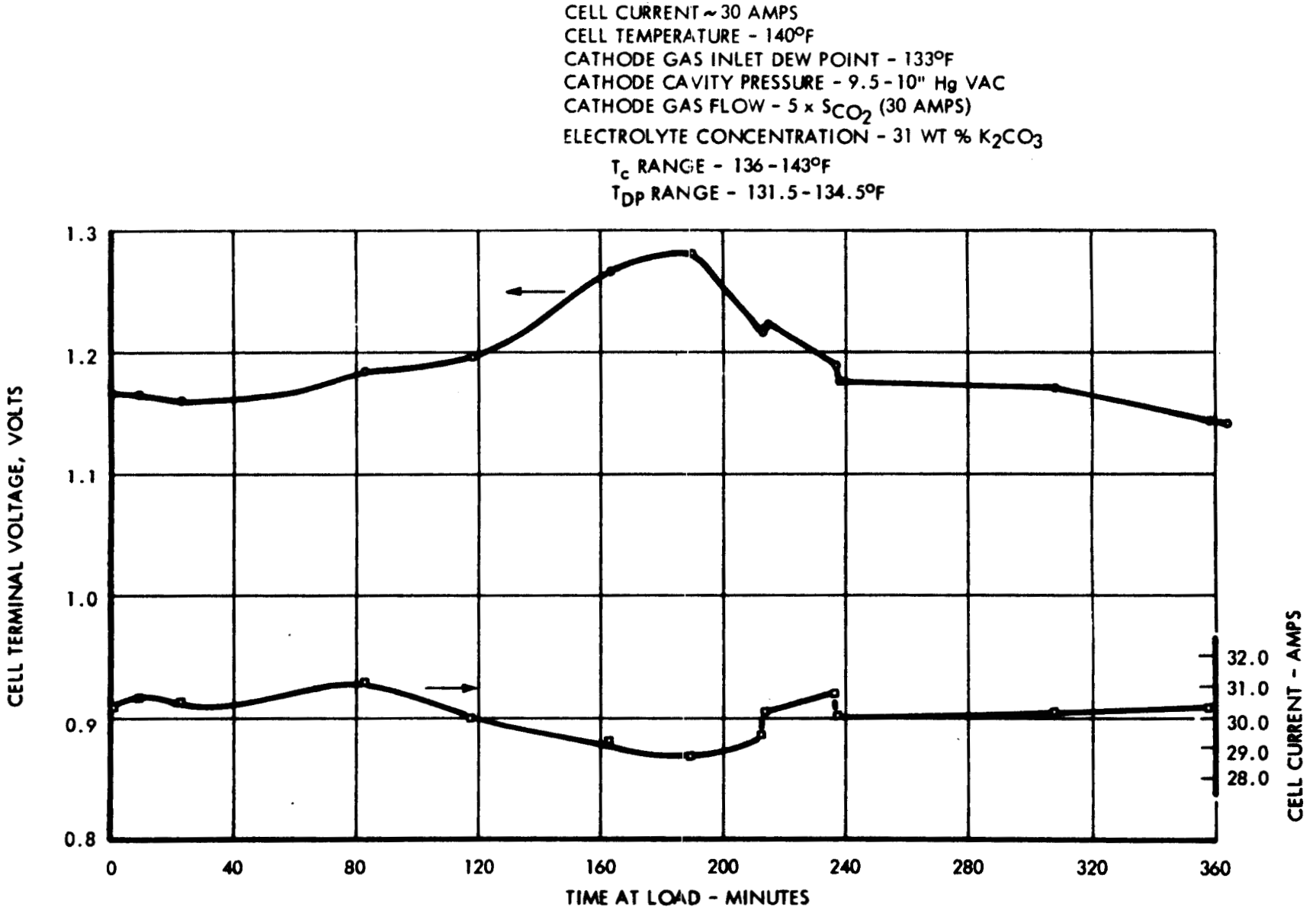

FIGURE 6-15 STAGE I CELL - POLARIZATION TIME DEPENDENCE, T = 140°F, I=30, 5 x S FLOW

6.2 Stage II

The assembly of the Stage II cell was more complex than the Stage I cell due to the recessed liquid cavity and gas diffusion plate. A gas-tight seal was established between the recessed cavity and the gas diffusion plate while maintaining electrical continuity. To eliminate unnecessary errors in measuring the cell potential, a wire was attached directly to the gas diffusion plate and passed out of the cell through one of the gas manifold outlets. Use of this wire by-passed the problems associated with connecting directly to the cathode end plate. The other lead for potential measurement was attached to the anode end plate since this end plate contacts the anode directly.

Electrolyte charging of the cell was the same as with Stage I. The cell was checked for internal sealing from cathode chamber to anode chamber and from cathode to liquid reservoir chamber. Upon establishment of a proper seal the cell was installed in the module and the test rig.

Normal test procedure followed during parametric testing was the same procedure outlined in Section 6.1 for Stage I.

6.2.1 Current Density Effect

Figure 6-16 presents the effect of cell current density on cell performance for the two cell operating temperatures. The current, given in amperes, has the same value as the current density in amps/ft^2, since the cell active electrode area is one square foot. At a cell temperature of 122^{o}F the highest current was 30 amperes since higher currents caused operating voltages in the region of possible electrolysis. All the data points were obtained using a cathode gas flow rate based on one times stoichiometric CO_2 requirement at a given cell operating current.

6.2.2 Carbon Dioxide Transfer

The per cent CO_2 in the anode gas and the CO_2 transfer rate as a function of cell current are given in Figure 6-17 for the two cell operating temperatures. Both the percentage and transfer rate decrease with increasing cell current density. The point at 22.5 amperes for the 122^{o}F cell temperature in low probably due to variations in experimental conditions or the actual decay with time of the transfer rate which was noted in the life testing. The 22.5 ampere point was the last data point taken on the Stage II short term tests.

6.2.3 Polarization Time Dependence

Figures 6-18 through 6-23 give the Polarization time dependence for each of the six test conditions. Operating conditions and cell operating current are also given for each run.

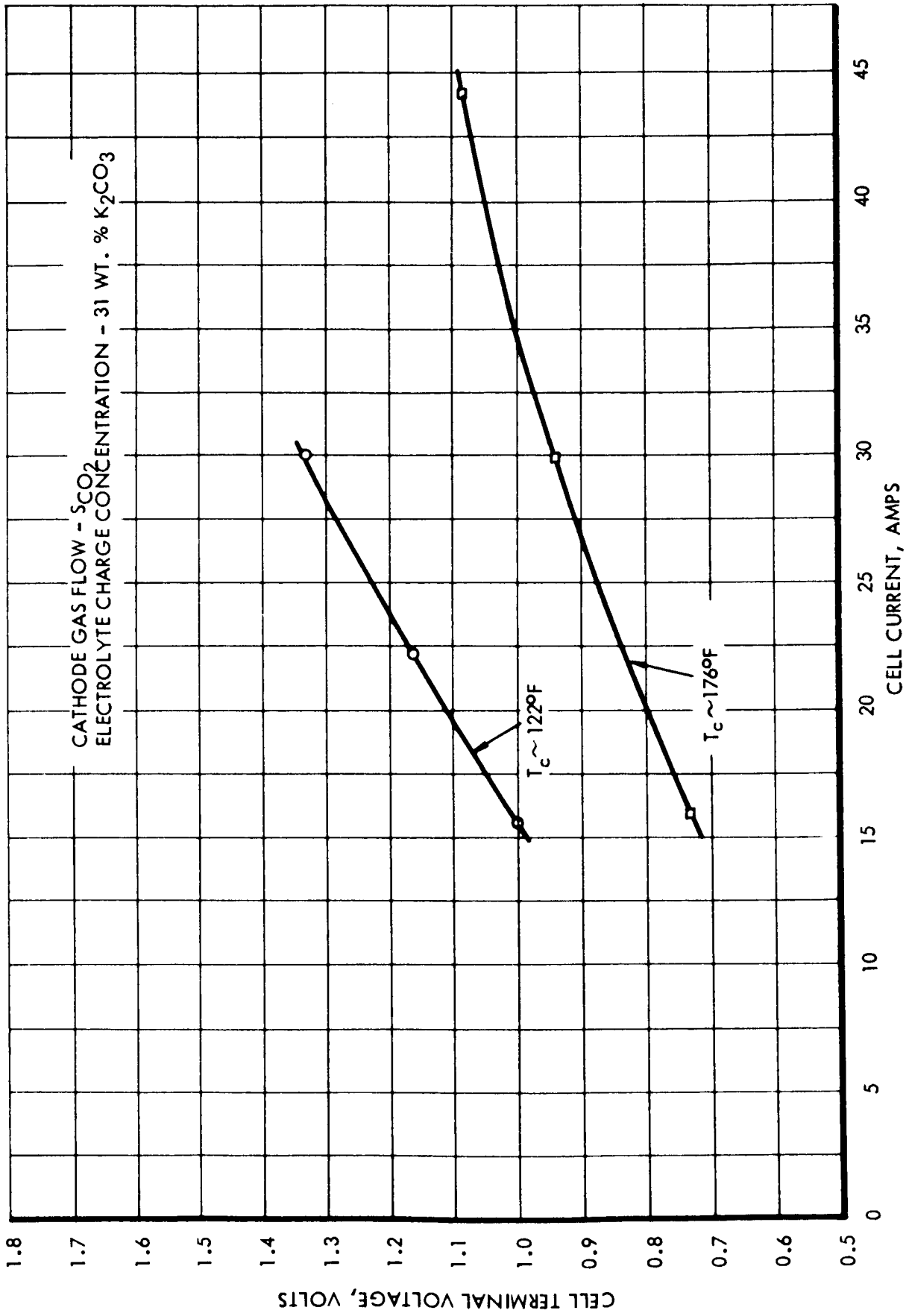

FIGURE 6-16 STAGE II CELL VOLTAGE AS A FUNCTION OF CELL CURRENT

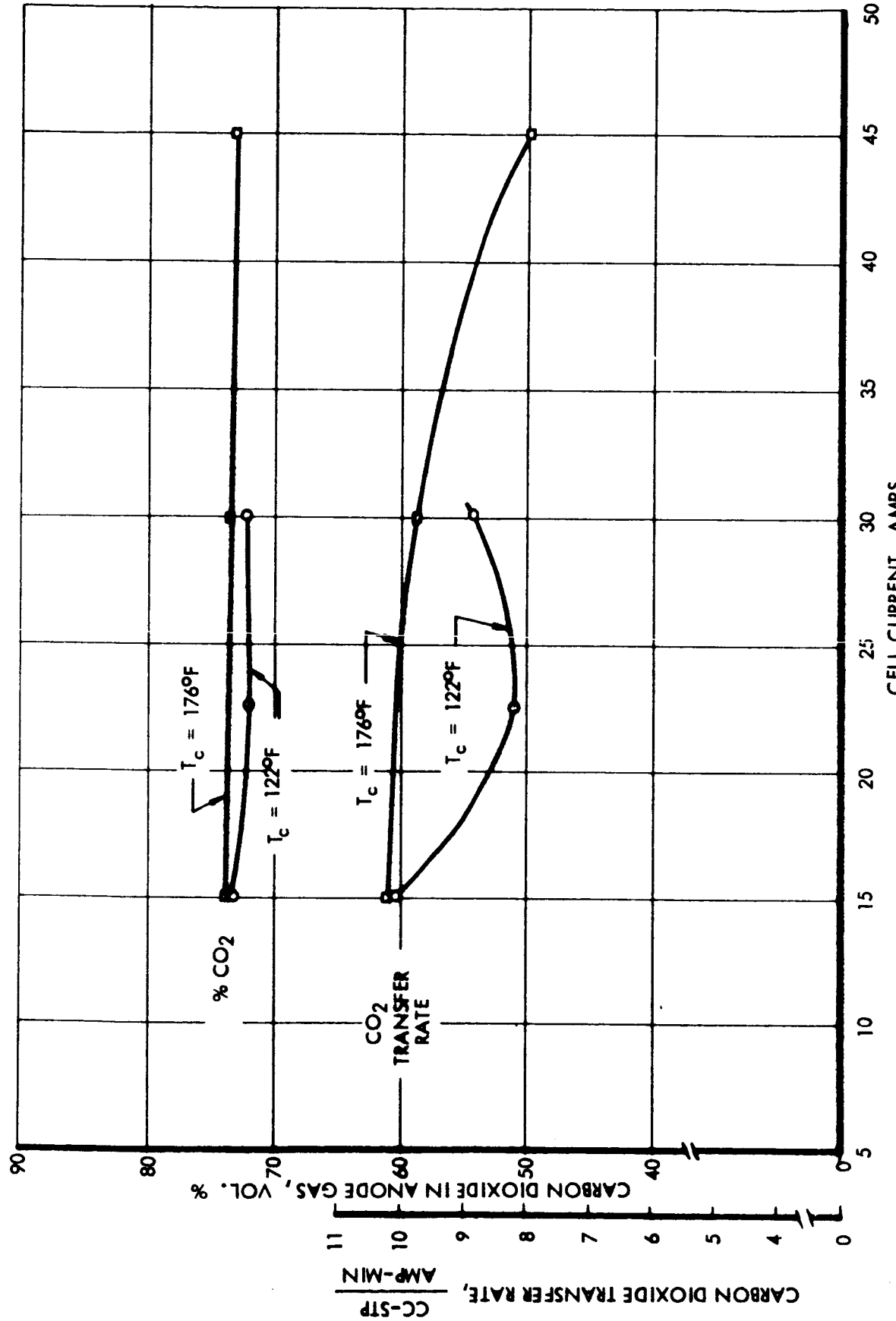

FIGURE 6-17 STAGE II CELL, CARBON DIOXIDE TRANSFER AS A FUNCTION OF CELL CURRENT

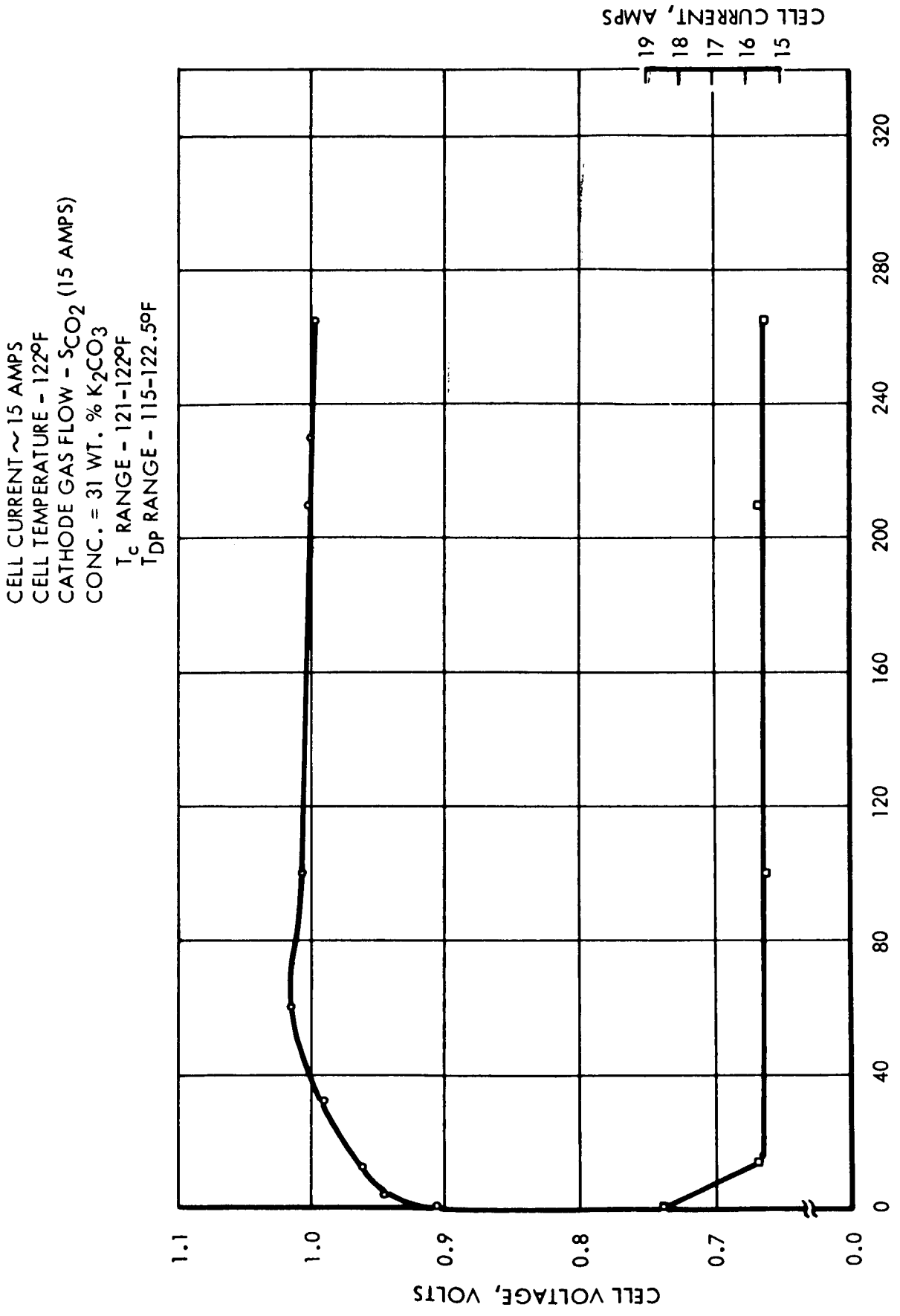

FIGURE 6-18 STAGE II CELL - POLARIZATION TIME DEPENDENCE, T = 122°F, I = 15

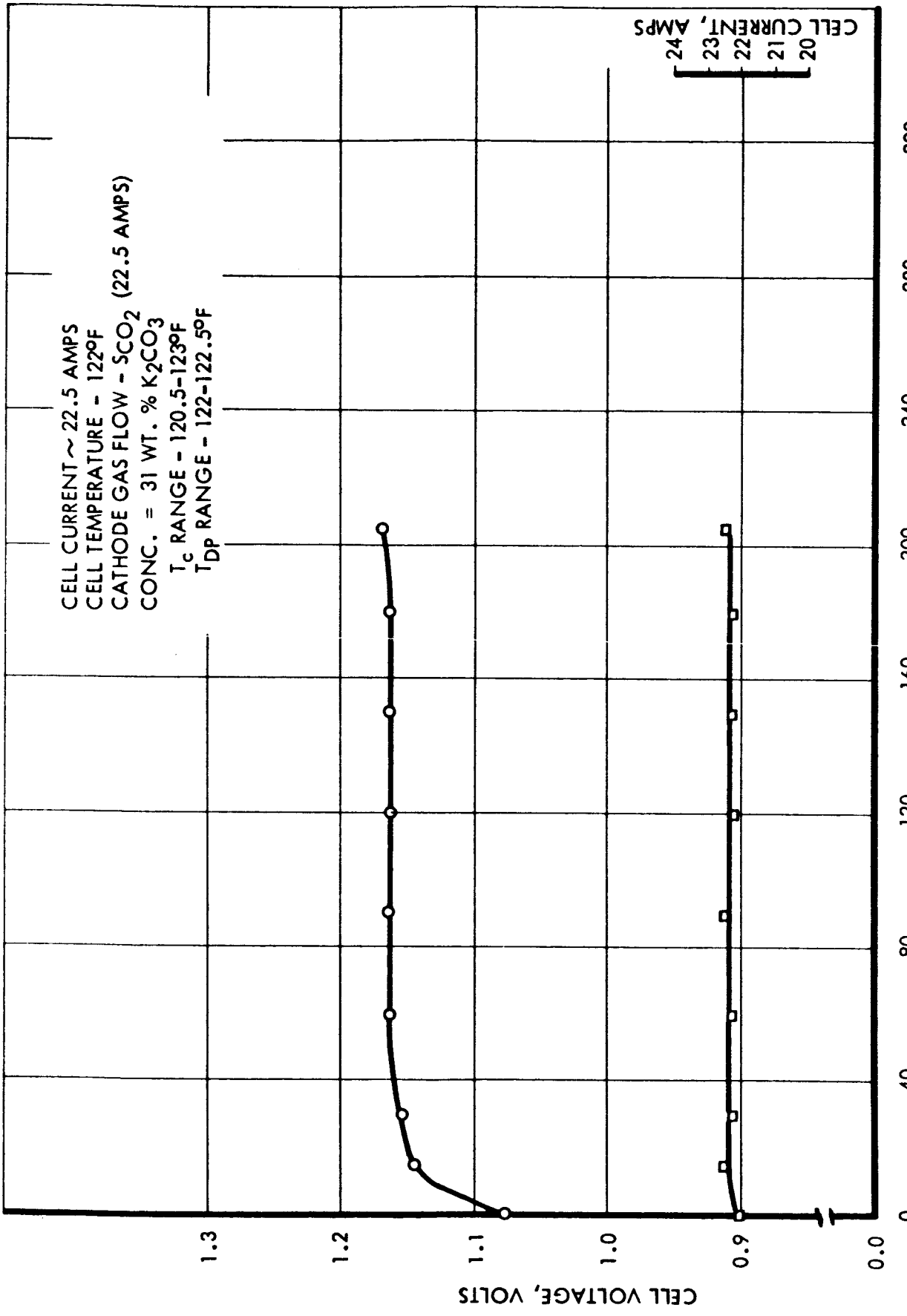

FIGURE 6-19 STAGE II CELL - POLARIZATION TIME DEPENDENCE, T = 122°F, I = 22.5

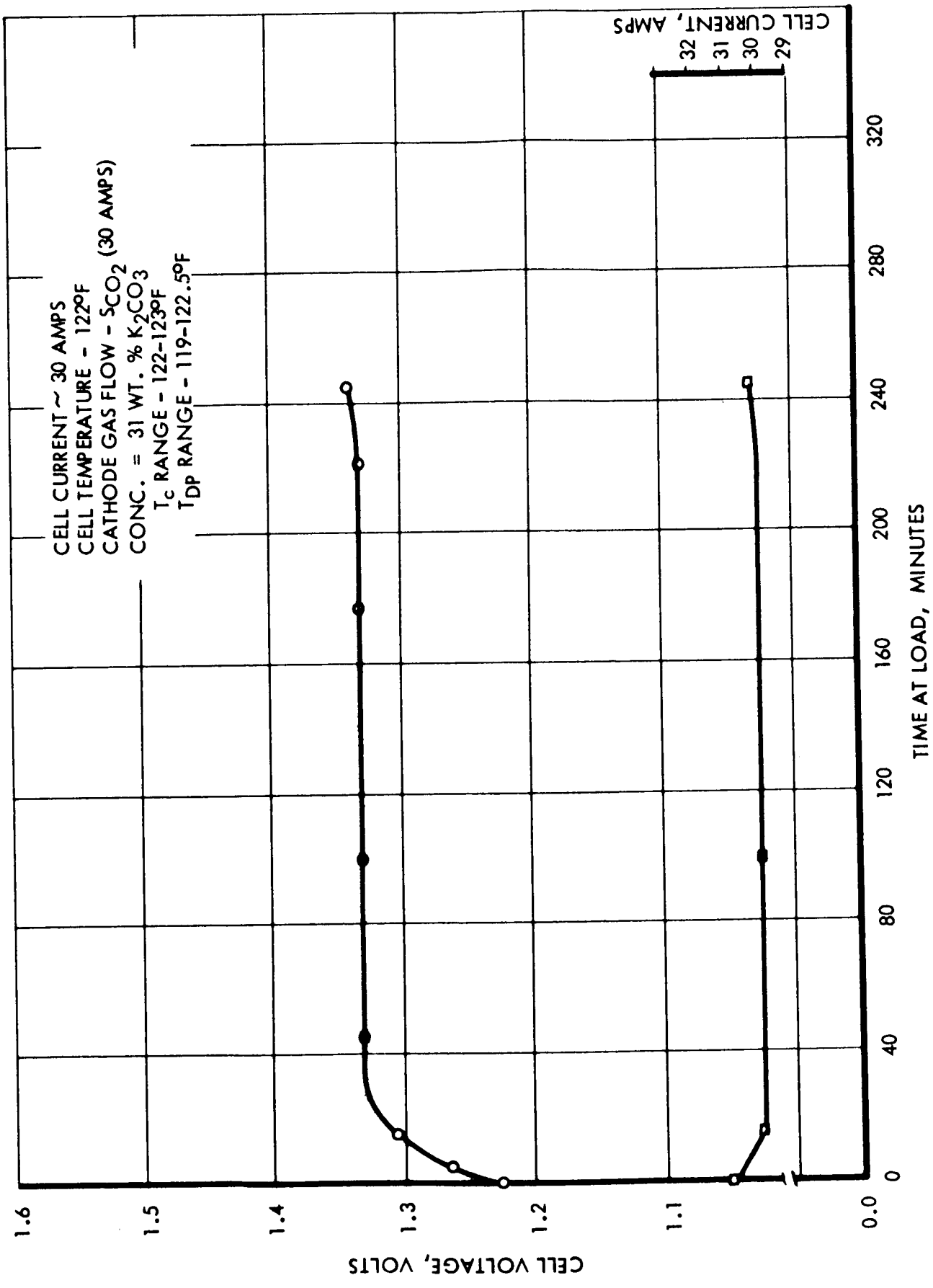

FIGURE 6-20 STAGE II CELL - POLARIZATION TIME DEPENDENCE, T = 122°F, I = 30

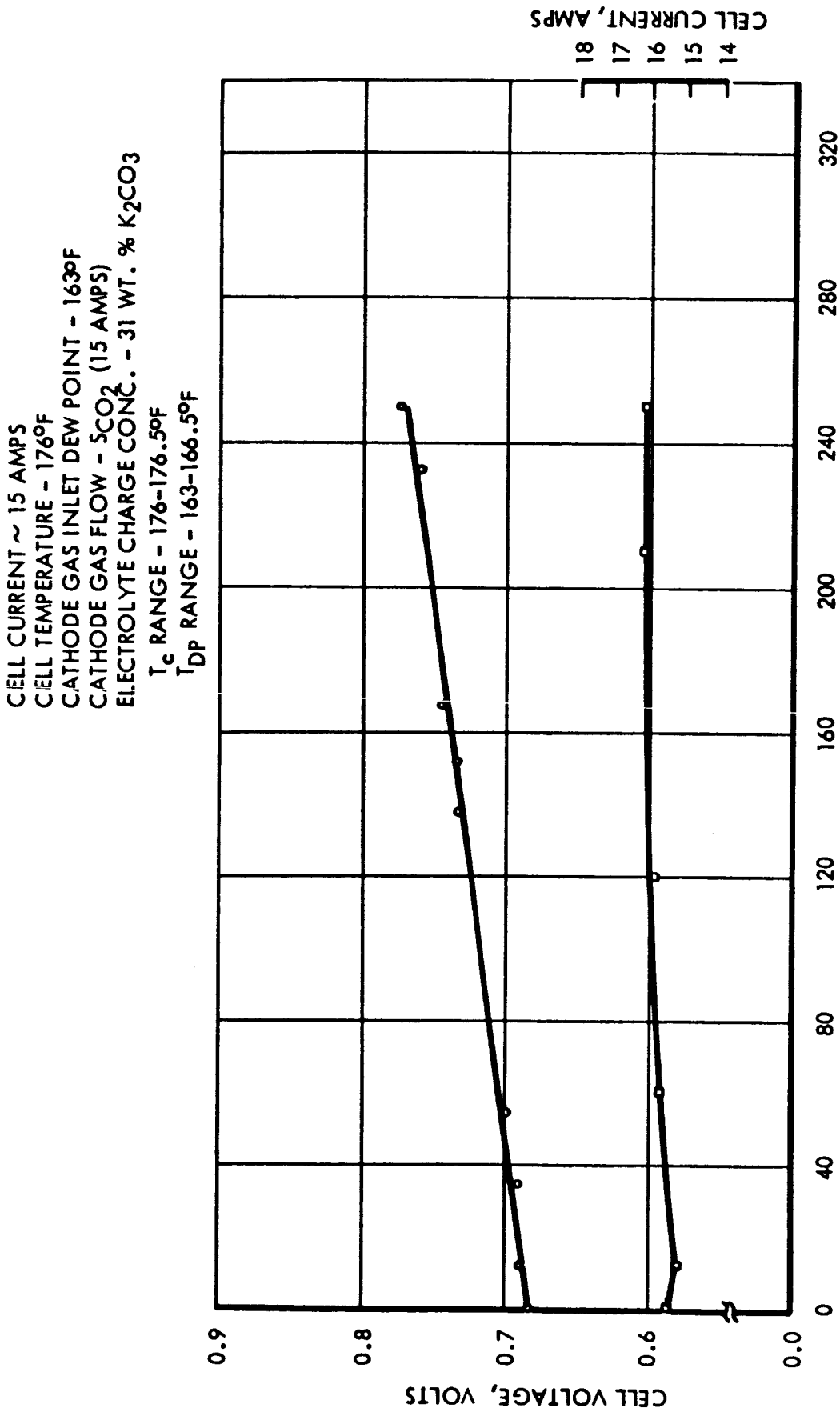

FIGURE 6-21 STAGE II CELL - POLARIZATION TIME DEPENDENCE, T = 176°F, I = 15

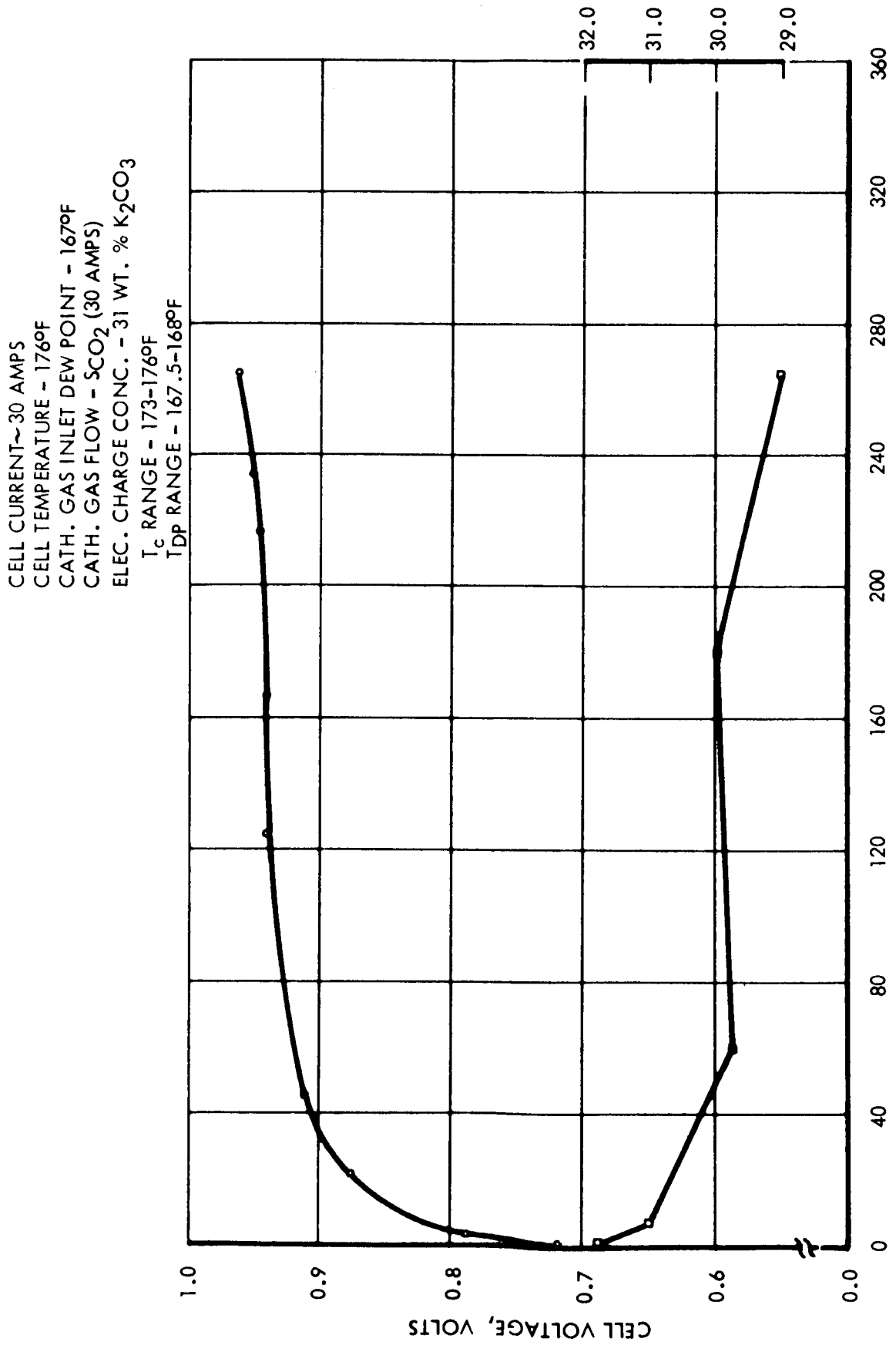

FIGURE 6-22 STAGE II CELL - POLARIZATION TIME DEPENDENCE, T = 176°F, I = 30

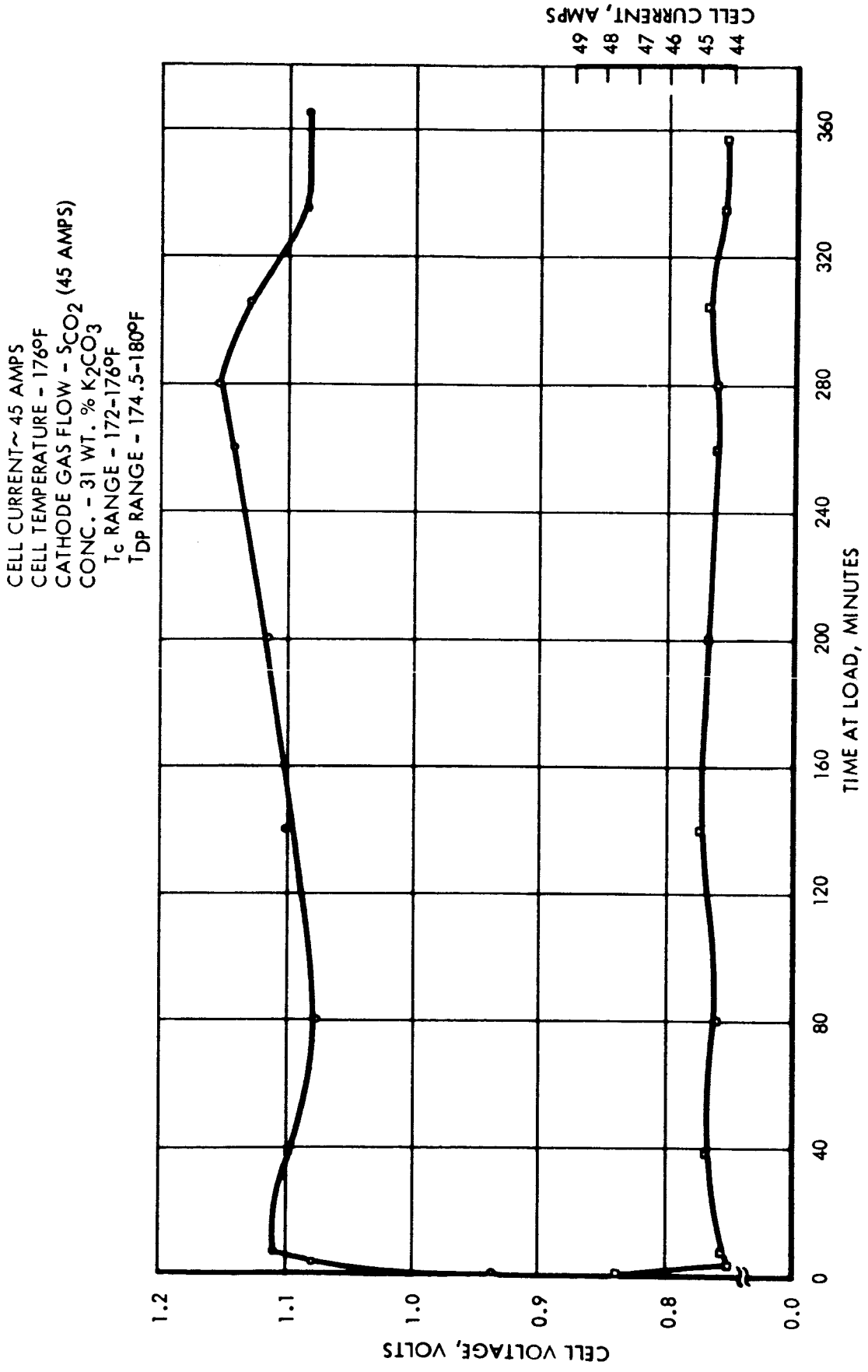

FIGURE 6-23 STAGE II CELL - POLARIZATION TIME DEPENDENCE, T = 176°F, I = 45

6.3 Stage III

Assembly of the Stage III cells was more difficult than either the Stage I or II cells due to cell complexity, lack of strength in the glass fiber matrix material and difficulty in installation of the tantalum wire screens used to enclose the water cavity matrix. It was required that the tantalum screen be anchored to thin strips of tantalum along the screen edge for installation in the cell since the screen could not be directly attached to the PVDC end plates.

After the assembly and charging procedures were completed, the seals between the anode and cathode cavities and cathode and water cavities were unsatisfactory. The cell was disassembled and reassembled with a sturdier matrix material, NORAMITE (crocidolite mineral fiber paper). Satisfactory sealing was obtained. Table 6-1 summarizes the short run made with this cell. The operation was not satisfactory due to the high cell operating voltage.

Table 6-1

Stage III Cell Operation - NORAMITE Matrix

Current	Voltage	Anode Gas Flow	Anode Gas O_2%	Cathode Gas O_2% Out	T_{cell}	$T_{humidifier}$
15 amps	1.31 volts	55 $\frac{cc\ STP}{MIN}$	97	0.5	149.5	143

A second cell was assembled again using the Whatman glass fiber matrix material. Also all the epoxy-glass fiber board gas manifold covers were replaced with teflon sheet manifold covers to prevent further problems of acid attack noted in the previous assembly. The cell was charged and installed in the test stand after satisfactory sealing was noted.

6.3.1 Current Density Effect

Figure 6-24 presents the effect of cell current density on cell performance for the two cell operating temperatures. The current, given in amperes, is somewhat less than the corresponding current density since the active electrode area for this stage is approximately 0.83 ft^2. In normal operation one would maintain the cathode gas flow rate such that close to stoichiometric oxygen flow would be obtained. However, for the experimental program manual control of this low flow ratio would be difficult to maintain. Therefore, the flow was maintained such that a minimum of 1.2 times stoichiometric oxygen was obtained.

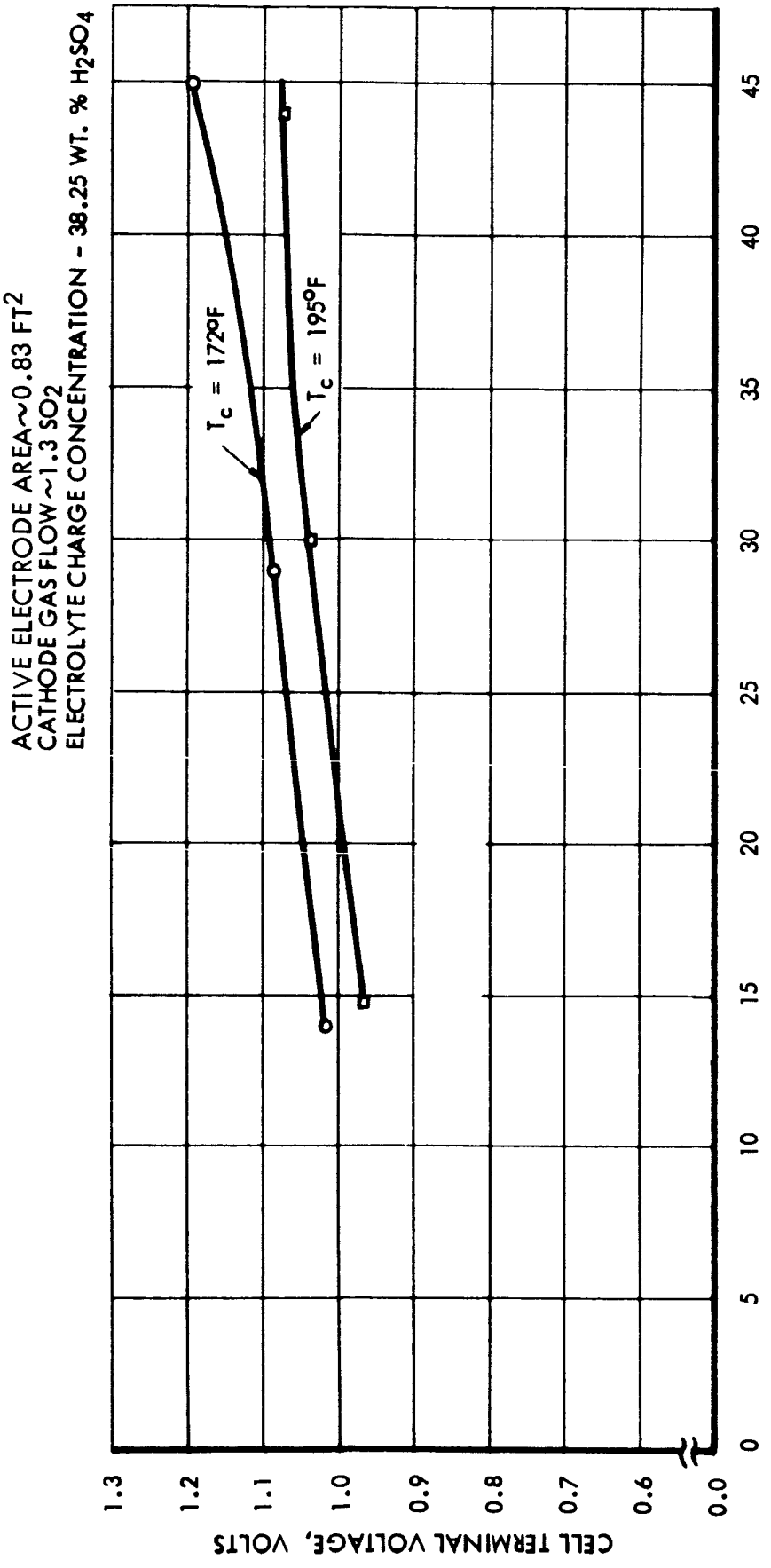

FIGURE 6-24 STAGE III CELL VOLTAGE AS A FUNCTION OF CELL CURRENT

6.3.2 Oxygen Transfer

The oxygen transfer rate for Stage III is presented in Table 6-2. As one would expect the rate is not effected to a great extent by either the cell temperature or current density in the normal cell operating range.

Table 6-2

$$\text{Stage III - Oxygen Transfer Rate} - \frac{\text{cc - STP}}{\text{AMP-MIN}}$$

$$\text{Theoretical } O_2 \text{ Transfer Rate} - 3.479$$

Cell Current	Cell Operating Temperature	
Amps	176°F	195°F
15	3.26	3.46
30	3.25	3.55
45	3.44	3.46

6.3.3 Polarization Time Dependence

Figures 6-25 through 6-30 give the polarization time dependence for each of the six test conditions. Operating conditions and cell operating current are also given for each run. Relatively smooth operation is shown in Figures 6-25 and 6-26. Explanation of results of other runs are as follows.

Figure 6-27 - Variations in current are due to drift in power supply and changing load as cell conditions changed. When the current change became significant, it was manually adjusted to the nominal operating point. Near end of run both current and cell voltage were relatively stable as the cell temperature and inlet gas dew point temperature were stabilized.

Figure 6-28 - During first 150 minutes of run, an attempt was made to control the cathode gas flow rate at too low a level causing wide fluctuations in both the cell current and voltage. At 150 minutes the cathode gas flow momentarily decreased to close to stoichiometric oxygen requirement. For a few minutes the current decreased to 9 amps while the voltage increased to approximately 1.6 volts. At this time the gas flow was set at 1.3 times stoichiometric O_2 flow to allow for a margin of error as the flow rates fluctuates due to slight changes in pressure drops in gas flow lines. After this change in gas flow rate stable operation is noted.

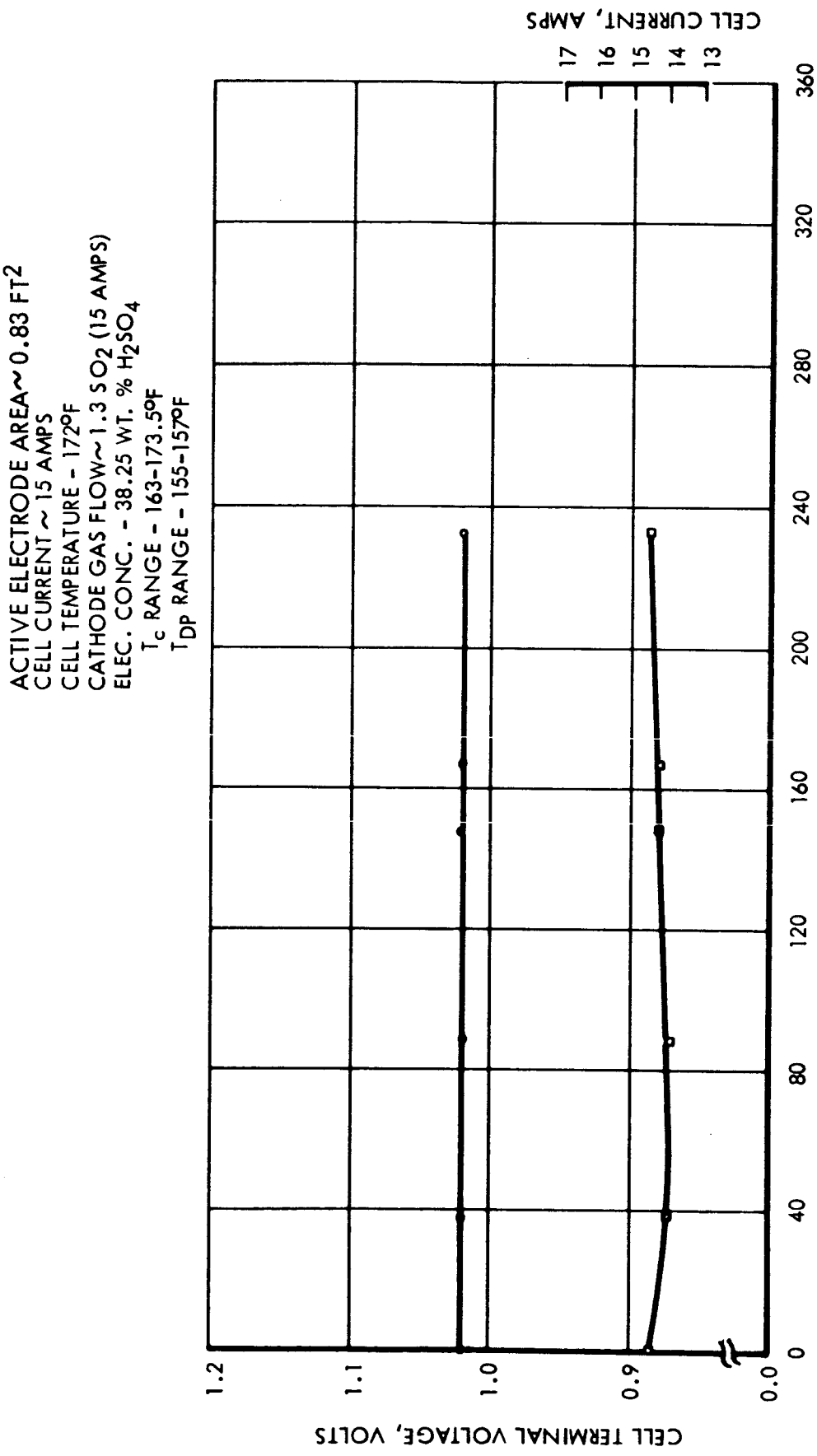

FIGURE 6-25 STAGE III CELL - POLARIZATION TIME DEPENDENCE, T = 172°F, I = 15

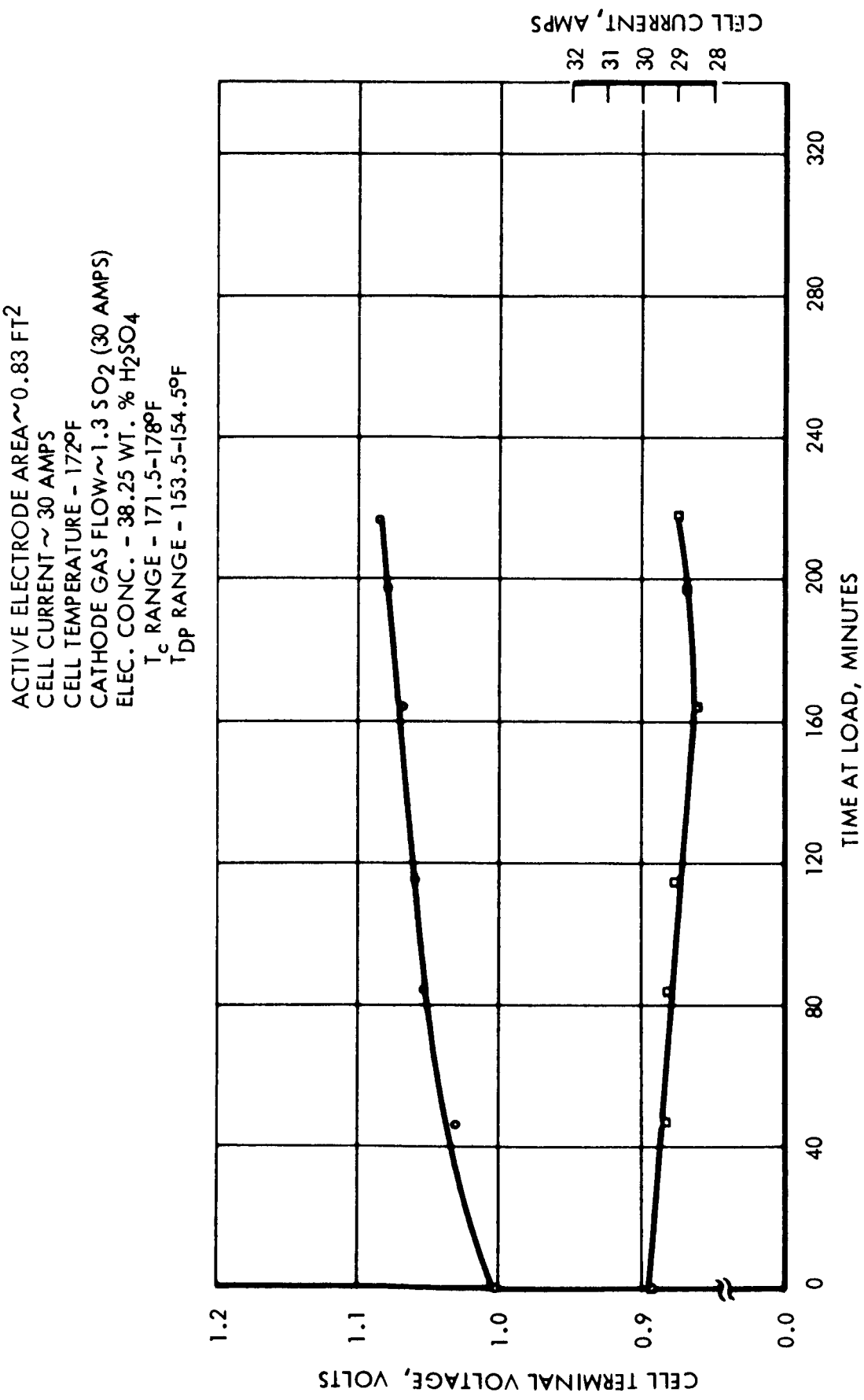

FIGURE 6-26 STAGE III CELL - POLARIZATION TIME DEPENDENCE, T = 172°F, I = 30

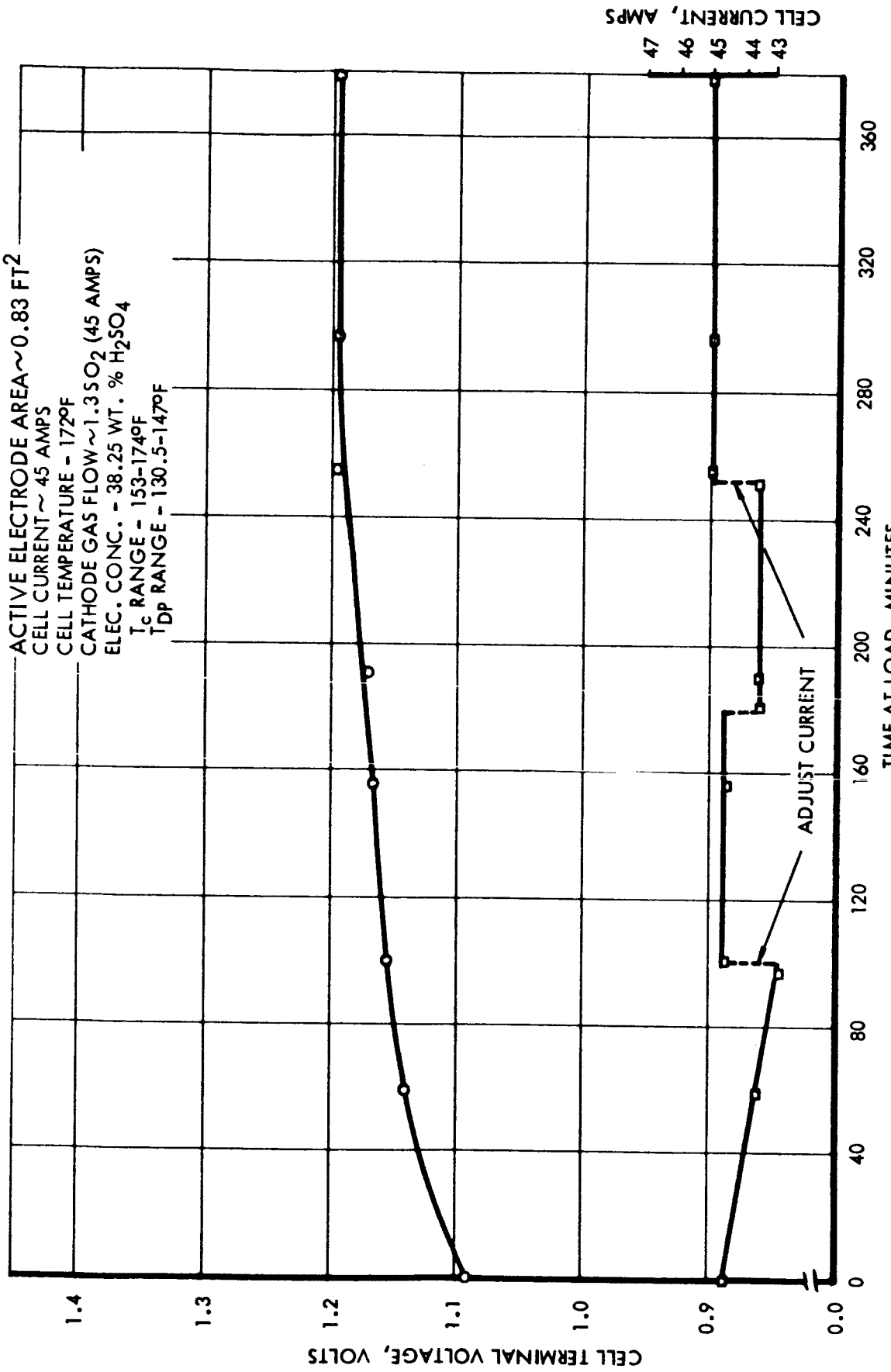

FIGURE 6-27 STAGE III CELL - POLARIZATION TIME DEPENDENCE, T = 176°F, I = 45

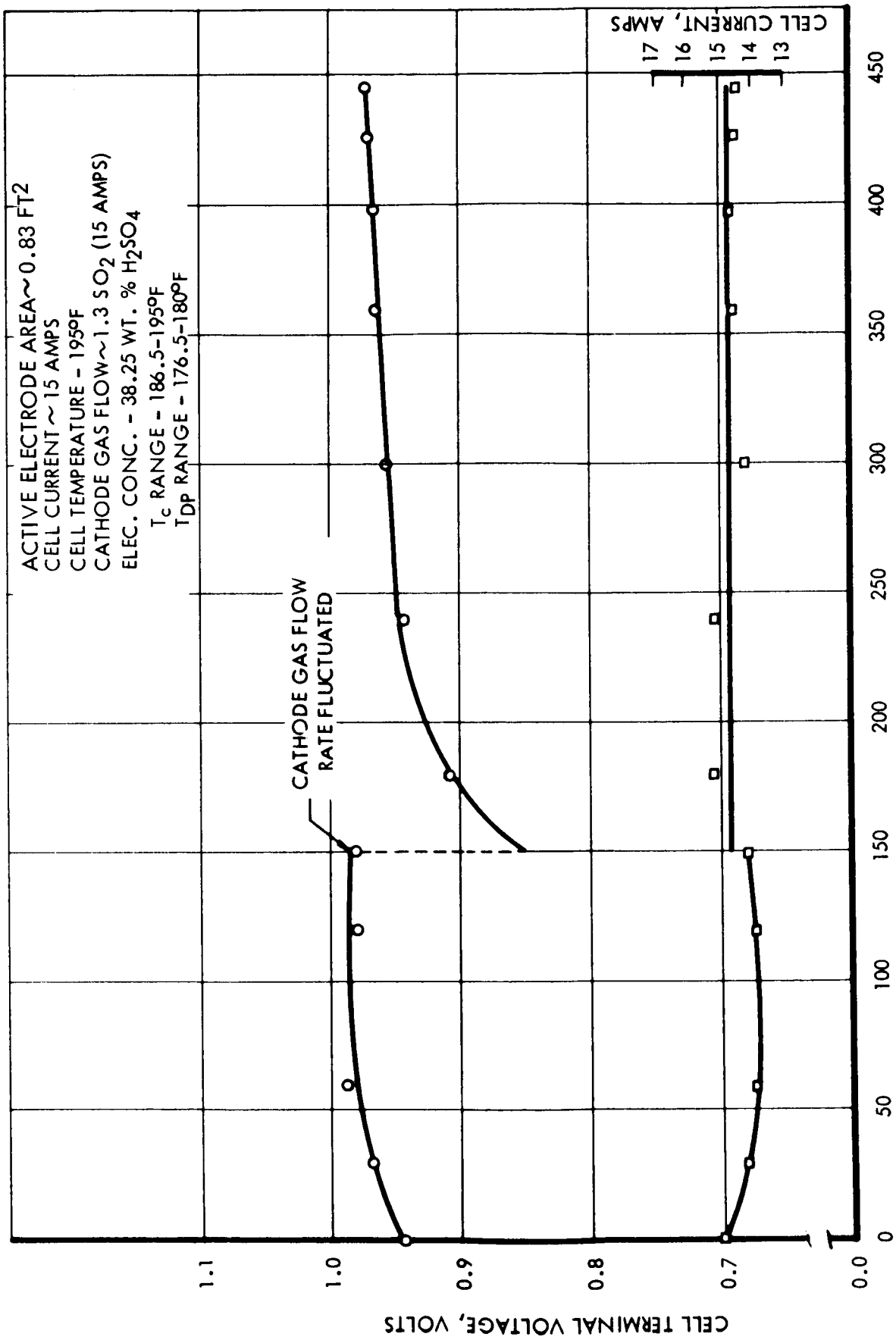

FIGURE 6-28 STAGE III CELL - POLARIZATION TIME DEPENDENCE, T = 195°F, I = 15

Figure 6-29 - Variations in cell current and voltage were due entirely to slight changes in cell operating conditions of temperature, inlet gas dew point and gas flow rate.

Figure 6-30 - Performance variation for first 320 minutes are due to fluctuations in cathode gas flow rate. Stable performance was achieved after switching to a bottled gas mixture of 20% O_2 and 80% CO_2 at 1.3 times stoichiometric O_2.

6.4 Stage II - Stage III Coupled Test

Short duration tests were conducted with the Stage II and III cells coupled, i.e., the anode-out gas of Stage II was used as the cathode-in gas for Stage III. With the output of Stage II held constant the current density in Stage III was varied to determine the maximum purity of carbon dioxide which could be obtained while still maintaining stable Stage III electrical performance. A rapid increase in Stage III cell voltage was obtained at a cathode gas flow ratio of 1.013 times stoichiometric O_2. Relatively stable performance is obtained at ratios approximating 1.04. Within the accuracy of the gas analysis equipment ($\pm$0.5%), all the oxygen was scrubbed out of the cathode stream leaving essentially 100% CO_2 in the cathode outlet stream. Table 6.3 lists operating conditions obtained during operation of the coupled cells.

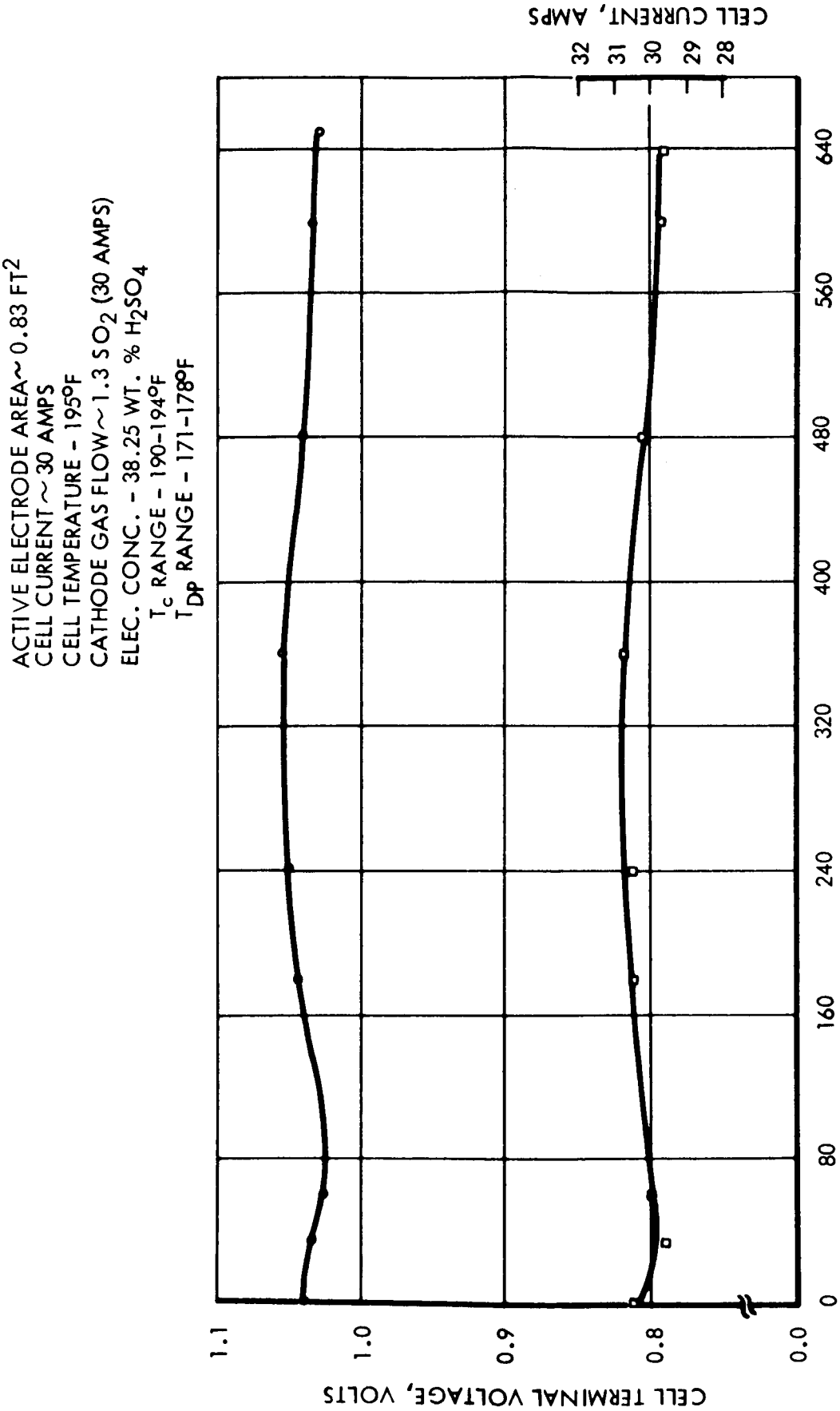

FIGURE 6-29 STAGE III CELL - POLARIZATION TIME DEPENDENCE, T = 195°F, I = 30

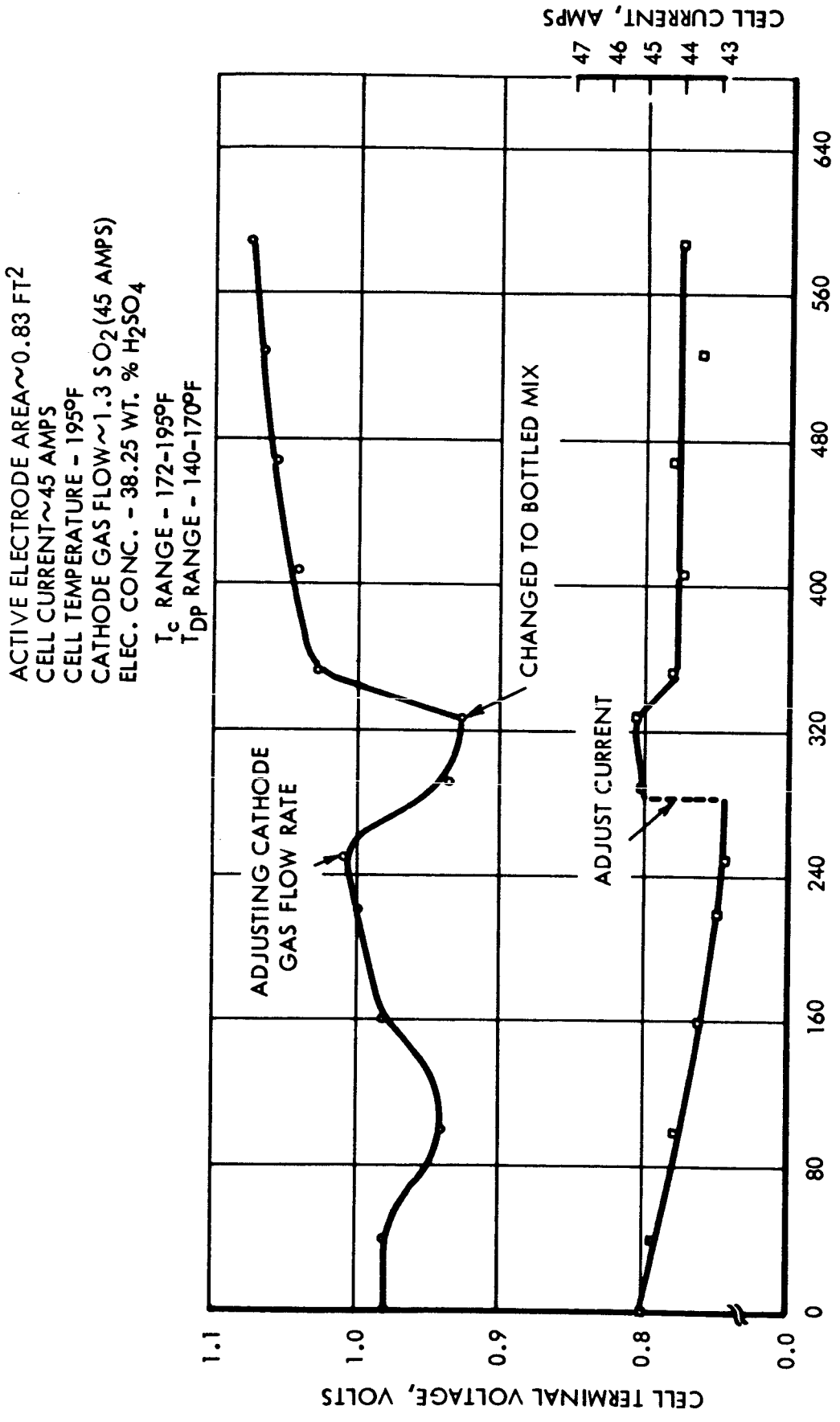

FIGURE 6-30 STAGE III CELL - POLARIZATION TIME DEPENDENCE, T = 195°F, I = 45

Table 6-3

Stage II - Stage III Coupled Test

Stage II Cell		Stage III Cell	
Current	- 20 amps	Current	- 19.50 amps
Voltage	- 0.833 volts	Voltage	- 0.980 volts
Cathode Gas In	- 42% O_2	Cathode Gas In	- 25.7% O_2
	58% CO_2		74.3% CO_2
Cathode Gas Out	- 68.5% O_2		@ 280 cc STP/MIN
	31.5% CO_2	Cathode Gas Out	- 100% CO_2 ($\pm$ 0.5%)
Anode Gas Out	- 25.7% O_2		@ 212 cc STP/MIN
	74.3% CO_2	Anode Gas Out	- 98.4% O_2 ($\pm$ 0.5%)
	@ 280 $\frac{\text{cc STP}}{\text{MIN}}$		@ 68.7 cc STP/MIN

7.0 LIFE TESTING

Prior to initiation of life tests, the Stage I cell which was used in parametric testing was disassembled in order to check for possible corrosion. Considerable corrosion was evident, in the form of black and green deposits on the anode end plate, on the anode, and in the matrix on the anode side. The cathode was in excellent condition. Some damage to the cathode end plate was in evidence in the form of breaks in the plating in the region where the matrix was compressed between the end plates. The cathode end plate is shown in Figure 7-1.

The anode end plate, with the severe corrosion, is shown in Figure 7-2. Note the sharp demarcation line at bottom of cell between a solid black area and a partially blackened area. This is attributed to electrolyte standing in the lower portion of the cell during cell operation. This pooling was avoided during the life test by allowing the cathode gas to flow through the cell from top to bottom, carrying out of the cell any free liquids formed by condensation.

Figure 7-3 shows the condition of the cathode after the parametric testing phase.

Due to the fact that most of the corrosion was on the anode and anode end plate, it was felt that the higher potential in this cell region contributed greatly to the corrosion. It was thus decided that the life tests were to be run at those operating conditions which would be reasonable from the system standpoint while maintaining minimum cell potentials. Thus all cells were to be run at 15 amperes and at the maximum temperature at which each cell had been operated in parametric tests.

Life testing for each stage was initiated with two cells operating. The same procedures of start-up, operation and shut-down as used during parametric testing were followed during the life testing program.

7.1 Stage I

Stage I testing was started using one cell assembled with unused end plates and one cell assembled with the corroded end plates which were used in the parametric tests.

7.1.1 Cell Operation

The cell using the old end plates performed poorly from the beginning of the

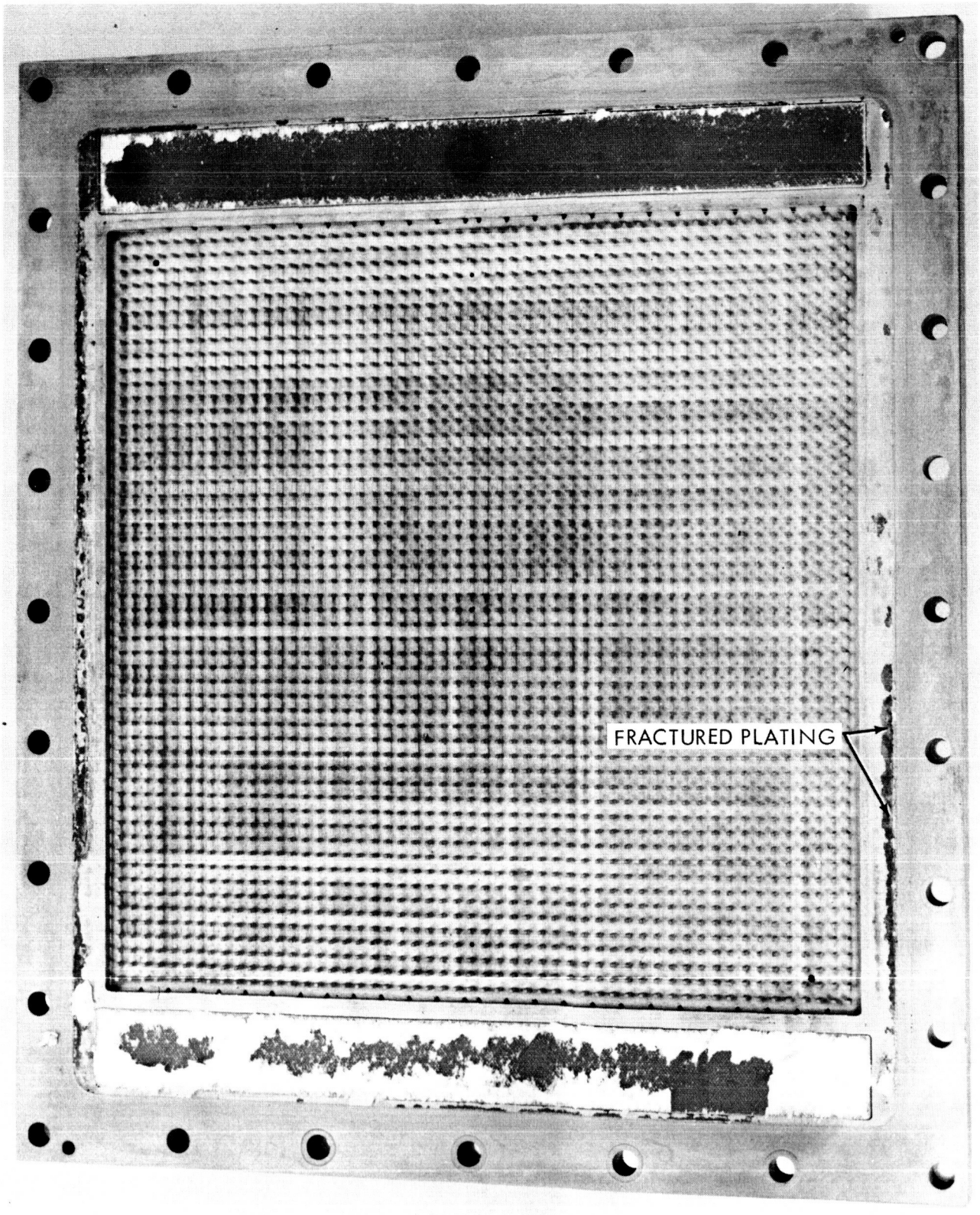

FIGURE 7-1 STAGE I CATHODE END PLATE, AFTER PARAMETRIC TESTS

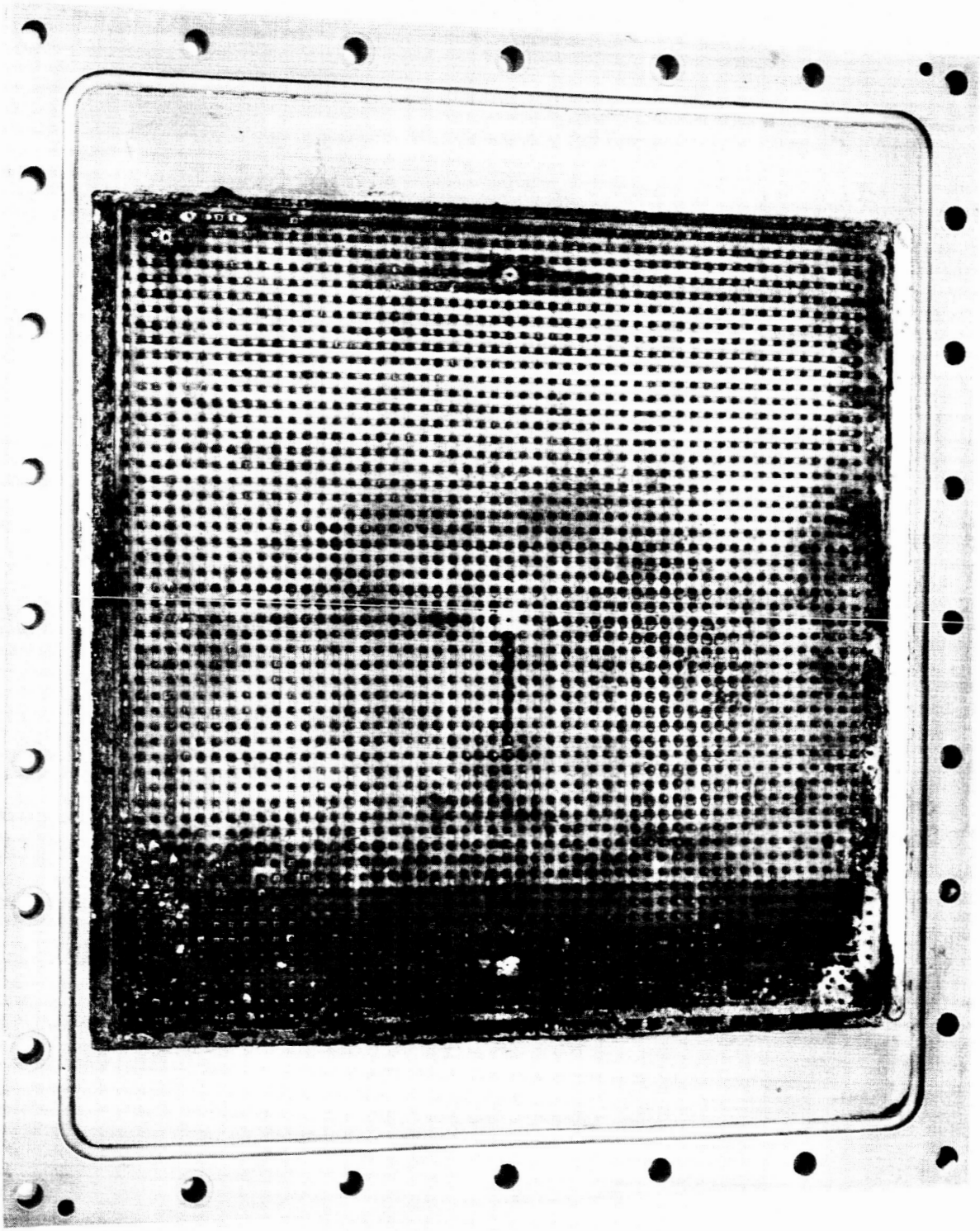

FIGURE 7-2 STAGE I ANODE END PLATE, AFTER PARAMETRIC TEST

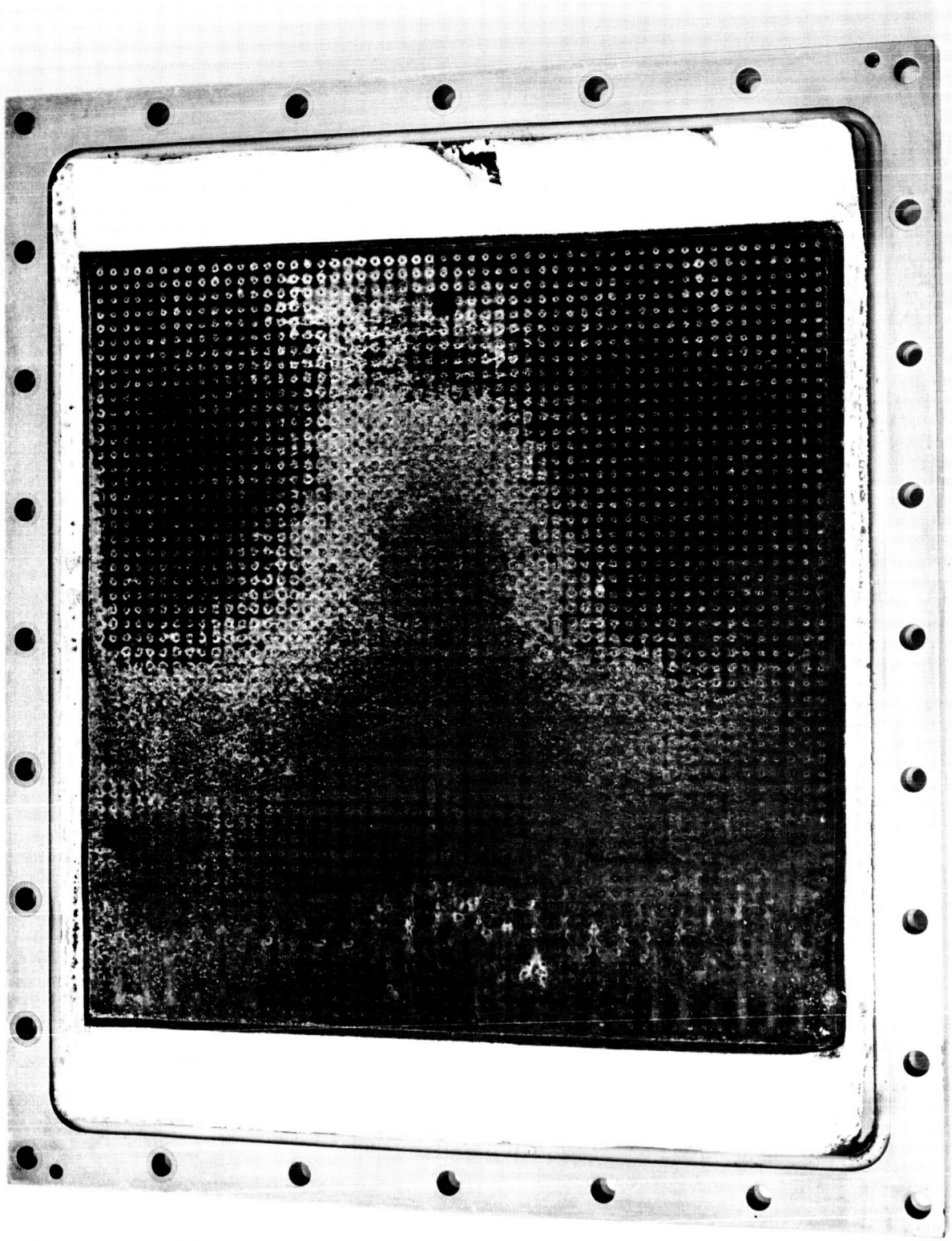

FIGURE 7-3 STAGE I CATHODE, AFTER PARAMETRIC TESTING

test period and could not be kept on test. The performance of cell number two is shown in Figure 7.4. Performance was erratic. The cell operation was stopped and restarted once due to failure of the vacuum pump and once due to extreme difficulty in dew point control of the inlet gas. The test was terminated after 152 hours of operation when the cell voltage reached 1.70 volts and could not be decreased by dew point temperature adjustment. Figure 7-5 gives a comparison of the cell operating temperature and the cathode gas humidifier temperature.

In addition to the electrical characteristics of the cell, the transfer of CO_2 across the cell is important in establishing cell performance. Figure 7-6 presents the CO_2 transfer rate as a function of cell operating time. Relatively stable and high transfer rates are obtained for approximately seventy hours and then a sharp decay in the transfer rate sets in. Satisfactory cell operation therefore existed only out to seventy hours. Note the sharp rise in cell voltage at seventy hours in Figure 7-4. Figure 7-7 presents the anode gas composition and flow rate as a function of running time.

7.1.2 Discussion of Results

In order to intelligently discuss the test results one must examine the cells internally for the effects of corrosion on cell operation. The sharp break in cell performance at seventy hours cannot be attributed to anything other than corrosion. It was initially believed that the erratic Stage I performance was due to difficulties with the dew point temperature control. However, it may be that dew point control difficulties were in fact caused by the effects of corrosion. If the electrolyte composition or concentration were markedly changed then one would have no way of knowing what the proper dew point temperature should be in order to maintain proper cell moisture balance. As cell operation became erratic, it was not possible to maintain a gas seal across the cell matrix and still maintain a suitable cell operating voltage. This mode of operation could occur if the electrolyte had (1) been washed out of the matrix or (2) the electrolyte had been consumed forming an insoluable compound with the cell materials and/or feed gases. A description of the used cell components follows.

The cathode end plate from cell number two is shown in Figure 7-8, indicating little or no corrosion except in the area where the compressed matrix was in contact with the plate. All gas ports and channels remained open and unrestricted.

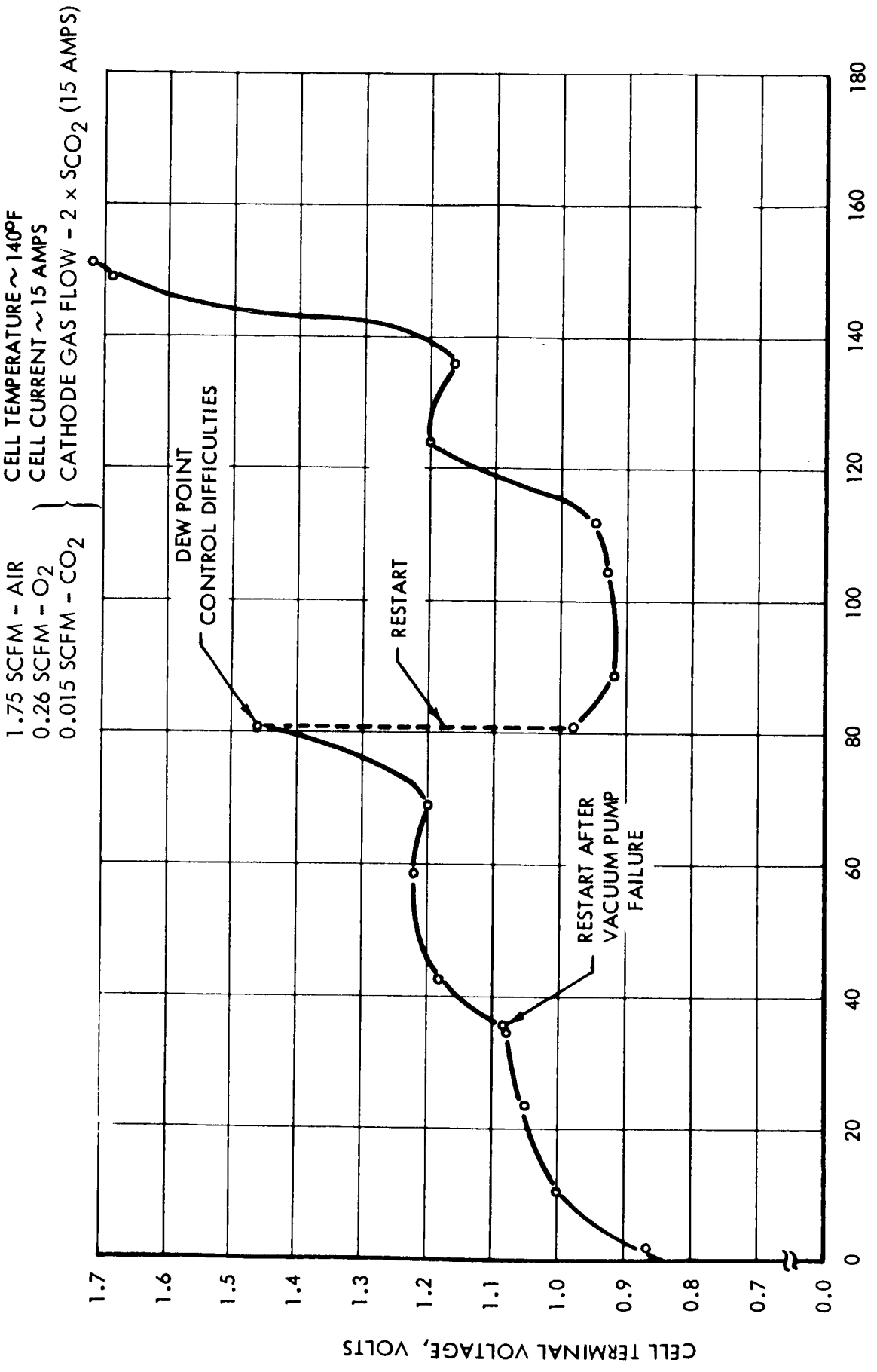

FIGURE 7-4 STAGE I - CELL #2, LIFE TEST PERFORMANCE

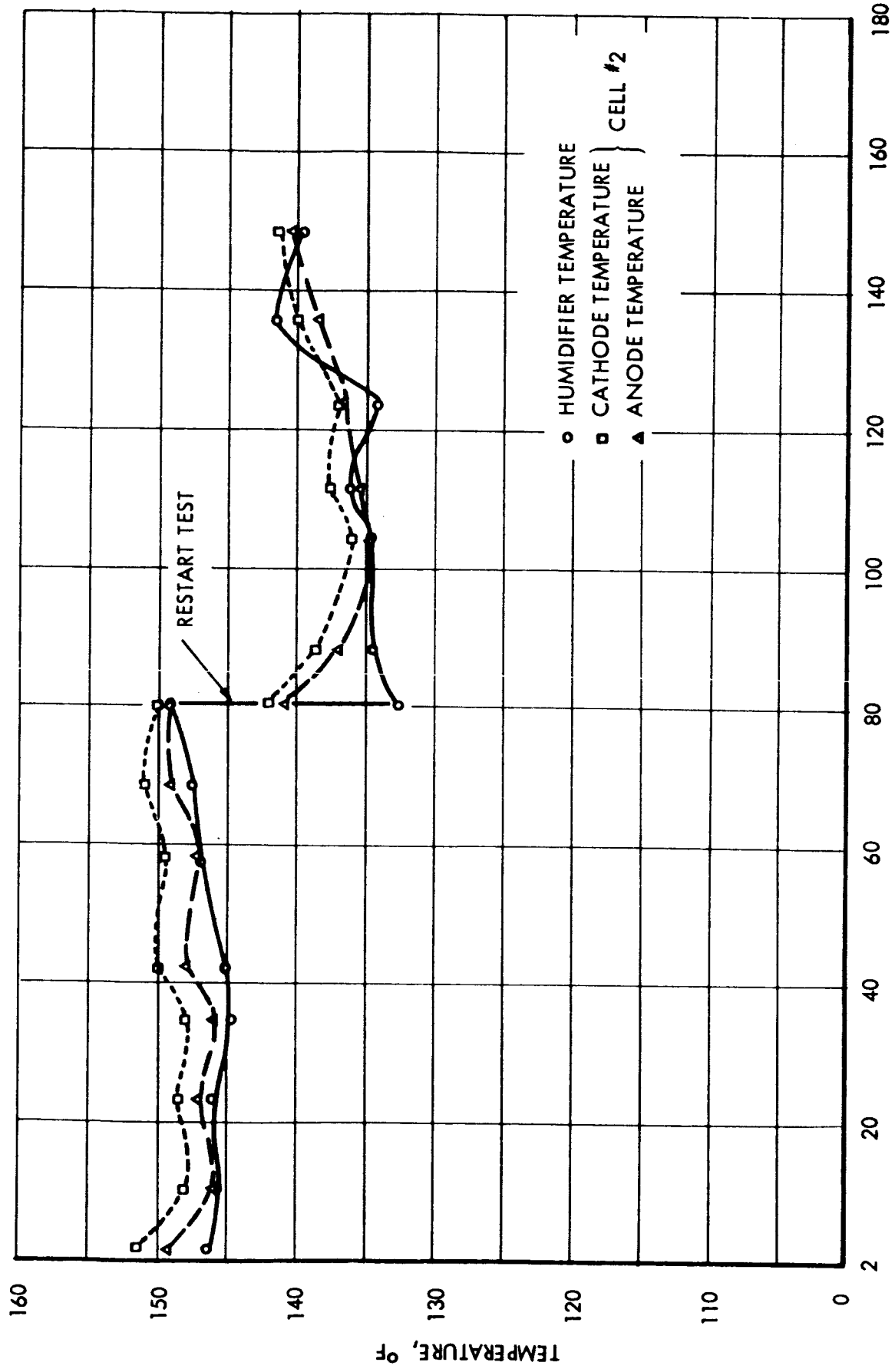

FIGURE 7-5 COMPARISON OF HUMIDIFIER AND CELL TEMPERATURE DURING STAGE I LIFE TEST

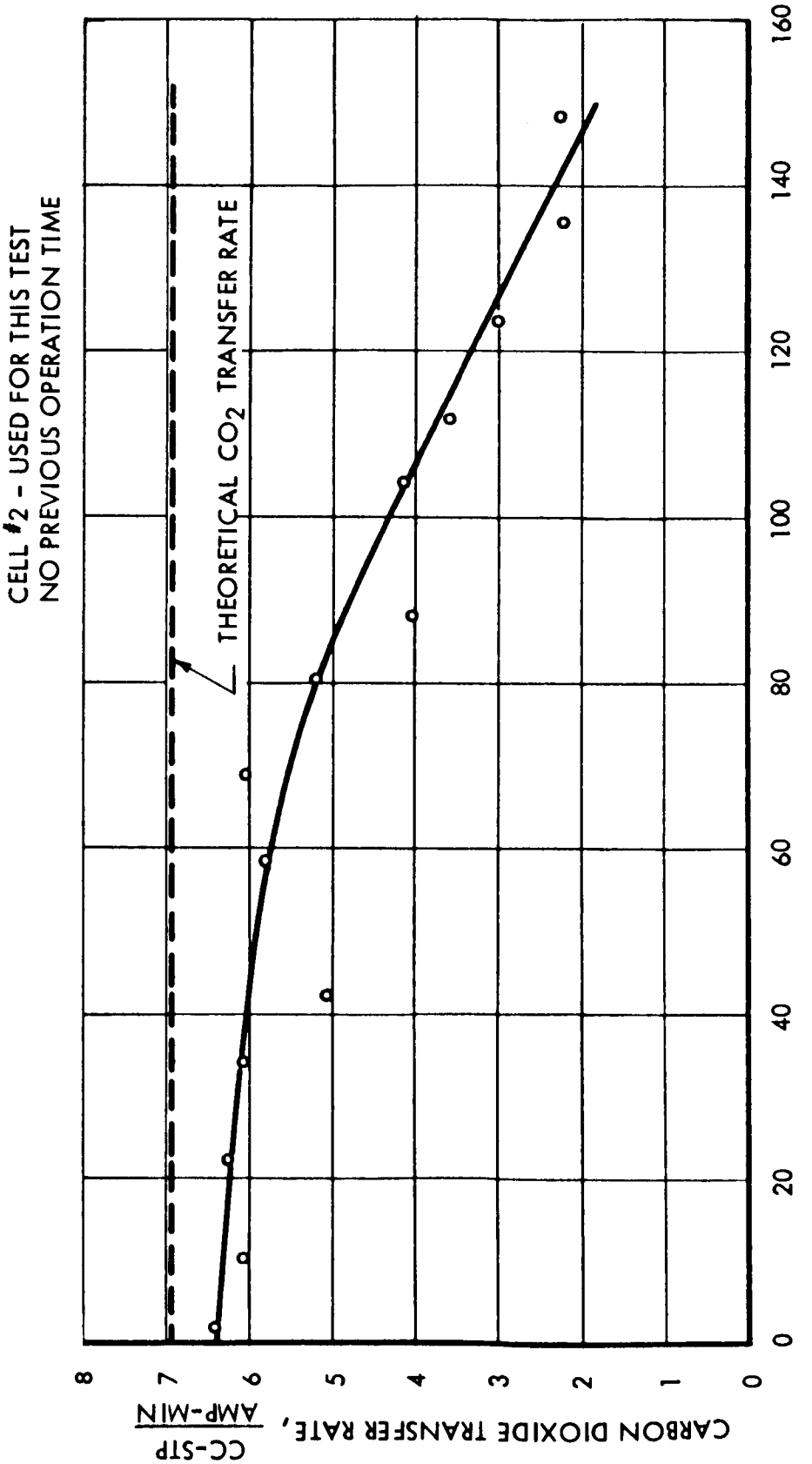

FIGURE 7-6 DECAY OF CO_2 TRANSFER RATE WITH TIME, STAGE I - LIFE TEST

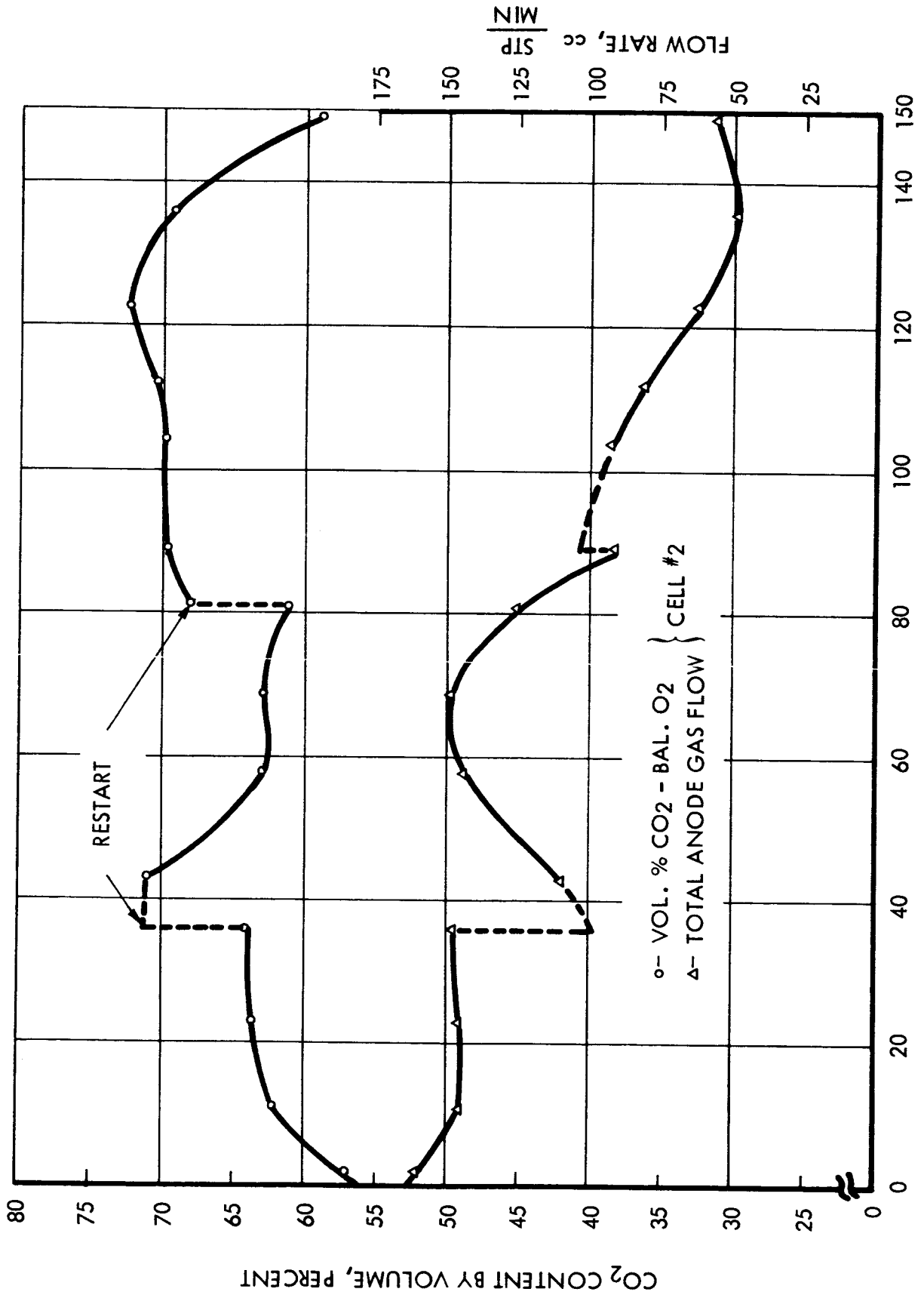

FIGURE 7-7 STAGE I - CELL #2, ANODE GAS OUTPUT - LIFE TEST

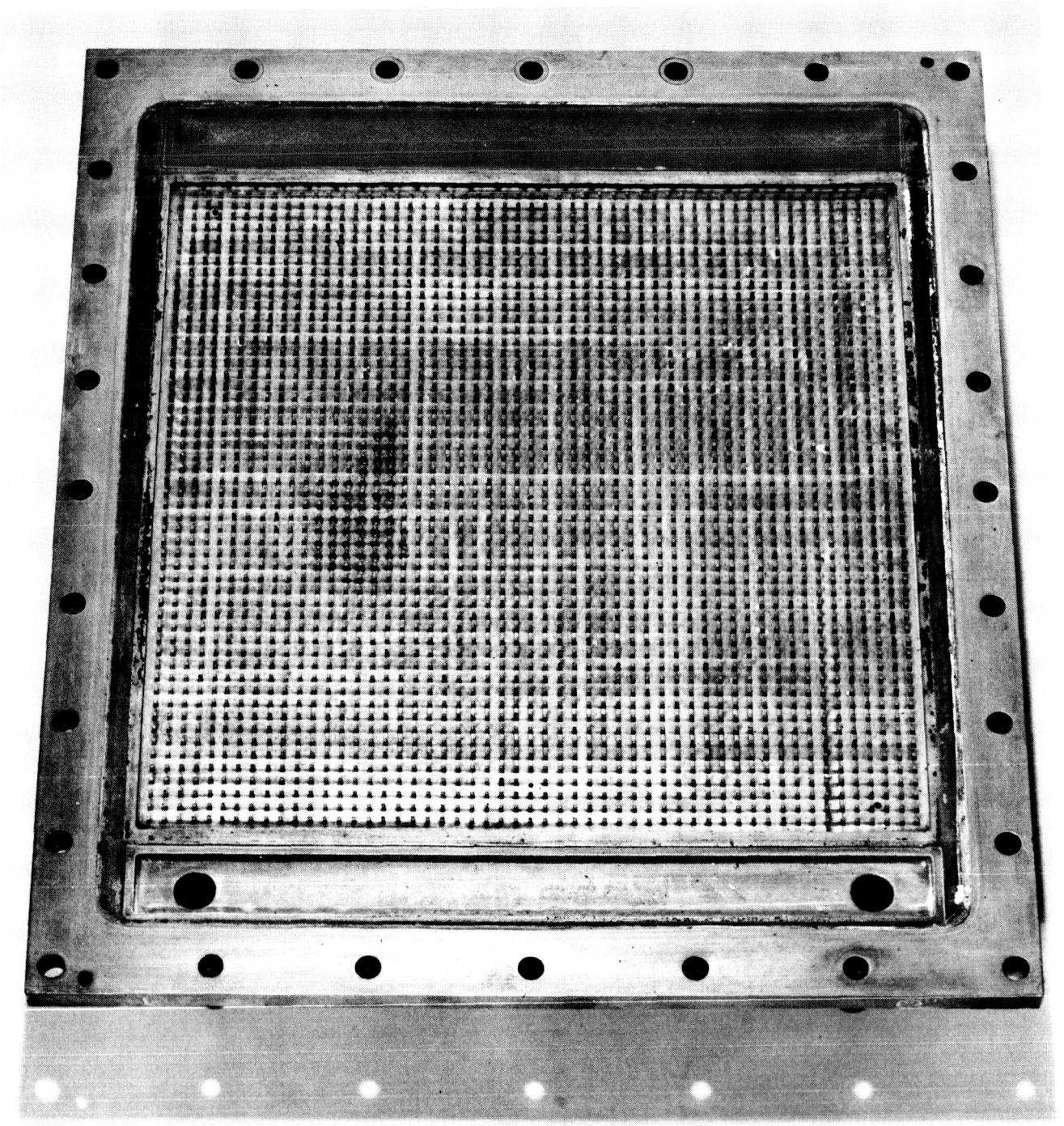

FIGURE 7-8 STAGE I CATHODE END PLATE, AFTER LIFE TEST

Both cell one and cell two anode end plates are shown in Figure 7-9. Cell number one, on right, is badly corroded over the entire cell area. The products of corrosion are light green in color except around the edge of the cell and on the pins where the substance is black. The bottom half of the cell had an extremely large amount of the green substance. Cell number two on the left, the newer piece, exhibits mostly a black product at cell bottom, on pins, and around edge of cell. Some green substance is also seen at very bottom of the cell. The heavy band of corrosion at the cell bottoms is probably due to high moisture content of cells at the bottom.

An enlarged section of cell number one is shown in Figure 7-10. The light colored residue is light green. The black residue is seen around the edge and on the pins. Corrosion is also seen near the O-ring groove edge.

The electrode-matrix pack from cell number one is shown in Figure 7-11, with the electrode peeled back, anode side up. On the electrode matrix side, and in the matrix a heavy black deposit is found, which causes the electrode to adhere to the matrix. This black deposit is not found on the cathode or cathode side of the matrix. The light areas on the electrode are caused by the green corrosion product. Where the screen is pulled back, corrosion of the electrode screen is evidenced by the large holes in the electrode screen base material. A discussion of the identity of the corrosion product is given in Section 7.2.2.

7.2 Stage II

Life testing of Stage II was initiated with a newly assembled cell and the cell used in the parametric testing phase. After 24 hours of operation cell two (new hardware) failed due to an internal electrical short. Probable cause for the short is discussed in Section 7.2.2. Testing was continued using cell number one.

7.2.1 Cell Operation

Cell voltage as a function of running time is given by Figure 7-12. During the first twenty hours of operation the cell was inadvertently run at 7.5 amperes rather than 15 amperes due to the installation of a new shunt prior to life test initiation. The change to 15 ampere is accompanied by the expected increase

FIGURE 7-9 STAGE I ANODE END PLATES - AFTER LIFE TEST

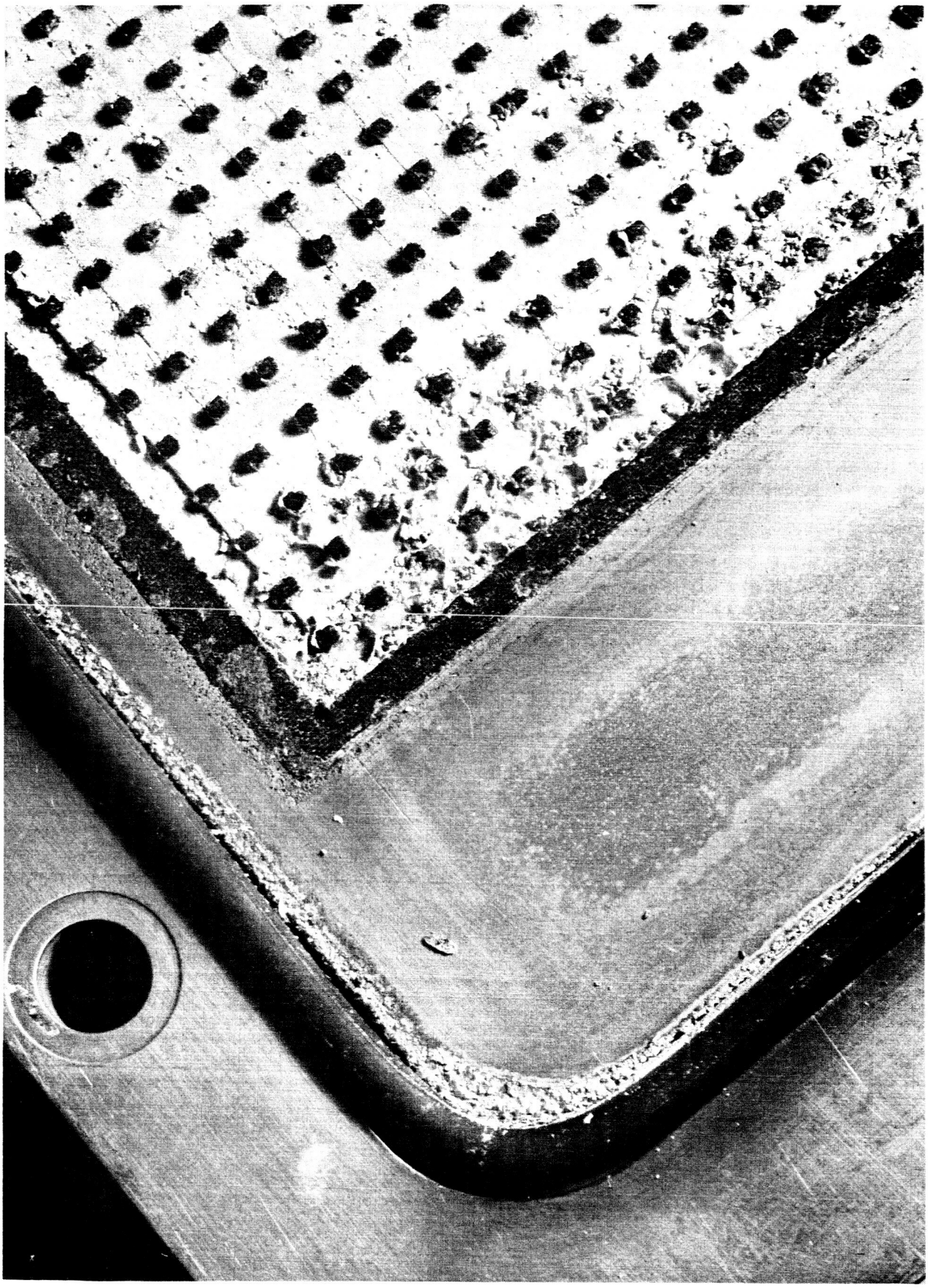

FIGURE 7-10 STAGE I, ANODE END PLATE CORROSION

FIGURE 7-11 STAGE I, ELECTRODE MATRIX PACK - ANODE SIDE UP

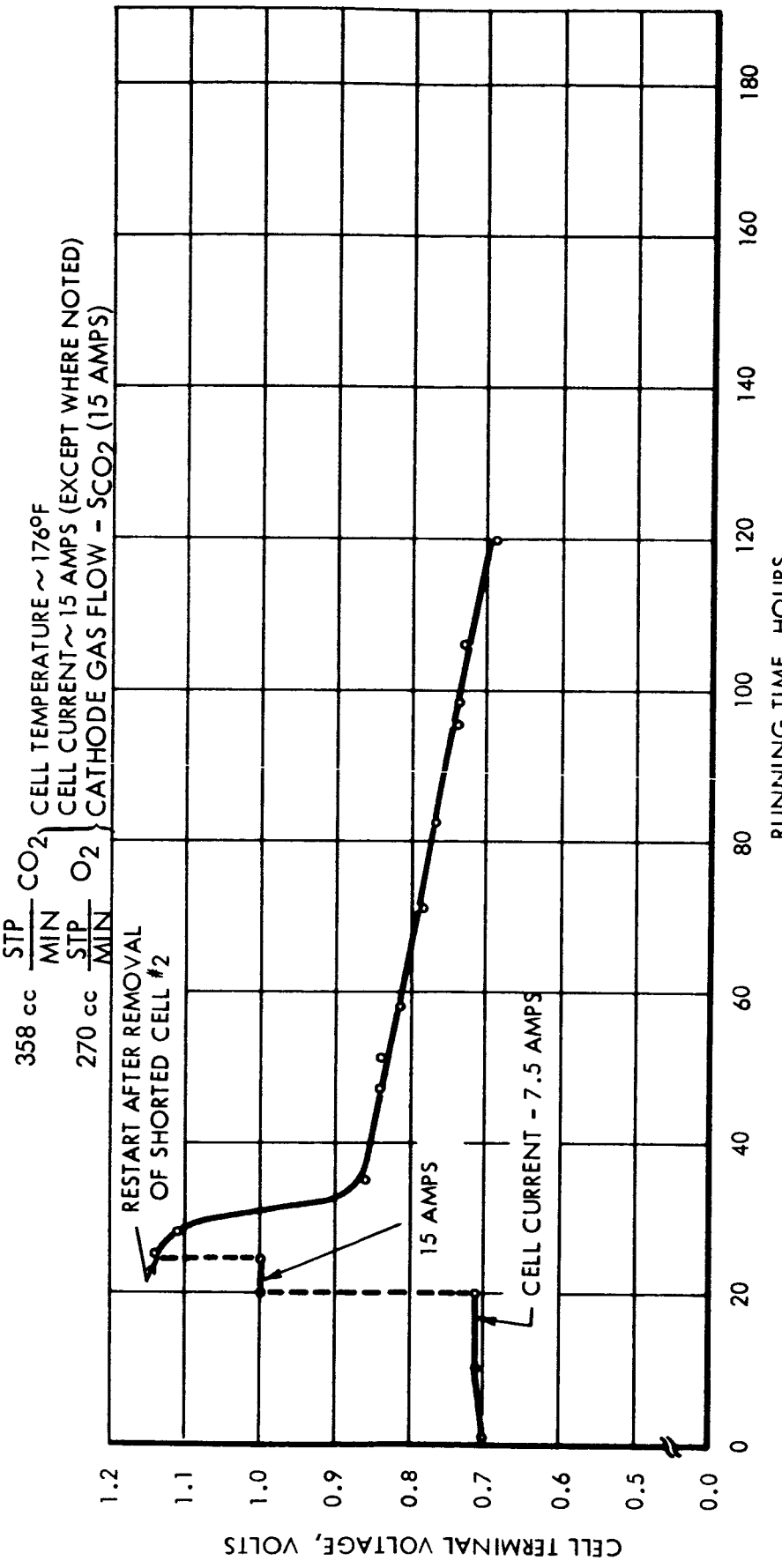

FIGURE 7-12 STAGE II - CELL #1, LIFE TEST PERFORMANCE

in cell voltage. At 24 hours, operation was ceased in order to remove the shorted number two cell from the module. A significant increase in the voltage of cell number one was noted upon restart. From that point on the cell voltage constantly decreased. Cause of this decrease is not known. Total running time for cell number one was 120 hours. Cell operation was ceased due to the low CO_2 transfer rate obtained at this time. The CO_2 transfer rate is shown in Figure 7-13. Note again satisfactory performance for approximately 60 hours and then a sharp continuous decreasc with operating time. Figure 7-14 shows anode gas composition and flow rate as a function of operating time. Cell and humidifier temperature are given in Figure 7-15.

7.2.2 Discussion of Results

The probable cause of the electrical short in cell number two can be seen in Figure 7-16. A close-up photograph reveals a layer of plating material adhering to the O-ring. Sufficient material (plating metal) had adhered to the O-ring to bridge the gap between metal end plates. Defective plating was the most probable cause of this effect since it was not observed in any of the other cells. Some corrosion products are also seen on the O-ring.

Figure 7-17 is a close-up of the gas diffusion plate from the same cell showing the corrosion which exposes the base metal of the component.

End plates from cell number one (used in both the parametric testing and life testing) are seen in Figures 7-18 and 7-19. As expected the cathode end plate, Figure 7-19, is relatively free of corrosion. However, the anode end plate was not corroded as expected. Only minor corrosion is in evidence and this is mostly in the form of green crystals, which had not been seen in any of the other cells. The corrosion which was seen in cell number two (operating for only 24 hours) was much more severe and was of the black and light green type noted in all other cells.

A close-up of the gas diffusion plate from cell number one shows the green crystalline type of corrosion product, Figure 7-20.

The electrode-matrix pack, cathode side up, is seen in Figure 7-21. The cathode screen has been pulled back to show the asbestos matrix. Black areas seen on the matrix appeared to have pulled away from the cathode and are not of the type seen on the anode side. The electrode screen retains its structural integrity.

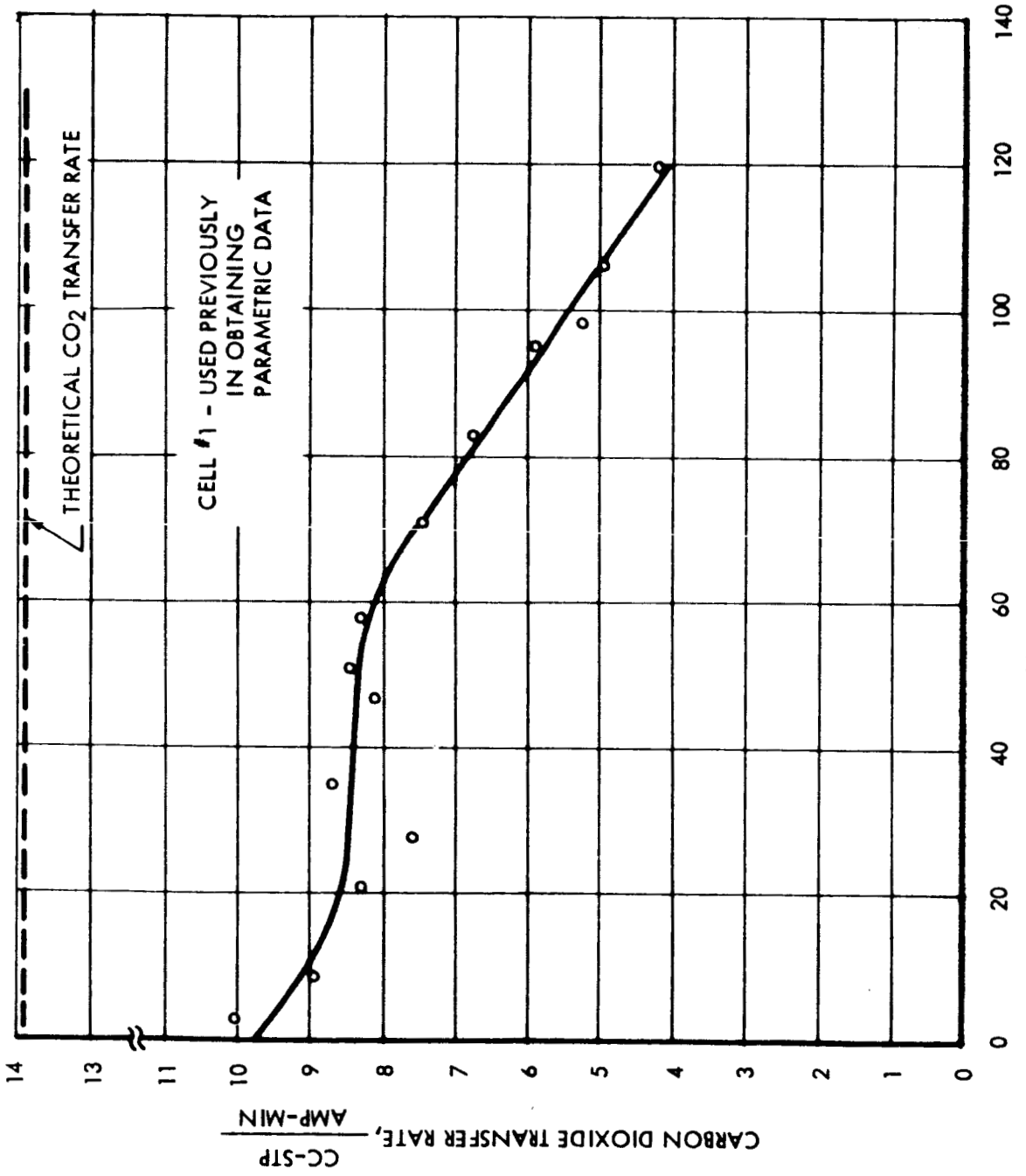

FIGURE 7-13 DECAY OF CO_2 TRANSFER RATE WITH TIME, STAGE II - LIFE TEST

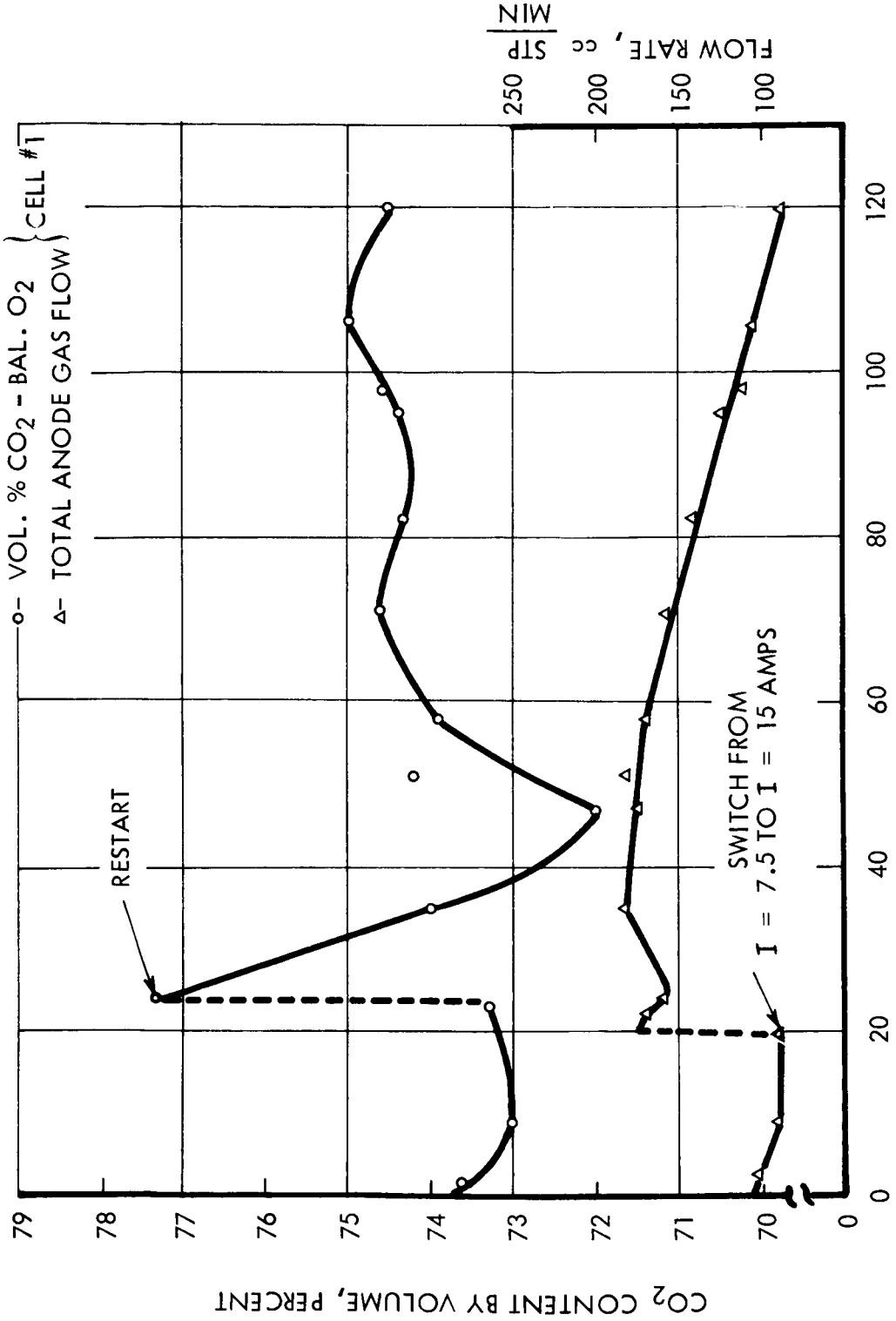

FIGURE 7-14 STAGE II - CELL #1, ANODE GAS OUTPUT - LIFE TEST

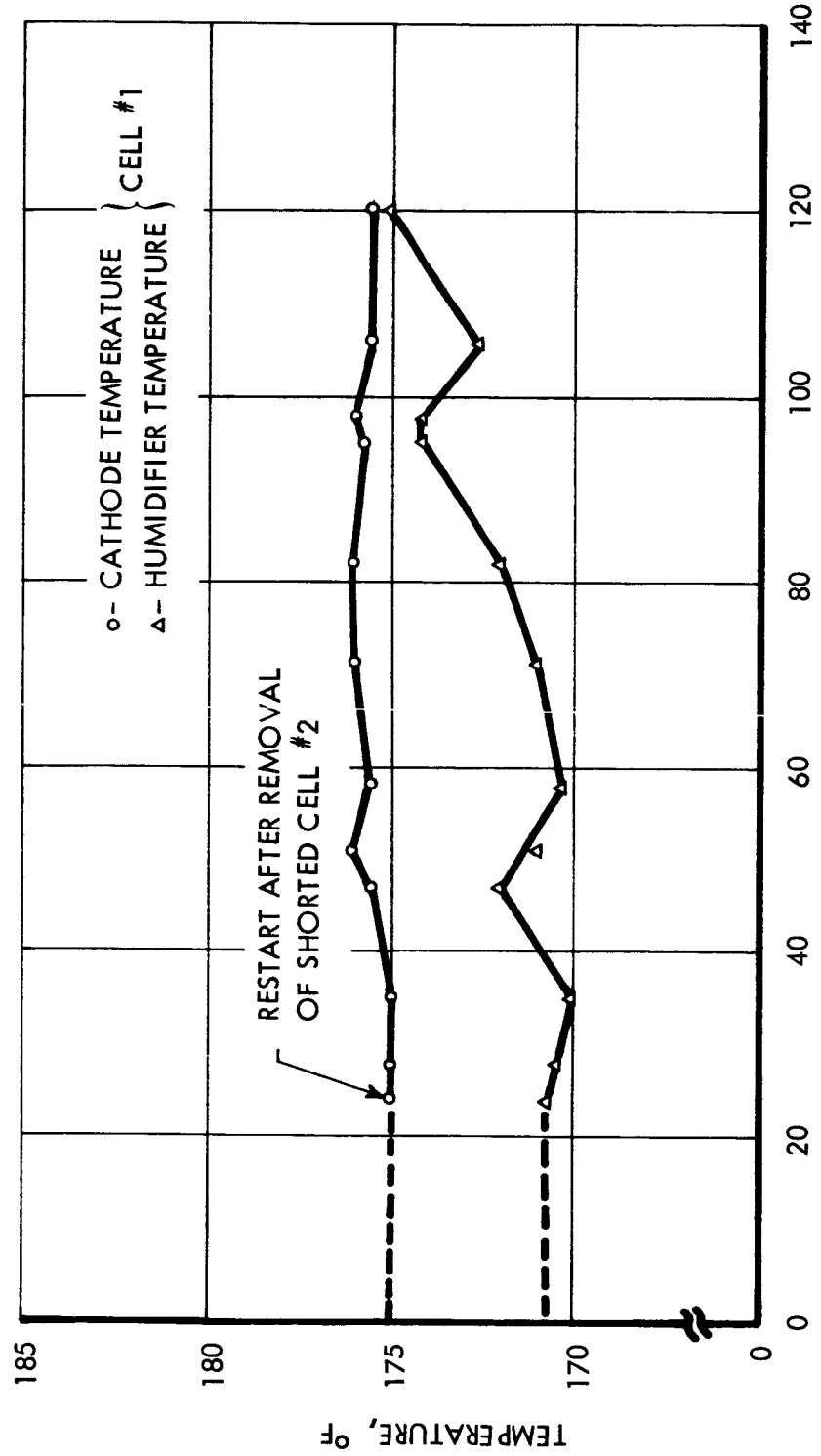

FIGURE 7-15 COMPARISON OF HUMIDIFIER AND CELL TEMPERATURE DURING STAGE II LIFE TEST

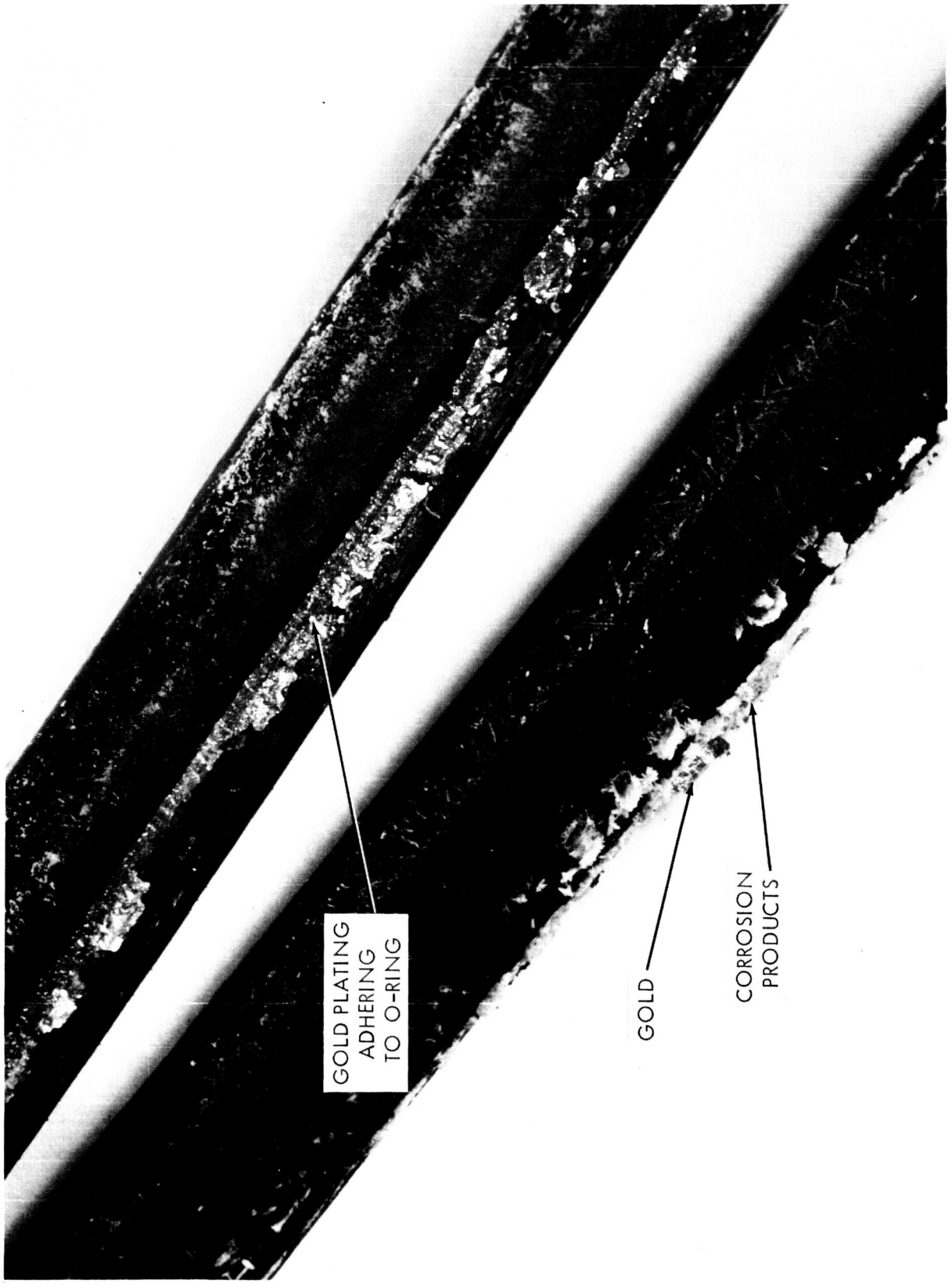

FIGURE 7-16 O-RING FROM SHORTED STAGE II CELL

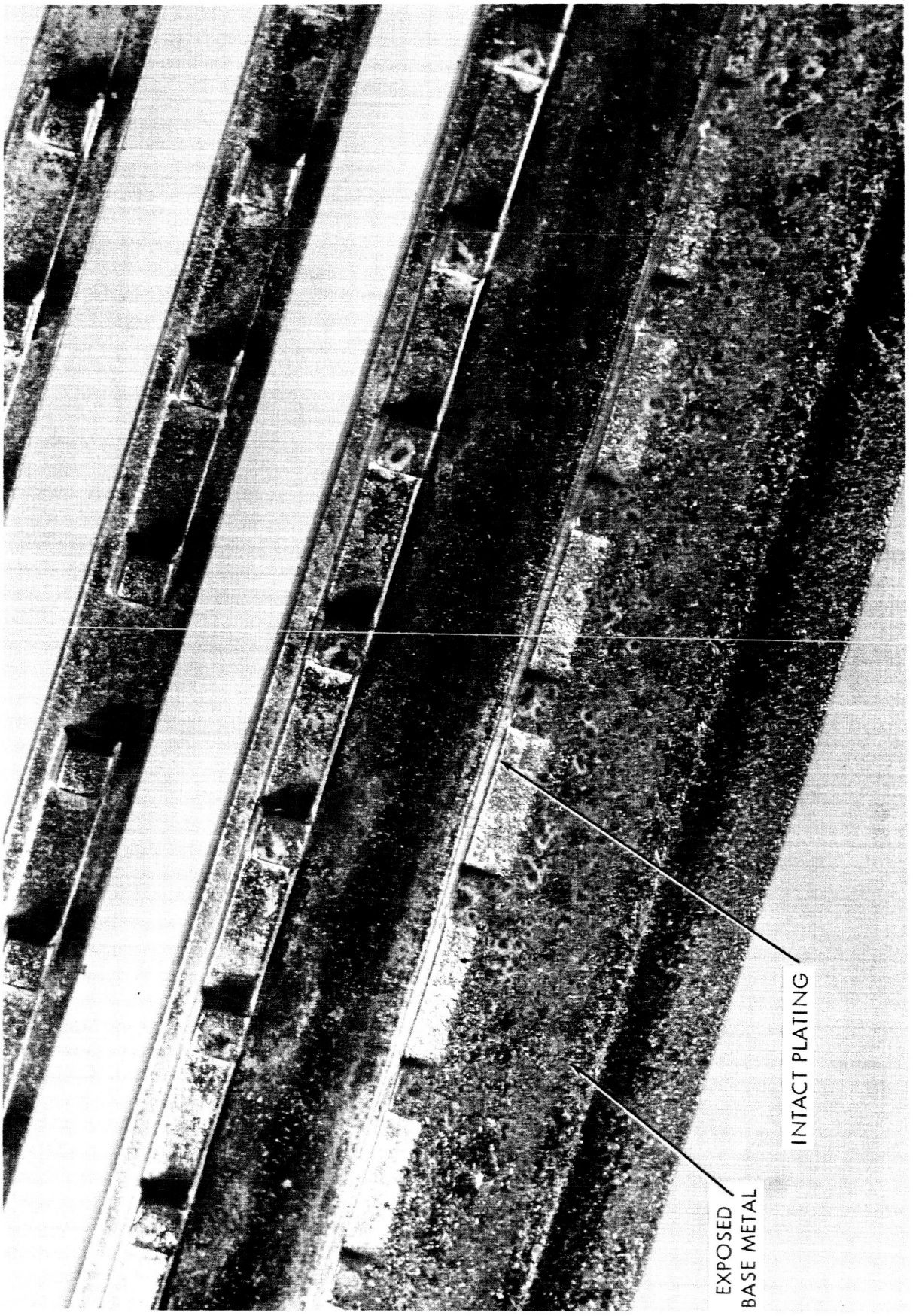

FIGURE 7-17 GOLD PLATED GAS DIFFUSION PLATE FROM SHORTED STAGE II CELL

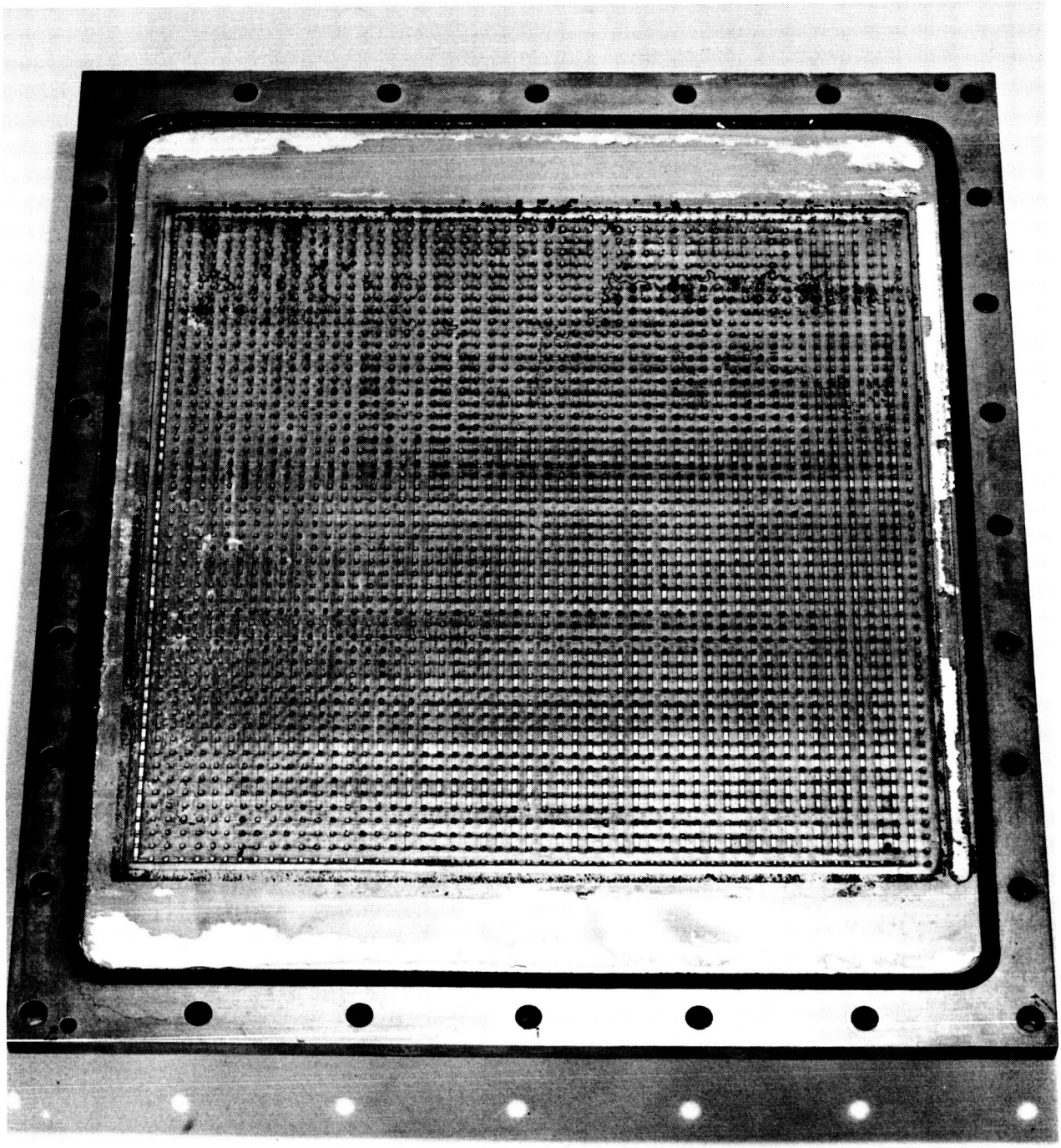

FIGURE 7-18 STAGE II ANODE END PLATE, CELL #1 AFTER LIFE TEST

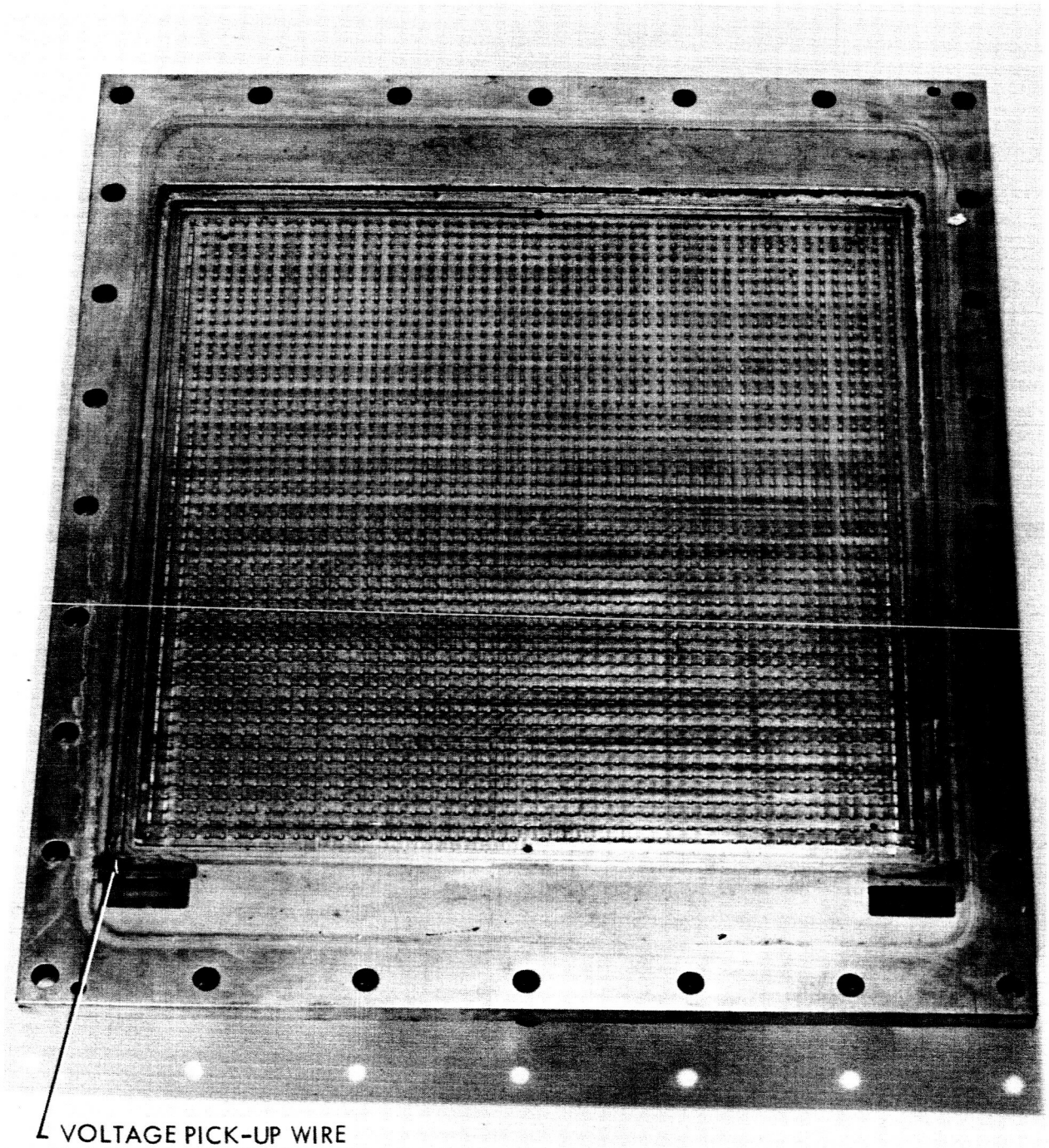

FIGURE 7-19 STAGE II CATHODE END PLATE, CELL #1 AFTER LIFE TEST

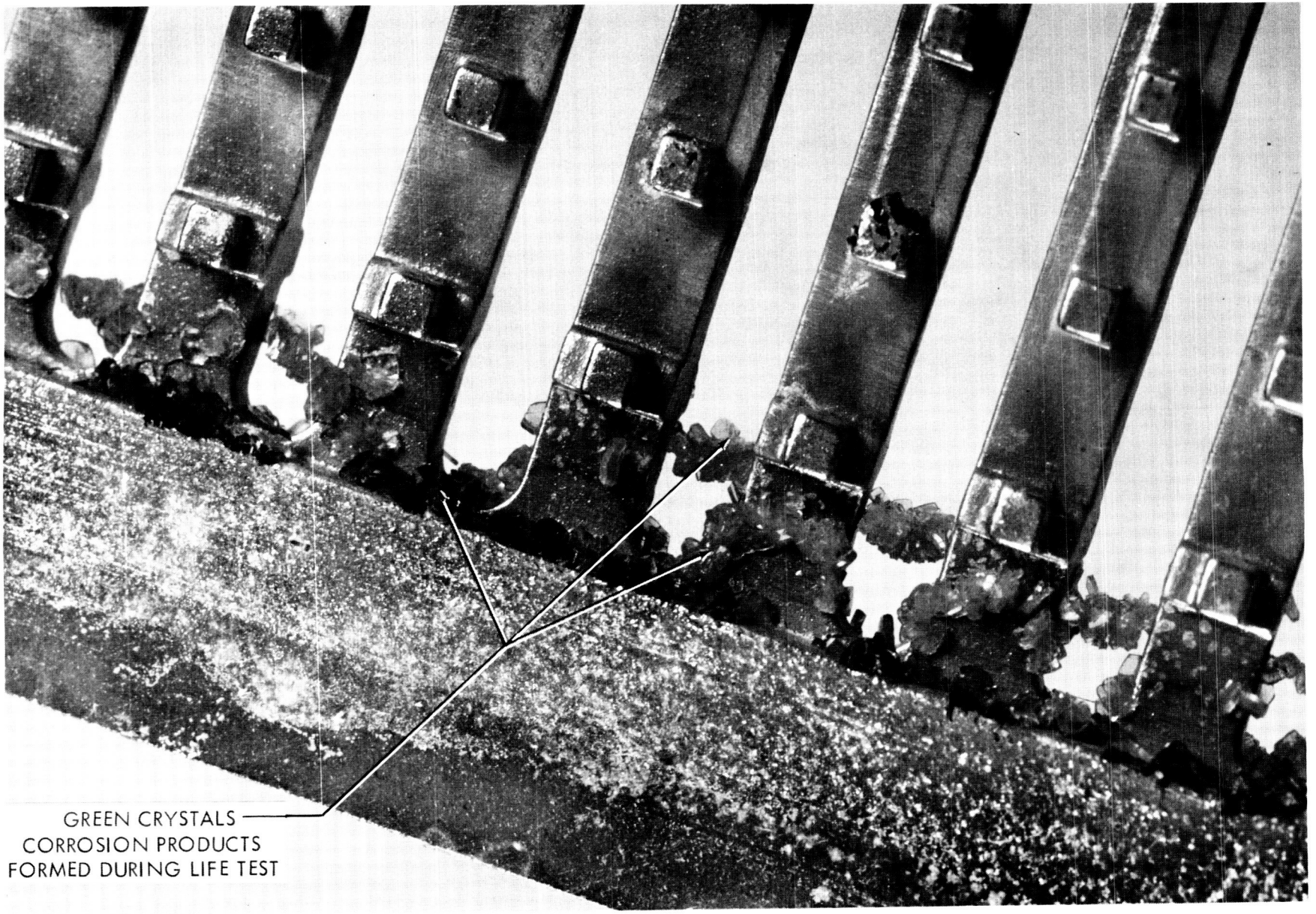

FIGURE 7-20 STAGE II GAS DIFFUSION PLATE, CORROSION PRODUCTS

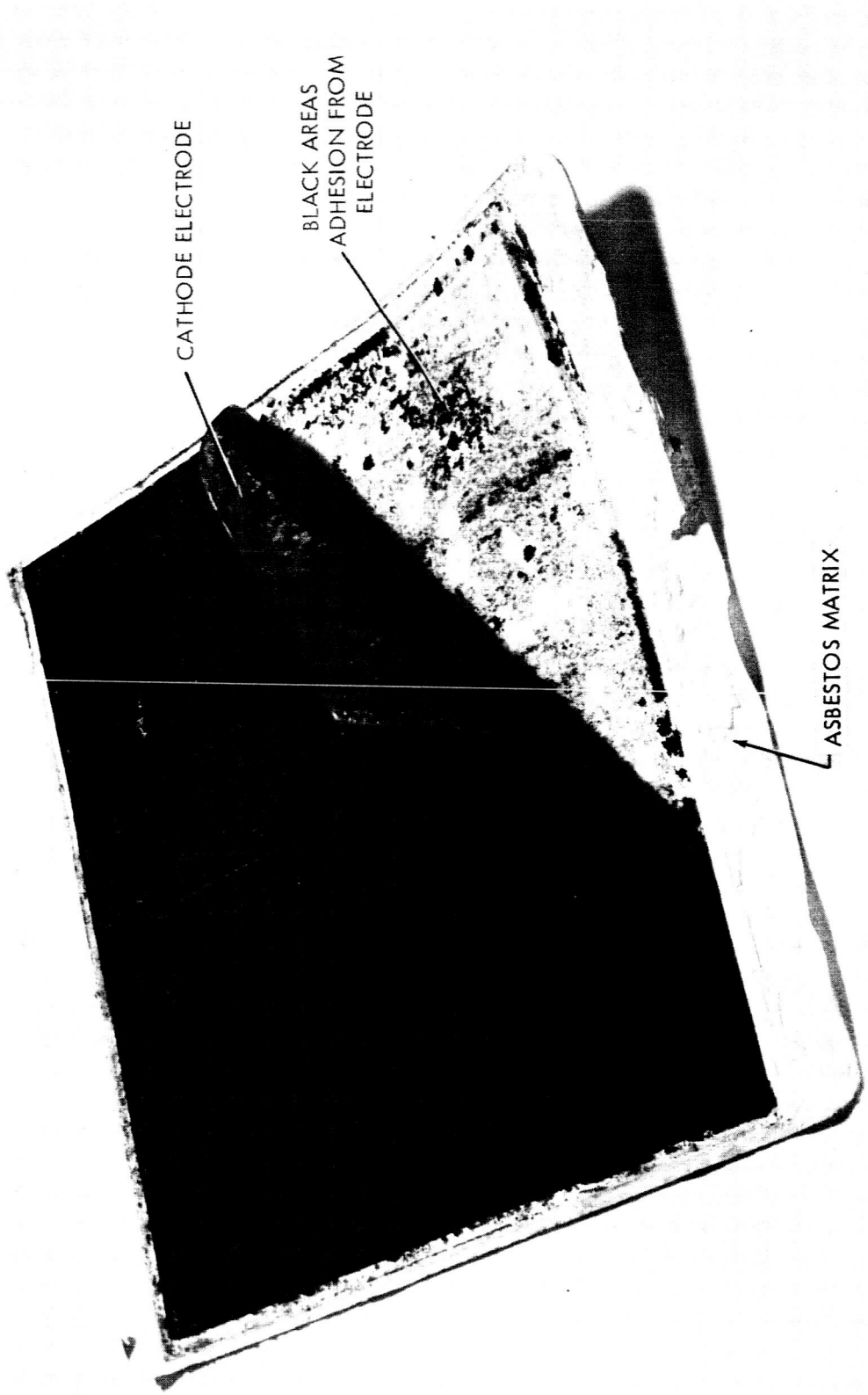

FIGURE 7-21 STAGE II ELECTRODE MATRIX PACK, CATHODE SIDE AFTER LIFE TEST

No explanation is offered for the continually decreasing cell voltage observed in the life test. The decay of the CO_2 transfer rate is attributed to formation of corrosion products.

An attempt was made to identify the products of corrosion. Both x-ray diffraction and spectrographic analyses were performed. In all samples the major constituents were potassium and nickel. Appreciable amounts of calcium and magnesium were present. The x-ray diffraction studies, yielded 50 or more discernible peaks on the diffraction chart. The most intense lines are not readily identifiable. $Ni(OH)_2$ was identified as correlating with some lines but not major lines. γ-NiOOH was also possible for some minor lines. Further studies will be required to definitely identify the compounds present. It is presently assumed that the major corrosion product is some form of nickel carbonate or oxidized nickel.

7.3 Stage III

Life testing of Stage III was conducted with a newly assembled cell and the cell which was used for parametric testing.

7.3.1 Cell Operation

Figure 7-22 presents the cell terminal voltage as a function of operating time for both cell number one and two. Both cells exhibited stable performance prior to developing an internal electrical short, as evidenced by the sharply decreasing cell voltage and anode gas output. Cell number two, the newly assembled cell operated for approximately 60 hours prior to indication of a short while cell number one operated properly for approximately 170 hours. Cell number one was stopped and restarted once due to a leak in the test rig plumbing. The oxygen transfer rate for each cell is given as a function of running time in Figure 7-23. Anode gas composition and flow are shown in Figure 7-24. Cell and humidifier temperature are shown in Figure 7-25.

7.3.2 Discussion of Results

The general condition of the acid cell hardware is shown in Figure 7-26. Cause of the electrical short is evident. Each cell exhibited a charred area in the PVDC material near the edge of the matrix. The matrix, Whatman GFB glass-fiber

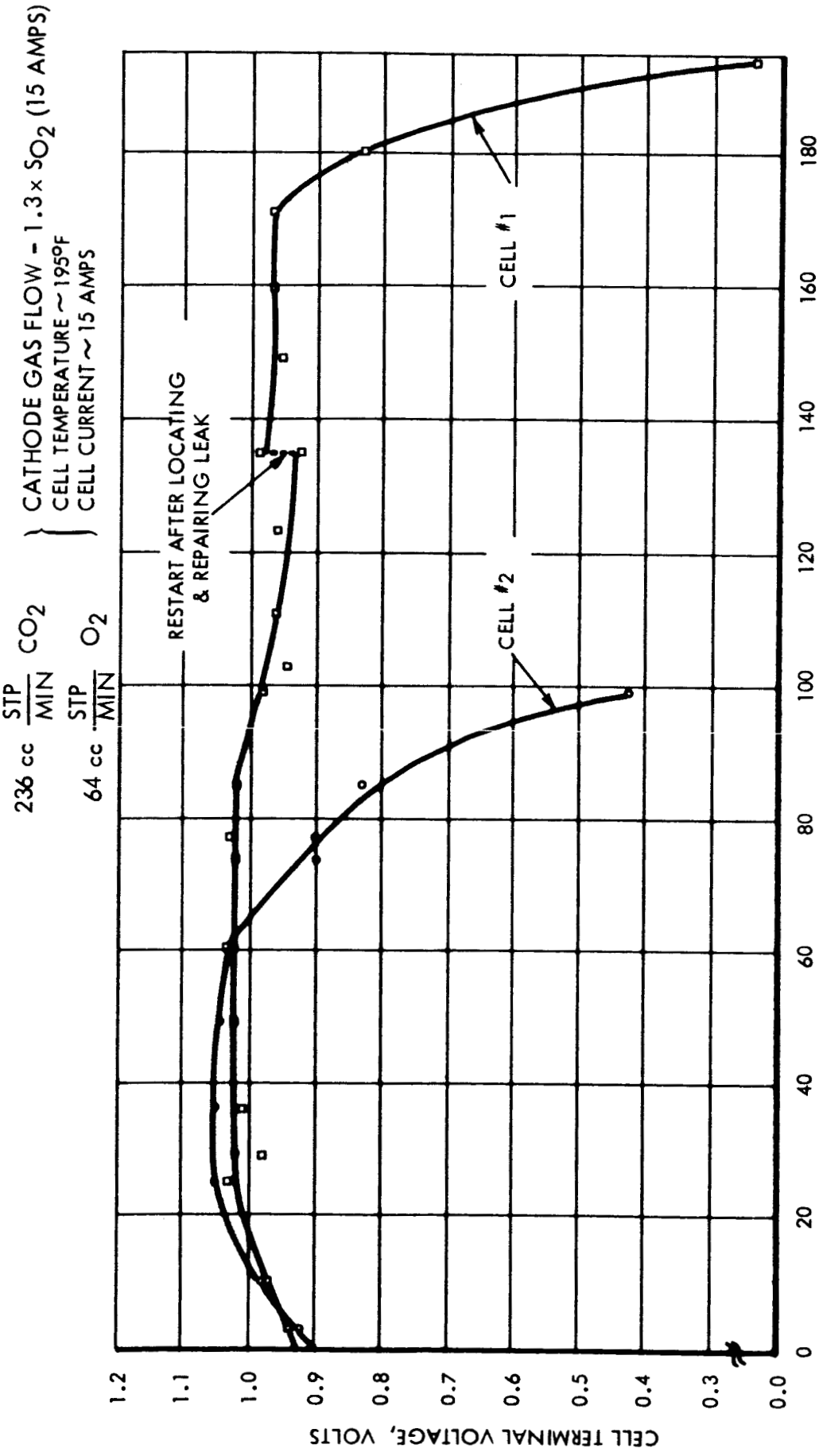

FIGURE 7-22 STAGE III - CELL #1 AND #2, LIFE TEST PERFORMANCE

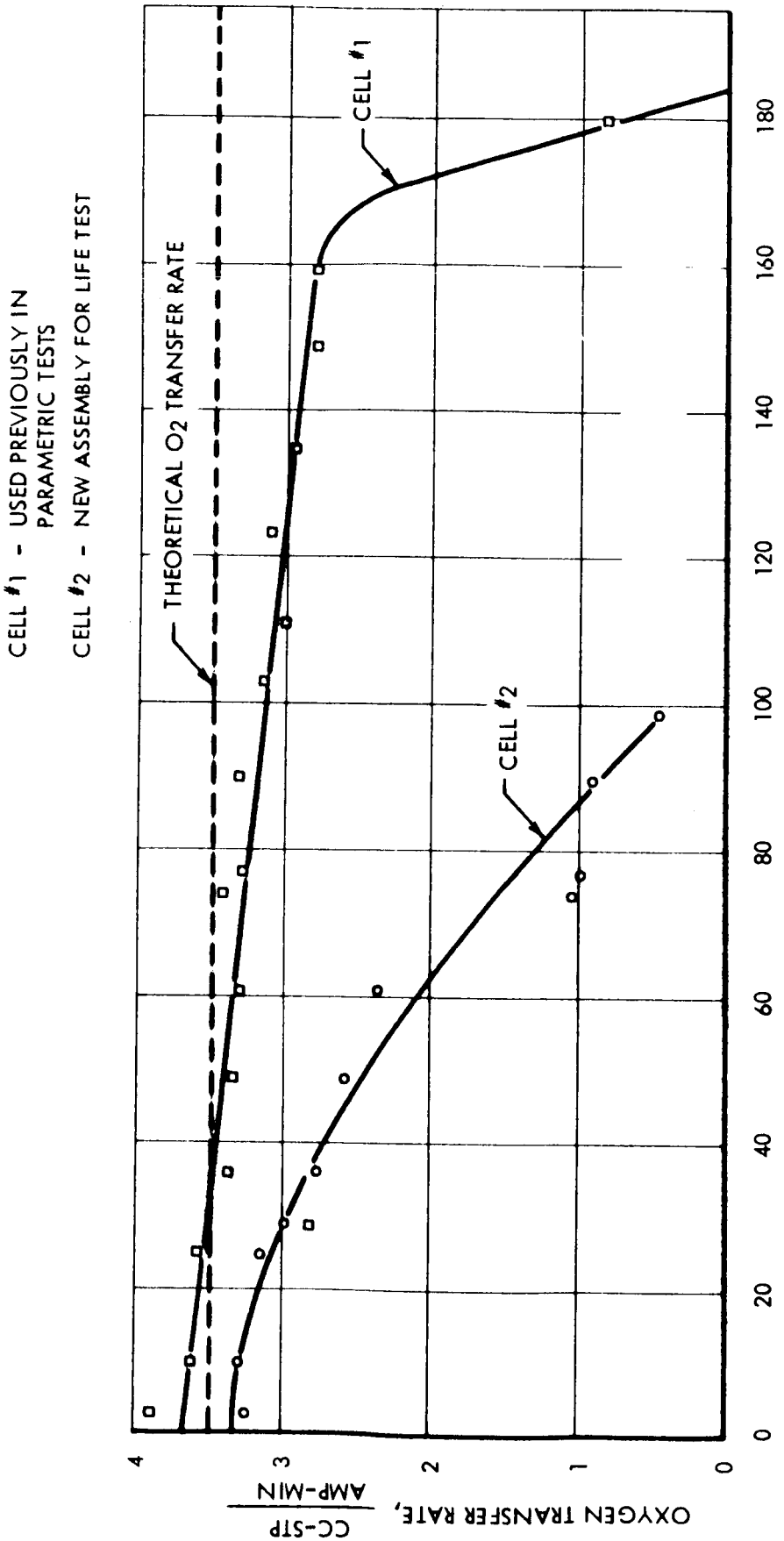

FIGURE 7-23 DECAY OF O_2 TRANSFER RATE WITH TIME, STAGE III - LIFE TEST

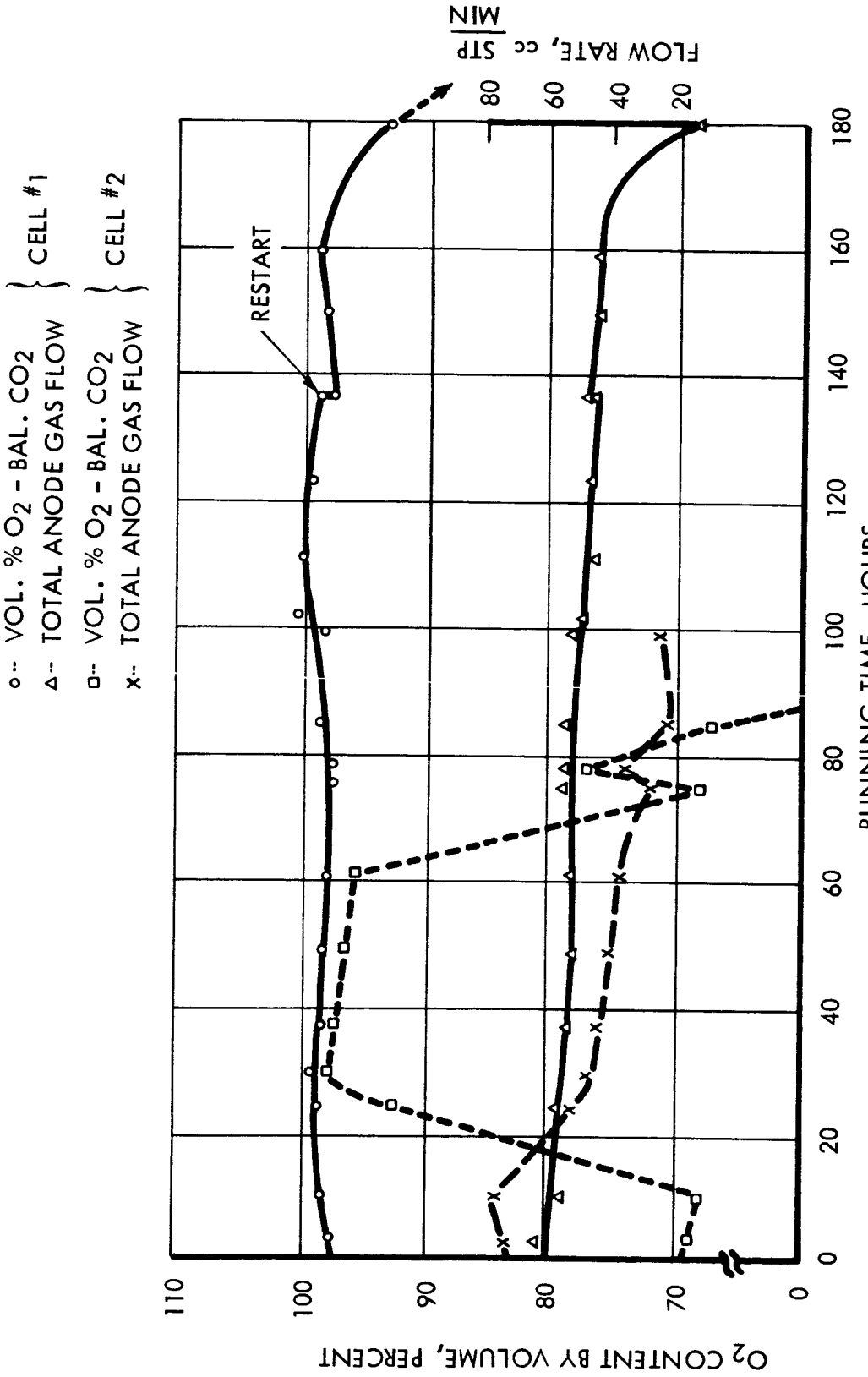

FIGURE 7-24 STAGE III, ANODE GAS OUTPUT - LIFE TEST

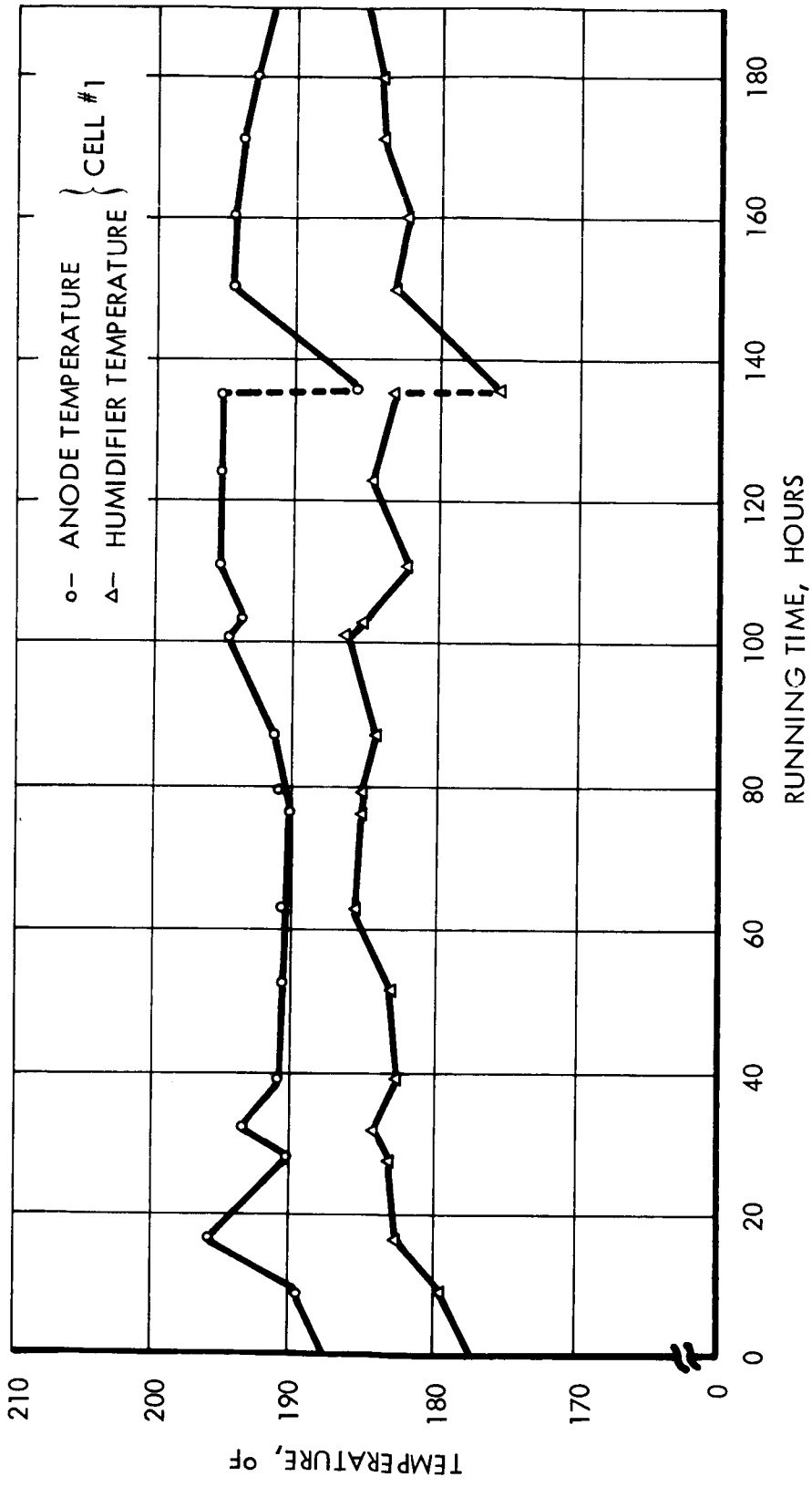

FIGURE 7-25 COMPARISON OF HUMIDIFIER AND CELL TEMPERATURE DURING STAGE III LIFE TEST

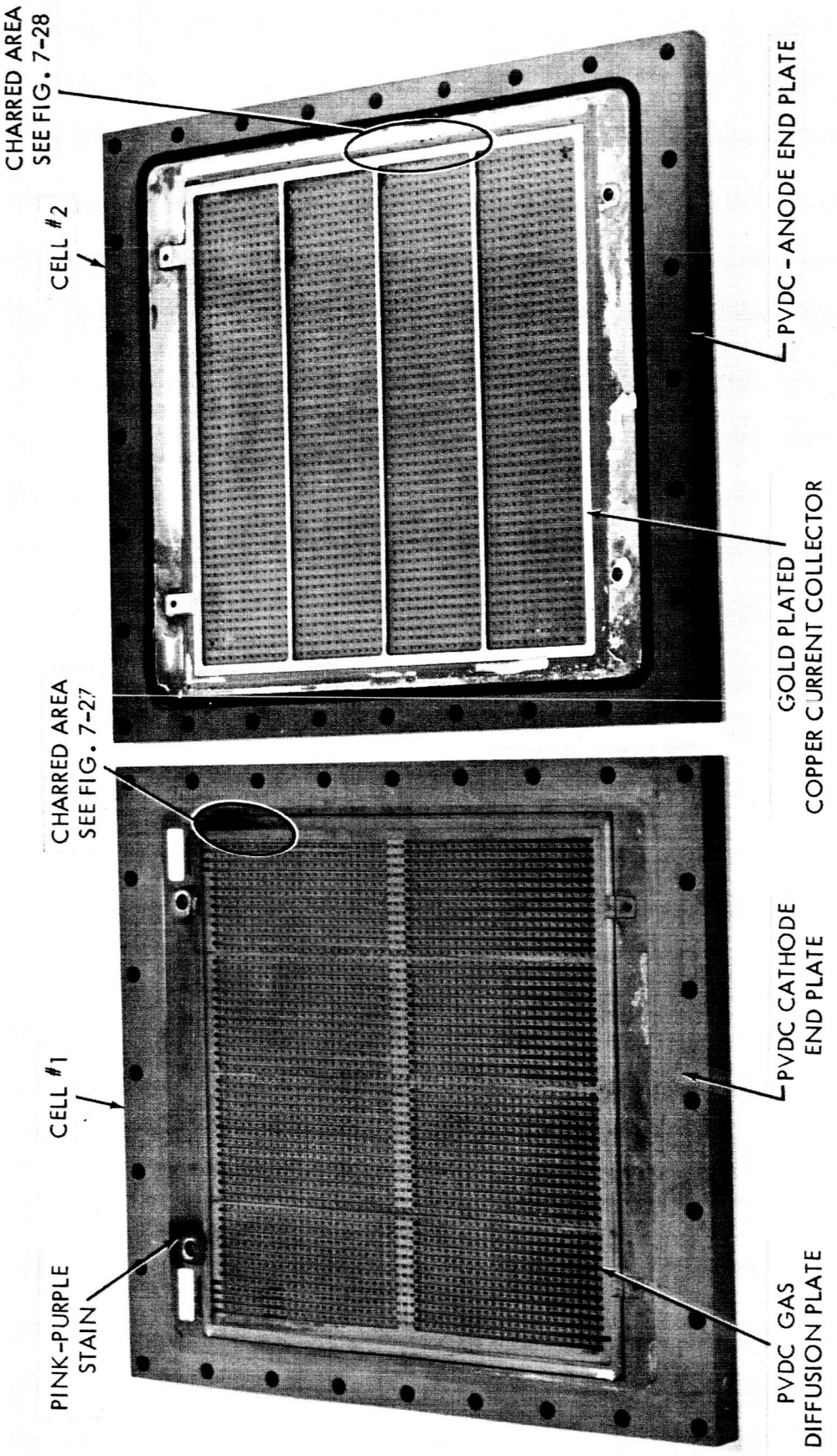

FIGURE 7-26 STAGE III COMPONENTS AFTER LIFE TEST

paper, is not physically strong, thus enabling the rough edges of the electrode screens to penetrate the matrix and cause the electrical shorts. High currents in the region of electrode contact caused localized heating and charring of the PVDC plastic end plates. Note also the stain (pink-purple in color) where the current collector tabs contact the end plates. This indicates that some gold did come off the gold plated current collectors in localized areas.

Figures 7-27 and 7-28 show close-up views of the charred areas of cell one and two respectively. The charring in cell number one was much more severe. Cell number one did drop off in voltage at a sharper rate than did cell number two indicating a much more severe short.

Post test condition of the matrix and electrodes from cell number one is seen in the photographs, Figures 7-29 and 7-30. Figure 7-30 shows the cathode side of the matrix and the cathode electrode, matrix side up. The anode side of the matrix and the anode electrode, matrix side up are seen in Figure 7-30. The stain which outlines the current collector shape on the cathode side is yellow-orange in color. This stain does not show on the anode side. Note also the difference in appearance between the cathode and anode electrodes. A significant amount of platinum has been lost from the cathode but not from the anode.

Figure 7-31 shows the matrix and electrode, cathode side up, from cell number two, exhibiting the same general characteristics noted in cell number one.

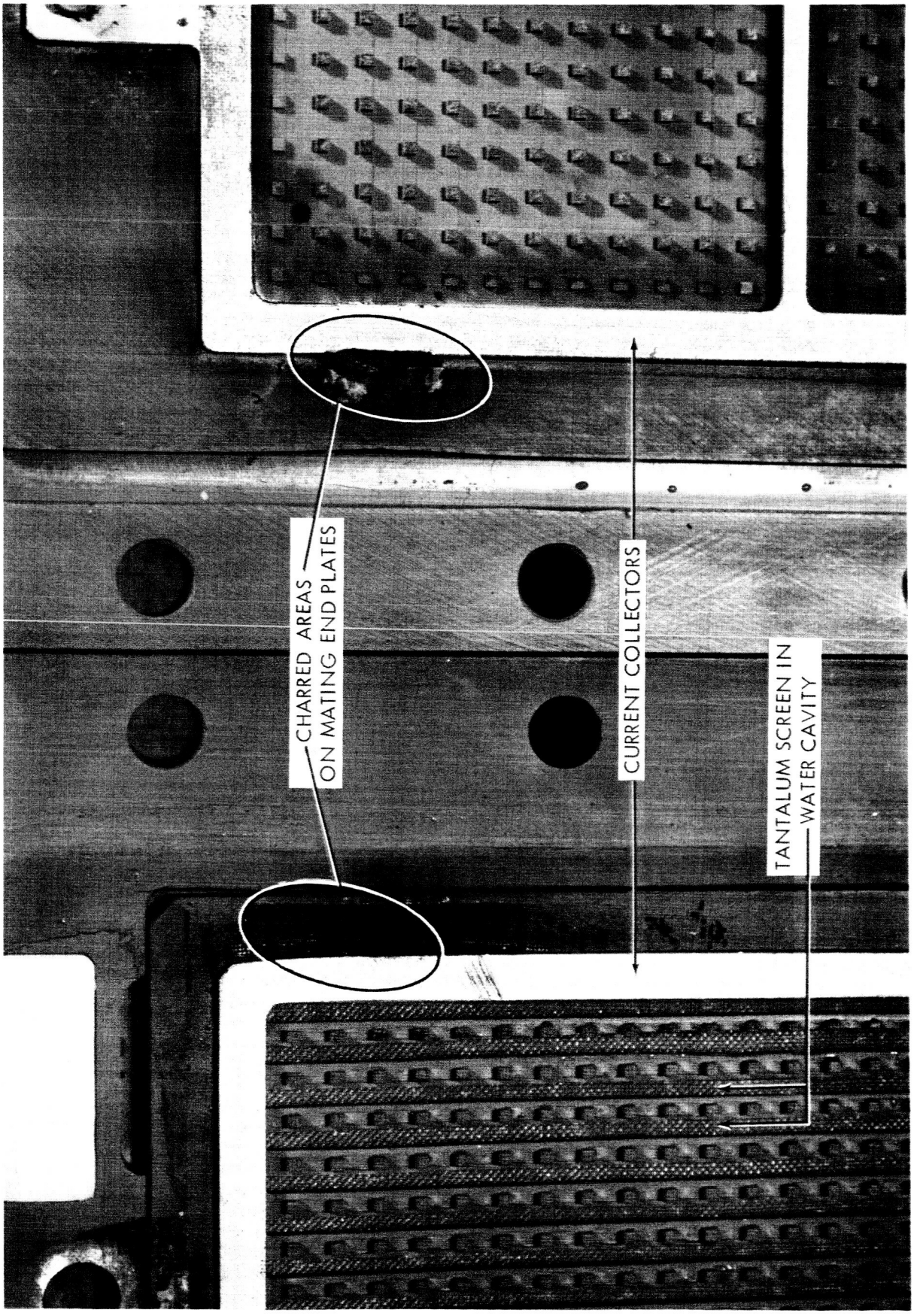

FIGURE 7-27 STAGE III - CELL #1, CHARRED AREAS IN SHORTED CELL

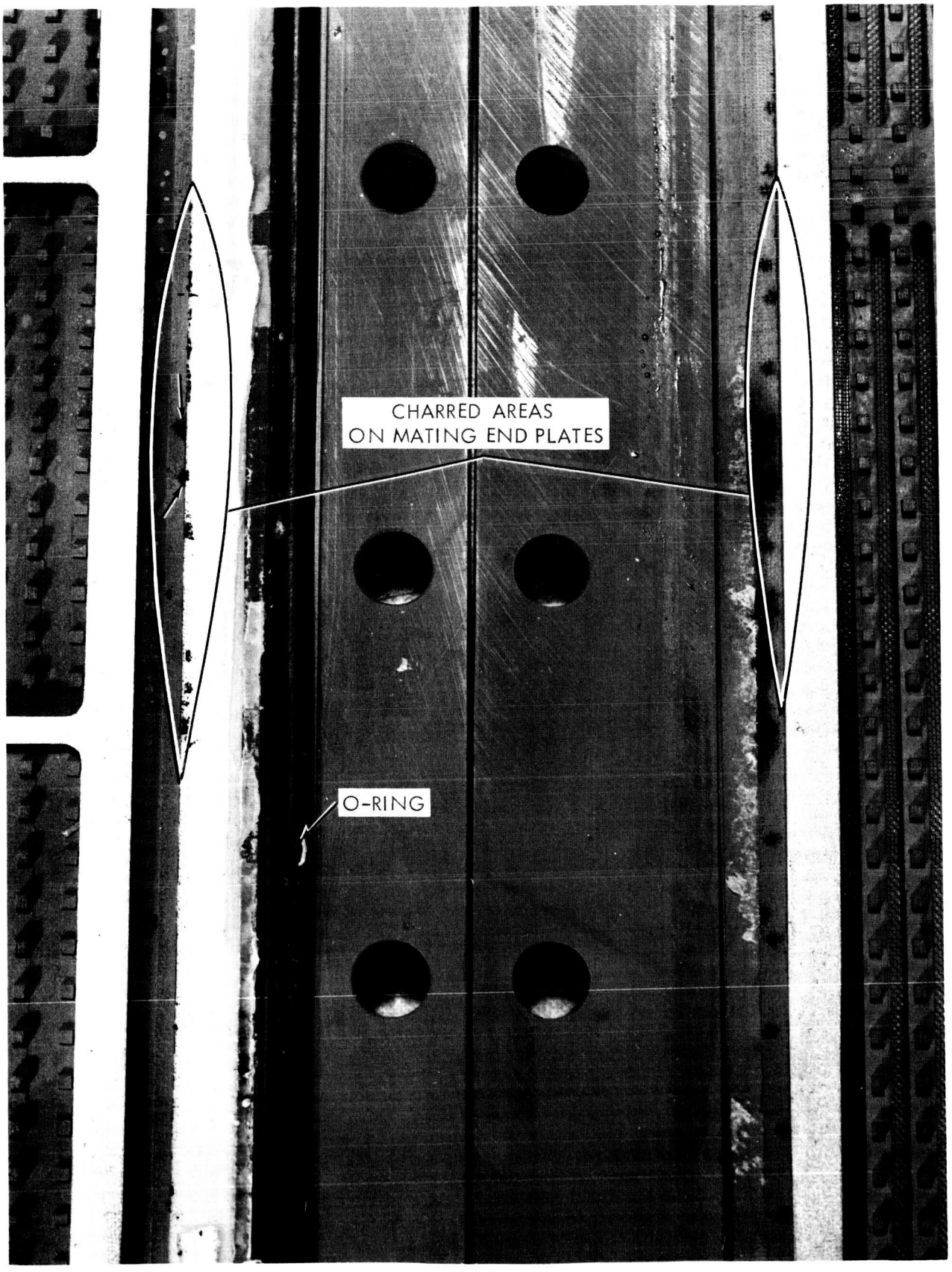

FIGURE 7-28 STAGE III - CELL #2, CHARRED AREAS IN SHORTED CELL

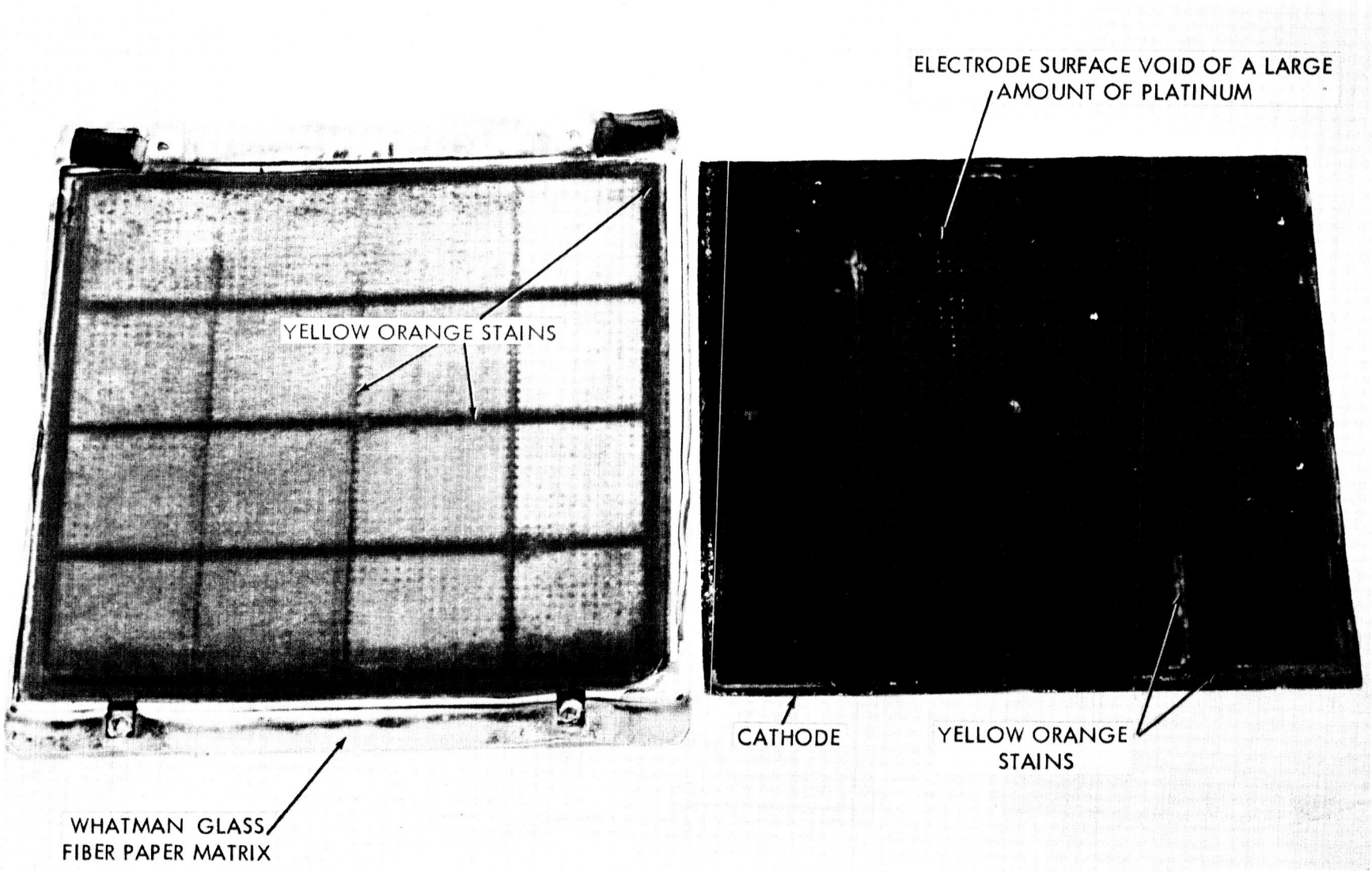

FIGURE 7-29 STAGE III - CELL #1, ELECTRODE MATRIX CATHODE SIDE

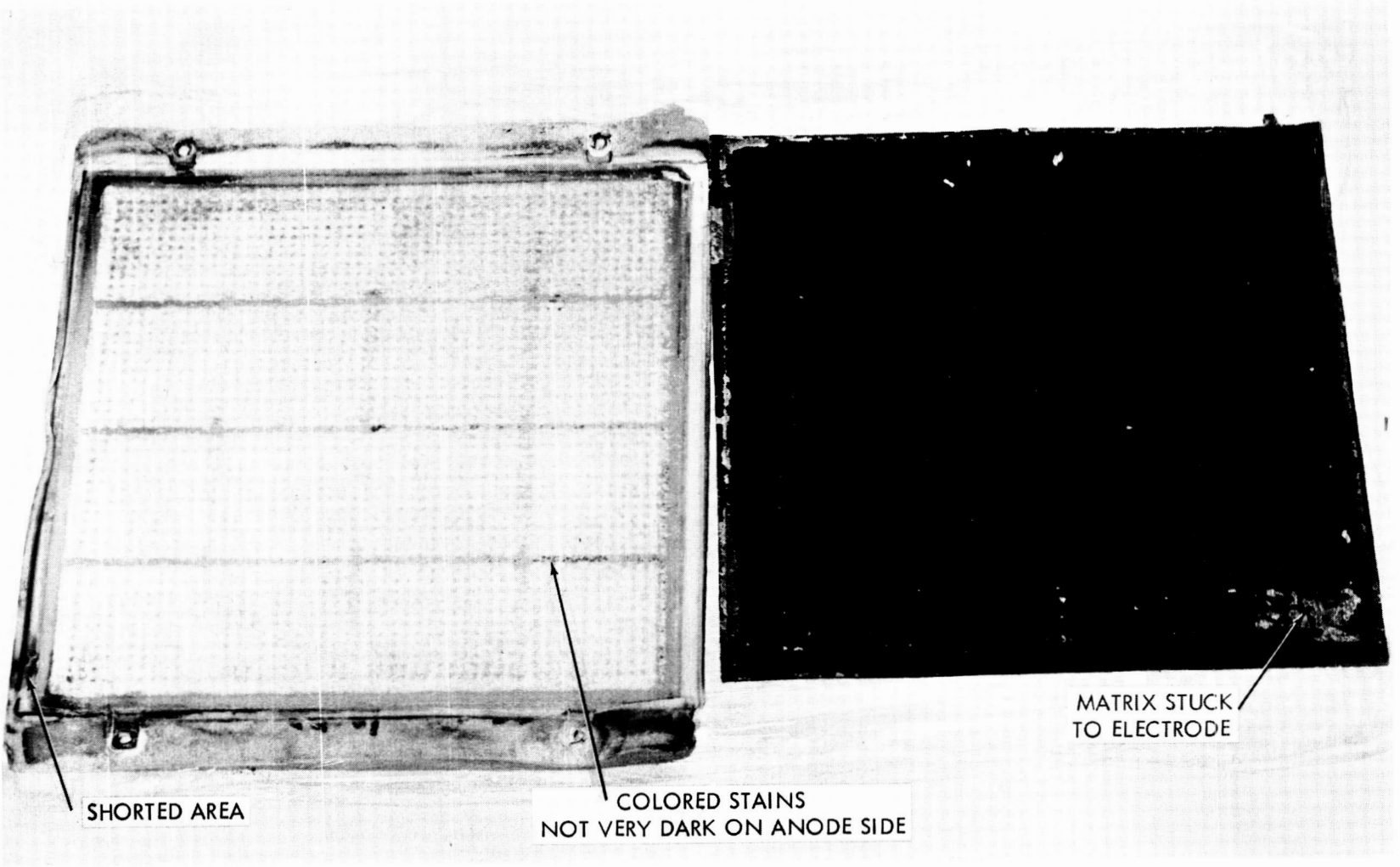

FIGURE 7-30 STAGE III - CELL #1, ELECTRODE MATRIX PACK ANODE SIDE

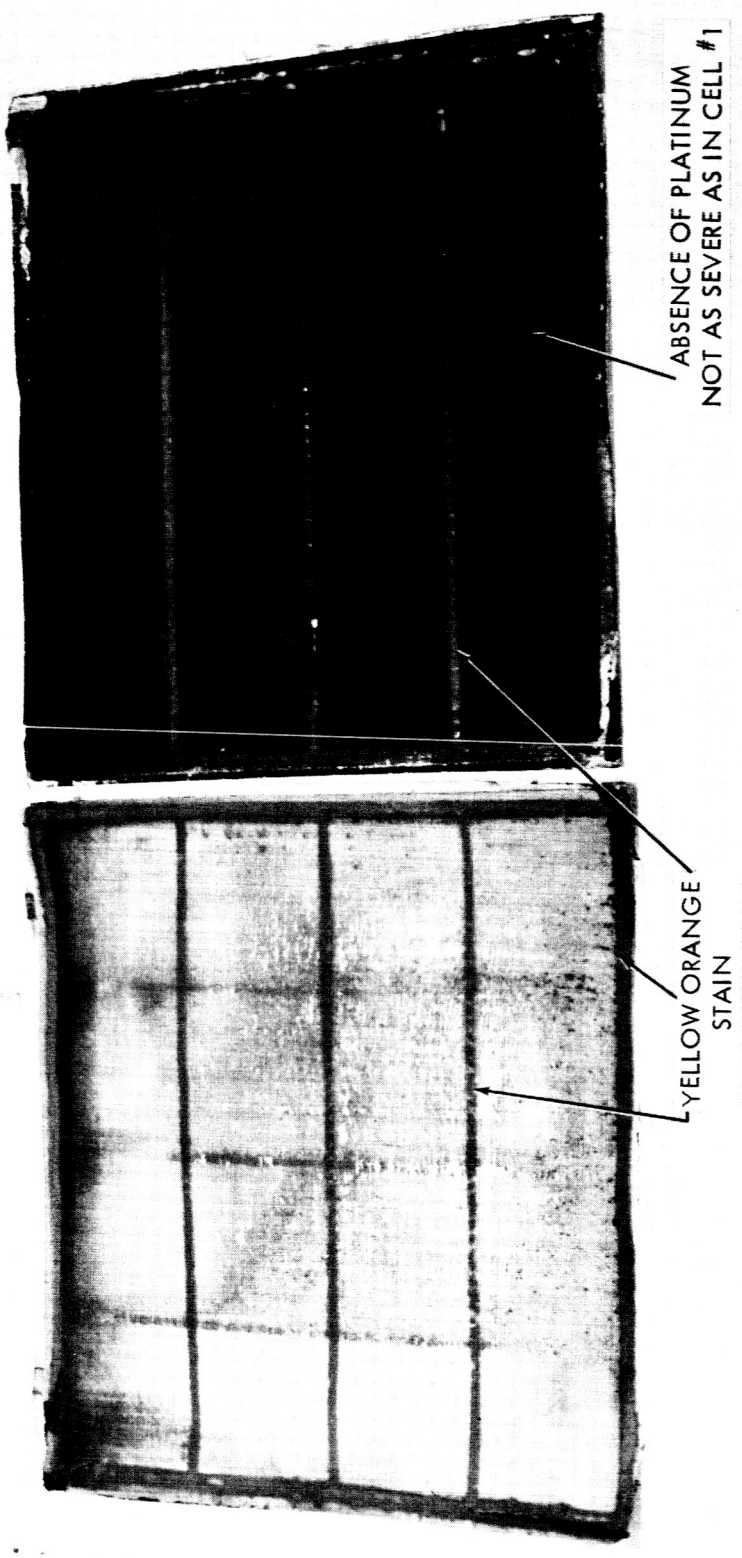

FIGURE 7-31 STAGE III - CELL #2, ELECTRODE MATRIX PACK - CATHODE SIDE

8.0 THERMAL BALANCE STUDY

A thermal balance study was conducted to determine operating characteristics which will yield a system having minimum weight while operating at temperatures and electrolyte concentrations required to achieve self-regulated temperature control. Preliminary system coolant requirements were also determined. A final detailed thermal balance would require actual vehicle system interface parameters.

8.1 System Description

The system used for this study is shown schematically in Figure 8-1. For the purposes of this analysis a three stage system was used even though a two stage system is recommended for future development.

Cabin air, before enetering the Stage I cathode, passes through the water vapor exchanger where it picks up both heat and water vapor from the Stage I cathode-out gas. In the Stage I cells the air is partially stripped of CO_2 and O_2, while picking up heat primarily by water evaporation. Before exhausting the air back to the cabin, it is cooled and dried in a condenser-separator. The recovered water is fed to a water feed reservoir. Flow of water from the reservoir to the Stage I water cavity is controlled by maintaining the water pressure just below the cathode gas cavity pressure through the use of a reference gas line to the cathode gas cavity and a spring connected to the feed diaphragm. Cooling of the cells is accomplished by evaporative cooling in the cell, while cooling of the cathode-out gas stream is accomplished by 1) the incoming cabin air and 2) the condenser-separator. Vehicle coolant flows through the condenser-separator.

The Stage I anode gas is fed to the Stage II cathode. Again cell cooling is accomplished by evaporation of water into the flowing cathode gas stream (and anode gas stream). The cathode-out gas flows through a condenser-separator before exhausting to the cabin. Water from the condenser-separator is fed to a water reservoir which serves as a common feed to both Stage II and Stage III.

A similar flow of Stage II anode gas into the Stage III cell is used. Cooling is again by evaporation. Water is removed from the cathode-out and the anode-out streams in condenser-separators. All condensed water is fed to the Stage II-III common water reservoir. Make-up water is added to the reservoirs as required.

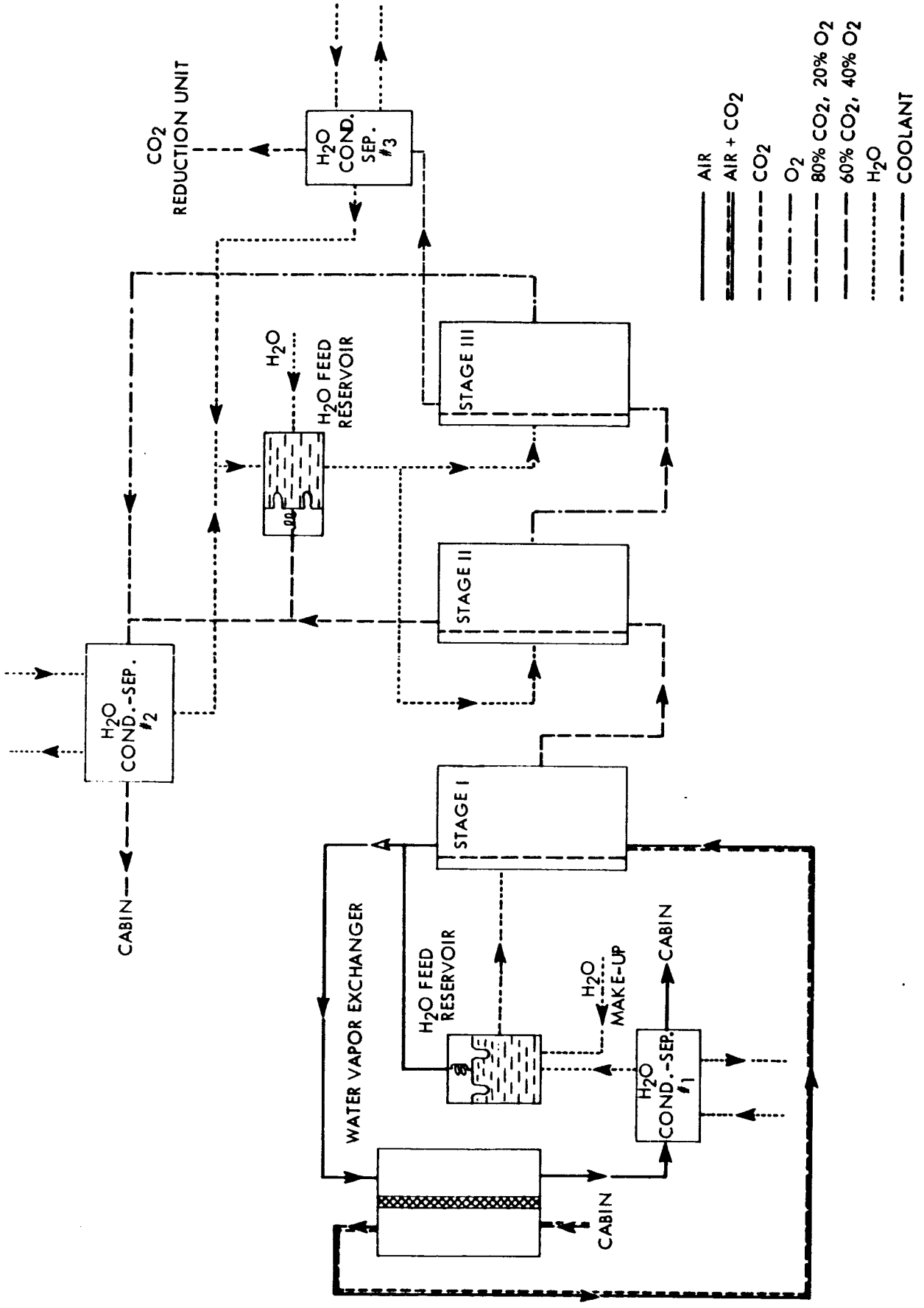

FIGURE 8-1 THREE STAGE CO_2 CONCENTRATION SYSTEM SCHEMATIC

8.2 Selection of Operating Conditions

In order to determine system cooling requirements we must first fix the cell operating temperatures and cell heat rejection requirements. Using the data obtained in the parametric testing phase, we optimize the weight of each stage as a function of current density for each stage with the cell temperature as a parameter.

The expressions used in calculating the current required for each stage are given below:

First Stage: $$\left[NI_a\right] \approx 553 \left(\dot{W}_{CO_2}\right)\left[2\,\frac{O_2\%\ A_{OI}}{CO_2\%\ A_{OI}}\right]\left[4\,\frac{O_2\%\ A_{OII}}{CO_2\%\ A_{OII}}\right]$$

Second Stage: $$\left[NI_a\right] \approx 276 \left(\dot{W}_{CO_2}\right)\left[4\,\frac{O_2\%\ A_{OII}}{CO_2\%\ A_{OII}}\right]$$

Third Stage: $$\left[NI_a\right] \approx 276 \left(\dot{W}_{CO_2}\right)\left[4\,\frac{O_2\%\ A_{OII}}{CO_2\%\ A_{OII}}\right] 1/S_{O_2}$$

where:

$\dot{W}_{CO_2}$ = removal rate of CO_2 in lbs/hr.

$O_2\%\ A_{OI}$ = percent O_2 in Stage I anode out.

$CO_2\%\ A_{OI}$ = percent CO_2 in Stage I anode out.

$O_2\%\ A_{OII}$ = percent O_2 in Stage II anode out.

$CO_2\%\ A_{OII}$ = percent CO_2 in Stage II anode out.

S_{O_2} = stoichiometric O_2 flow ratio = 1.03.

The calculations are based on a CO_2 removal rate of 9.34 pounds per day, sufficient capacity for four men. The percentages of CO_2 and O_2 out of each stage vary with the cell current density and temperature. This data is obtained from the parametric tests reported in Section 6.0. The current required

is calculated as a function of cell current density for each stage at various operating temperatures. Knowing the required current, the cell stack weight and power are calculated. Table 8-1 summerizes the calculations for each stage.

TABLE 8-1

WEIGHT OPTIMIZATION OF STAGE I, II, AND III

	Cell Temp °F	Cell Current Density ASF	Current Required, Amps	Cell Voltage, Volts	Cell Power, Watts	Total Weight, lbs
STAGE I	90	15	542	1.220	660	314
	90	20	592	1.320	780	332
	116	15	400	1.100	440	220
	116	30	432	1.300	560	220
	116	40	828	1.425	1180	421
	140	15	512	0.935	476	254
	140	30	432	1.135	488	199*
	140	45	532	1.250	664	242
STAGE II	122	15.5	154	0.996	154	83
	122	22.25	166	1.170	194	87
	122	30.25	162	1.340	217	88
	176	16.25	154	0.770	118	69
	176	29.00	154	0.962	148	67*
	176	45.00	158	1.110	176	70
STAGE III	172	16.5	213	1.018	217	111
	172	33.5	213	1.082	232	96
	172	52	213	1.195	255	96
	195	17	213	0.968	206	107
	195	35	213	1.034	221	91
	195	51	213	1.070	228	88*

Those operating conditions which yield the minimum weight for each stage are indicated by an asterisk. The effect of thermal requirements were not considered in these calculations since specific temperatures and types of coolant fluids with resultant weight penalties are not known. For the above calculations a power penalty of 300 pounds per kilowatt was assumed.

8.3 Thermal Analysis

Based on the table above, the net heat inputs for the three stages of the CO_2 concentration system are 488, 148 and 228 watts for the first, second and third stages respectively. Removal of heat by evaporation of water into the process gases is feasible. The vapor transfer device used in conjunction with Stage I will work in principle, but data is not now available on transfer rates at given concentration gradients; therefore sizing of the device is not now possible.

Calculations for three condensers to lower dew points of various exit gases to 45°F show that the total coolant flow required is 1286 lb/hr. The temperature rise of the coolant (FC-75) is taken as 10°F and the specific heat as 0.23 BTU/lb °F. The flow could be lowered by changing to a fluid of greater specific heat, i.e. ethylene glycol and H_2O. Such a solution might have a specific heat of 0.75 which would require the coolant flow to be 395 lb/hr. With FC-75, the individual flows would be 711 lb/hr for condenser 1, 215 lb/hr for condenser 2, and 360 lb/hr for condenser 3. Use of an alternate fluid could change these to 218 lb/hr, 66 lb/hr, and 110 lb/hr.

The thermal characteristics and operating conditions for the three stages, the three condenser-separators and the vapor transfer device are summarized in Tables 8-2 through 8-8. Assumptions used in making these thermal calculations were:

1. Cooling is accomplished by only evaporation of water in cells.
2. Perfect gases.
3. No heat transfer with surroundings.
4. All gases saturated with vapor except inlet to condenser number 2.
5. All vapor exits via the cathode out-gas in Stage I.

Preliminary system optimization indicates that Stage I should be operated at 140°F, but the thermal balance study indicates a self-controlling system with the first stage operating at 131°F. A change in the thermal balance is not

warranted here since all factors of vehicle integration were not considered in the initial weight optimization. When all factors are considered, such as integration with vehicle heating and cooling loops, then a much more precise calculation can be made. The indications at the moment are that a system can be operated at conditions, such that a reasonable mode of temperature control is possible. The weight and power requirements of the systems are attractive enough for further development.

A sample calculation is shown in Appendix A for Stage II and condenser 2.

TABLE 8-2

STAGE I - THERMAL CHARACTERISTICS

	CATHODE IN	CATHODE OUT	ANODE
O_2 lb/hr			6.92 lb/day
CO_2 lb/hr			12.56 lb/day
N_2 lb/hr			0
TOTAL lb/hr	141.6	140.8	19.48 lb/day
HUMIDITY RATIO lb/lb	0.0652	0.0760	0.0426
DEW POINT °F	100°F	105°F	105°F
TOTAL PSIA	10	10	13

BTU REMOVED	1665 BTU/hr
H_2O EVAP	1.52 lb/hr
CELL TEMP.	131°F
ELEC. CONC.	~ 50 WT% K_2CO_3

TABLE 8-3

STAGE II - THERMAL CHARACTERISTICS

	CATHODE IN	CATHODE OUT	ANODE
O_2 lb/day	6.92	4.52	2.40
CO_2 lb/day	12.56	3.20	9.36
TOTAL lb/day	19.48	7.72	11.76
HUMIDITY RATIO	0.0426	0.646	0.572
DEW POINT °F	99°F	172°F	172°F
TOTAL PSIA	11	11	11

BTU REMOVED	504 BTU/hr
H_2O EVAP.	10.9 lb/day
CELL TEMP.	176°F
ELEC. CONC.	~ 20 WT% K_2CO_3

TABLE 8-4

STAGE III - THERMAL CHARACTERISTICS

	CATHODE IN	CATHODE OUT	ANODE
O_2 lb/day	2.40	0.08	2.32
CO_2 lb/day	9.36	9.36	-
TOTAL lb/day	11.76	9.44	2.32
HUMIDITY RATIO	0.572	1.88	2.58
DEW POINT °F	169°F	186°F	186°F
TOTAL PSIA	10.5	10.5	10.5

BTU REMOVED	18,600 BTU/day
H_2O EVAP.	16.42 lb/day
CELL TEMP.	195°F
ELEC. CONC.	~32.5 WT% H_2SO_4

TABLE 8-5

VAPOR TRANSFER DEVICE - THERMAL CHARACTERISTICS

	GAS FROM CABIN	GAS TO STAGE I	GAS FROM STAGE I	GAS TO CONDENSER 1
COMPOSITION	AIR	AIR	AIR	AIR
LB/HR	141.6	141.6	140.8	140.8
HUMIDITY RATIO	0.00934	0.0652	0.0760	0.02014
DEW POINT °F	45°F	100°F	105°F	66°F
TOTAL PSIA	10	10	10	10

TABLE 8-6

CONDENSER 1 - THERMAL CHARACTERISTICS

	GAS IN	GAS OUT	COOLANT IN	COOLANT OUT
FLOW LB/HR	140.6	140.6	711	711 (FC-75)
DEW POINT °F	66°F	45°F	-	-
°F DIFF. OUT-IN	21		10	
PRESSURE		10 PSIA		
COMPOSITION	~AIR	~AIR		
HUMIDITY RATIO	0.02014	0.00934		
Q, BTU/HR	1635			

TABLE 8-7

CONDENSER 2 - THERMAL CHARACTERISTICS

	GAS IN CATHODE STAGE II	GAS IN ANODE STAGE III	GAS OUT	COOLANT
FLOW LB/DAY	7.22	2.32	9.54	215 lb/hr (FC-75)
HUMIDITY RATIO	0.646	2.58	0.00768	
DEW POINT	172°F	186°F	45°F	
PRESSURE	11 PSIA	10.5 PSIA	10 PSIA	
O_2	4.52	2.32	6.84	
CO_2 LB/DAY	3.2		3.2	
TEMP. DIFF. °F				10
Q, BTU/DAY	11,911			

TABLE 8-8

CONDENSER 3 - THERMAL CHARACTERISTICS

	GAS IN	GAS OUT	COOLANT
FLOW LB/DAY	9.44	9.44	360 lb/hr (FC-75)
(CO_2)	9.36	9.36	
O_2	0.08	0.08	
HUMIDITY RATIO	1.88	0.00610	
DEW POINT °F	186°F	45°F	
PRESSURE	10 PSIA		
TEMP. DIFF. °F			10
Q, BTU/DAY	19,909		

9.0 CONCLUSIONS

Based on the experimental results obtained, the following conclusions are believed to be justified:

1. The actual process used for concentrating carbon dioxide studied under this contract is feasible.
2. Performance of all three stages meets or exceeds performance predictions based on past tests with TRW plastic laboratory cells.
3. Wide variations in cell operating conditions, for all three stages, can be tolerated without irreversible cell performance degradation.
4. Gas flow rate to the cathode of each stage need not exceed the following values for satisfactory performance:

   a. Stage I - $2 \times S_{CO_2}$

   b. Stage II - $1 \times S_{CO_2}$

   c. Stage III - $1.03 \times S_{O_2}$

5. Operation of the process is feasible at elevated cell temperatures.
6. Operation of all three cell stages is feasible at current densities exceeding 45 ASF. The upper limit at elevated cell temperatures has not been determined.
7. Thermal analysis indicates cooling of each stage by water evaporation from a liquid reservoir is possible.
8. The present materials used for Stage I and II are not suitable for long term operation. This includes the end plates and the electrodes (nickel base screen).
9. Non-porous gold plated components appear to be satisfactory for long term Stage III cell operation.
10. A better matrix material for long term Stage III cell operation is required.
11. Loss of platinum from the Stage III cell cathode appears to be a long term operating problem.

12. A detailed materials study program is required to:

    a. Establish the mechanisms for the corrosion processes observed.

    b. Provide materials for suitable long term operation.

APPENDIX A

THERMAL BALANCE CALCULATION

The following sample calculation is presented to illustrate the technique used in determining the thermal operating characteristics of the various components of a three stage CO_2 concentration system. Stage II and condenser 2 were chosen as representative system components. Operating conditions are to be determined which allow the cells to operate at a temperature and electrolyte concentration such that cell cooling and electrolyte concentration control are accomplished within the cell by water addition and evaporation. The same general procedure of these calculations apply to the analysis performed in Section 3.1.

Stage II - Cell Stack

Figure A-1 presents a flow schematic for the Stage II cells.

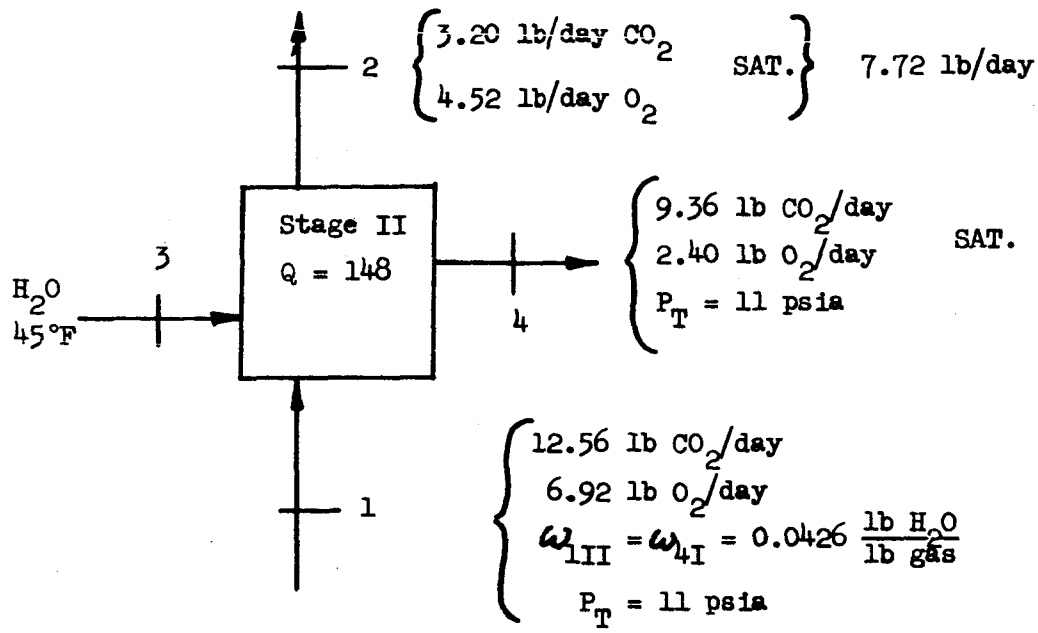

FIGURE A-1 STAGE II FLOW SCHEMATIC

where

P_T = total pressure

ω = humidity ratio

Amount of heat removed:

$$Q = 148 = 504 \text{ BTU/hr} = 12{,}100 \text{ BTU/day}$$

$$\text{Water Evaporated} = \frac{\text{Heat Removed}}{\text{Change in Enthalpy}} = \frac{12{,}100}{\Delta h_{Evap}} = \frac{12{,}100}{(1122)_{140°F} - 13} = 10.9 \text{ lb/day}$$

Water evaporated is equal to sum of water removed or added by each gas stream.

Therefore

$$10.9 \text{ lb/day} = \omega_2 \dot{M}g_2 + \omega_4 \dot{M}g_4 - \omega_1 \dot{M}g_1$$

where $\dot{M}g$ = mass flow rate of gas.

Humidity ratio of gas flows are given by

$$= \frac{\text{Mol Wt } H_2O}{\text{Mol Wt gas}} \times \frac{\text{Vapor Pressure of water}}{\text{Total Pressure - Vapor Pressure}}$$

$$\therefore \omega_2 = \frac{18}{Mg_2} \frac{Pv}{11-Pv}$$

$$\text{where } Mg_2 = \frac{1}{\frac{3.2}{7.72 \times 44} + \frac{4.52}{7.72 \times 32}} = 36.1$$

$$\omega_2 = \frac{18}{36.1} \frac{Pv}{11-Pv} = .498 \frac{Pv}{11-Pv}$$

and

$$\omega_4 = \frac{18}{Mg_4}\left(\frac{Pv}{11-Pv}\right) = \frac{18}{40.8} \frac{Pv}{11-Pv} = .442 \frac{Pv}{11-Pv}$$

$$\text{where } Mg_4 = \frac{1}{\frac{9.36}{11.76 \times 44} + \frac{2.40}{11.76 \times 32}} = 40.8$$

Water removed =

$$10.9 = 0.498 \times (7.72) \frac{Pv}{11-Pv} + 0.442 \times (1176) \frac{Pv}{11-Pv} - \underbrace{0.0426 \times 19.48}_{\text{from Stage I}}$$

$$11.72 = \frac{Pv}{11-Pv}\ (3.84 + 5.19)$$

$$1.3 = \frac{Pv}{11-Pv}$$

$$Pv = 14.29 - 1.3\ Pv$$

$$Pv = 6.21$$

From steam tables

Dew Point = 172°F

An electrolyte concentration of approximately 20 wt. percent K_2CO_3 will have a dew point of 172°F at a temperature of 176°F.

Since Pv = 6.21, we find

$$\omega_2 = 0.498 \times \frac{6.21}{4.79} = 0.646\ \frac{\text{lb } H_2O}{\text{lb gas}}$$

and

$$\omega_4 = 0.442 \times \frac{6.21}{4.79} = 0.572\ \frac{\text{lb } H_2O}{\text{lb gas}}$$

Condenser 2

Condenser 2 removes water from both the cathode outlet gas of Stage II and the anode outlet gas of Stage III. The flow schematic for condenser 2 is shown in Figure A-2.

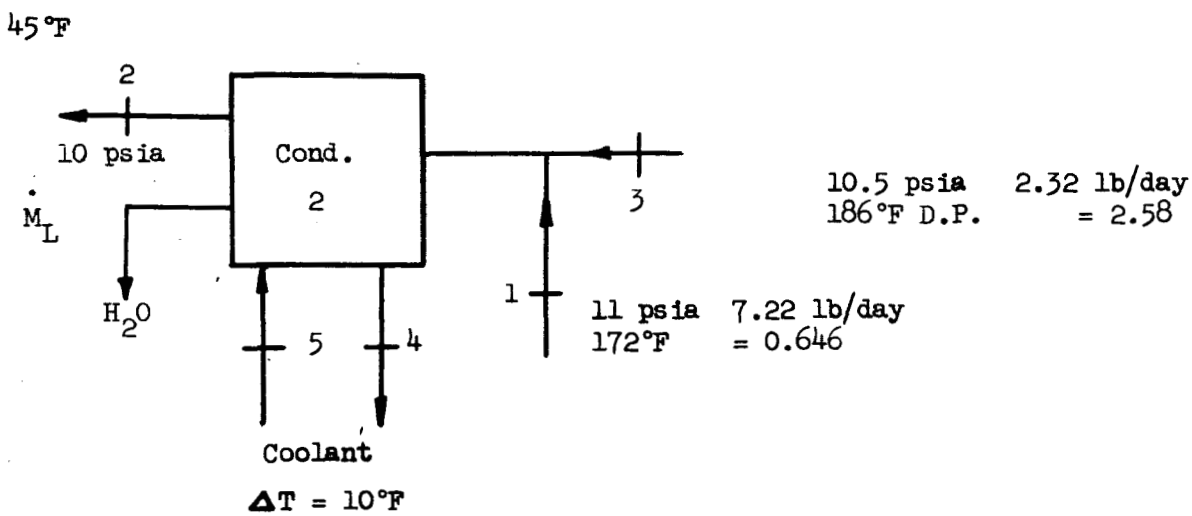

FIGURE A-2. CONDENSER 2 FLOW SCHEMATIC

$\dot{M}_L$ = mass flow of liquid

$$Q = \omega_2 \dot{M}g_2 h_2 - \omega_1 \dot{M}g_1 h_1 - \omega_3 \dot{M}g_3 h_3 + \dot{M}_L h_L$$

$$\omega_2 = \frac{18}{Mg_2} \frac{(0.147)}{9.853} = \frac{18}{34.9} \frac{(0.147)}{9.853} = 0.00768$$

where $$Mg_2 = \frac{1}{\frac{7.22}{9.54 \times 36.1} \times \frac{2.32}{9.54 \times 32}} = 34.9$$

$$Q = 0.00768(9.54)1081 - 0.646(7.22)1135. - 2.58(2.32)1140.5 + \dot{M}_L h_L$$

$$\dot{M}_L = -0.00768(9.54) + 0.646(7.22) + 2.58(2.32) = 10.733$$

$$\dot{M}_L h_L = 10.733(13)$$

$$Q = 79 - 5290 - 6840 + 140 = -11,911 \text{ BTU/day}$$

$$\text{Coolant Flow (FC-75)} = \frac{11,911}{.23 \times 10 \times 24} = 215 \text{ lb/hr}$$

CONTRACT NAS3-7638

National Aeronautics & Space Administration
Washington, D. C. 20546
Attention: A. L. Ingelfinger, Code RBB (3)

National Aeronautics & Space Administration
Scientific and Technical Information Facility
P. O. Box 5700
Bethesda, Maryland 20014 (2)

National Aeronautics & Space Administration
Lewis Research Center
21000 Brookpark Road
Cleveland, Ohio 44135
Attention: B. Lubarsky, MS 500-201
R. L. Cummings, MS 500-201
H. J. Schwartz, MS 500-201
John Dilley, MS 500-309
Technology Utilization Office, MS 3-19
Solar & Chemical Power Branch
Project Manager, MS 500-201
Library, MS 3-7
Report Control, MS 5-5
V. Hiavin, MS 3-14

National Aeronautics & Space Administration
Ames Research Center
Biotechnology Division
Moffett Field, California 94035
Attention: S. E. Belsley
E. Gene Lyman
P. D. Quattrone

National Aeronautics & Space Administration
Langley Research Center
Hampton, Virginia 23365
Attention: W. N. Gardner, MORL Studies Office
F. W. Booth, MORL Studies Office
R. W. Stone, Jr., Space Mechanics Div.
D. C. Popma, Life Support Systems Development Section
R. A. Bruce, Flight Vehicles and Systems Division
H. K. Clark, Flight Vehicles and Systems Division
R. W. Johnson, Applied Materials and Physics Division
R. S. Osborne, Applied Materials and Physics Division

NASA Manned Spacecraft Center
Crew Systems Division
Houston, Texas 77058
Attention: R. S. Johnston
Mr. Gill
W. W. Guy
R. E. Smylie
M. I. Radnofsky

NASA Manned Spacecraft Center
Houston, Texas 77058
Attention: N. Belasco, Code EC7

NASA Manned Spacecraft Center
Advanced Spacecraft Technology Division
Houston, Texas 77058
Attention: W. E. Stoney

NASA Western Operations Office
Santa Monica, California 90406
Attention: P. Pomerantz

Bureau of Naval Weapons
Washington, D. C. 20360

Bureau of Ships (Code 679)
Refrigeration, Air Conditioning & Pump Branch
Washington, D. C. 20360

Department of the Navy
Special Projects Office (SP-003)
Washington, D. C. 20360
Attention: Commander H. D. Baldridge

Department of the Army
Office of Chief of Engineers
Washington, D. C.
Attention: J. E. Malcolm, ENGMC-ED

Brooks Air Force Base
San Antonio, Texas
Attention: Col. A. Swan
Col. G. Wise

Air Force Space Systems Division
El Segundo, California
Attention: Col. A. Karstens

Wright-Patterson AFB
Wright-Patterson AFB, Ohio 45433
Attention: Mr. Roundy, MRMBR
Mr. F. Ebersbach, SENXP
Mr. L. V. Larson, SENPO
Mr. Bud Caston, SESSV
Mr. W. Savage, FDFE

Aerojet-General Corporation
Building 60, Department 206
Azusa, California
Attention: W. T. Shatzer, Spacecraft Division

Aerospace Corporation
Vehicle Systems Department
Systems Research & Planning Division
El Segundo, California

AiResearch Manufacturing Company
9851 Sepulveda Boulevard
Los Angeles, California
Attention: W. L. Burris

Arde, Incorporated
P. O. Box 286
Paramus, New Jersey
Attention: Jack Zeff

Arthur D. Little, Incorporated
Acorn Park
Cambridge, Massachusetts
Attention: A. C. Tobey

Bendix Aviation Corporation
Pioneer-Central Division
Davenport, Iowa
Attention: I. H. MacMillan

The Boeing Company
1625 K Street, N. W.
Washington, D. C.
Attention: P. L. Sommer

Borg-Warner Corporation
Research Center
Des Plaines, Illinois
Attention: R. L. Kuehner

Douglas Aircraft Company, Incorporated
M&SSD
3000 Ocean Park Boulevard
Santa Monica, California
Attention: Terry Secord

Dynatech Corporation
17 Tudor Street
Cambridge, Massachusetts
Attention: W. W. Welsh, Jr.

General American Transportation Corp.
MRD Division
7501 N. Natchez Avenue
Niles, Illinois
Attention: H. E. Thorpe

General Dynamics Corporation
Electric Boat Division
Groton, Connecticut
Attention: Dr. Petracelli

General Dynamics/Convair
P. O. Box 166
San Diego, California
Attention: Dr. Armstrong
Mr. Drake

General Electric Company
Advanced Technology Laboratory
Schenectady, New York
Attention: F. W. Van Luik, Jr.

Grumman Aircraft Engineering Corp.
Bethpage, Long Island, New York
Attention: C . J. Briody, Jr.

Hamilton Standard
Division of United Aircraft Corp.
1725 DeSales Street, N. W.
Washington, D. C.
Attention: E. J. Wulff

Hamilton Standard
Division of United Aircraft Corp.
Windsor Locks, Connecticut
Attention: J. S. Tupper

Honeywell
2435 Virginia Avenue, N. W.
Washington, D. C.
Attention: W. T. Herring

IIT Research Institute
1755 Massachusetts Avenue, N. W.
Washington, D. C.
Attention: A. D. Farrell

University of Iowa
Department of Chemical Engineering
Iowa City, Iowa
Attention: Prof. K. Kammermeyer

International Business Machine Company
Air Rights Building
Bethesda, Maryland
Attention: John Fuscoe

John Hopkins University
Applied Physics Laboratory
Charles & 34th Streets
Baltimore, Maryland
Attention: Dr. Evans

Ling-Temco-Vought, Incorporated
Astronautics Division
7015 Guld Freeway, Room 235
Houston, Texas
Attention: P. J. Carlton

Ling-Temco-Vought, Incorporated
Environmental Control
P. O. Box 6267
Dallas, Texas
Attention: G. B. Whisenhunt, Jr.

Lockheed Aircraft Corporation
Missile and Space Division
Flight Sciences Department
Palo Alto, California

McDonnell Aircraft Corporation
Civil Space Systems
P. O. Box 516
St. Louis, Missouri
Attention: M. T. Eldridge

S. G. McGriff Associates
National Bank Building
100 South Royal Street
Alexandria, Virginia 22314

The Marquardt Corporation
888 17th Street, N. W.
Washington, D. C.
Attention: W. W. Eckard

The Marquardt Corporation
Power Systems Division
16555 Saticoy Street
Van Nuys, California
Attention: W. H. Straly

Martin Company
Baltimore, Maryland
Attention: Arnold Gross,
Mail Number 395

New York University
College of Engineering
Research Division
New York 53, New York
Attention: Dr. R. Contini

North American Aviation, Incorporated
808 17th Street, N. W.
Washington, D. C.
Attention: G. P. Hillery
E. R. Kessler

North American Aviation, Incorporated
International Airport
Los Angeles, California
Attention: Mr. Paselk

North American Aviation, Incorporated
Space & Information Systems Division
12214 Lakewood Boulevard
Downey, California
Attention: J. W. Mohlman
Mr. Sexton

Northrop Corporation
Northrop Space Laboratories
1730 K. Street, N. W.
Washington, D. C.
Attention: L. K. Jensen

Norair Div., Northrop Corporation
3901 West Broadway
Hawthorne, California
Attention: B. N. Pridmore Brown

Radiation Applications, Incorporated
36-40 37th Street
Long Island City, New York
Attention: Dr. E. J. Henley

Rand Development Corporation
420 Lexington Avenue
New York 17, New York
Attention: G. H. Bookbinder

Republic Aviation Corporation
Conklin Street
Farmingdale, Long Island, New York

Ryan Aeronautical Company
2701 Harbor Drive
San Diego, California

Space/Defense Corporation
1600 North Woodward Avenue
Birmingham, Michigan
Attention: M. D. Ross

Space-General Corporation
Marketing Division
9200 E. Flair Drive
El Monte, California
Attention: B. Moxon

Spacelabs, Incorporated
15521 Lanark Street
Van Nuys, California
Attention: B. L. Ettelson

Space Technology Laboratories, Incorporated
Systems Design Department
One Space Park
Redondo Beach, California
Attention: F. H. Kaufman

TRW Inc.
23555 Euclid Avenue
Cleveland, Ohio 44117
Attention: A. D. Babinsky (3)

Union Carbide Corporation
Linde Division
777 14th Street, N.W.
Washington, D. C.
Attention: G. A. Kazanjian

United Aircraft Corporation
Pratt & Whitney Aircraft Division
1725 DeSales Street, N. W.
Washington, D. C.
Attention: J. S. Nuzum

Westinghouse Electric Corporation
Atomic Defense & Space Products
1625 K Street, N. W.
Washington, D. C.
Attention: W. Anderson

Westinghouse Electric Corporation
P. O. Box 2278
Pittsburgh, Pennsylvania
Attention: D. Archer

Whirlpool Corporation
300 Broad Street
St. Joseph, Michigan
Attention: Dr. N. G. Roth

TRW EQUIPMENT LABORATORIES
A DIVISION OF TRW INC. • CLEVELAND, OHIO 44117